Mechanistic Studies of Rhodium-Catalysed Intermolecular Hydroacylation

James Barwick-Silk

University College, University of Oxford

September 2018

Declaration

The work described in this thesis is entirely the work of the author except where specifically indicated. This thesis has not been previously submitted for a degree, diploma or any other qualification at The University of Oxford or elsewhere.

James Barwick-Silk

September 2018

Acknowledgments

What a journey, where to begin? Well, considering this doctorate has been undertaken at The University of Oxford, the traditional way, by thanking my supervisors (in alphabetical order) Andrew Weller and Michael Willis. They have both provided excellent supervision throughout my DPhil, which has allowed me to flourish as a chemist. I would like to thank Andy for teaching me the importance of scientific rigour and creativity in the pursuit of my passion; the understanding of catalytic mechanism. I would like to thank Mike for giving me the intellectual freedom to pursue my own scientific ideas and curiosities.

Less traditionally, at the time of writing anyway, I would like to thank the Centre for Doctoral Training: Synthesis for Biology and Medicine (SBM), for the opportunity to undertake my doctoral studies. Without the SBM, I would not have had the unique opportunity to collaborate so seamlessly between the Weller and Willis groups.

On the subject of research groups, I would like to thank the Weller group members past and present, I have been consistently amazed and inspired by your passion for the understanding of chemistry, you are all a credit to yourselves. Thanks to Mark for his distinct lack of supervision when I joined the lab; Alasdair for the extensive and intensive chats about chemistry (football and Geoffrey Boycott); Gemma for being an all-round star; the Devon boys for, well thanks for the proofing anyway!; Antonio for your wise (bald) head; Anna, just keep dancing; and last (and probably least) the Part II's for keeping us entertained. A special thanks must go to my Part II Louisa, you were a pleasure to supervise and you taught me more about practising chemistry than you'll ever know.

Now for the Willis group, wow, what a fantastic time I had in F2 when I started. I challenge anyone to have a better lab bay than Manu, Danny, Me, Concrete, Tim, Yiding, Maitane and Nate. I'm glad we prioritised listening to music over doing columns! A shout out to the whole group, especially for the Christmas parties, I hope the tradition of breaking MCR tables is long continued. A special thanks goes to Mataine, Vincent and Sang you all were, and will continue to be, great friends. Mataine, thanks for your brilliant supervision, including for the legendary May Day reaction. Vincent and Sang, thank you for all the crazy nights out, including our trip to Korea.

I would like to thank the JACS editorial team for accepting my work to be published in the journal. Since spending hours of my undergraduate degree reading JACS articles, it was a dream of mine to have my name alongside the great chemists who have published in the journal. I am immensely proud of this achievement.

Anyway, the legendary May Day reaction. Well, it wouldn't exist without the unique tradition of celebrating May Day morning on Magdalen bridge, an event that will bring me back to Oxford in the future. Thank you to all those who have celebrated May Day with me, you know who you are.

I'm grateful for all the friends I made away from the lab including those from Univ. and SBM, with a special mention to the 19 Boulter Street crew, Giulio and Shane, that house will forever feel like a home, thank you for sharing it with me.

Now for the important people in my life; Sara, I will be forever grateful for the compassion and understanding you have shown me. You have treated my goals and ambitions as yours, I cannot ask for more. Richard, you have been selfless in your support of me through an immensely challenging time, I am proud to call you a friend, and what you have taught me will stand me in good stead for the rest of my life. Mum, I know you will be proud of whatever Adam and I achieve in life, and because of this unconditional love I have accomplished this doctorate; and will go on to achieve much more. And finally, Dad, I would like to dedicate this thesis in your memory, I miss you dearly and know how proud you were and would be of me. You nurtured my curious and analytical mind, which was essential for starting and finishing this doctorate, I will use these qualities in all my future endeavours.

Abstract

Chapter 1 – Introduction: The concept of rhodium-catalysed intermolecular hydroacylation is introduced. The research that has led to significant improvements in substrate scope and catalytic activity are described, with the reactions being classified into three sub-groups: aldehyde-tethered hydroacylation, alkene-tethered hydroacylation and non-tethered hydroacylation. The mechanistic studies that have facilitated these developments are then detailed.

Chapter 2 – Mechanistic Studies of *β*-Amido Aldehyde Hydroacylation: One of the recent developments in aldehyde-tethered hydroacylation has been the use of *β*-amido aldehyde substrates. This chapter describes the mechanistic studies of the reaction of a *β*-amido aldehyde substrate with 1-octyne, catalysed by the Rh(I)-complex [Rh(*cis*-κ^2-$_{P,P}$-DPEPhos)(acetone)$_2$][BAr$^F{}_4$].

Chapter 3 – Cyclotrimerisation and Optimisation of Hydroacylation: In chapter 2, cyclotrimerisation of 1-ocytne was discovered to be a competitive side-reaction with hydroacylation under certain conditions. The mechanism of the cyclotrimerisation reaction is explored with the pre-catalyst [Rh(*cis*-κ^2-$_{P,P}$-DPEPhos)(acetone)$_2$][BAr$^F{}_4$], and the point at which the reactions become competitive is discovered. This understanding is then used to optimize the catalyst loading, reagent stoichiometry, reaction concentration and reaction temperature, leading to the realisation of an exceptionally efficient, and selective, gram-scale hydroacylation process.

Chapter 4 – Non-tethered Aldehyde Hydroacylation of Acrylates: The discovery of a non-tethered aldehyde Tishchenko reaction catalysed by [Rh(Cy$_2$PCH$_2$PCy$_2$)(η^6-fluoroarene)][AlO$^F{}_4$] complexes, in weakly coordinating fluoroarene solvents is described. The subsequent discovery and optimization of a hydroacylation reaction of non-tethered aldehydes with acrylates, catalysed by a {Rh(DPEPhos)}$^+$ catalyst system in 1,2-difluorobenzene is detailed.

Abbreviations

Å	angstrom(s)
Ac	acetate
acac	acetylacetone
AcOH	acetic acid
$AlO^F{}_4$	$Al(OC(CF_3)_3)_4$
anal.	analytical
app.	apparent
aq.	aqueous
Ar	aryl group
Ar^F	$3,5\text{-}C_6H_3(CF_3)_2$
atm	atmosphere
b	branched
$BAr^F{}_4$	$B(3,5\text{-}C_6H_3(CF_3)_2)_4$
BMIM	1-butyl-3-methylimidazolium hexafluorophosphate
boc	*tert*-butyloxycarbonyl
br	broad
Bu	butyl
$CbCl_6$	*closo*-$CB_{11}H_6Cl_6$
CI	chemical ionisation
cod	cyclooctadiene
COSY	correlation spectroscopy
Cy	cyclohexyl
d	doublet
DCE	1,2-dichloroethane
dcpb	1,4-*bis*(dicyclohexyl-phosphino)butane
dcpe	*bis*(dicyclohexylphosphino)-ethane
dcpm	*bis*(dicyclohexylphosphino)-methane
deg	degree(s)
dfb	difluorobenzene
DMAP	4-dimethylaminopyridine
DMF	dimethyl formamide
DMSO	dimethyl sulfoxide
DoE	design of experiments
DPE(cy)Phos	(oxydi-2,1-phenylene)-bis[dicyclohexyl] phosphine
DPEPhos	(oxydi-2,1-phenylene)-bis(diphenylphosphine)
dppb	1,4-*bis*(diphenylphosphino)-butane
dppe	1,2-bis(diphenylphosphino)-ethane
dppf	1,1′-ferrocenediyl-bis(diphenylphosphine)
dppp	1,3-*bis*(diphenylphosphino)-propane
dtbpm	*bis*(di-*tert*-butylphosphino)-methane
E	entgegen
e.e	enantiomeric excess
eq.	equivalents
ESI	electrospray ionisation
Et	ethyl
fac	facial
FT	Fourier transformation
g	gram(s)
GC	gas chromatography
h	hour(s)
HA	hydroacylation
hept	heptyl
Hex	*n*-hexyl
HRMS	high resolution mass spectrometry
Hz	Hertz
i	iso
intens.	intensity
IR	infrared spectroscopy

J	coupling constant
K_{eq}	equilibrium constant
KIE	Kinetic Isotope Effect
k_{obs}	observed rate constant
L	ligand or litre(s)
l	linear
LRMS	low resolution mass spectrometry
M	molar
m	multiplet or mili
m/z	mass to charge ratio
Me	methyl
MeCN	acetonitrile
mer	meridional
min(s)	minute(s)
mol	mole
mol%	mole percentage
MS	mass spectrometry
n	normal
N	normal
nbd	norbornadiene
NMR	nuclear magnetic resonance
nOe	nuclear Overhauser effect
nOeSY	2D nuclear Overhauser effect spectroscopy
o	ortho
Pent	pentyl
pfb	pentafluorobenzene
Ph	phenyl group
PMI	process mass intensity
ppm	parts per million
Pr	propyl
Py	pyridine
PyBOP	benzotriazol-1-yl-oxytripyrrolidinophosphonium hexafluorophosphate
q	quartet
quint	quintet
R	generic group
rpm	revolutions per minute
rr	regioisomer ratio
rt	room temperature
sat.	saturated
SIPHOS-PE	*N*-Dimethyl-[(*R*)-1,1′-spirobiindane-7,7′-diyl]phosphoramidite
t	triplet
T	temperature
t	tertiary
temp.	temperature
THF	tetrahydrofuran
TG	tethering group
TLC	thin layer chromatography
TLS	turnover limiting step
ToF	time of flight
TOF	turnover frequency
TON	turnover number
VT	variable temperature
X	counterion anion
XantPhos	4,5-*bis*(diphenylphosphino)-9,9-dimethylxanthene
Z	zusammen
δ	chemical shift (ppm)
υ	wavenumber

Table of Contents

Chapter 1: Introduction

1.1. Metal Catalysed Cross-Coupling Reactions in Drug Discovery

Metal-catalysed C–C bond-forming cross-coupling reactions have revolutionised organic synthesis since their discovery in the 1970's;[1,2] to the extent that, a statistical analysis of Medicinal Chemistry reactions by major pharmaceutical companies, over a 1 year period, revealed that 19% of the reactions performed were Pd-catalysed Suzuki cross-couplings.[3] The reason for the popular use of metal-catalysed cross-coupling reactions is that the reactions are efficient, chemoselective and the functional groups required for reactivity are widely accessible. These reaction characteristics facilitate the synthesis of large compound libraries by a combinatorial-type chemistry approach, a key technique used in drug discovery.[4] However, the number of different cross-coupling reactions employed in medicinal chemistry synthesis are severely limited, which is believed to be narrowing the chemical space explored in drug discovery,[5] which in turn, is hampering the discovery of new active drug compounds.[6] An ideal approach to solving this problem is to develop new metal-catalysed C–C bond forming cross-coupling reactions, that possess similar reaction characteristics to those currently employed but create distinct C–C bonds, and therefore readily facilitate access to different chemical space.

1.2. Hydroacylation

A reaction that has the potential to possess the characteristics described above is intermolecular-hydroacylation, the 100% atom economic union of an aldehyde and an alkene/alkyne to form a ketone/enone respectively, with the concomitant formation of a C–C bond (Scheme 1.1).[7]

Figure 1.1. Intermolecular-hydroacylation

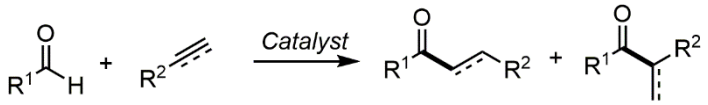

Aldehydes and alkenes are readily accessible functional groups, while chemoselectivity can be engineered using catalyst design, thus making the reaction an ideal candidate for application in medicinal chemistry. Furthermore, the product ketones/enones are distinct in structure to the biaryls

formed by aryl-aryl cross-coupling reactions, which means the reaction will facilitate research into different chemical space. A variety of transition metal catalysts have been used in intermolecular-hydroacylation, including ruthenium, cobalt, iridium, nickel and rhodium, with rhodium(I)-phosphine-chelated catalysts being the most commonly employed, as they support the largest substrate scope.[8] A general mechanism for hydroacylation with rhodium(I)-phosphine-chelated catalysts is depicted in Scheme 1.1

Scheme 1.1. General mechanism of intermolecular-hydroacylation

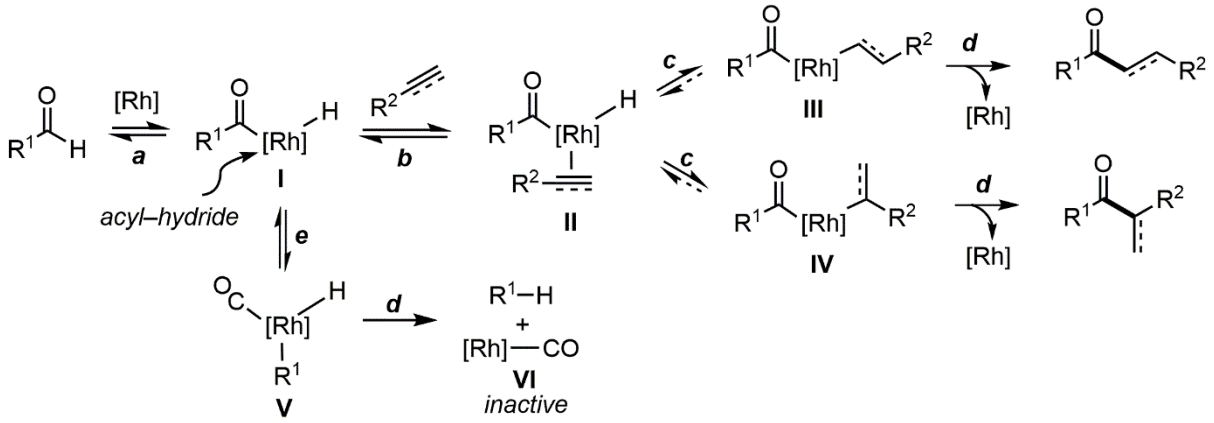

a. oxidative addition; ***b***. co-ordination; ***c***. migratory insertion; ***d***. reductive elimination; ***e***. decarbonylation

Oxidative addition of the aldehyde with the Rh(I)-catalyst forms the Rh(III)-acyl-hydride complex **I**, coordination of alkene/alkyne forms the alkene/alkyne bound intermediate **II**. Migratory insertion of the alkyne/alkene affords either the linear acyl-alkenyl-intermediate **III**, or the branched acyl-alkenyl-intermediate **IV**. Subsequent reductive elimination from **III** and **IV** then produces the linear and branched ketone/enone products respectively, while reforming the Rh(I)-catalyst. A competitive process to productive hydroacylation occurs by bifurcation of the reaction pathway at the acyl-hydride intermediate. This intermediate, if a vacant site on rhodium is present, can undergo (reversible) decarbonylation to provide the alkyl-hydride intermediate **V**, which can undergo irreversible reductive elimination to form a Rh-carbonyl complex **VI** and an alkane.

Over the past 46 years significant research efforts have been devoted to developing rhodium(I)-phosphine-chelated hydroacylation reactions; with a goal to develop reactions that are fast, reliable and possess broad substrate scope, key characteristics for application in medicinal chemistry. This introduction focusses upon the development of intermolecular-hydroacylation catalysed by rhodium(I)-

phosphine-chelated catalysts; in particular how catalyst systems have been developed to increase catalyst activity and/or substrate scope. The first section will outline the catalyst systems that been reported, briefly remarking on key mechanistic observations and the second section will present the detailed mechanistic studies that have been published.

1.3. Discovery of Intramolecular-Hydroacylation

Direct reductive decarbonylation of aldehydes promoted by Wilkinson's catalyst was discovered before rhodium catalysed hydroacylation, and was first reported by Tsuji and Ohno in 1965 (Scheme 1.2).[9]

Scheme 1.2. Rhodium-promoted reductive decarbonylation

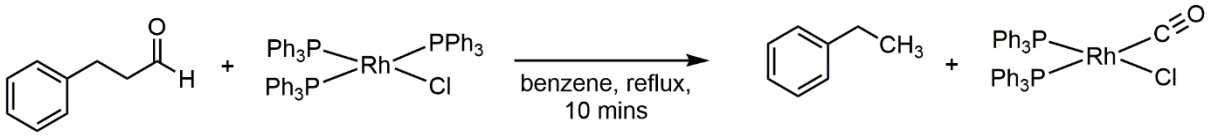

Since the report of these stoichiometric and mild reductive decarbonylation reaction conditions, the reaction has found widespread application in organic synthesis.[10] Although no direct evidence was reported, the mechanism was suggested to proceed by the now accepted pathway, *via* an acyl-hydride intermediate.[11]

In 1972 Sakai and colleagues discovered that by reacting Wilkinson's catalyst with substituted 4-pentanals, the product of intramolecular-hydroacylation was observed alongside a product of reductive decarbonylation (Scheme 1.3).[12]

Scheme 1.3. Rhodium promoted intramolecular-hydroacylation of a substituted 4-pentanal

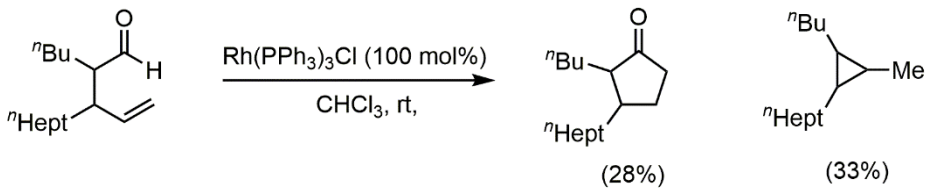

This is the first reported example of a hydroacylation reaction. A variety of substituted cyclopentanone hydroacylation products were synthesised, alongside the corresponding tri-substituted cyclopropane reductive decarbonylation products. The formation of a cyclopropane by reductive

decarbonylation, rather than a substituted butene product, indicates that intramolecular-hydride insertion into the alkene occurred before reductive C–C bond formation.

1.4. Early Development Intramolecular-Hydroacylation

The intramolecular-hydroacylation of 4-pentanal **1.1** was subsequently established as a catalytic reaction, with several groups developing new rhodium(I)-phosphine-chelated catalyst systems, which increased both the turnover number (TON) and turnover frequency (TOF) of the reaction (Table 1.1).

Table 1.1. Catalyst systems for intramolecular-hydroacylation of 4-pentanal

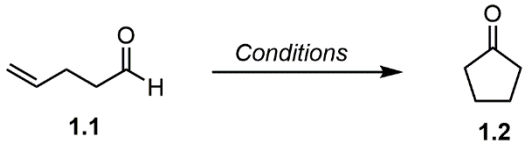

Entry	Conditions	Yield of 1.2 (%)
1	$Rh(PPh_3)_3Cl$ (10 mol%), C_2H_4 Sat. $CHCl_3$, rt, 88 h	72%
2	$[Rh(cod)Cl]_2$ (5 mol%) $P(4\text{-}MeC_6H_4)_3$ (10 mol%), C_2H_4 Sat. CH_2Cl_2, rt	97%
3	$[Rh(dppe)]_2[ClO_4]_2$ (1 mol%), CD_2Cl_2, 20 °C, 5 mins	95%

In 1976 Lochow and Miller reported that the combination of Wilkinson's catalyst (10 mol%) with 4-petenal **1.1** in an ethene saturated solution of chloroform afforded a 72% yield of cyclopentanone **1.2** (Table 1.1, Entry 1).[13] It was postulated that the ethene reduced the rate of reductive decarbonylation, by occupying the vacant site in the rhodium coordination sphere required for decarbonylation. Larock and colleagues, in 1980, also found that using ethene saturated solvents provided increased hydroacylation activity and reported that the $[Rh(cod)Cl]_2$ (5 mol%), $P(4\text{-}MeC_6H_4)_3$ (10 mol%) catalyst system provided the optimum yield of cyclopentanone **1.2** (97%, Table 1.1, Entry 2) from the conditions they screened.[14] A significant breakthrough in TON and TOF for hydroacylation was reported by Bosnich and Fairlie in 1988.[15] They used the cationic rhodium *bis*-phosphine catalyst system of $[Rh(dppe)]_2[ClO_4]_2$ (1 mol%) with CD_2Cl_2 as solvent and achieved a remarkable 95% yield of cyclopentanone within 5 mins (Table 1.1, Entry 3). A detailed mechanistic study of the reaction was performed and is discussed later. It was proposed that cationic nature of the Rh-complex is key to high catalytic activity due to promoting the formation of coordinatively unsaturated, and therefore reactive, catalytic intermediates.

Since this seminal work by Bosnich and Fairlie, cationic rhodium *bis*-phosphine catalyst systems have been extensively used in intramolecular-hydroacylation. Research has been focused on developing stereoselective transformations[16] and synthesising larger membered ring systems (6, 7 and 8 membered rings),[17] through judicious choice of ligand and substrate design.

1.5. Development of Intermolecular-Hydroacylation

Miller and Lochow disclosed the first example of intermolecular-hydroacylation at the same time as reporting their conditions for the intramolecular-hydroacylation of 4-pentantal (Scheme 1.4).[13]

Scheme 1.4. Intermolecular-hydroacylation of 4-pentantal with ethene

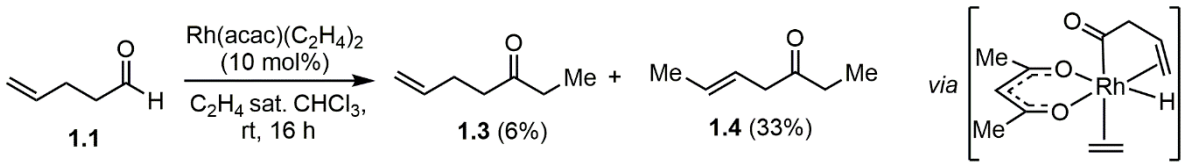

They found that by simply switching the catalyst to the [Rh(acac)(PPh_3)$_2$] complex, combined with ethene saturated chloroform as solvent, the products of intermolecular-hydroacylation, 6-hepten-3-one **1.3** and *trans*-5-hepten-3-one **1.4** were isolated in 6% and 33% yields respectively. It was later shown that the reaction of 3-pentanal **1.5** under the same conditions only afforded *trans*-2-pentanal **1.6** as product in 27% yield, formed by rhodium catalysed alkene-isomerisation (Scheme 1.5).[18]

Scheme 1.5. Attempted ethene hydroacylation with 3-pentanal and hexanal

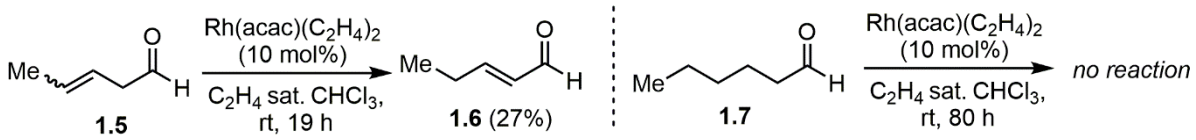

This result is consistent with the product of the hydroacylation with 4-pentenal, *trans*-5-hepten-3-one **1.4** (See Scheme 1.4), being formed by isomerisation of 6-hepten-3-one **1.3**, rather than by ethene hydroacylation with 3-pentanal. It also shows that the position of the remote alkene group is critical for intermolecular-hydroacylation reactivity. This was further exemplified in the reaction of hexanal **1.7** where no reactivity, including reductive decarbonylation, was detected after an 80 h reaction time.

1.6. Aldehyde-Tethered Hydroacylation

These seminal investigations by Miller and colleagues represent the first example of an 'aldehyde-tethered' intermolecular-hydroacylation. An aldehyde-tethered hydroacylation is a hydroacylation reaction which is assisted by a remote-functional group, that can coordinate to rhodium, and is directly attached (i.e. 'tethered') to the aldehyde. The role of tether in the reaction is two-fold, firstly to promote coordination and subsequent oxidative addition of the aldehyde. Its second role is to retard reductive decarbonylation by: i) constraining the product of decarbonylation to an unfavourable 4-membered rhodacyle and ii) filling a vacant site in the rhodium coordination sphere to prevent the decarbonylation step (Figure 1.2)

Figure 1.2 Role of the aldehyde-tethering group

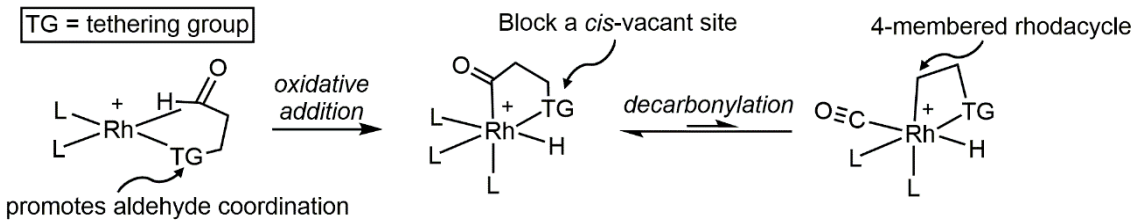

In Miller and colleague's reaction the alkene group is functioning as the tethering group and since this work several other tethering groups have been employed in Rh-catalysed hydroacylation; this next section will discuss the application of these tethering groups in intermolecular hydroacylation reactions (Figure 1.3).

Figure 1.3. Tethering groups used in Rh-catalysed hydroacylation

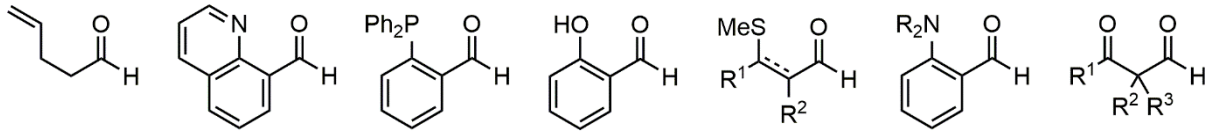

After Suggs' initial report of stoichiometric hydroacylation of quinoline carboxaldehyde with 1-octene in 1978 (*vide infra*),[19] Jun and colleagues, in 1994, reported a catalytic reaction with Wilkinson's catalyst that produced 2 turnovers with styrene as the alkene substrate.[20] Jun and Lee subsequently reported a hydroacylation that could achieve up to 7 turnovers by using 2-(diphenylphopshino) benzaldehyde as

the alkene substrate with 5 equivalents 1-propene and $[RhCl(cod)]_2$ as catalyst, without an auxiliary phosphine ligand, however harsh conditions were required and poor substrate scope was achieved.[21]

1.7. Salicylic Aldehyde Hydroacylation

A breakthrough in catalytic reactivity was reported by Miura and colleagues in 1997.[22] When they reported the reaction of salicylic aldehyde derivatives with alkynes catalysed by $[Rh(cod)Cl]_2$, dppf and Na_2CO_3; which afforded the corresponding enones in excellent yield while using low catalyst loadings (2 mol% [Rh]) (Scheme 1.6).

Scheme 1.6. Hydroacylation of salicylic aldehyde and alkynes

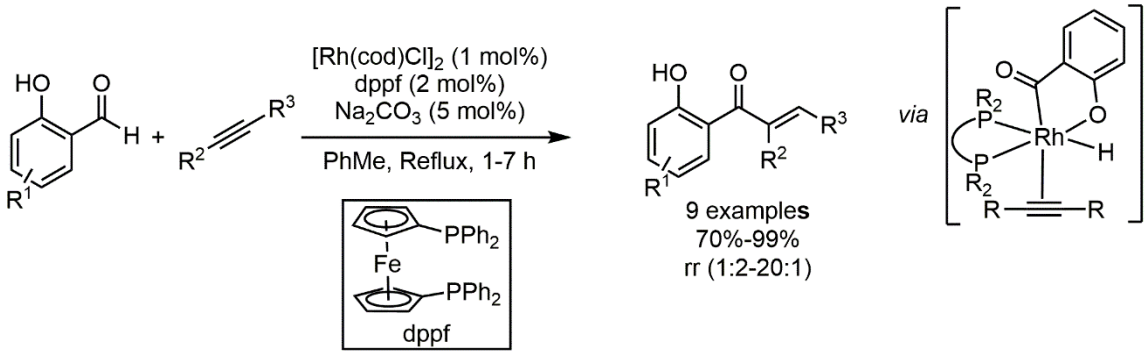

Catalytic base was found to be critical to reactivity, which was proposed to deprotonate the phenol group of the salicylic aldehyde, to enable the formation of a Rh-phenolate complexes. It was also found that the wide bite angle[23] dppf *bis*-phosphine ligand was crucial for high reactivity. Limitations of the methodology were the poor linear/branched enone ratios observed for terminal alkynes and the poor reactivity with alkenes, only vinyltrimethylsilane underwent appreciable reactivity using similar conditions.[24]

Since this initial report of the hydroacylation of salicylic aldehydes, significant research has been focussed on extending the alkene substrate scope. A noteworthy development was made by Suemune and colleagues in 2004, when they reported the hydroacylation of salicylic aldehyde and 1,4-pentadienes and 1,5-hexadienes (Scheme 1.7).[25]

Using catalytic amounts of Wilkinson's catalyst and sodium acetate, high yields of mixtures of branched/linear (b/l) ketone products were isolated. The branched ketone products were usually

Scheme 1.7. Hydroacylation of salicylic aldehyde and dienes

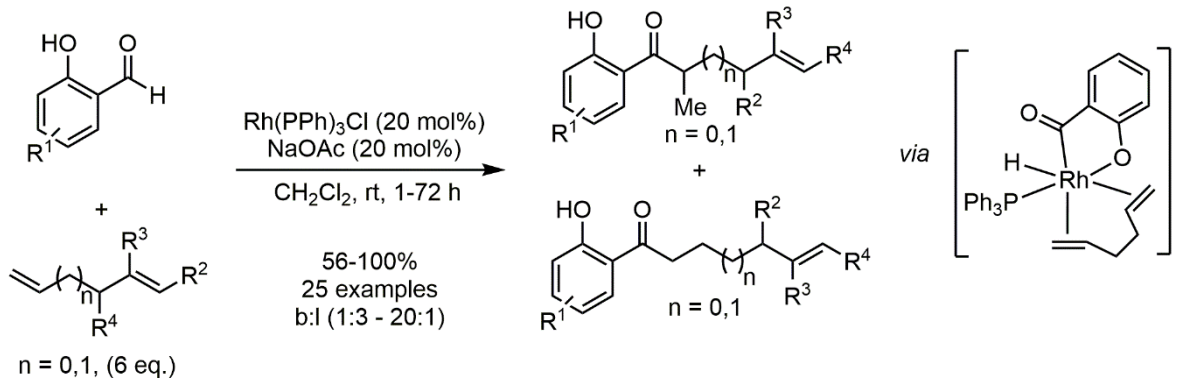

favoured over linear products and when substituted alkenes were employed, the unsubstituted alkene reacted in preference to the substituted alkene. Importantly, the reaction of 1-hexene, under similar reaction conditions, only afforded a 4% yield of the corresponding linear ketone hydroacylation product, and in the reaction of benzaldehyde no hydroacylation reactivity was observed. This demonstrated that both the salicylic aldehyde and the diene functionality is critical for reactivity. Which led to Suemune and colleagues to propose that the a double-tethering effect from both the diene and salicylic aldehyde was in operation, with both tethering groups reducing the rate of reductive decarbonylation.

It was also noted that the tethered-alkene favoured the branched hydroacylation product over the linear hydroacylation product. This preference is observed in other salicylic aldehyde hydroacylation systems with tethered-alkenes, including enamides[26] and 1,5-thiophenylether alkenes.[27] The subtly of this effect was exemplified by Dong and colleagues, in 2010, using the $[Rh(cod)Cl]_2$, chiral monodentate phosphine SIPHOS-PE ligand and K_3PO_4 catalyst system. They observed that: the branched ketone product is favoured in the reactions of 1,5-thiophenylether alkenes, whereas the linear ketone product is favoured in the reaction of 1,4-thiophenylether alkenes (Scheme 1.8).

The difference in regiochemistry can be explained by the preferred formation of 5-membered alkyl-rhodacycles, after hydride insertion into the alkene, instead of 4/6-membered alkyl-rhodacycles. Dong and colleagues utilised this regioselectivity switch, to develop a highly enantioselective reaction of 1,5-thiophenylether alkenes with moderate substrate scope.

After the development of the double tethered diene hydroacylation, Suemune and colleagues sought to develop hydroacylation with non-tethered alkenes and salicylic aldehyde. After their initial report of

Scheme 1.8. Hydroacylation of salicylic aldehyde with 1,4 and 1,5-thiophenylether

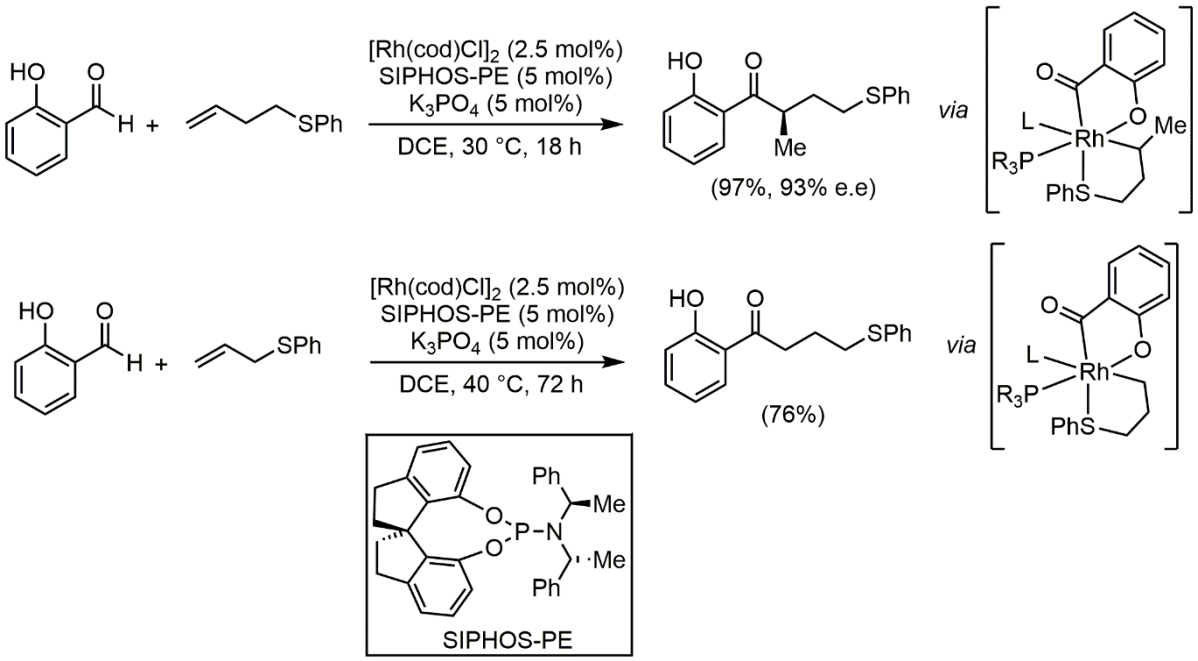

hydroacylation with norbornadiene in 2005,[28] which was subsequently developed into an enantioselective reaction by Bolm and colleagues,[29] they reported the beneficial effect of adding superstiochometric quantities of acetonitrile in the reaction of simple terminal alkenes with salicylic aldehyde.[30] The reaction conditions where otherwise similar to that reported for the reaction of 1,6/1,5-dienes and 2 turnovers of hydroacylation was achieved with a small set of terminal alkenes. Despite this improvement in reactivity, not until 2012 was a general and high yielding hydroacylation of terminal alkenes and salicylic aldehyde reported (Scheme 1.9).

Scheme 1.9. Hydroacylation of salicylic aldehyde and a terminal alkene

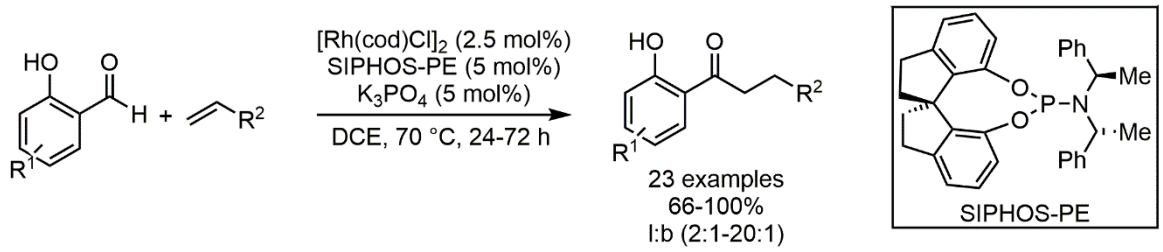

The reaction was reported by Dong and colleagues using similar reaction conditions to those reported for their asymmetric reaction of 1,5-thiophenylether alkenes. Interestingly, in both reactions an equal stoichiometry of the monodentate phosphine and [Rh] was used, which is in contrast to all other

hydroacylation reactions discussed. The authors showed that the (R_a,*R*,*R*)-SIPHOS-PE ligand was crucial for high activity, with other bulky phosphine and phosphoramidite ligands providing significantly lower yields. The diastereomer of ligand also proved critical, with the (S_a,*R*,*R*)-SIPHOS-PE ligand proving to be much less active. The authors speculate that the steric bulk and electronics of the phosphoramidite ligand promote, the potentially turnover-limiting, reductive elimination step.

1.8. *β*-S-Substituted Aldehyde Hydroacylation

All the systems discussed so far use a neutral rhodium-phosphine catalyst systems; in 2004 Willis and colleagues employed the cationic catalyst system reported by Bosnich, for the intramolecular-hydroacylation of 4-pentanals, in the intermolecular-hydroacylation of *β*-S-substituted aldehydes with activated alkenes (Scheme 1.10).[31]

Scheme 1.10. Hydroacylation of a *β*-S-substituted aldehyde and activated alkenes

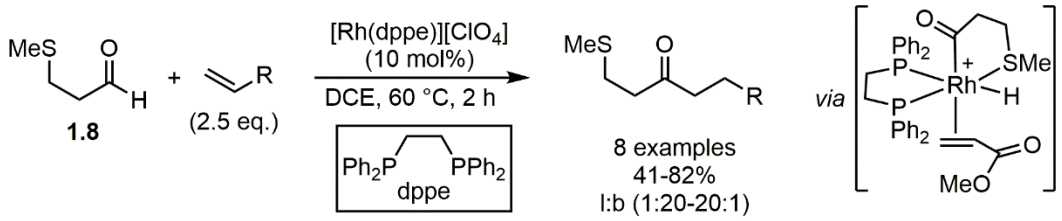

A broad range of activated alkene substrates could be employed, although high catalyst loadings of 10 mol% were required. Interestingly, a switch in reactivity to reductive-aldol-hydroacylation was observed when acrylonitrile, methyl-vinyl ketone and phenyl acrylate were employed as the alkene coupling partner (Scheme 1.11).[32]

Mechanistic studies indicated that the reaction proceeds *via* an aldol reaction from the branched acyl-alkenyl intermediate **II**, followed by reductive elimination of the ester product from the so formed acyl-ester complex **III**. The reaction also required 10 mol% catalyst, as well as 5 equivalents of the alkene coupling partner to afford good yields. Following this report, significant efforts into developing more active catalyst systems, that can control reaction selectivity and increase the reaction substrate scope, were undertaken by the Willis and Weller groups. With the Willis group focussing organic methodology and the Weller group focussing on mechanism and catalyst design (Figure 1.4).

Scheme 1.11. Reductive-aldol-hydroacylation of *β*-S-substituted aldehyde

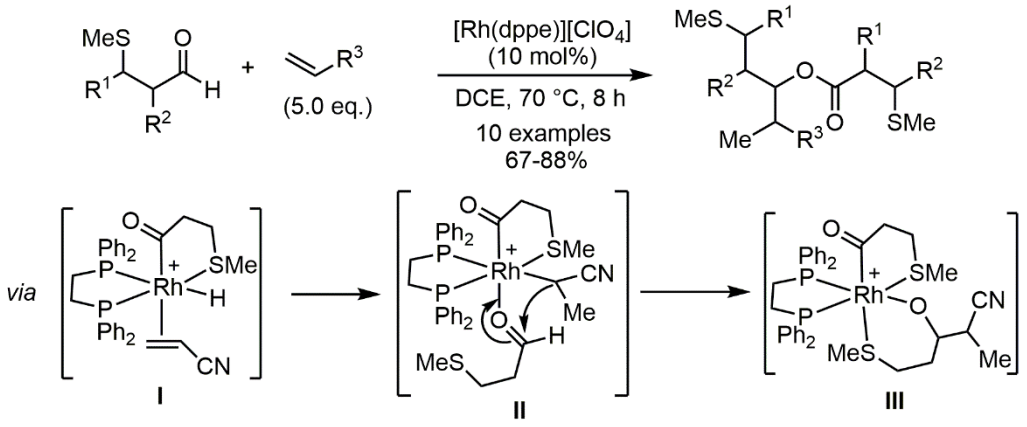

Figure 1.4. Catalyst design for hydroacylation with *β*-S-substituted aldehydes

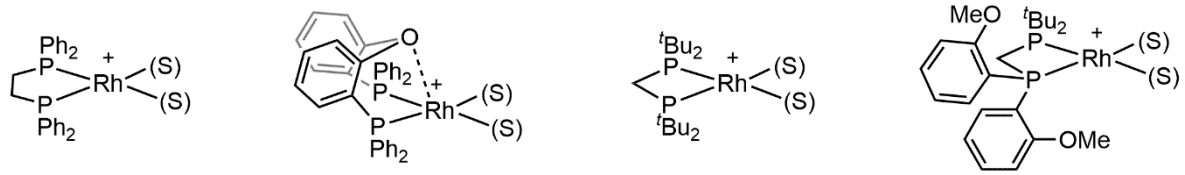

The first improvement in reactivity was reported in 2006, by applying the 2nd generation catalyst system which utilised the hemilabile DPEPhos ligand and acetone as solvent.[33,34] The catalyst system reduced the catalyst loadings and reaction time required in the reaction of methyl acrylate, to 1 h and 5 mol% respectively (compared 4 h and 10 mol% with the dppe catalyst system), and extended the substrate scope to terminal alkenes and terminal/internal alkynes. Detailed mechanistic studies were undertaken, which indicated that the oxygen atom in the POP backbone coordinates to the Rh in a hemilabile fashion, which decreases the rate of deleterious of reductive decarbonylation, by blocking a *cis*-vacant site. The 3rd generation catalyst system, reported in 2012, provided another significant improvement in catalytic activity. The catalyst system utilised small-bite-angle *bis*-phosphine ligands, including dtbpm ($^tBu_2PCH_2P^tBu_2$), which reduced the catalyst loadings required for the reaction of terminal alkenes with 3-(methylthio)propanal **1.8** to 0.5 mol% for a 3 h reaction time.[35] Application of the small bite angle PNP ligand $Cy_2P(NMe)PCy_2$ in the reaction of terminal alkynes, provided high catalyst activity and excellent linear/branched selectivity.[36] It was postulated that the small bite angle

ligands accelerate the, often turnover-limiting, reductive elimination step of the hydroacylation reactions. Further optimization of the small-bite-angle ligand scaffold, to include *ortho*-anisole and *tert*-butyl substituents on each phosphine (AmpaPhos, ($^{t}Bu_2PCH_2P(^{o}C_6H_4OMe)_2$)), resulted in the unprecedented reaction of *β*-S-substituted aldehydes with un-activated internal alkenes.[37] The positive effect of the 4th generation catalyst system was rationalised by the bulky phosphine substituents promoting the hydride insertion step, a challenging step for internal alkenes.

The Willis group have since demonstrated the synthetic utility of the developed catalyst systems, to synthesise hydroacylation products that can be converted into heterocycles in one further synthetic step. The heterocycles synthesised include furans,[38] pyrroles,[39] dihydropyrroles,[39] quinolines,[40] pyrazoles,[41] pyrimidines,[41] and isoxazoles.[41] However, all these products still contain the sulphur tethering group, which is often not a synthetically desirable functional group, particularly for medicinal chemistry applications. One approach to this problem has been to develop 'traceless' hydroacylation reactions that either remove, functional group convert, or directly functionalise the sulphur group in the hydroacylation product.[42–48]

1.9. Aniline and Carbonyl Aldehydes in Hydroacylation

Another approach to increasing the utility of the hydroacylation products has been to extend the substrate scope of the aldehyde to containing more synthetically useful functional groups. Bolm and colleagues first reported the use of an aniline aldehyde in their work on enantioselective salicylic aldehyde hydroacylation with norbornene.[29] Willis and colleagues reported a more extensive substrate scope in the reaction of protected anilines with alkynes, which could be directly transformed into dihydro-4-quinolones in one step (Scheme 1.12).[49]

Scheme 1.12. Aniline aldehyde hydroacylation

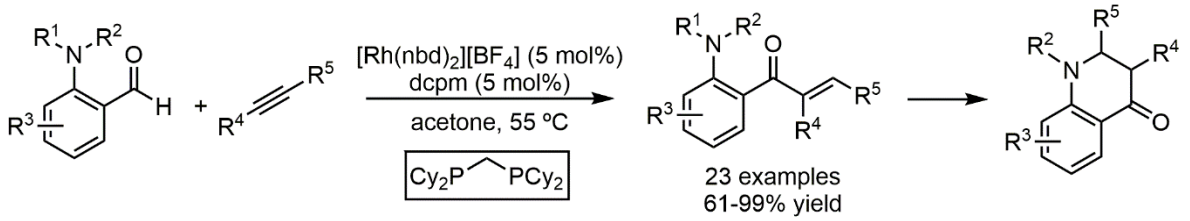

Extending the aldehyde substrate scope further, Willis and colleagues reported the hydroacylation of amides, esters and ketones. The authors found that using different catalyst systems, in which the bidentate phosphine was varied, provided the best yields and selectivity for different substrate combinations (Scheme 1.13).[50]

Scheme 1.13. *β*-Amido, ester and ketone aldehyde hydroacylation

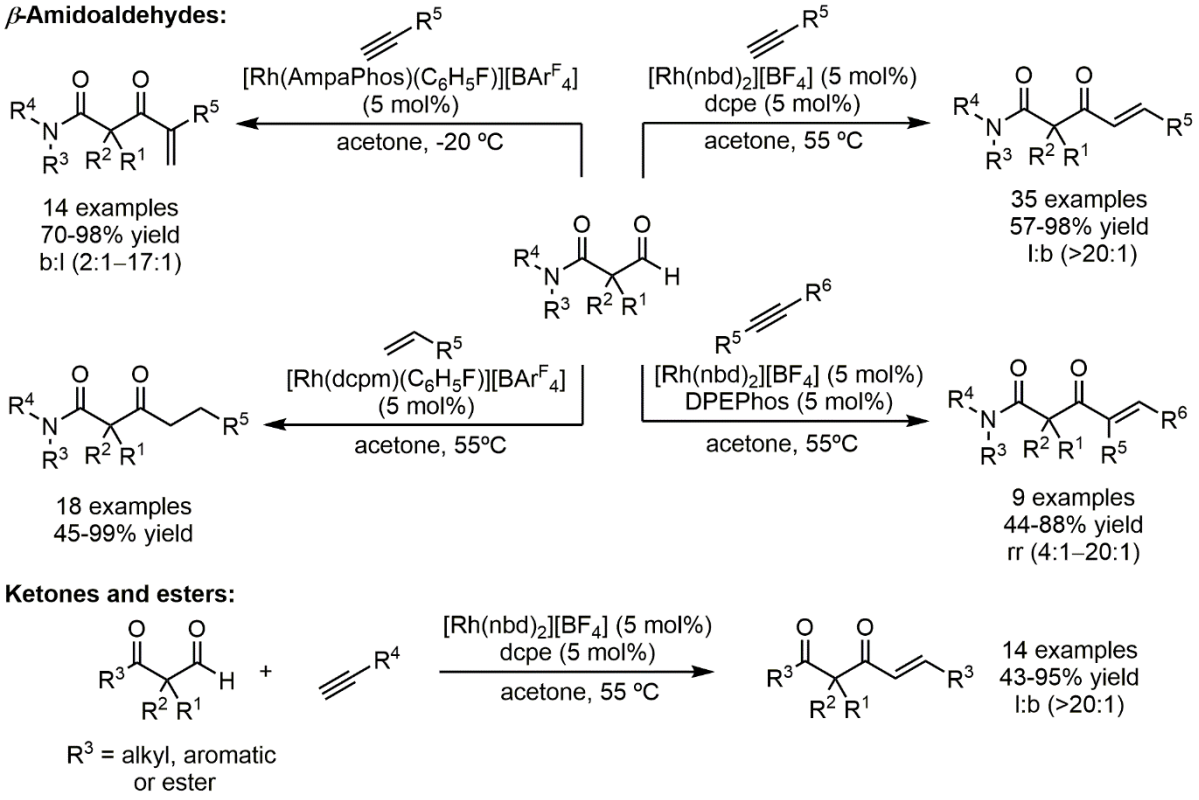

A remarkable substrate scope was reported, particularly with alkyne coupling partners. In the reactions of terminal alkynes, dcpe provided the highest linear to branched selectivity, while using AmpaPhos as ligand, at –20 ºC, switched the selectivity in favour of the branched enone products. In the reactions of unsymmetrical internal alkynes, DPEPhos provided the best regioselectivity and in the reaction of terminal alkenes, remarkably, dcpm was the only ligand to provide any reactivity. *α*-Disubstituted *β*-ketones and *β*-esters didn't provide any reactivity with alkenes, however, high yields and linear/branched ratios were obtained with terminal alkynes, with dcpe proving to be the most effective ligand.

Overall, significant research of aldehyde-tethered hydroacylation has been explored by various groups, which has led to the development of general intermolecular-hydroacylation reactions with a

subset of aldehyde tethers including phenolate, thioether, aniline and amide groups

1.10. Alkene-Tethered Hydroacylation

Since the breakthrough of aldehyde-tethered hydroacylation, considerable efforts have been invested in developing intermolecular-hydroacylation reactions that do not require a tethered aldehyde. Inspired by the double chelation-controlled reactions of salicylic aldehyde with tethered alkenes, several hydroacylation reactions of aldehydes with tethered alkenes have since been realised. In 2007 Tanaka and colleagues reported the hydroacylation of acrylamides with non-tethered aldehydes catalysed by a cationic rhodium catalyst system with the wide bite-angle ligand dppb (Scheme 1.14).[51]

Scheme 1.14. Acrylamide hydroacylation with non-tethered aldehydes

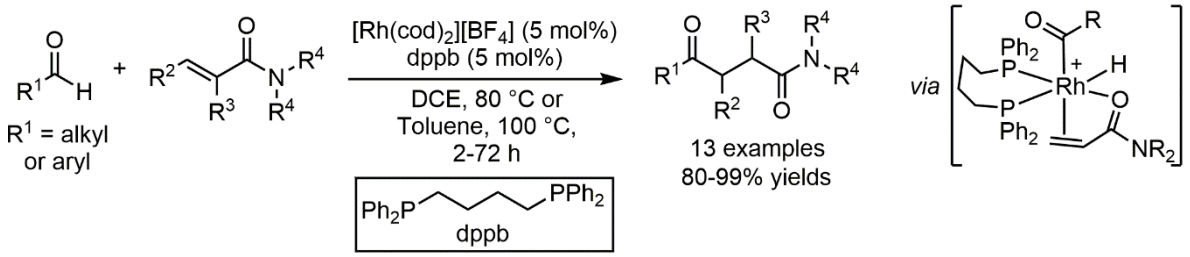

Notably, high linear selectivity was reported for all substrates, with primary and secondary aliphatic aldehydes as well as aromatic aldehydes being tolerated. Interestingly, aromatic aldehydes required higher reaction temperatures of 100 ºC compared to 80 ºC for aliphatic aldehydes. Methyl-substitution of the at the α and β-position of the alkene also provided high yields of their corresponding ketone products and an enantioselective reaction with methyl acrylamides was subsequently reported.[52] Tanaka and colleagues proposed that the amide and alkene groups of the acrylamide simultaneously coordinate to rhodium, which after formation of the acyl-hydride, retards reductive decarbonylation by reducing the concentration of unsaturated acyl-hydride intermediates. The tethering effect of the acrylamide is supported by the poor reactivity observed with *N*-methylmaleimide and methacrylate. *N*-methylmaleimide provided no reactivity and only a 55% yield was reported when methacrylate was used as the reaction solvent with 10 mol% catalyst. (Scheme 1.15).

It is postulated that no reactivity is observed with *N*-methylmaleimide because the alkene and amide groups cannot coordinate simultaneously to rhodium. Whereas poor reactivity is observed with methyl

Scheme 1.15. Acrylate hydroacylation with non-tethered aldehydes

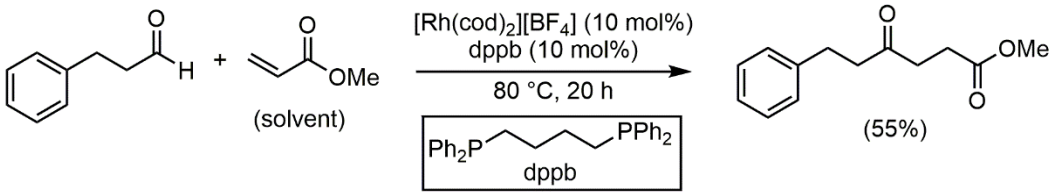

acrylate because the ester group possesses reduced Lewis basicity compared to amides, and therefore are more likely to form unsaturated acyl-hydride intermediates, able to undergo reductive decarbonylation.

Dong and colleagues developed an alkene-tethered hydroacylation by further exploring the use of the phenolate tethering group.[53] They employed the small-bite-angle ligand dcpm, in combination with the neutral rhodium complex $[Rh(cod)(OMe)]_2$ to catalyse the reaction between vinylphenols and non-tethered aldehydes to afford a range of branched ketones (Scheme 1.16).

Scheme 1.16. Vinylphenol hydroacylation with non-tethered aldehydes

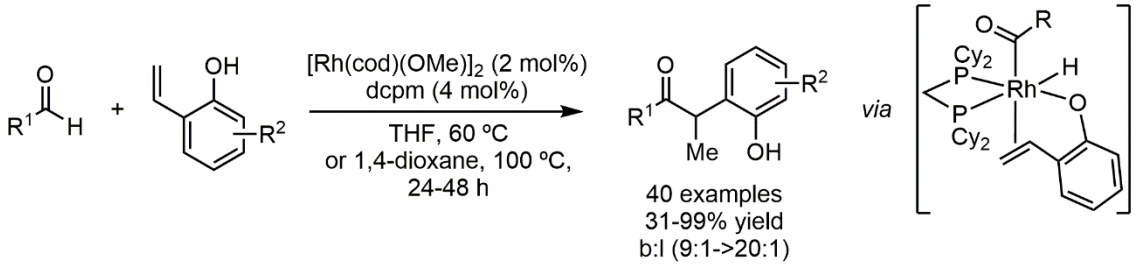

The use of the small-bite-angle ligand dcpm ($Cy_2PCH_2PCy_2$) is vital for high catalytic activity and as with Tanaka and colleague's acrylamide system, aromatic aldehydes required increased reaction temperatures compared to aliphatic substrates (100 and 60 ºC respectively). Mechanistic studies were undertaken which led to the authors proposing that the dcpm ligand played a role in promoting oxidative addition.[54] An elegant extension of this work was reported by Zhang and Guo in 2017, where they reported the hydroacylation of vinyl cyclobutanols with non-tethered aldehydes to afford 1,5-diketones (Scheme 1.17).[55]

The vinyl cyclobutanol is proposed to initially coordinate through both the alkene and alkoxide functional groups, formed by deprotonation with the catalytic base. A subsequent rearrangement of the

Scheme 1.17. Vinyl cyclobutanols hydroacylation with non-tethered aldehydes

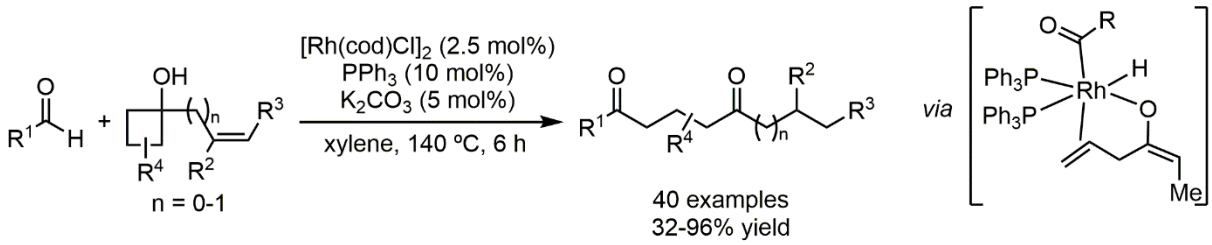

cyclobutanol *via* β-carbon cleavage, β-hydride elimination and hydride insertion forms an acyl-enol-alkene complex that can undergo the hydroacylation sequence with the aldehyde. Under the optimized reaction conditions using monodentate triphenylphosphine as ligand, both aliphatic and aromatic aldehydes were tolerated and a wide substrate scope of vinyl cyclobutanols was reported.

1.11. Non-Tethered Hydroacylation

To make hydroacylation a truly general process, reactions that do not require tethering groups on either substrate are highly desirable. Expanding on the initial report of Lochow and Miller on the intermolecular-hydroacylation of 4-pentanals with ethene, Millstein and colleagues extended the substrate scope to non-tethered aldehydes using the η^5-indenyl Rh-complex Rh(η^5-C_9H_7)(C_2H_4)$_2$ as the catalyst (Scheme 1.18).[56]

Scheme 1.18 Hydroacylation of non-tethered aldehydes and ethene

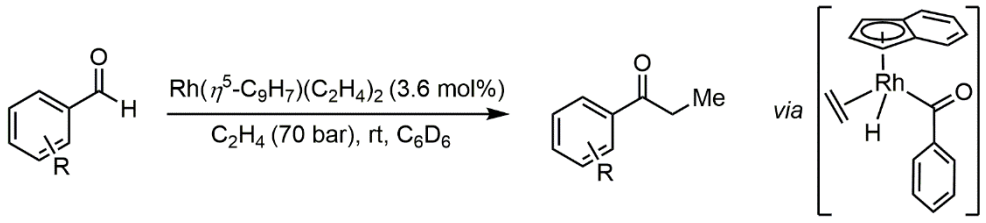

High pressures of ethene were required to prevent catalyst decomposition and facilitate catalytic turnover, leading to no reductive decarbonylation being observed under the optimized conditions. However, limited reactivity was reported when acetaldehyde and formaldehyde were used as substrates due to catalyst decomposition. Deuterium labelling studies were carried and indicated that: i) oxidative addition of aldehyde is irreversible, ii) hydride insertion is fast and reversible and iii) ethene substitution does not occur from the acyl-hydride-ethene intermediate.

Brookhart and colleagues also utilised a neutral half-sandwich rhodium-complex, $[Rh(C_5Me_4CF_3)(CH_2CH_2SiMe_3)_2]$, in the hydroacylation of aromatic aldehydes with simple terminal and internal alkenes (Scheme 1.19).[57]

Scheme 1.19. Hydroacylation of non-tethered aromatic aldehydes with alkenes

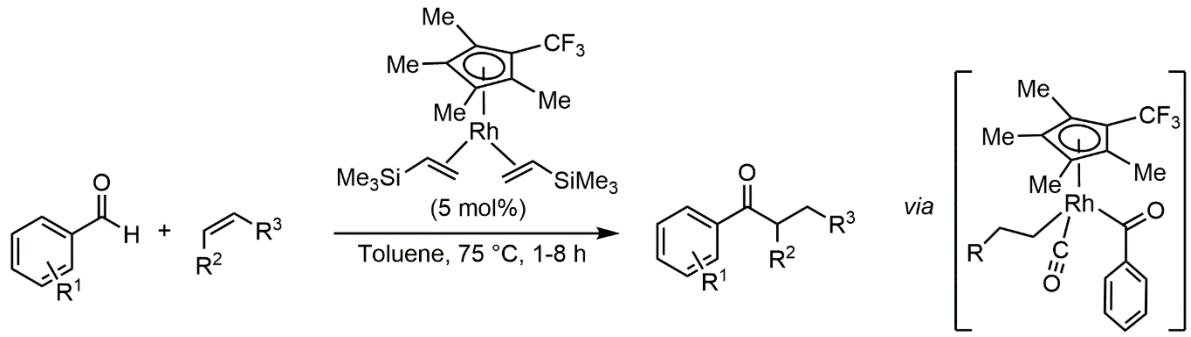

A detailed study of the reaction revealed a unique mechanism, in which one of the resting states of the reaction is an acyl-alkyl-carbonyl complex, indicating that decarbonylation is reversible. Overall reductive decarbonylation does not occur from this complex because reductive elimination of the alkane from the 18-electron, octahedral half-sandwich complex is disfavoured; compared to the rate of reductive elimination of the ketone product.

Jun and colleagues also developed a hydroacylation of non-tethered aldehydes and non-tethered alkenes, as well as acrylates, using 2-amino-3-picoline and benzoic acid as co-catalysts (Scheme 1.20).[58–60]

Scheme 1.20. 2-amino-3-picoline catalysed hydroacylation

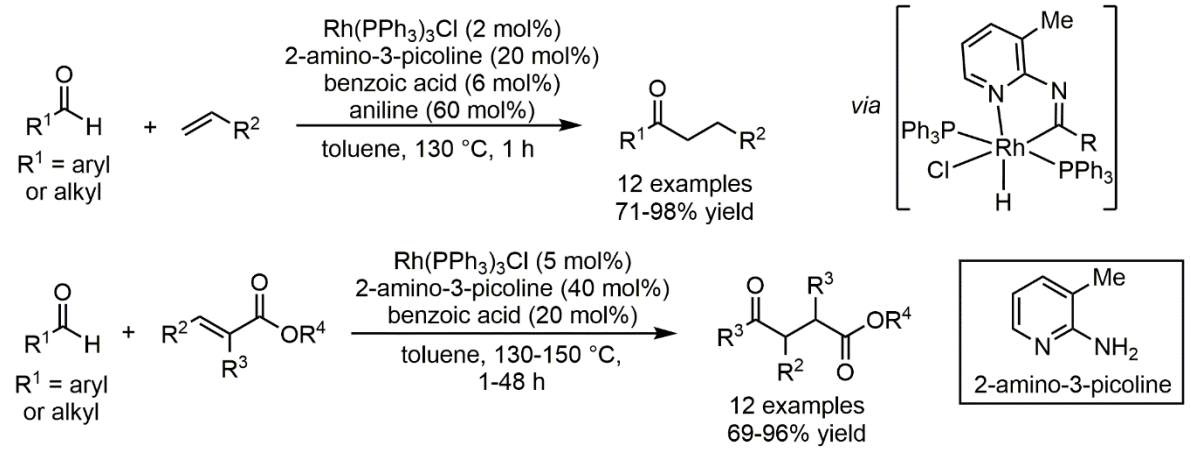

Aliphatic and aromatic aldehydes were tolerated in both reactions, although tertiary aliphatic aldehydes provided no yield. The 2-amino-3-picoline catalyst acts as a transient tethering group, assisting oxidative addition and slowing reductive decarbonylation. The first step of the reaction is the condensation reaction of 2-amino-3-picoline and the aldehyde to form an aldimine, which can undergo hydroacylation to form the corresponding imine. Subsequent hydrolysis to the ketone affords the hydroacylation product and liberates the 2-amino-3-picoline catalyst. The isolation of an iminoacyl-hydride rhodium species was reported by Suggs in 1979,[61] with Jun's first catalytic process being reported in 1997. Jun and colleagues later reported benzoic acid as a co-catalyst, which accelerates the condensation of the 2-amino-3-picoline and subsequent hydrolysis steps. More mild reaction conditions have since been reported by Breit and co-workers by using a bifunctional aminopicoline-phosphine ligand that could also reversibly condense with the substrate.[62]

Overall, significant progress has been made into the development of a remarkable number of catalytic intermolecular-hydroacylation systems. However, a truly general process, applicable for medicinal chemistry and materials synthesis, is yet to be discovered. In the case of the Suzuki cross-coupling reaction, significant mechanistic studies underpinned the discovery of the now often employed catalyst systems.[63] The next section discuss the efforts to understand the mechanism of hydroacylation, in order to facilitate reaction development.

1.12. Mechanistic Studies of Hydroacylation

In 1979, Suggs isolated and characterised the first stable rhodium(III)-acyl-hydride complexes by the reaction of Wilkinson's catalyst with quinoline carboxaldehyde, followed by treatment with silver tetrafluoroborate (Scheme 1.21).[19]

Scheme 1.21. Acyl-hydride synthesis with quinoline carboxaldehyde

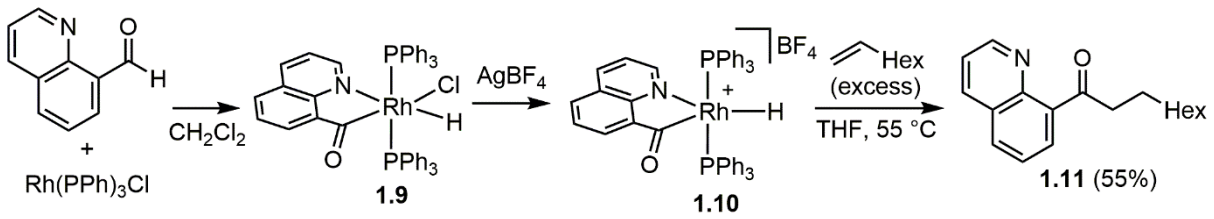

Both complexes **1.9** and **1.10** were characterised by elemental analysis, IR spectroscopy and ^{1}H NMR spectroscopy, with the hydride region of ^{1}H NMR spectra containing the characteristic double of triplets at δ −11.9 [J_{RhH} = 15 Hz; J_{PH} = 6 Hz] and δ −10.7 [J_{RhH} = 20 Hz; J_{PH} = 6 Hz] for complexes **1.9** and **1.10** respectively. Interestingly, both complexes required elevated temperatures for decarbonylation to be observed, despite the cationic complex possessing a vacant site. Coordinative unsaturation appeared to be advantageous in the reaction with 1-octene, with only the cationic complex **1.10** displaying hydroacylation reactivity with excess 1-octene to yield **1.11**. This seminal work represented the first time hydroacylation was observed directly from an acyl-hydride intermediate, consistent with it being a catalytic intermediate.

Millstein subsequently reported the synthesis of several acyl-hydride intermediates with 4-pentenal and non-tethered aldehydes using the neutral Rh(I)-complex $Rh(PMe_3)_3Cl$ (Scheme 1.22).[64–66]

Scheme 1.22. Acyl-hydride synthesis with $Rh(PMe_3)_3Cl$

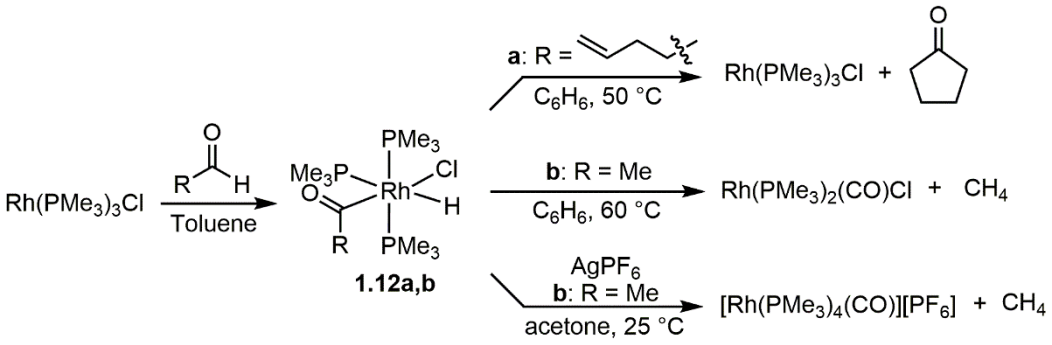

The isolated neutral Rh(III)-acyl-hydride complexes were stable at room temperature, which was attributed to the reduced propensity of the trimethyl phosphine ligand to dissociation, compared to bulkier monodentate phosphine ligands (i.e. triphenylphosphine). Upon heating, the 4-pentanal acyl-hydride complex **1.12a** afforded a 72% yield of cyclopentanone hydroacylation product. Heating the acetaldehyde acyl-hydride **1.12b** complex also resulted in decomposition, but by reductive decarbonylation to afford methane. Interestingly, the rate of reductive decarbonylation was significantly increased by the addition of silver hexafluorophosphate in acetone, with the reaction proceeding immediately at room temperature. The increased rate was postulated to be due to the formation of the coordinatively unsaturated cationic complex, which promotes migration of the CO group.

The observed low stability is in contrast with the high stability of the cationic quinoline carboxaldehyde acyl-hydride **1.10**, which also possesses a vacant site. The marked difference in stability can be rationalized by the tethering group preventing reductive decarbonylation by disfavouring the initial decarbonylation step, due to the formation of an unfavourable 4 membered alkyl-rhodacyle; in the case of a non-tethered aldehyde a rhodacyle is not formed.

In order to gain mechanistic insight into the intermolecular-hydroacylation between 4-hexenal and ethene, Miller and colleagues, in 1980, performed deuterium labelling studies with 4-hexenal-d_1 (Scheme 1.23).[67]

Scheme 1.23. Deuterium labelling studies for the hydroacylation between 4-hexenal-d_1 and ethene

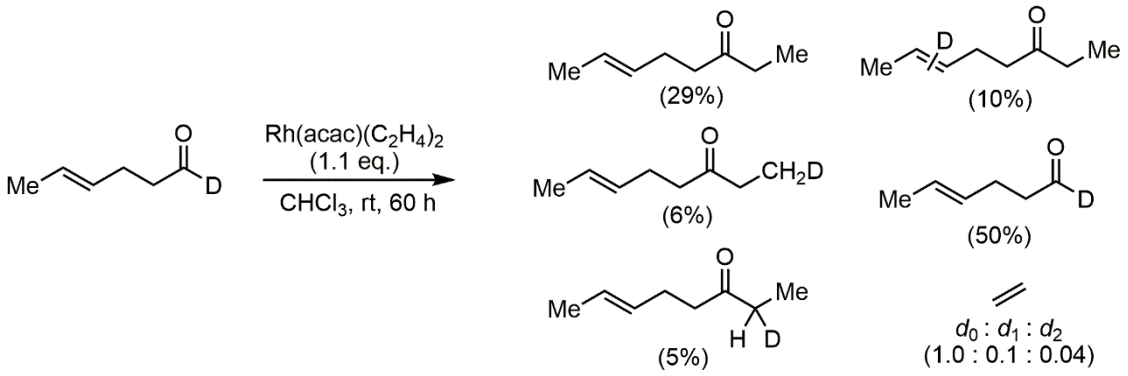

They reported a qualitative KIE isotope effect, with 4-hexenal-d_1 reacting at a slower rate than 4-hexenal. Deuterium scrambling was observed to the α and β-positions of the enone product as well as to both alkene positions, ^{2}H-incoporation into recovered alkene was observed alongside minimal ^{2}H-loss from recovered aldehyde. A hydroacylation mechanism consistent with these observations was proposed (Scheme 1.24).

Irreversible oxidative addition of aldehyde to form acyl-hydride intermediate **II** is followed by reversible hydride insertion into coordinated ethene, which forms the acyl-alkyl intermediate **III**. From intermediate **III**, reductive elimination produces hydroacylation product. To account for the observed distribution of deuterium into both ketone positions and in recovered ethene, reversible ethene coordination from intermediate **II** and reversible hydride insertion must be in operation. Because hydride insertion is reversible and scrambles the deuterium label, it means that if oxidative addition was reversible deuterium would be lost from unreacted 4-hexenal-d_1, however, this is not observed.

Scheme 1.24. Mechanism of the hydroacylation between 4-hexenal-d_1 and ethene

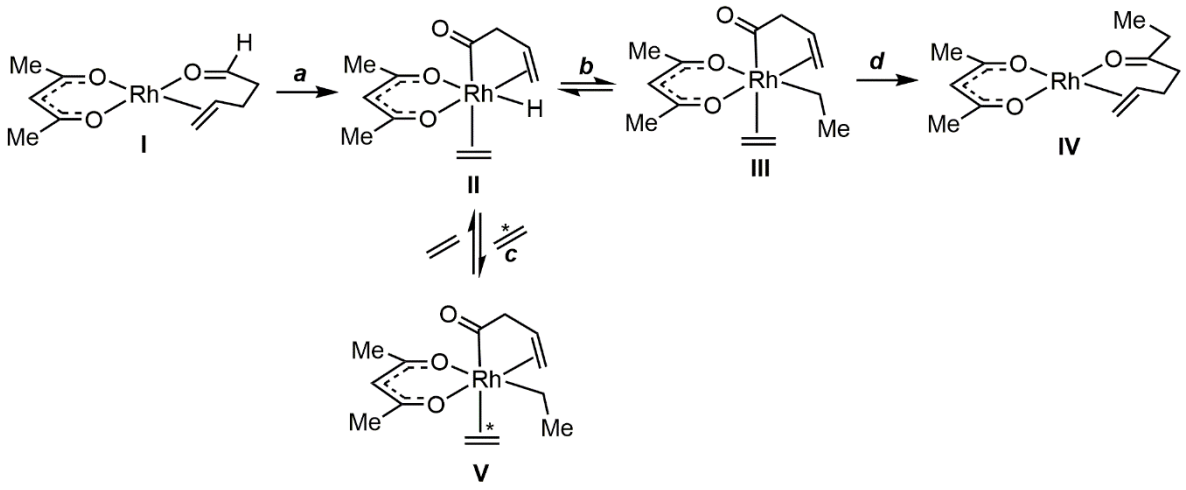

a. oxidative addition; ***b***. hydride insertion; ***c***. ligand substitution ***d***. reductive elimination

Miller and Lochow further studied the effect of ethene concentration during their kinetic studies of the intramolecular-hydroacylation of 4-petenal to form cyclopentanone (Table 1.1).[67] They found that TONs increased with increased ethene concentration, leading the authors to suggest that added ethene slows the rate of reductive decarbonylation. This postulation was supported by Bosnich and Farlie's studies into the same reaction but with the more active cationic *bis*-phosphine catalyst $[Rh(dppe)]_2[ClO_4]_2$. Their studies showed that as substrate concentration increased TON's increased, alongside a decreased rate of reductive decarbonylation. Bosnich and Farlie, agreeing with Miller and colleague's postulation for ethene concentration, suggested that the increased substrate concentration prevented reductive decarbonylation, by reducing the equilibrium concentration of unsaturated acyl-hydride intermediates able to undergo reductive decarbonylation (Scheme 1.25).

Scheme 1.25. Coordination of substrate to acyl-hydride intermediate

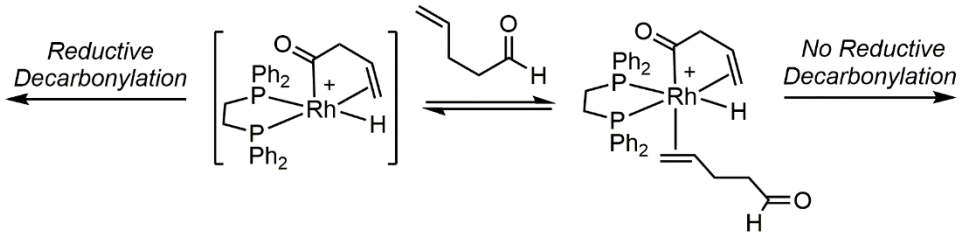

Recent density functional theory calculations for Bosnich's system have, however, given an alternative explanation: that the coordination of substrate reduces the barrier of ketone reductive elimination, relative to the energy barrier for overall reductive decarbonylation.[68]

Bosnich and Farlie could not determine the resting state in the intramolecular-hydroacylation of 4-pentenal but inferred significant mechanistic information from extensive deuterium labelling studies. These studies, at the time of publication, represented the most complete understanding of hydroacylation, and revealed that: aldehyde oxidative addition, hydride insertion and decarbonylation are fast and reversible steps. They also showed that, reductive elimination to form hydroacylation product is irreversible and rate limiting, and that reductive elimination to form reductive decarbonylation product is irreversible. They also studied the reactivity of the complexes formed by reductive elimination, $[Rh(dppe)(CO)_2][ClO_4]$ and $[Rh(dppe)(CO)(acetone)][ClO_4]$, and observed that both were inactive toward hydroacylation, with the latter complex promoting reductive decarbonylation of pentanal.

The next significant mechanistic study of intermolecular-hydroacylation was carried out by Weller and colleagues in 2008, when they characterized several catalytic intermediates in the hydroacylation of *β*-S-substituted aldehyde, 2-(methylthio)benzaldehyde catalysed by the Rh(I)-complex $[Rh(cis\text{-}\kappa^2\text{-}_{P,P}DPEPhos)(acetone)_2][CbCl_6]$ ($CbCl_6$ = *closo*-$CB_{11}H_6Cl_6$) (Scheme 1.26).[33,34]

The mechanism follows the prototypical hydroacylation steps of oxidative addition, hydride insertion and reductive elimination. The hemilabile DPEPhos ligand was proposed to stabilise low-coordinate catalytic intermediates, which was suggested to be beneficial to catalysis by slowing the rate of reductive decarbonylation, by blocking a vacant site in the acyl-hydride intermediate **1.16**. This stabilisation also facilitated the characterization of catalytic intermediates that could not be observed with simple *bis*-phosphine ligands.[69] Although alkene coordinated intermediate **I** could not be observed, the product of hydride insertion $[Rh(mer\text{-}\kappa^3\text{-}_{P,O,P}\text{-}DPEPhos)(CH_2CH_2CO_2Me)(COC_6H_4SMe)][CbBr_6]$ **1.17** was characterised by ESI-MS and $^1H/^{31}P\{^1H\}$ NMR spectroscopy by the addition of methacrylate to the isolated acyl-hydride complex **1.16**, this represented the first time an acyl-alkyl complex has been characterised in a hydroacylation. Consistent with the generally proposed mechanism for hydroacylation until this study.

Scheme 1.26. Mechanism of 2-(methylthio)benzaldehyde hydroacylation with methacrylate[a]

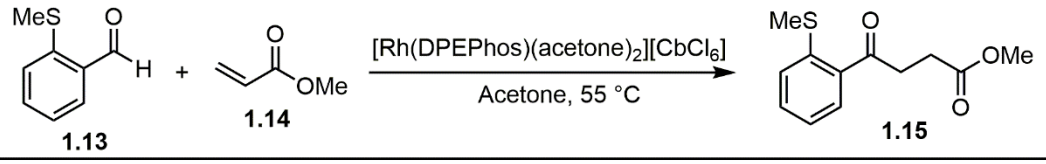

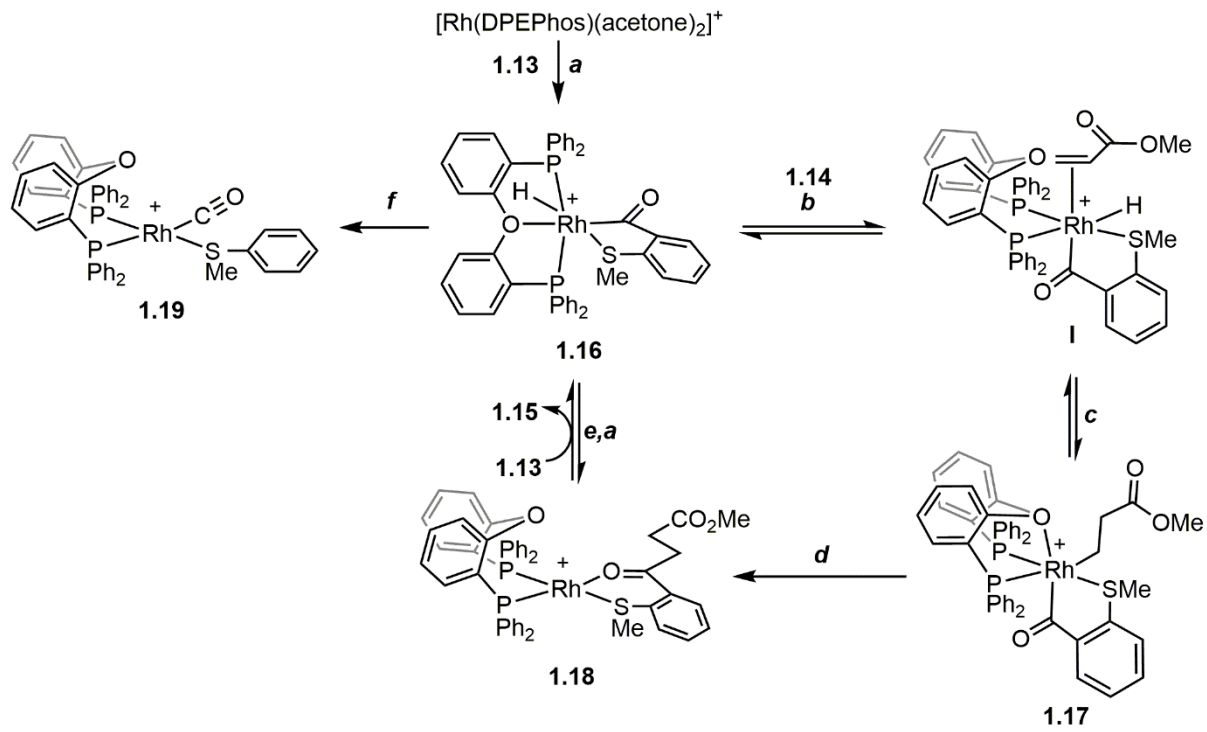

a. oxidative addition; ***b***. ligand coordination; ***c***. hydride insertion; ***d***. reductive elimination; ***e***. ligand substitution; ***f***. reductive decarbonylation

[a]$CbCl_6$ anions omitted for clarity

The acyl-hydride intermediate, [Rh(*mer*-κ^3-$_{P,O,P}$-DPEPhos)(H)(COC_6H_4SMe)][$CbBr_6$] **1.16**, as well as the analogous complexes [Rh(*mer*-κ^3-$_{P,O,P}$-DPEPhos)(H)($COCH_2CH_2SMe$)][$CbBr_6$] **1.20** and [Rh(*mer*-κ^3-$_{P,O,P}$-XantPhos)(H)($COCH_2CH_2SMe$)][$BAr^F{}_4$] **1.21**[69] were synthesised independently and characterised by single X-ray diffraction, NMR spectroscopy, elemental analysis and ESI-MS (Figure 1.5).

Figure 1.5. Isolated acyl-hydride intermediates

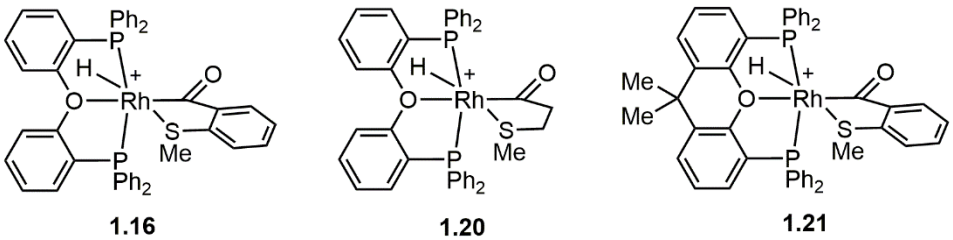

The rate of reductive elimination was monitored by ^{1}H NMR spectroscopy for each complex, in an acetone solution at room temperature for 1 week, during this time: **1.16** underwent complete reductive decarbonylation, **1.20** underwent 50% reductive decarbonylation and **1.21** underwent no reductive decarbonylation. The increased stability of the aryl-aldehyde compared to the alkane-aldehyde was rationalised by the increased rigidity of the aryl-backbone disfavouring the decarbonylation step. The stability of the XantPhos complex compared to the DPEPhos complex was attributed to the increased binding of the ether linkage in XantPhos relative to the DPEPhos, disfavouring decarbonylation by reducing the concentration of 5-coordinate intermediates formed by dissociation of the ether linkage.

Increased reactivity of DPEPhos compared to XantPhos was also observed in the hydroacylation of 3-(methylthio)propanal, with methacrylate. Weller and colleagues reported kinetic data for this reaction using a range of *bis*-phosphine ligands including DPEPhos and XantPhos in 2010.[69] The ligand not only affected the rate of hydroacylation but also affected the reaction selectivity (Table 1.2).

Table 1.2. Ligand effects in the hydroacylation of 3-(methylthio)propanal and methyl acrylate

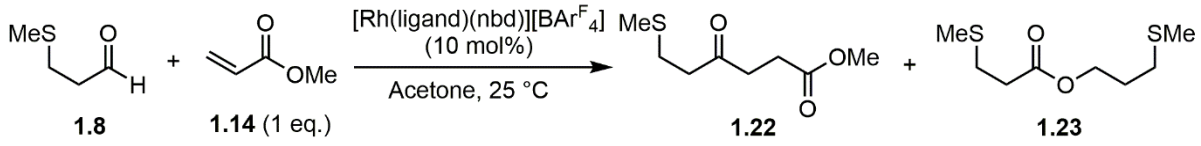

Entry	Ligand	Time (h)	Yield of **1.22** (%)	Yield of **1.23** (%)	Initial rate of **1.22** formation ($\times 10^{-3}$ Mh^{-1})	Initial rate for **1.23** formation ($\times 10^{-3}$ Mh^{-1})
1	DPEPhos	20	93	7	96 ± 6	3 ± 1
2	XantPhos	145	10	20	2 ± 2	2 ± 4
3	dppe	60	91	8	30 ± 2	1 ± 3
4	dppp	100	38	62	21 ± 1	25 ± 3
5	dppb	8	50	50	134 ± 10	136 ± 2

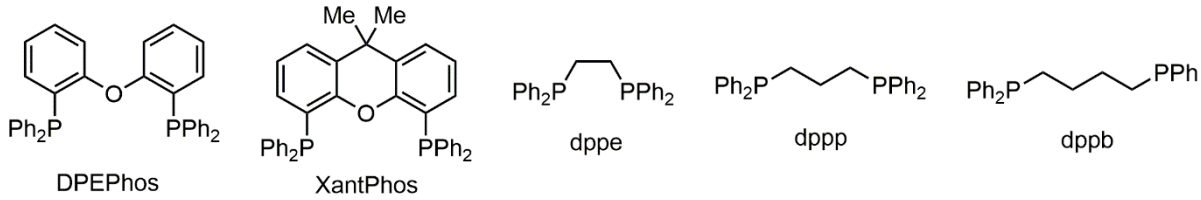

Alongside the hydroacylation product **1.22**, the Tishchenko ester product **1.23** is also observed. This product is proposed to be formed by a hydroacylation-type reaction where the acyl-hydride intermediate

reacts with another equivalent of aldehyde rather than alkene, which forms the ester product after reductive elimination. Both DPEPhos and dppe provided high selectivity for hydroacylation, whereas, Xantphos, dppp and dppb gave a mixture of products. It was postulated that increased ligand bite-angle increased the rate of Tishchenko reactivity compared to hydroacylation. A notable exception was the DPEPhos ligand, where it was postulated that the hemilabile coordination of the oxygen atom prevents aldehyde coordination, but not alkene coordination, promoting alkene-hydroacylation reactivity. A general trend for increased initial rate of hydroacylation was observed with increasing ligand bite-angle with the expectation of the XantPhos ligand. This was again rationalised by the strong binding of the ether linkage in the XantPhos acyl-hydride complex, preventing coordination of alkene or aldehyde.

Having established the mechanism of the{Rh(DPEPhos)}-catalysed hydroacylation with methyl acrylate, Weller and colleagues next studied the mechanism of alkyne hydroacylation using the same catalyst system (Scheme 1.27).

The reaction produces a 3:1 mixture of linear : branched enone products **1.25a/b**, with the formation of both following the archetypal hydroacylation steps of oxidative addition, hydride insertion and reductive elimination. Monitoring of the reaction profile revealed interesting kinetics, including an accelerated period at the early stages of catalysis. During the first few turnovers of the reaction, the linear product was formed almost exclusively, and after this time a ~2 : 1 ratio of linear : branched products was observed until complete consumption of both substrates. This observed change in selectivity and reaction rate also coincided with the compete conversion of the rhodium pre-catalyst to the resting state of the reaction after the initial accelerated period. This complex was identified as the acyl-alkenyl complex **1.27**, which was isolated from the reaction mixture and characterised by single-crystal X-ray diffraction, elemental analysis, NMR spectroscopy and ESI-MS. Once this resting state is formed, the rate of formation of the linear hydroacylation product is determined by the rate of conversion from the acyl-alkenyl complex **1.27** to linear product, *via* complexes **1.28 → 1.16 → I→ II**. Direct conversion *via* the acyl-hydride-alkyne complex **I** was ruled out by kinetic modelling of the reaction, which showed that hydride insertion to form the branched acyl-alkenyl complex **1.27** is irreversible. Overall, combined with the accelerated formation of linear product at the start of the reaction, this means the turnover-limiting step is the same for the formation of both branched and linear products.

Scheme 1.27. Mechanism of 2-(methylthio)benzaldehyde hydroacylation with alkyne 1.24

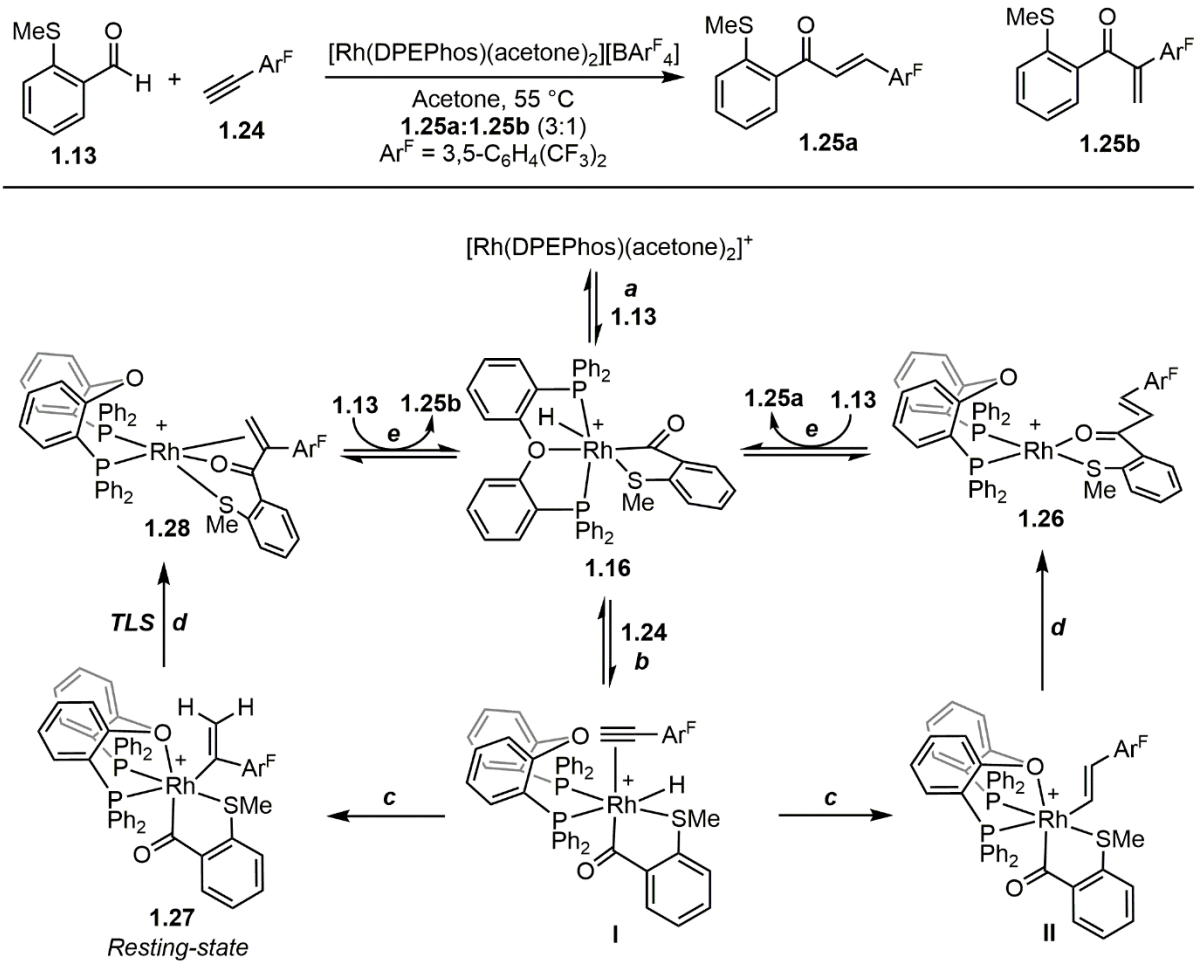

a. oxidative addition; ***b***. ligand coordination; ***c***. hydride insertion; ***d***. reductive elimination; ***e***. ligand substitution

[a] BAr^F_4 anions omitted for clarity

The turnover-limiting step (TLS) was determined by measuring the reaction kinetics and a KIE. *Pseudo*-zero kinetics were observed when the acyl-alkenyl complex **1.27** is the reaction resting state, meaning the turnover-limiting step (for both linear and branched products) is reductive elimination from **1.27**. Consistent with turnover-limiting reductive elimination, a kinetic isotope effect of 1.0 ± 0.1 was observed with formyl deuterated aldehyde, 2-(methylthio)benzaldehyde-d_1. An implication of irreversible hydride insertion from intermediate **I** to form complex **1.27** is that, when the turnover limiting steps of the reactions are the same (i.e. after complete formation of resting sate **1.27**) the relative rates of linear : branched hydride insertion determines the ratio of formed linear/branched ketone products. Before formation of the acyl-alkenyl resting state, the TLS of the reactions are different, with the TLS for linear product formation being lower in energy than branched product formation, resulting

in high selectivity for linear/branched hydroacylation product, during the initial accelerated period.

Weller and colleagues also studied the mechanism of hydroacylation with the 3rd and 4th generation small-bite-angle catalyst systems, which promoted much faster catalysis with alkenes and alkynes (see Figure 1.4). The mechanism proceeds *via* the typical steps of oxidative addition, hydride insertion and reductive elimination (Scheme 1.28).[35–37]

Scheme 1.28. Mechanism of 2-(methylthio)benzaldehyde hydroacylation with akenes using small-bite-angle catalyst systems

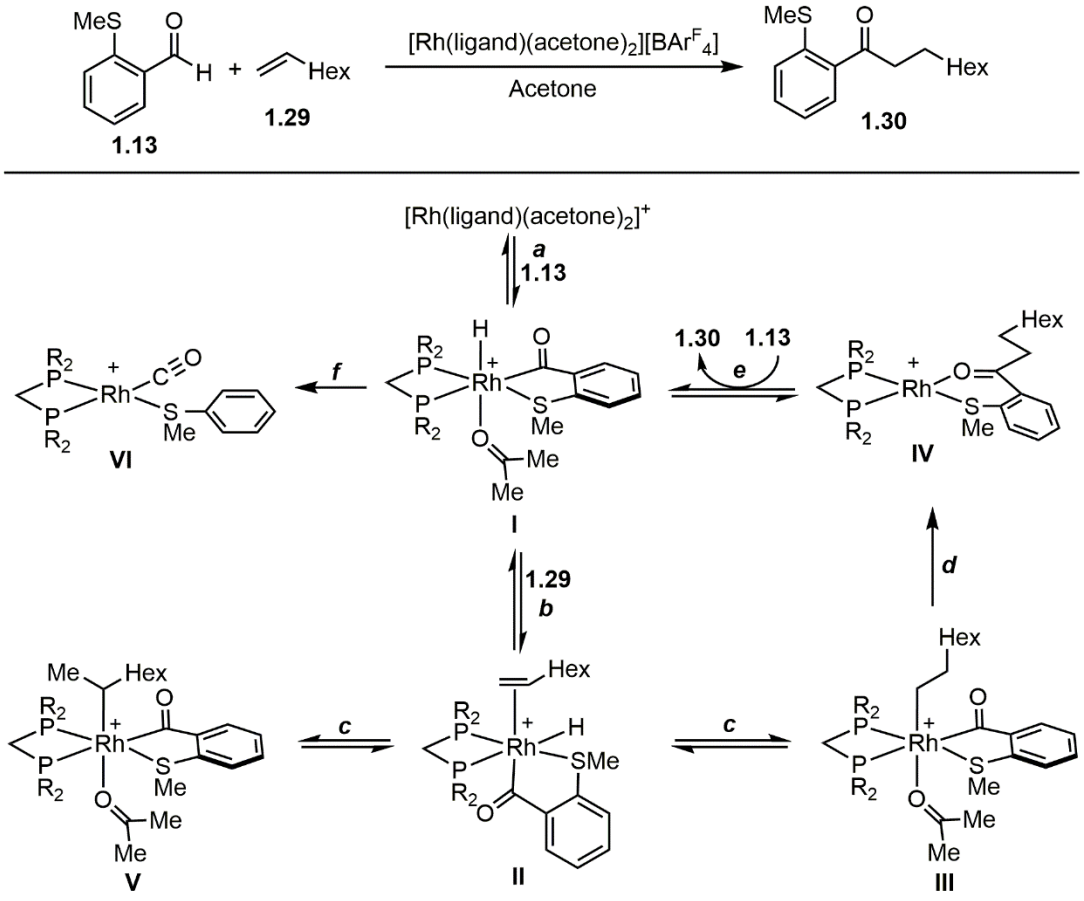

[a]BAr^F_4 anions omitted for clarity

Significant kinetic and speciation studies were performed, which indicated that reductive decarbonylation of aldehyde **1.13**, as well as hydroacylation, is significantly faster with the small bite angle ligands compared to DPEPhos. A more stable analogue of the acyl-hydride intermediate **I** (with coordinated acetonitrile instead of acetone) was characterized by single crystal x-ray diffraction, elemental analysis, NMR spectroscopy and ESI-MS.

During their studies with 1-octene, using both dtbpm and AmpaPhos as ligands, deuterium labelling studies revealed that aldehyde oxidative as well as hydride insertion (to form both linear and branched acyl-alkyl intermediates **III** and **V**) are reversible and in operation during catalysis. The measured linear : branched ratios (which were >20 : 1 for both catalysts) are therefore determined by the relative rates of irreversible reductive elimination from the respective linear/branched acyl-alkyl intermediates (**III**/**V**), with reductive elimination to form the linear product being significantly favoured. Valuable insights into the effect of reaction concentration were also observed, with increased reaction concentration leading to higher TON's, which was attributed to a reduction in the relative rate of reductive decarbonylation compared to hydroacylation. This effect can be rationalised by the rate of hydroacylation, and not reductive decarbonylation, being dependant on alkene concentration.

For both systems, as well as catalysis with 1-octyne using dtbpm as ligand, KIE's were measured using the initial rates method with the formyl deuterated aldehyde, 2-(methylthio)benzaldehyde-d_1. All three reactions had equivalent KIE's: i) 1-octene/dtbpm = 1.4 ± 0.2,[35] ii) 1-octene/AmpaPhos = 1.4 ± 0.1,[37] and iii) 1-octyne/dtbpm = 1.6 ± 0.2. [36] The authors proposed that the small but measurable KIEs were caused by an equilibrium kinetic isotope effect, with reductive elimination being the turnover limiting step.

Dong and colleagues reported mechanistic investigations into their hydroacylation reaction between salicylic aldehydes and simple alkenes using the $[Rh(cod)Cl]_2$, SIPHOS-PE, K_3PO_4 catalyst system (see Scheme 1.9). They performed extensive deuterium labelling studies with terminal alkenes, which indicated that oxidative addition and branched hydride insertion are reversible and at equilibrium during the reaction. Interestingly, linear hydride insertion was found to be reversible but not at equilibrium during the reaction, indicating that the barrier to reductive elimination from the acyl-alkyl intermediate is similar to, but lower in energy than β-hydride elimination. Detailed kinetic studies could not be performed due to the insolubility of the deprotonated salicylic aldehyde in the reaction solvent, 1,2-dichloroethane. However, qualitative kinetic measurements did indicate that the deprotonated salicylic aldehyde is the component reactive to oxidative addition, and that increased alkene concentration prevents catalyst decomposition by slowing reductive decarbonylation.

Dong and colleagues later showed how the mechanism of hydroacylation is subtly altered in the reaction of vinylphenol with non-tethered aldehydes. They performed extensive speciation studies alongside kinetic measurements, an abbreviated mechanism is shown in Scheme 1.29.

Scheme 1.29. Mechanism of vinyl phenol hydroacylation with non-tethered aldehydes

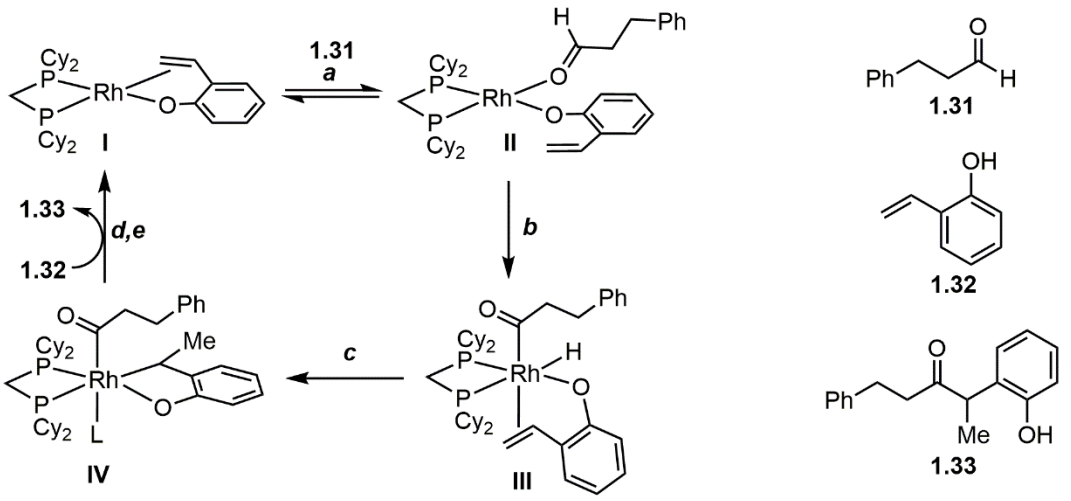

a. ligand coordination; ***b***. oxidative addition; ***c***. hydride insertion; ***d***. reductive elimination; ***e***. ligand substitution

The active catalytic resting states were observed by $^{31}P\{^{1}H\}$ NMR spectroscopy and characterized *in situ* by ^{1}H NMR spectroscopy to be complexes **I** and **II**. Complex **II** was postulated as being the only species reactive toward oxidative addition, forming intermediate **III** which undergoes hydride insertion followed by reductive elimination to yield the branched ketone product. No decarbonylation was observed throughout their studies, which was explained by the formed acyl-hydride complex **III**, being 6-coordinate and coordinatively saturated. Therefore, decarbonylation is disfavoured, relative to hydride insertion followed by reductive elimination, to the already coordinated alkene. A KIE = 2.5 ± 0.2 was measured when using formyl deuterated hydrocinnamaldehyde-d_1. This is consistent with oxidative addition of the aldehyde being the rate-limiting step, which is consistent with the observed first order kinetics is aldehyde concentration, and zero order kinetics in alkene concentration. During this study no deuterium scrambling was observed, indicating that hydride insertion is an irreversible reaction.

Of the work discussed, one of the most significant recent developments in hydroacylation has been the development of aldehyde-tethered hydroacylation with *β*-amido/ester/ketone aldehydes. Not only are the functional groups synthetically useful, their reactivity is interesting from a mechanistic

viewpoint, because the tethering groups would be expected to possess attenuated coordinating ability to rhodium, compared to the commonly employed *β*-sulphur and salicylic aldehydes. From the understanding of hydroacylation presented, attenuated coordination would be expected to promote deleterious reductive decarbonylation, by facilitating the formation of low coordinate Rh-complexes. Despite this, an extraordinary substrate scope was reported, which was facilitated by judicious choice of ligand and substrate combination. In chapters 2 and 3 of this thesis the mechanistic studies that aided the design and development of these aldehyde substrates is detailed. These studies employed a {Rh(DPEPhos)}$^{+}$ catalyst because, as shown, this ligand is catalytically active with these substrates and can facilitate the characterization of catalytic intermediates. In the third chapter, the understanding gained the mechanistic studies of *β*-amido-aldehyde hydroacylation is then applied to the development of hydroacylation reactions with non-tethered aldehydes.

1.13. References

1 A. De Meijere, S. Brase and M. Oestreich, *Metal Catalyzed Cross-Coupling Reactions and More*, Wiley-VCH, 2012.

2 Cross Coupling Reactions in Organic Synthesis, *Chem. Soc. Rev.*, 2011, **40**, 4877–5208.

3 J. Boström, D. G. Brown, R. J. Young and G. M. Keserü, *Nat. Rev. Drug Discov.*, DOI:10.1038/nrd.2018.116.

4 J. P. Kennedy, L. Williams, T. M. Bridges, R. N. Daniels, D. Weaver and C. W. Lindsley, *J. Comb. Chem.*, 2008, **10**, 345–354.

5 D. G. Brown and J. Boström, *J. Med. Chem.*, 2016, **59**, 4443–4458.

6 S. Y. Chow and A. Nelson, *J. Med. Chem.*, 2017, **60**, 3591–3593.

7 M. C. Willis, *Chem. Rev.*, 2010, **110**, 725–748.

8 A. Ghosh, K. F. Johnson, K. L. Vickerman, J. A. Walker and L. M. Stanley, *Org. Chem. Front.*, 2016, **3**, 639–644.

9 J. Tsuji and K. Ohno, *Tetrahedron Lett.*, 1965, **6**, 3969–3971.

10 A. Korotvicka, D. Necas and M. Kotora, *Curr. Org. Chem.*, 2012, **16**, 1170–1214.

11 K. Ohno and J. Tsuji, *J. Am. Chem. Soc.*, 1968, **90**, 99–107.

12 K. Sakai, J. Ide, O. Oda and N. Nakamura, *Tetrahedron Lett.*, 1972, **13**, 1287–1290.

13 C. F. Lochow and R. G. Miller, *J. Am. Chem. Soc.*, 1976, **98**, 1281–1283.

14 R. C. Larock, K. Oertle and G. F. Potter, *J. Am. Chem. Soc.*, 1980, **102**, 190–197.

15 D. P. Fairlie and B. Bosnich, *Organometallics*, 1988, **7**, 936–945.

16 K. L. Vickerman and L. M. Stanley, *Org. Lett.*, 2017, **19**, 5054–5057.

17 J. S. Arnold, E. T. Mwenda and H. M. Nguyen, *Angew. Chem. Int. Ed.*, 2014, **53**, 3688–3692.

18 K. P. Vora, C. F. Lochow and R. G. Miller, *J. Organomet. Chem.*, 1980, **192**, 257–264.

19 J. W. Suggs, *J. Am. Chem. Soc.*, 1978, **100**, 640–641.

20 C.-H. Jun, J.-S. Han, J.-B. Kang and K. Sun-Il, *Bull. Korean Chem. Soc.*, 1994, **15**, 204–209.

21 L. Hyuk and C.-H. Jun, *Bull. Korean Chem. Soc.*, 1995, **16**, 66–68.

22 K. Kokubo, K. Matsumasa, M. Miura and M. Nomura, *J. Org. Chem.*, 1997, **62**, 4564–4565.

23 P. Dierkes and P. W. N. M. van Leeuwen, *J. Chem. Soc. Dalt. Trans.*, 1999, **0**, 1519–1530.

24 K. Kokubo, K. Matsumasa, Y. Nishinaka, M. Miura and M. Nomura, *Bull. Chem. Soc. Jpn.*, 1999, **72**, 303–311.

25 M. Imai, M. Tanaka, K. Tanaka, Y. Yamamoto, N. Imai-Ogata, M. Shimowatari, S. Nagumo, N. Kawahara and H. Suemune, *J. Org. Chem.*, 2004, **69**, 1144.

26 H.-J. Zhang and C. Bolm, *Org. Lett.*, 2011, **13**, 3900–3903.

27 M. M. Coulter, K. G. M. Kou, B. Galligan and V. M. Dong, *J. Am. Chem. Soc.*, 2010, **132**, 16330–3.

28 K. Tanaka, M. Tanaka and H. Suemune, *Tetrahedron Lett.*, 2005, **46**, 6053–6056.

29 R. T. Stemmler and C. Bolm, *Adv. Synth. Catal.*, 2007, **349**, 1185–1198.

30 M. Imai, M. Tanaka, S. Nagumo, N. Kawahara and H. Suemune, *J. Org. Chem.*, 2007, **72**, 2543–2546.

31 M. C. Willis, S. J. McNally and P. J. Beswick, *Angew. Chem. Int. Ed.*, 2004, **43**, 340–343.

32 M. C. Willis and R. L. Woodward, *J. Am. Chem. Soc.*, 2005, **127**, 18012–18013.

33 G. L. Moxham, H. E. Randell-Sly, S. K. Brayshaw, R. L. Woodward, A. S. Weller and M. C. Willis, *Angew. Chem. Int. Ed.*, 2006, **45**, 7618–7622.

34 G. L. Moxham, H. Randell-Sly, S. K. Brayshaw, A. S. Weller and M. C. Willis, *Chem. Eur. J.*, 2008, **14**, 8383–8397.

35 A. B. Chaplin, J. F. Hooper, A. S. Weller and M. C. Willis, *J. Am. Chem. Soc.*, 2012, **134**, 4885–4897.

36 I. Pernik, J. F. Hooper, A. B. Chaplin, A. S. Weller and M. C. Willis, *ACS Catal.*, 2012, **2**, 2779–2786.

37 A. Prades, M. Fernández, S. D. Pike, M. C. Willis and A. S. Weller, *Angew. Chem. Int. Ed.*, 2015, **54**, 8520–8524.

38 P. Lenden, D. A. Entwistle and M. C. Willis, *Angew. Chem. Int. Ed.*, 2011, **50**, 10657–10660.

39 M. K. Majhail, P. M. Ylioja and M. C. Willis, *Chem. Eur. J.*, 2016, **22**, 7879–7884.

40 J. D. Neuhaus, S. M. Morrow, M. Brunavs and M. C. Willis, *Org. Lett.*, 2016, **18**, 1562–1565.

41 R. N. Straker, M. K. Majhail and M. C. Willis, *Chem. Sci.*, 2017, **8**, 7963–7968.

42 S. R. Parsons, J. F. Hooper and M. C. Willis, *Org. Lett.*, 2011, **13**, 998–1000.

43 M. Arambasic, J. F. Hooper and M. C. Willis, *Org. Lett.*, 2013, **15**, 5162–5165.

44 J. F. Hooper, R. D. Young, A. S. Weller and M. C. Willis, *Chem. Eur. J.*, 2013, **19**, 3125–3130.

45 J. F. Hooper, R. D. Young, I. Pernik, A. S. Weller and M. C. Willis, *Chem. Sci.*, 2013, **4**, 1568–

1572.

46 A. Bouisseau, M. Gao and M. C. Willis, *Chem. Eur. J.*, 2016, **22**, 15624–15628.

47 J. F. Hooper, S. Seo, F. R. Truscott, J. D. Neuhaus and M. C. Willis, *J. Am. Chem. Soc.*, 2016, **138**, 1630–1634.

48 M. Gao and M. C. Willis, *Org. Lett.*, 2017, **19**, 2734–2737.

49 M. Castaing, S. L. Wason, B. Estepa, J. F. Hooper and M. C. Willis, *Angew. Chem. Int. Ed.*, 2013, **52**, 13280–13283.

50 T. J. Coxon, M. Fernández, J. Barwick-Silk, A. I. McKay, L. E. Britton, A. S. Weller and M. C. Willis, *J. Am. Chem. Soc.*, 2017, **139**, 10142–10149.

51 K. Tanaka, Y. Shibata, T. Suda, Y. Hagiwara and M. Hirano, *Org. Lett.*, 2007, **9**, 1215–1218.

52 Y. Shibata and K. Tanaka, *J. Am. Chem. Soc.*, 2009, **131**, 12552–3.

53 S. K. Murphy, A. Bruch and V. M. Dong, *Angew. Chem. Int. Ed.*, 2014, **53**, 2455–9.

54 S. K. Murphy, A. Bruch and V. M. Dong, *Chem. Sci.*, 2015, **6**, 174–180.

55 R. Guo and G. Zhang, *J. Am. Chem. Soc.*, 2017, **139**, 12891–12894.

56 T. B. Marder, D. C. Roe and D. Milstein, *Organometallics*, 1988, **7**, 1451–1453.

57 A. H. Roy, C. P. Lenges and M. Brookhart, *J. Am. Chem. Soc.*, 2007, **129**, 2082–2093.

58 C.-H. Jun, L. Hyuk and J.-B. Hong, *J. Org. Chem.*, 1997, **62**, 1200–1201.

59 C.-H. Jun, D.-Y. Lee, H. Lee and J.-B. Hong, *Angew. Chem. Int. Ed.*, 2000, **39**, 3070–3072.

60 C.-H. Jun, E.-A. Jo and J.-W. Park, *Eur. J. Org. Chem.*, 2007, 1869–1881.

61 J. W. Suggs, *J. Am. Chem. Soc.*, 1979, **101**, 489–489.

62 N. R. Vautravers, D. D. Regent and B. Breit, *Chem. Commun.*, 2011, **47**, 6635.

63 J. F. Hartwig, *Inorg. Chem.*, 2007, **46**, 1936–47.

64 D. Milstein, *J. Am. Chem. Soc.*, 1982, **104**, 5227–5228.

65 D. Milstein, *J. Chem. Soc. Chem. Commun.*, 1982, **0**, 1357.

66 D. Milstein, *Organometallics*, 1982, **1**, 1549–1551.

67 K. P. Vora, C. F. Lochow and R. G. Miller, *J. Organomet. Chem.*, 1980, **192**, 257–264.

68 I. F. D. Hyatt, H. K. Anderson, A. T. Morehead and A. L. Sargent, *Organometallics*, 2008, **27**, 135–147.

69 R. J. Pawley, G. L. Moxham, R. Dallanegra, A. B. Chaplin, S. K. Brayshaw, A. S. Weller and M. C. Willis, *Organometallics*, 2010, **29**, 1717–1728.

Chapter 2: Mechanistic Studies of *β*-Amido Aldehyde Hydroacylation

2.1. Introduction

To develop hydroacylation reactions that could be applied beyond small scale organic synthesis in areas such as polymer, biological and process chemistries, systems that combine both catalyst stability and activity are highly desirable. We envisaged that this could be achieved by combining the stable Rh{DPEPhos}$^{+}$ catalyst system with a highly active aldehyde substrate. Our aldehyde substrate design incorporates a weakly chelating *β*-amido group to: i) assist in aldehyde oxidative addition, by promoting initial aldehyde coordination ii) promote reductive elimination, by facilitating the formation of a 5-coordinate intermediate and iii) prevent product inhibition, by forming a product that is a relatively labile ligand. The aldehyde design also includes an *α*-tertiary centre, to disfavour reductive decarbonylation by decreasing the enthalpy of the so formed tertiary M−C bond after the initial decarbonylation step (Figure 2.1).[1]

Figure 2.1. Aldehyde design

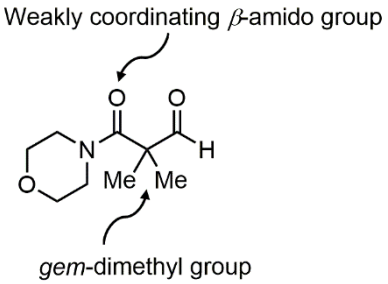

These *β*-aldehyde substrates and the related *β*-ester and *β*-keto-aldehydes proved to be effective hydroacylation substrates and their synthetic utility has recently been reported.[2] This chapter focuses on the kinetic studies of this new system, which reveal that reductive decarbonylation is not operative during catalysis, no product inhibition is observed, and that the turnover limiting step of the reaction is hydride insertion.

2.2. Synthesis of Acyl-hydride Intermediates

The Rh(I)-complex [Rh(*cis*-κ^2-$_{P,P}$-DPEPhos)(acetone)$_2$][BAr$^F_4$] **2.1** was generated *in situ* by

hydrogenation of [Rh(*cis*-κ^2-$_{P,P}$-DPEPhos)(nbd)][BAr^F_4] (nbd = norbornadiene).[3,4] To this complex, the addition of one equivalent of aldehyde **2.2a** in acetone-d_6 resulted in the formation of the acyl-hydride complex [Rh(*mer*-κ^3-$_{P,O,P}$-DPEPhos)(H)(COC{$(CH_3)_2$}CO{NC_4H_8O})][BAr^F_4] **2.3a** in quantitative yield, on time of mixing as observed by NMR spectroscopy (Scheme 2.1).

Scheme 2.1. DPEPhos acyl-hydride complex synthesis[a]

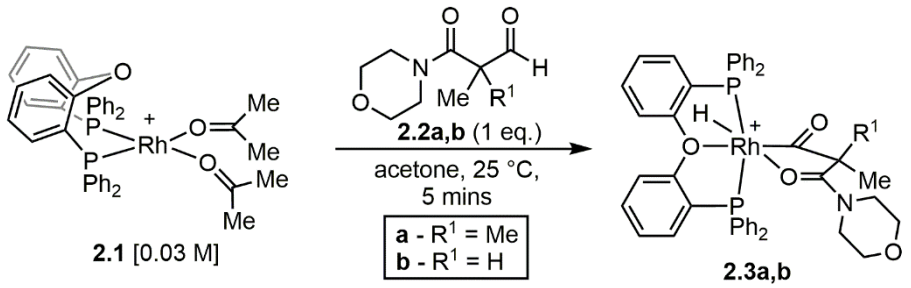

[a]BAr^F_4 anions omitted for clarity

An immediate colour change from red to light yellow occurred, signalling the formation of a Rh(III) complex, which was characterized by NMR spectroscopy and electrospray ionisation mass spectrometry (ESI-MS). In the $^{31}P\{^1H\}$ NMR spectrum of complex **2.3a**, a single environment at δ 25.2 [J_{RhP} = 127 Hz] is observed, indicating that identical phosphorus environments are bound to a Rh(III) center.[5] In the hydride region of the ^1H NMR spectrum, a doublet of triplets is observed at δ –14.6 [J_{RhH} = 27.5; J_{PH} = 9.5 Hz]. A single methyl environment, relative integral 6, is observed for the tertiary centre on the aldehyde. In the $^{13}C\{^1H\}$ NMR spectrum, the acyl-carbon is observed as a doublet of triplets at δ 224.0 [J_{RhC} = 37.0; J_{PC} = 6.0 Hz]. These data are consistent with an acyl-hydride located *cis* to both phosphines and a *mer*-κ^3 arrangement of the DPEPhos ligand.

The same reaction was performed using the secondary aldehyde, 2-methyl-3-morpholino-3-oxopropanal **2.2b**, which resulted in the formation of the analogous complex [Rh(*mer*-κ^3-$_{P,O,P}$-DPEPhos)(H)(COC{(CH_3)(H)}CO{NC_4H_8O})][BAr^F_4] **2.3b**. The resulting NMR spectra reflect that there is no longer a mirror plane in the Rh-cation, with the $^{31}P\{^1H\}$ NMR spectrum showing a tightly coupled ABX doublet of doublets with a large trans ^{31}P–^{31}P coupling:[5] δ 31.3 [J_{PP} = 319; J_{RhP} = 129 Hz] and δ 22.9 [J_{PP} = 319; J_{RhP} = 129 Hz]. In the hydride region of the ^1H NMR spectrum, an apparent doublet of triplets at δ –14.9 [J_{RhH} = 29.0; J_{PH} = 9.0 Hz] is observed. Similarly, an apparent doublet of

triplets is observed in the $^{13}C\{^{1}H\}$ NMR at δ 220.3 [J_{RhC} = 37.0; J_{PC} = 5.5 Hz] for the acyl-carbon. The signals appear as apparent doublet of triplets due to the similarity of the coupling with the inequivalent ^{31}P nuclei.

The synthesis of an analogous XantPhos complex [Rh(*mer*-κ^3-$_{P,O,P}$-XantPhos)(H)(COC{(C_4H_8)}CO{NC_4H_8O})][BAr^F_4] **2.5** was achieved by addition of the cyclopentyl *β*-amido-aldehyde **2.2c** to the known Rh(I) complex [Rh(*mer*-κ^3-$_{P,O,P}$-XantPhos)(η^2-PhCCPh)] **2.4** in acetone. A colour change from dark red to light yellow occurred upon time of mixing, and full conversion to acyl-hydride **2.5** was confirmed by $^{31}P\{^{1}H\}$ NMR spectroscopy (Scheme 2.2).

Scheme 2.2. XantPhos acyl-hydride complex synthesis[a]

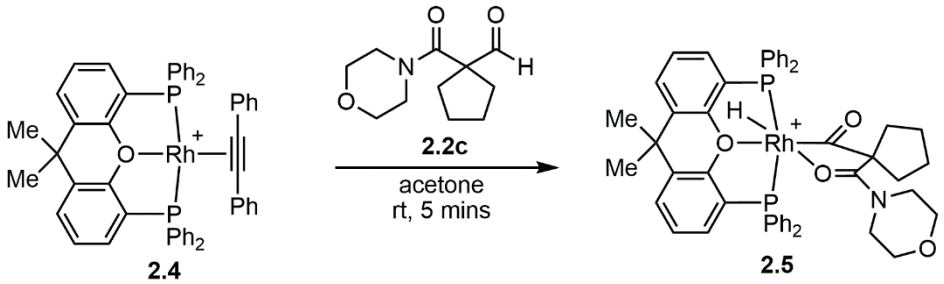

[a] BAr^F_4 anions omitted for clarity

Upon isolation by crystallisation from 1,2-diflurobenzne/pentane **2.5** was fully characterised by single crystal X-ray diffraction, NMR spectroscopy and ESI-MS (Scheme 2.2). The key NMR data is similar to the DPEPhos-acyl-hydride complex; in the ^{1}H spectrum the hydride appears at δ –14.7 as a doublet of triplets [J_{RhH} = 27.2; J_{PH} = 9.3 Hz] and the *gem*-dimethyl groups on the XantPhos backbone appear as two distinct singlets at δ 1.84 and δ 1.81. The $^{31}P\{^{1}H\}$ NMR spectrum displays a doublet at δ 29 [J_{RhP} = 128 Hz] and the acyl group in the $^{13}C\{^{1}H\}$ NMR spectrum is observed as a doublet of triplets at δ 224.0 [J_{RhC} = 36.7 Hz; J_{PC} = 5.9 Hz]. The solid-state structure of **2.5** confirms that the C–H activation of the aldehyde has occurred to give an acyl-hydride with a supporting *β*-amide Rh···O interaction (Figure 2.2).

The structure is in agreement with the assignment made from the ^{1}H NMR data for acyl-hydrides **2.3a,b** and **2.5**. The XantPhos ligand adopts a *mer*-κ^3-$_{P,O,P}$-XantPhos geometry with the acyl group siting trans to the XantPhos ligand's oxygen atom [Rh1–C40, 1.9408(16); Rh1–O1, 2.2895(10)Å]; the

Figure 2.2. Crystal structure of complex 2.5[a]

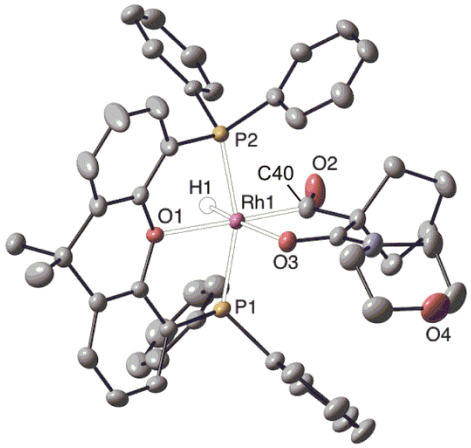

[a]Displacement ellipsoids are shown at the 50% probability level. Selected bond distances (Å) and angles (deg): Rh1−H1, 1.45(2); Rh1−O1, 2.2895(10); Rh1−O3, 2.1584(10); Rh1−C40, 1.9408(16); Rh1−P1, 2.2803(4); Rh1−P2, 2.2702(4); P1−Rh1−P2, 160.651(14); $[BAr^F{}_4]^-$ anions are not shown.

hydride ligand was located and freely refined. The ligand arrangement is as expected based on the *trans*-influence of the ligands. The acyl and hydride groups, which are strong *trans*-influence ligands, are *trans* to the DPEPhos-ether and the *β*-amido groups, both weak *trans*-influence ligands. The analogous Rh(III) acyl hydride complexes [Rh(*mer*-κ^3-$_{P,O,P}$-XantPhos)(H)($COCH_2CH_2SMe$)][$BAr^F{}_4$],[6] [Rh(*mer*-κ^3-$_{P,O,P}$-DPEPhos)(H)($COCH_2CH_2SMe$)][$BAr^F{}_4$][3,4] have been synthesised from the *β*-*S*-aldehyde 3-(methylthio)propanal and possess analogous structures to the reported *β*-amido-acyl-hydrides (**2.3a,b** and **2.5**).

2.3. Decarbonylation of Acyl-Hydride Complexes

Both complexes **2.3a** and **2.3b** are stable for at least 24 hours in acetone-d_6 (0.2 M) at 25 ºC as measured by $^{31}P\{^1H\}$ NMR spectroscopy. However, when heated to 55 °C only complex **2.3b** gradually evolved to give the product of reductive decarbonylation [Rh(*mer*-κ^3-$_{P,O,P}$-DPEPhos)(CO)][$BAr^F{}_4$], **2.6**, alongside free 1-morpholinopropan-1-one **2.7** (Scheme 2.3).

This result demonstrates the secondary aldehyde undergoes reductive decarbonylation at a significantly faster rate compared to the analogous tertiary aldehyde. In the ^{31}P NMR spectrum of the reaction with secondary acyl-hydride **2.3b** a new broad doublet at δ 35 [J_{RhP} = 124 Hz] appeared and increased in intensity with the concurrent disappearance of the starting material signals (Figure 2.3).

Scheme 2.3. Reactivity of acyl-hydrides 2.3a and 2.3b to decarbonylation[a]

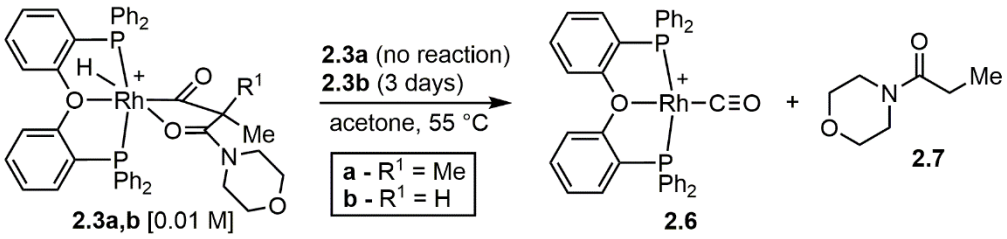

[a]BAr^F_4 anions omitted for clarity

Figure 2.3. $^{31}P\{^1H\}$ NMR spectra of decarbonylation reaction A) Complex 2.3b; B) After 1 day; C) After 3 Days

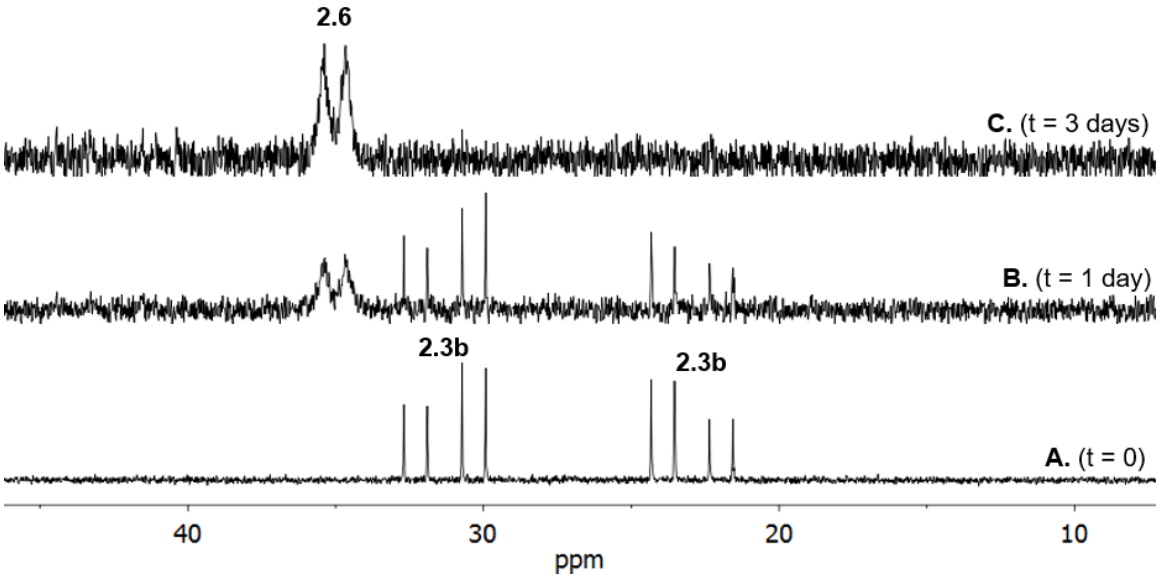

The new broad resonance at δ 35 was ascribed to the Rh(I) complex [Rh(*mer*-κ^3-$_{P,O,P}$-DPEPhos)(CO)][BAr^F_4] **2.6** (*vide infra* for full characterisation). When the reaction was followed by ^{1}H NMR spectroscopy, disappearance of the starting material hydride resonance at δ –14.9 was observed, alongside the appearance of resonances corresponding to reductive decarbonylation product 1-morpholinopropan-1-one **2.7**.

To interrogate why a broad ^{31}P resonance is observed for carbonyl complex **2.6**, NMR spectroscopy at 220K was performed. The ^{31}P NMR resonance became a well-defined doublet at δ 35.0 [J_{RhP} = 124 Hz] (Figure 2.4).

Interestingly, a similarly sharp resonance was observed after removal of the organic amide **2.7** by precipitation of the complex with pentane. These observations suggest that the broad signal

Figure 2.4. $^{31}P\{^{1}H\}$ NMR spectra carbonyl complex 2.6 in the presence of amide 2.7 at A) 298 K; B) 220K[a]

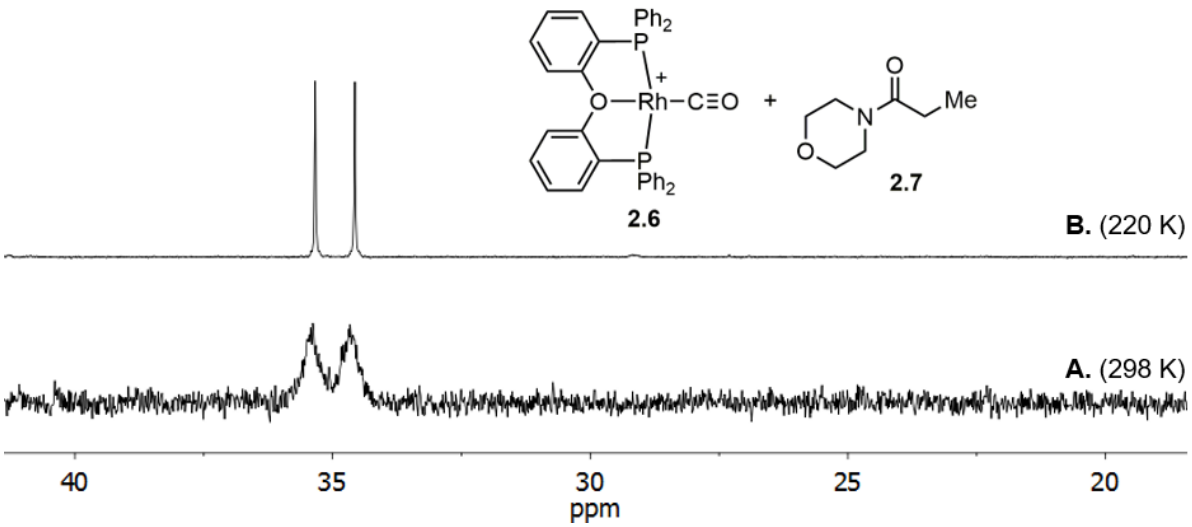

[a]BAr^{F}_{4} anion omitted for clarity

Scheme 2.4 Equilibrium of amide coordination

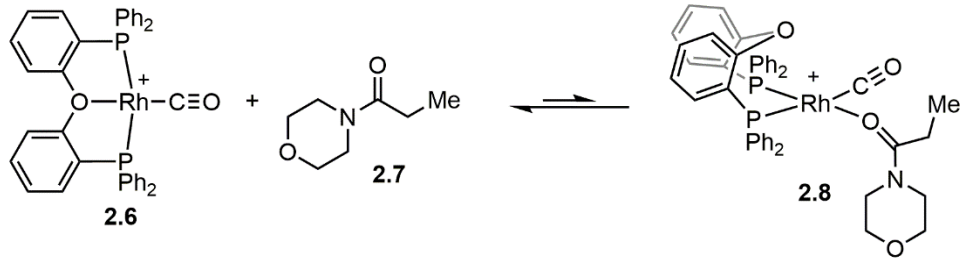

[a]BAr^{F}_{4} anions omitted for clarity

in the presence of amide **2.7** is caused by a small equilibrium to the amide co-ordinated complex **2.8** (Scheme 2.4).

The ^{31}P environments in complex **2.8** are inequivalent and would appear in the $^{31}P\{^{1}H\}$ NMR as 2 sets of doublet of doublets, however, because the equilibrium lies so far to carbonyl complex **2.6** only a broad signal that closely corresponds to complex **2.6** is observed. The related carbonyl complex [Rh(*cis*-κ^{2}-$_{P,P}$-DPEPhos)(CO)(EtSMe)][*closo*-$CB_{11}H_{6}Cl_{6}$] was previously synthesized by reductive decarbonylation from the acyl-hydride [Rh(*mer*-κ^{3}-$_{P,O,P}$-DPEPhos)(H)($COCH_{2}CH_{2}SMe$)][BAr^{F}_{4}].[3,4] NMR studies at 220K and analysis by single crystal X-ray diffraction indicated that the thioether was co-ordinated to rhodium in solution as well as in the solid state, these results exemplify the attenuated coordination of the amide group compared to the thioether group to rhodium.

Having isolated the carbonyl complex **2.6** by precipitation it was also characterized by ESI-MS and IR spectroscopy with a carbonyl stretching frequency observed in the IR at 2017 cm^{-1} (thin film, CD_2Cl_2). The analogous [Rh(*mer*-κ^3-$_{P,O,P}$-XantPhos)(CO)][BF_4] has been previously characterized by single crystal X-ray diffraction and ^{31}P NMR spectroscopy and IR spectroscopy, displaying a doublet at δ 37 [J_{RhP} = 122 Hz][7] and an IR stretching frequency of 2014 cm^{-1} (thin film, CH_2Cl_2).[8] Both pieces of data compare well to the synthesised DPEPhos analogue **2.6**.

2.4. Monitoring of Catalysis

Having developed an acyl-hydride complex that does not undergo reductive decarbonylation, this provided the rare opportunity to study the mechanism of hydroacylation in the absence of this deleterious process. Using similar conditions that were used for the organic reaction scope, the reaction of aldehyde **2.2a** (0.75 M) and 1-octyne **2.9** (0.98 M) with [Rh(*cis*-κ^2-$_{P,P}$-DPEPhos)(acetone)$_2$][$BAr^F{}_4$] **2.1** (5 mol%) in acetone-d_6 at 25 ºC was monitored by ^1H NMR spectroscopy using the [$BAr^F{}_4$] anion as an internal reference (Figure 2.5).

After 1 h, a >98% ^1H NMR yield of enones **2.10a**/**2.10b** (15 : 1, linear : branched) and a 4% NMR yield of cyclotrimerisation products **2.11a**/**2.11b** (2 : 1, 1,2,4-tri-*n*-hexyl benzene : 1,3,5-tri-*n*-hexyl benzene) was observed. 1-Octyne was consumed by a first order process over three half-lives [k_{obs} = 5.57 (± 0.04) × 10^{-4} s^{-1}]. The resting state of the system was monitored by both ^{31}P NMR and ^1H NMR spectroscopy (by measuring the hydride signal at δ –14.6, [Figure 1, purple diamonds]), this revealed that the concentration of the acyl-hydride complex **2.3a** remained constant during the first 37 minutes of the reaction and was the only observed rhodium species. At this the point (*ca*. 37 mins) the aldehyde **2.2a** (Figure 1, red triangles) was fully consumed and the yield of enones **2.10a**/**2.10b** was ~94%. After 37 minutes, acyl-hydride is consumed and the resting state changes to one characterized by multiple signals between δ 24–23 in the $^{31}P\{^1H\}$ NMR spectrum, with no hydride signal observed in the ^1H NMR spectrum (the nature of these complexes will be discussed in Chapter 3). During this time the formation of enones **2.10a**/**2.10b** continues, but with an increased rate of 1-octyne consumption due to cyclotrimerisation to form tri-*n*-hexylbenzene products **2.11** (Figure 1, filled

Figure 2.5. Catalytic Reaction Profile[a]

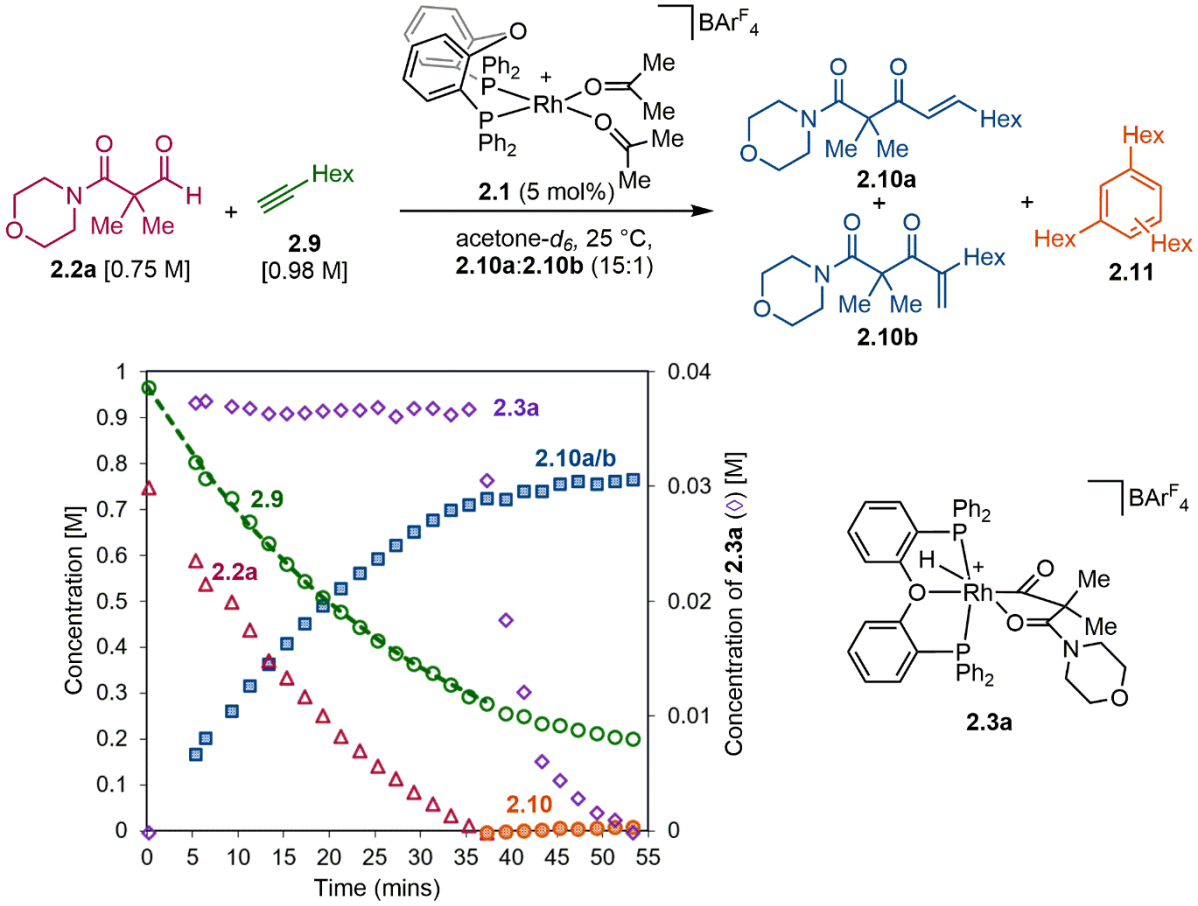

[a]Reaction profile (first 55 min) as measured by ^{1}H NMR spectroscopy. Left axis: red △ = aldehyde **2.2a**, green ○ = 1-octyne **2.9**, blue ■ = enones **2.10a** and **2.10b**, and orange ● = tri-*n*-hexylbenzenes **2.11**. Dotted green line = first-order model for the consumption of 1-octyne **2.9**. Right axis: purple ◇ = acyl-hydride, **2.3a**.

orange circles). This is a relatively slow process and only a 10% ^{1}H NMR yield of tri-*n*-hexylbenzenes **2.11** is observed after 2 hours with some 1-octyne **2.9** remaining.

To probe whether cyclotrimerisation only occurs when no free aldehyde remains in solution a reaction starting with an excess of aldehyde **2.2a** (0.9 M) compared to 1-octyne **2.9** (0.75M) under otherwise identical conditions was performed. The resting state remained as the acyl-hydride **2.3a** throughout the reaction, complete consumption of 1-octyne **2.9** was observed and no tri-*n*-hexylbenzene products **2.11a**/**2.11b** were detected.

2.5. Initial Rates

To determine the kinetic order of the reagents in the hydroacylation reaction an analysis by the initial rates method was performed. The rate of the formation of enones **2.10a/2.10b** up to 15% yield

was measured by ^{1}H NMR spectroscopy. Under the initial rate conditions of aldehyde **2.2a** [0.2 M], 1-octyne [0.18 M] and *bis*-acetone catalyst **2.1** [0.01 M] in acetone-d_6 at 25 ºC, the reaction was shown to give a >98% yield of enones **2.10a/2.10b** with a 15 : 1 (linear : branched) ratio after 5 hours, with an initial rate = 3.25 (±0.03) x 10^{-5} Ms^{-1} (Table 2.1, Entry 3). The full results for the variation of the initial concentrations of aldehyde **2.3a**, alkyne **2.9**, rhodium catalyst **2.1** and product **2.10b** are shown in Table 2.1 along with the initial rate/concentration plots in Figure 2.6.

Table 2.1. Initial rates of reaction varying the initial concentration of aldehyde, alkyne, rhodium catalyst and product

Entry	[Aldehyde] M	[Alkyne] M	[Rh. Cat.] M	[Product] M	Rate (10^{-5} Ms^{-1})
1	0.20	0.045	0.01	-	0.89 ± 0.02
2	0.20	0.090	0.01	-	1.67 ± 0.01
3	0.20	0.18	0.01	-	3.25 ± 0.03
4	0.10	0.18	0.01	-	3.04 ± 0.05
5	0.40	0.18	0.01	-	3.26 ± 0.05
6	0.20	0.18	0.005	-	1.44 ± 0.06
7	0.20	0.18	0.01	-	5.95 ± 0.06
8	0.20	0.18	0.01	0.10	3.28 ± 0.09
9	0.20	0.18	0.01	0.40	3.4 ± 0.1

By varying the concentration of the reaction components, the analysis found the reaction to be 1st order in 1-octyne **2.9** concentration (Figure 2.6, A), 0th order in aldehyde **2.2a** concentration (Figure 2.6, B) and 1st order in *bis*-acetone catalyst **2.1** concentration (Figure 2.6, C). These results indicate that 1-octyne is involved in a step before the turnover limiting step and after the observed resting state, and that aldehyde **2.2a** is either involved in a step after the turnover limiting step or is incorporated into the observed resting sate.

The order of 1 in catalyst concentration rules out a dimer-monomer catalyst equilibrium being in operation.[9,10] Product inhibition was also probed by initial rates (Figure 2.6, D), with no inhibition observed even with 40 equivalents of enones **2.11a**/**2.11b** compared to *bis*-acetone catalyst **2.1**. In the Rh-catalysed hydroacylation of *β-S*-aldehydes with small-bite angle catalysts, such as [Rh{^{t}Bu$_2$PCH$_2$P(*o*-C$_6$H$_4$OMe)$_2$}(C$_6$H$_5$F)][BAr$^{F}_4$], the resting state of the reaction becomes a product

Figure 2.6. Initial rate plots for hydroacylation[a]

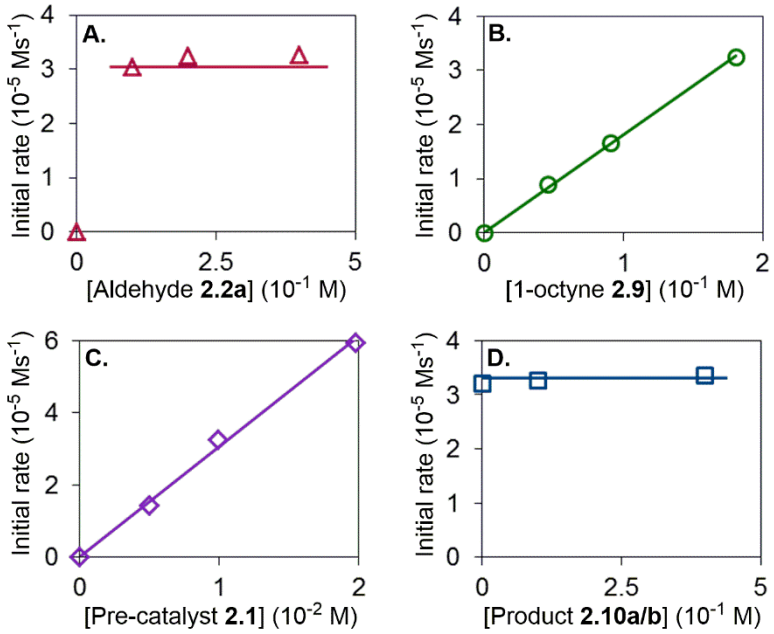

A: Aldehyde **2.2a**, ([1–octyne] = 0.18 M, [**2.1**] = 0.01 M); **B**: 1–octyne **2.9**), ([aldehyde] = 0.20 M, [**2.1**] = 0.01 M); **C**: Catalyst **2.1**, ([1–octyne] = 0.18 M, [aldehyde] = 0.20 M); **D**: Product **2.10a/2.10b** varied: ([1–octyne] = 0.18 M, [aldehyde] = 0.20 M, [**2.1**] = 0.01 M).

bound-complex, which means the kinetics, if studied, will likely exhibit product inhibition.[11,12] That product bound complexes are not observed during *β*-amido aldehyde hydroacylation further exemplifies the attenuated donating ability of the *β*-amido group compared to *β*-S-group.

These results are consistent with the observed monomeric acyl-hydride **2.3a** resting state, where its concentration is unchanged until free aldehyde is consumed. It is also consistent with the *pseudo* 1st order model described for 1-octyne consumption during catalysis (Figure 2.2). These observations support that oxidative addition of the aldehyde is fast and strongly favours the Rh(III) acyl-hydride resting state **2.3a**. From this resting state, alkyne coordination will be followed by hydride insertion and reductive elimination, with the turnover limiting step being contained within this sequence.

2.6. Reversibility of Oxidative Addition

To probe whether aldehyde oxidative addition to form acyl-hydride is an irreversible reaction step, 1 equivalent of the cyclopentyl-*β*-amido aldehyde **2.2c** was added to acyl-hydride **2.3a**. This afforded an equilibrium mixture of acyl-hydrides **2.3a** and **2.3c** (K_{eq} = 0.75) within 5 minutes (Scheme 2.5).

Scheme 2.5. Addition of aldehyde 2.2c to acyl-hydride 2.3a[a]

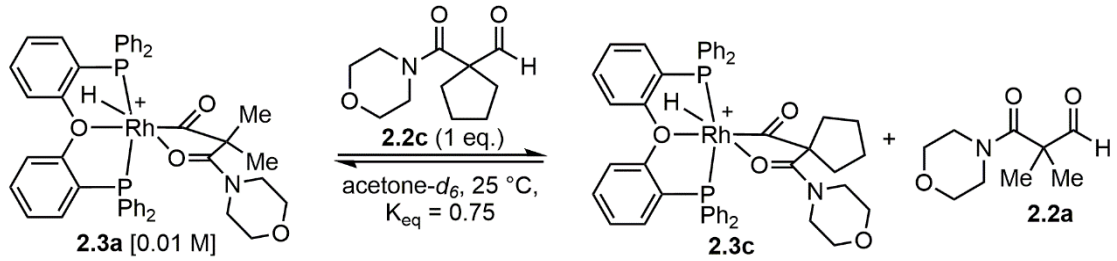

[a]BAr^F_4 anions omitted for clarity

In the ^{1}H NMR spectrum, the aldehyde resonance corresponding to dimethyl aldehyde **2.2a** is observed alongside a new hydride signal at δ −14.5. In the ^{31}P NMR spectrum a new doublet at δ 26.6 [J_{RhP} = 129 Hz] is observed, which corresponds to the Rh(III) complex [Rh(*mer*-κ^3-$_{P,O,P}$-DPEPhos)(H)(COC{C_4H_8}CO{NC_4H_8O})] **2.3c**. This result indicates that oxidative addition of aldehyde is fast and reversible on the reaction timescale. However, the equilibrium must be significantly shifted towards acyl-hydride, to the point where no *bis*-acetone complex **2.1** is observed by NMR spectroscopy.

The acyl-hydride complex **2.3c** was synthesized and characterized independently and displayed similar data to aldehyde **2.2a**: a single environment at δ 26.6 [J_{RhP} = 127 Hz] is observed in ^{31}P{^{1}H} spectrum and in the hydride region of the ^{1}H NMR spectrum a doublet of triplets is observed at δ −14.5 [J_{RhH} = 27.5; J_{PH} = 9.5 Hz]. In the ^{13}C{^{1}H} NMR spectrum the acyl-carbon is observed as a doublet of triplets at δ 225.1 [J_{RhC} = 36.0; J_{PC} = 5.5 Hz].

2.7. Using Acetonitrile as a Probe Ligand

Further evidence of reversible oxidative addition of aldehyde was observed in the reaction of acyl-hydride with acetonitrile, which was used to probe the binding of monodentate ligands to acyl-hydride **2.3a**. Addition of 20 equivalents of acetonitrile afforded a golden yellow solution of an equilibrium mixture of two new complexes in a 2.8 : 1.0 : 2.5 ratio of **2.3a** : **2.12** : **2.13** as measured by ^{31}P{^{1}H} NMR spectroscopy (Scheme 2.6).

Scheme 2.6. Addition of acetonitrile to acyl-hydride 2.3a[a]

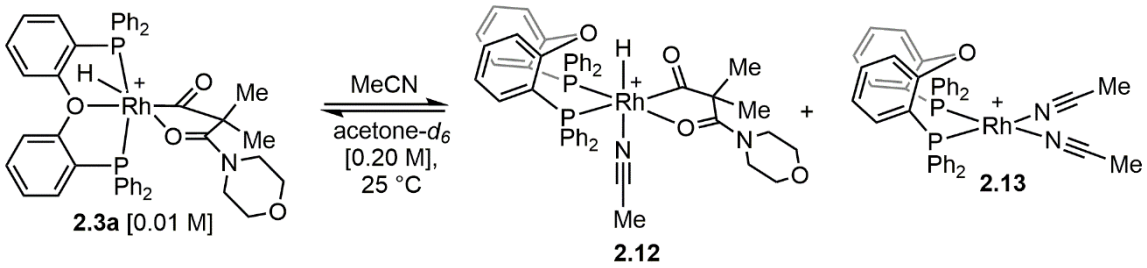

Eq. MeCN	Eq. 2.2a	2.3a : 2.12 : 2.13
20	0	2.8 : 1.0 : 2.5
20	20	3.9 : 1.0 : 0
200	20	0.5 : 1.0 : 0.3

[a]BAr^F_4 anions omitted for clarity

The two new complexes are assigned as the Rh(III) complex [Rh(*cis*-κ^2-$_{P,P}$-DPEPhos)(H)(MeCN)(COC{$(CH_3)_2$}CO{NC_4H_8O})][BAr^F_4] **2.12** and the Rh(I) complex [Rh(*cis*-κ^2-$_{P,P}$-DPEPhos)$(MeCN)_2$][BAr^F_4] **2.13**, which appears as a doublet at δ 34.3 [J_{RhP} = 181 Hz] in the ^{31}P NMR spectrum. Concomitant free aldehyde **2.2a** was also observed in the ^{1}H NMR spectrum. Complex **2.13** was synthesised independently by hydrogenation of [Rh(*cis*-κ^2-$_{P,P}$-DPEPhos)(nbd)][BAr^F_4] in MeCN, with a golden yellow solution being formed after 15 minutes reaction time. In the ^{1}H NMR spectrum of the precipitated complex a singlet at δ 1.66 (relative integral 6) was observed, corresponding to methyl groups of the acetonitrile. In the ESI-MS the $[Rh(DPEPhos)(MeCN)]^+$ fragment (m/z = 682.10) was observed, indicating that one of the MeCN ligands is labile upon ionisation by ESI-MS.

The equilibrium formed upon addition of MeCN to acyl-hydride **2.3a** was probed by addition of aldehyde (20 equivalents) to the reaction mixture which gave a 3.9 : 1.0 : 0 mixture of **2.3a** : **2.12** : **2.13** (Figure 2.7, B), addition of a further 180 equivalents of acetonitrile afforded a 0.5 : 1.0 : 0.3 mixture (Figure 2.7, C).

Acyl-hydride complex [Rh(*cis*-κ^2-$_{P,P}$-DPEPhos)(H)(MeCN)(COC{$(CH_3)_2$}CO{NC_4H_8O})][BAr^F_4] **2.12** was characterized *in-situ* by NMR spectroscopy. In the $^{31}P\{^1H\}$ NMR spectrum a doublet of doublets at δ 45.6 [J_{RhP} = 174; J_{PP} = 7 Hz)] and at δ 11.8 [J_{RhP} = 67; J_{PP} = 7 Hz] was observed. The small J_{PP} coupling is consistent with an unsymmetrical Rh(III) complex with the phosphines in a *cis*-arrangement, the significant difference in the J_{RhP} coupling constants indicates that one phosphine is

Figure 2.7. $^{31}P\{^{1}H\}$ NMR spectra of the addition of acetonitrile to acyl-hydride[a]

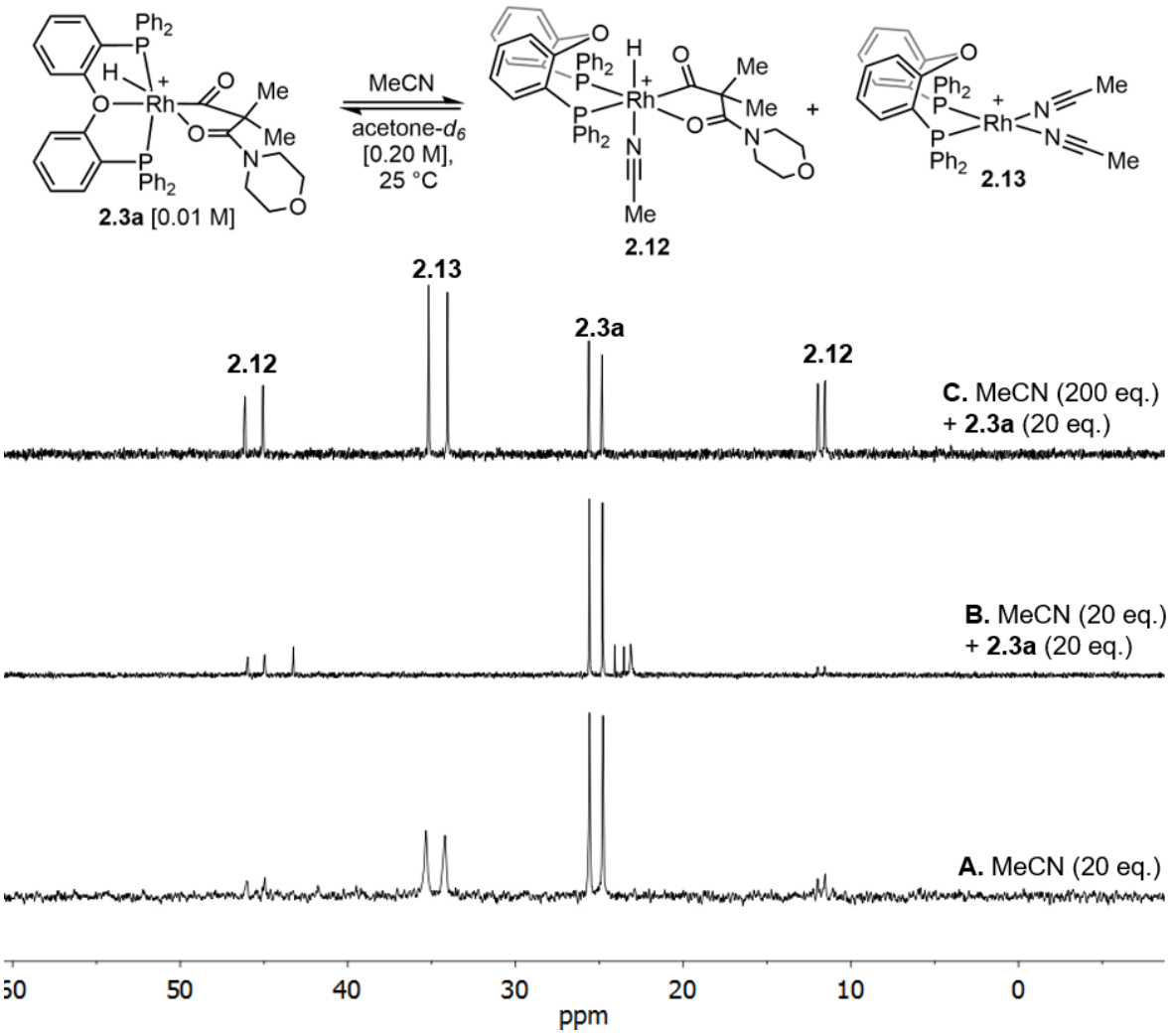

[a]BAr^{F}_{4} anions omitted for clarity

trans to a strong *trans*-influence ligand (either hydride or acyl) while the other is *trans* to a weak *trans*-influence ligand (MeCN, amide or DPEPhos ether).

In the hydride region of the ^{1}H NMR spectrum a new apparent triplet of doublets is observed at δ –15.8 [J_{RhH} = 20.0; J_{PH} = 20.0; J_{PH} = 8.0 Hz], as confirmed by $^{1}H\{^{31}P\}$ NMR spectroscopy. This is consistent with the hydride being axial and *cis* to two phosphorus atoms in different environments, thus making the acyl *trans* to one of the phosphorous atoms. Much larger *trans*-PH coupling [J_{PH} = 169 Hz] are found in Rh(III) acyl-hydride complexes such as [Rh(*cis*-κ^{2}-$_{P,P}$-diphosphine)(H)($COCH_2CH_2SMe$)][BAr^{F}_{4}], where the hydride is equatorial and *trans*-to a phopshine.[6]

The Rh(III)-acetonitrile adducts of [Rh(*cis*-κ^{2}-$_{P,P}$-DPEPhos)(H)($COCH_2CH_2SMe$)(MeCN)]

[*closo*-$CB_{11}H_6Cl_6$] complexes have been previously reported and interestingly 3 different isomers were observed compared to the one isomer of **2.12**; the analogous isomer to **2.12** was characterized by single X-ray diffraction.[7] The acetonitrile complex **2.12** could be a model for alkyne binding in catalysis and illustrates that nucleophiles can bind to the acyl-hydride, the step required before migratory insertion of alkyne.

2.8. Alkene Isomerisation

An alkene could also serve as a model for alkyne binding and reactivity. 20 equivalents of 1-octene were added to the deuterated acyl hydride complex **2.3a-*d*$_1$**, which was synthesized in an analogous fashion to acyl-hydride **2.3a** with formyl-deuterated aldehyde **2.2a-*d*$_1$** (*vide infra* for synthesis) (Scheme 2.7).

Scheme 2.7. Catalytic isomerisation of 1-octene with acyl-hydride 2.3a-*d*$_1$ and 2.1[a]

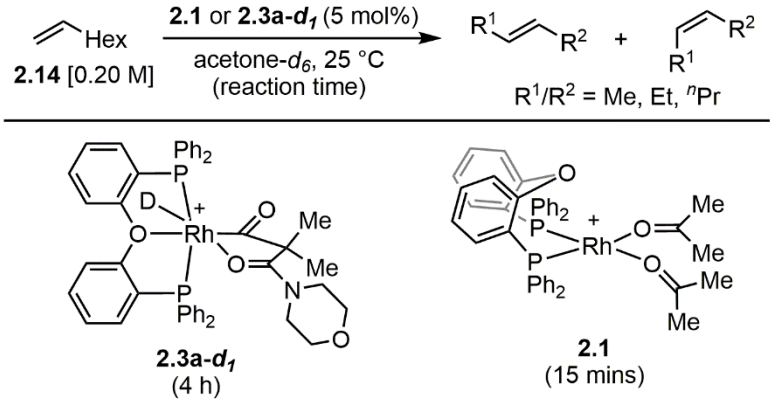

[a]BAr^F_4 anions omitted for clarity

No hydroacylation was detected and after 4 hours 1-octene **2.14** was isomerized to an undefined mixture of internal alkenes as observed by GC, ^{1}H NMR and ^{13}C NMR spectroscopy. In the ^{1}H NMR a broad peak was observed between δ 5.5–5.3, in the ^{13}C{^{1}H} NMR spectrum multiple alkene environments were observed from δ 133–124. There are two commonly implicated mechanisms for alkene isomerisation by cationic rhodium catalysts (Scheme 2.8).

Mechanism A (Scheme 2.8) proceeds *via* a Rh(III)-hydride intermediate **I**, hydride migratory insertion to the coordinated alkene results in a Rh-alkyl intermediate **II**, without change in rhodium oxidation state. From this intermediate *β*-hydride elimination can occur to form alkene bound

Scheme 2.8. Mechanisms of alkene isomerisation

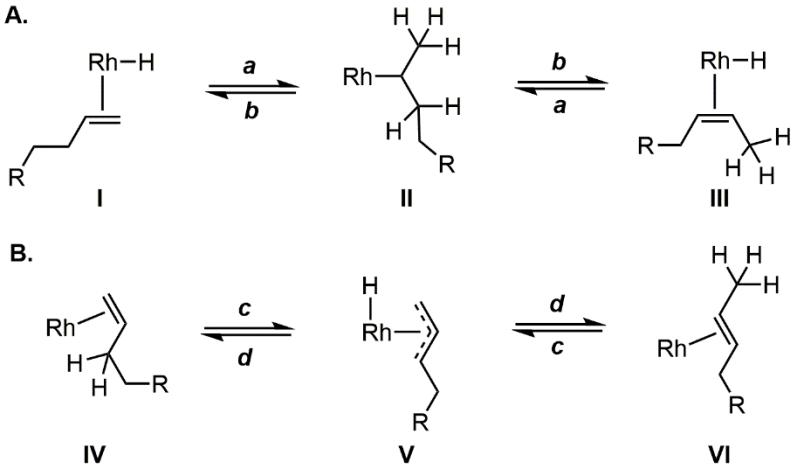

a. migratory insertion; ***b***. *β*–hydride elimination; ***c***. oxidative addition; ***d***. reductive elimination

rhodium-hydrides **I** or **III**, with intermediate **III** representing an overall isomerisation of the bound alkene. Further migratory insertion/*β*-hydride elimination sequences will result in the formation of a mixture of internal alkenes, with a mixture of alkene geometries.

Mechanism B (Scheme 2.8) proceeds *via* a Rh(I)-alkene bound intermediate **IV**, oxidative addition of the allylic alkene proton forms the Rh(III)-allyl hydride intermediate **V**. From this intermediate reductive bond formation can occur to provide either Rh(I)-alkene coordinated intermediates **IV** or **VI**, intermediate **VI** represents an overall alkene isomerisation from intermediate **IV**. Further sequences of oxidative addition/reductive bond formation will also afford a mixture of internal alkenes, with a mixture of alkene geometries.

If mechanism A (Scheme 2.8) was in operation *via* the acyl-deuteride intermediate **2.3a-*d*$_1$**: i) deuterium would be scrambled into the isomerized alkenes and ii) concomitant formation of non-deuterated acyl-hydride intermediate **2.3a** would be observed.[12,13] Under the reaction conditions in Scheme 2.7 no deuterium scrambling to the alkene was observed by ^{2}H NMR spectroscopy and no hydride resonance for **2.3a** was observed to the detection limit of ^{1}H NMR spectroscopy.

It was therefore proposed that the alkene isomerisation proceeds by Mechanism B, which is enabled by reversible aldehyde oxidative addition (See Scheme 2.5). To interrogate this, the reaction of Rh(I)

bis-acetone complex **2.1** with 1-octene was carried out (Scheme 2.7), which resulted in complete conversion to the internal alkene isomers within 15 minutes (compared to 3 h for acyl-hydride **2.3a**), several examples of Rh(I)-mediated alkene isomerisation have been reported.[14,15]

2.9. Synthesis of a Product-Bound Complex

To determine why no product inhibition is observed during catalysis, the product bound complex was synthesized by addition of 4 equivalents of enone **2.10a** to the Rh(I) *bis*-acetone complex **2.1** in acetone. The reaction mixture turned a darker shade of red and the reaction was complete within 5 minutes as measured by $^{31}P\{^{1}H\}$ spectroscopy (Scheme 2.9).

Scheme 2.9. Synthesis of product-bound complex and its reaction with aldehyde[a]

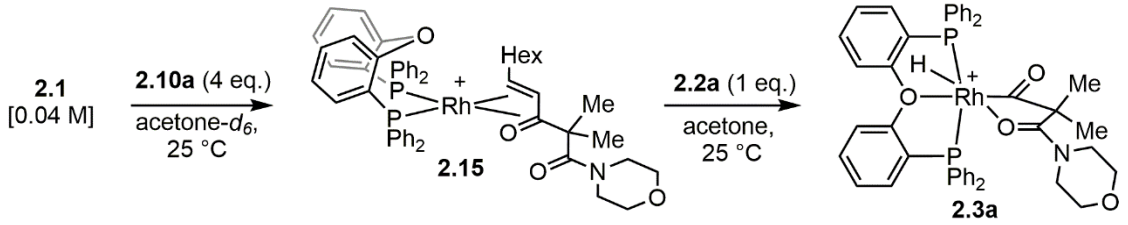

[a] BAr^{F}_{4} anions omitted for clarity

Removal of excess enone by precipitation of the complex in pentane allowed for characterisation of the Rh(I) complex [Rh(*cis*-κ^2-$_{P,P}$-DPEPhos)(**2.10a**)][BAr^{F}_{4}] **2.15** by ^{1}H NMR and ^{31}P NMR as well as by ESI-MS. At room temperature broad peaks were observed in both NMR spectra which became sharper at 190 K, this is potentially due to ring flipping of the DPEPhos ligand on the NMR timescale.[16,17]

The ^{31}P NMR spectrum at 190 K showed a doublet of doublets at δ 33.0 [J_{RhP} = 160; J_{PP} = 50 Hz] and at δ 25.0 [J_{RhP} = 190; J_{PP} = 50 Hz] which is indicative of an unsymmetrical Rh(I) complex with *cis*-phosphines. In the ^{1}H NMR spectrum (190 K) the alkene peaks are shifted upfield, with the α-enone proton appearing as an apparent triplet at δ 5.10 [J_{PH} = 7.5; J_{HH} = 7.5] and the β-enone proton appearing as an apparent pentet at δ 2.34 [J_{PH} = 7.5, J_{HH} = 7.5, J_{HH} = 7.5]. The methyl groups were observed in two distinct environments, one at δ 1.55 and the other at δ 0.63, due to their different environments relative to the DPEPhos backbone.

Addition of 1 equivalent of aldehyde **2.2a** to a solution of product bound complex **2.15** (0.02 M) in acetone resulted in a rapid color change of the solution to light yellow, which was due to the formation of the acyl hydride complex **2.3a** on time of mixing, as confirmed by $^{31}P\{^{1}H\}$ NMR spectroscopy. This demonstrates that rapid ligand exchange and oxidative addition of aldehyde **2.3a** occurs, consistent with no observed product inhibition during catalysis.

2.10. Kinetic Isotope Effect Studies

To provide insight into the turnover limiting step of the reaction kinetic isotope effect (KIE) studies were undertaken. The deuterated aldehyde **2a-*d*$_1$** was synthesised with 98% deuterium incorporation in 54% yield by a chemoselective Raney nickel mediated reduction of the *β*-amido-nitrile **2.16** (Scheme 2.10).

Scheme 2.10. Synthesis of deuterated aldehyde 2.2a-*d*$_1$

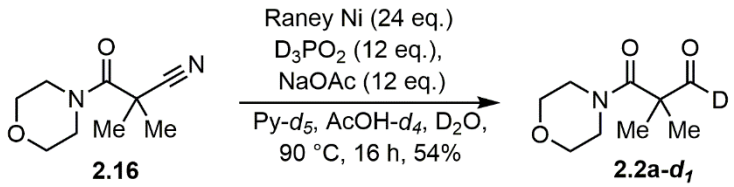

The aldehyde peak was observed as a singlet in the ^{2}H NMR spectrum at δ 9.63 and the level of deuterium incorporation was determined by the relative integrals of the aldehyde peak compared to the *gem*-dimethyl resonance in in the ^{1}H NMR spectrum. The reaction was conducted in a mixture of pyridine-d_5, acetic acid-d_4 and D_2O as solvent at 90 ºC with hypophosphourous acid-d_3 as a deuteride source. Initial experiments using non-deuterated pyridine and acetic acid-d_1 (AcOD) gave only 73% deuterium incorporation, indicating that deuterium scrambling to at least one of these the solvents was in operation. Analysis of the reaction mixture by ^{2}H NMR spectroscopy displayed a broad peak at δ 7.9–7.5, suggesting that deuterium had been incorporated into the *meta* and *para* positions of the pyridine ring, incorporation to the *ortho* position (δ 8.5) was not observed.[18] Nickel-mediated pyridine C–H functionalisation have been reported and could be the mechanism by which deuterium was scrambled.[19,20] It could not be determined whether deuterium had been incorporated into the methyl group of acetic acid, due to the predominant and broad D_2O peak.

The synthesised deuterated aldehyde **2.3a-*d*$_1$** was then used to measure the KIE of the hydroacylation using the initial rates method with two parallel samples, measuring the rate of enone formation. Conditions of aldehyde **2.2a** [0.2 M], 1-octyne [0.18 M] and *bis*-acetone catalyst **2.1** [0.01 M] in acetone-d_6 at 25 ºC were used and a KIE of 1.5 (± 0.1) was measured (Scheme 2.11).

Scheme 2.11. KIE for the reaction of deuterated aldehyde 2.2a-*d*$_1$

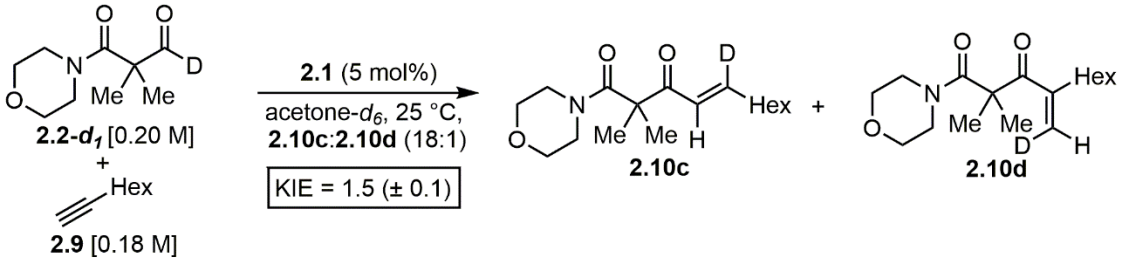

A KIE close to unity has been reported for an alkyne hydroacylation where reductive bond formation is proposed to be turnover limiting.[21] KIEs of between 1.4 and 1.7 have been reported for hydroacylation systems where the turnover limiting step is proposed to be either hydride insertion, or reductive bond formation preceded by reversible hydride insertion into an alkene (an equilibrium isotope effect[22,23]).[11–13] In reactions, including hydroacylation, where irreversible aldehyde C–H bond oxidative cleavage is proposed to be the turnover limiting step, larger KIE's = 2.4–2.9 have been measured.[24–26] The measured KIE [1.5 (± 0.1)] is also consistent with those reported for hydride insertions into alkenes/alkynes at group 9 metals.[27,28] A KIE of 1.1 (± 0.1) was measured when deuterated 1-octyne **2.6-*d*$_1$** was used under otherwise identical conditions (Scheme 2.12).

Scheme 2.12. KIE for the reaction of deuterated aldehyde 2.2a-*d*$_1$

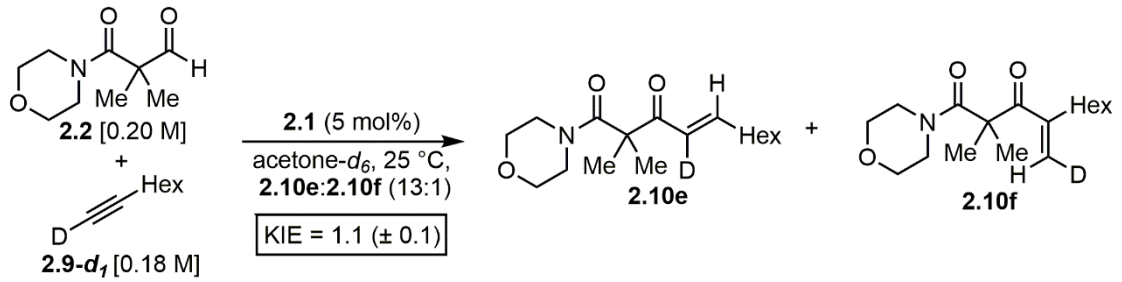

This suggests that C–H activation of the alkyne is not the irreversible turnover limiting step. Such C–H activation processes have been implicated in the related Ru-catalysed hydroamidation of alkynes,

which occur *via* a vinyldiene intermediate and show KIEs of 1.5–2.3.[29]

Based on these observations, hydride insertion is proposed to be turnover limiting, rather than reductive bond formation, which would be expected to have a KIE close to 1 in the absence of equilibrium isotope effects. We consider such an equilibrium unlikely, as reversible hydride insertion involving alkynes is rare.[27]

These labelling studies also show that deuterium is incorporated into both the linear and branched enone products with a stereochemistry consistent with *syn*–migratory insertion of the hydride into the alkyne. The position of deuteration for the linear enones was deduced by the changes in coupling to the non-deuterated alkene proton. In order to assign the position of deuteration for the branched enones, selective nOe experiments in acetone-d_6 before column chromatography were carried out. The *gem*-alkene protons in non-deuterated enone **2.10b** were compared with the single observed resonance in the deuterated analogues **2.10d** and **2.10f** (Scheme 2.13).

Scheme 2.13. A) Assignment of germinal protons in branched-enone 2.10b by nOe; B) Assignment of deuterated products

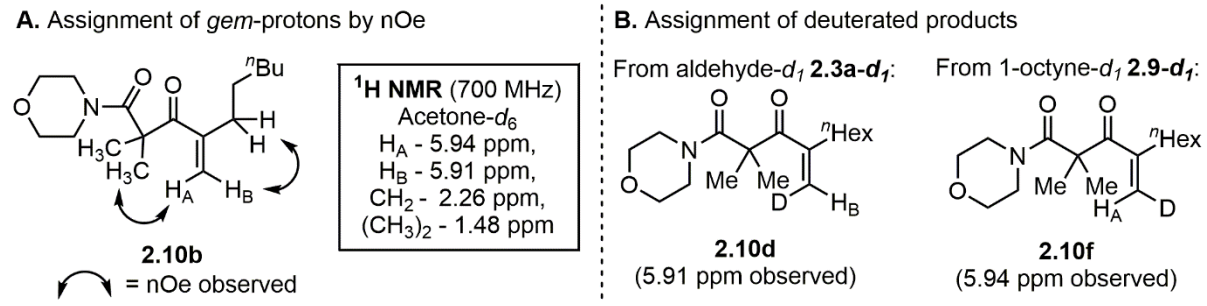

The nOe's in enone **2.10b** were observed between the gem-dimethyl (δ 1.48) and H_A (δ 5.94) as well as between the allylic-CH_2 group (δ 2.26) and H_B (5.91). The product of the reaction with deuterated aldehyde **2.3a-d_1** afforded enone **2.10d** with one alkene resonance at δ 5.91, which corresponds to H_B and the reaction with deuterated alkyne **2.9-d_1** afforded enone **2.10f** with one alkene resonance at δ 5.94, which corresponds to H_A.

Because deuterium incorporation is dependent on the location of the starting deuterium label, this implies that competitive scrambling of the *gem*-positions of the branched alkene product through a Rh(V)-metallacyclopropene intermediate is not occurring. This process is observed in the

hydroacylation reactions of 2-(methylthio)benzaldehyde **2.17** with alkynes catalysed by {Rh(DPEPhos)}$^{+21}$ or {Rh(^{i}Pr$_2$P(NMe)P^{i}Pr$_2$)}$^{+11}$ based catalysts, where deuterium was incorporated into both *gem*-positions of the branched enone product **2.18b** in 1 : 1 ratio (Scheme 2.14).

Scheme 2.14. Deuterium scrambling of the *gem*-alkene protons in the hydroacylation of 2-(methylthio)benzaldehyde with alkynes *via* a metallocyclopropene intermediate[a]

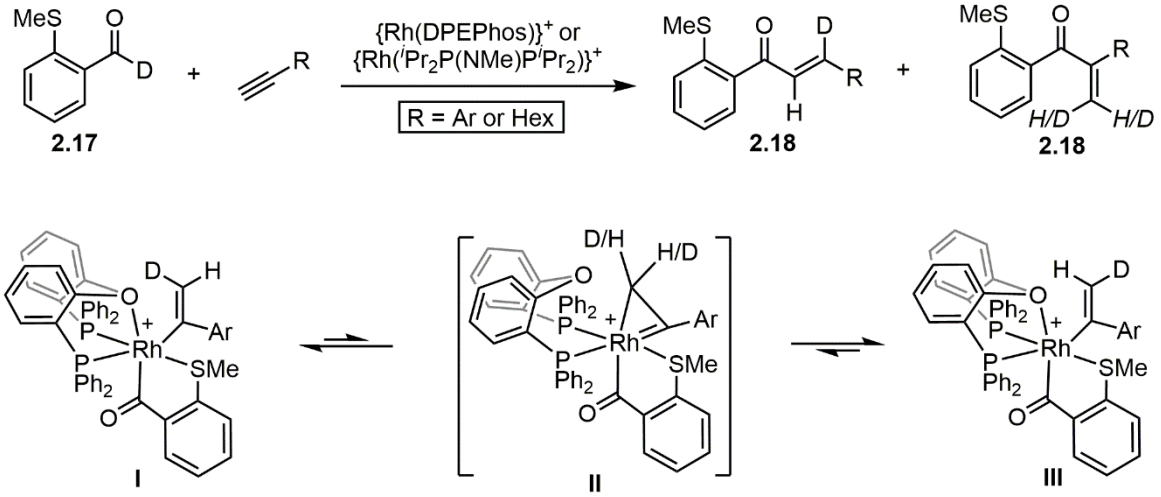

[a]BAr^{F}_4 anions omitted for clarity

The deuterium scrambling is proposed to occur *via* Rh(V)-metallacyclopropene **II** which is formed from the branched acyl-alkenyl intermediate **I**. The position of the H and D atoms in the alkenyl group does not determine their resultant positions in the metallacyclopropene, which means in the reverse reaction, both isomers of the acyl-alkenyl intermediates (**I** and **III**) are formed, resulting in a 50/50 mixture. This process can only occur because formation of the Rh(V)-metallacyclopropene intermediate **II** is competitive with reductive bond formation from the branched acyl-alkenyl intermediate **I**. Interestingly, in the hydroacylation of 2-(methylthio)benzaldehyde with the {Rh(DPEPhos)}$^{+}$ catalyst system, the turnover limiting step of the reaction was shown to be irreversible reductive bond formation from branched acyl-alkenyl intermediate **I**/**III**. In contrast, during the hydroacylation with *β*-amido aldehyde **2.2a-*d*$_1$** the formation of the metallacyclopropene intermediate must not be competitive with reductive bond formation, and we propose that hydride insertion is the turnover limiting step of the reaction (*vide supra*). This may suggest that reductive bond formation from the branched acyl-alkenyl intermediate for the *β*-amido aldehyde reaction has a lower energy barrier than for the 2-(methylthio)benzaldehyde system, resulting in hydride insertion

becoming turnover limiting and no deuterium scrambling *via* the Rh(V)-metallacyclopropene intermediate. However, the *β*-amido ligand slowing the rate of metallacyclopropene formation cannot be ruled out as an alternative explanation.

2.11. Hydroacylation Mechanism

A mechanism consistent with all the collected data is shown in Scheme 2.15.

Scheme 2.15. Hydroacylation mechanism with DPEPhos[a]

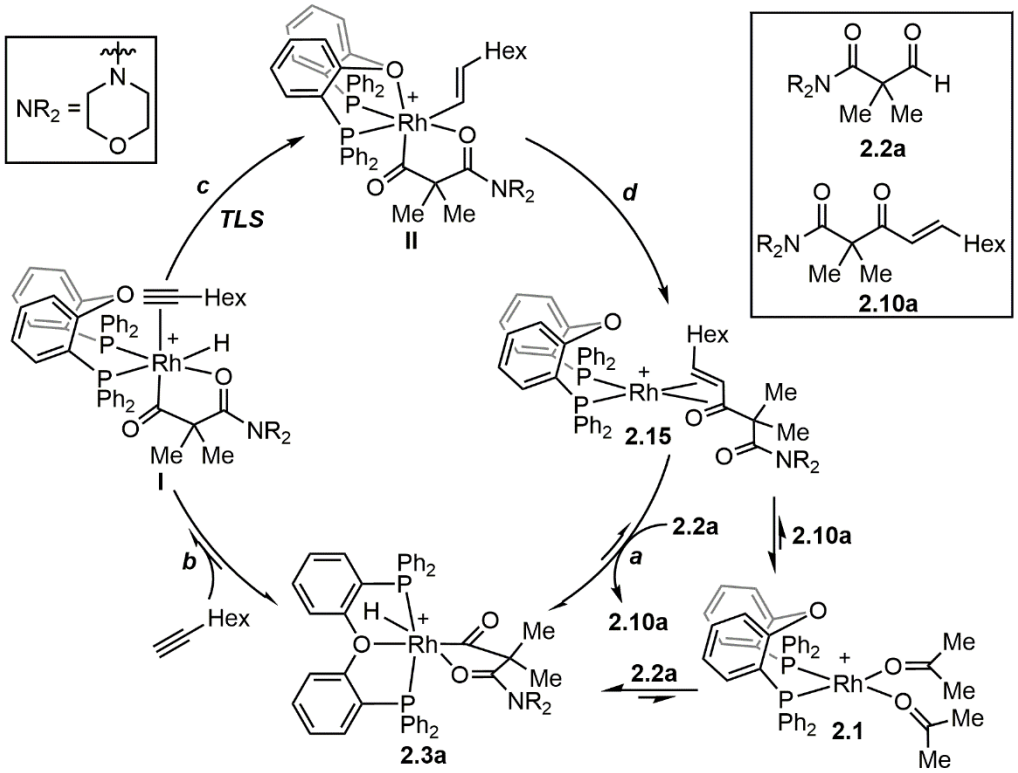

[a]BAr^F_4 anions omitted for clarity

Initial reaction of aldehyde **2.2a** with the *bis*-acetone pre-catalyst **2.1** forms the acyl-hydride complex **2.3a**. This step is reversible, but the equilibrium lies significantly to the acyl-hydride, resulting in the reaction being zero order in aldehyde. Subsequent reaction with alkyne (in which the reaction is 1st order) (step ***b***), with a change in coordination geometry for the DPEPhos ligand from κ^3 to κ^2, gives the alkyne coordinated intermediate **I** which undergoes turnover limiting migratory insertion (step ***c***) to form the alkenyl-acyl intermediate **II**. We propose this step is also selectivity determining with regard to linear/branched isomers. Subsequent reductive bond formation forms

enone-bound complex **2.15** (step ***d***). No product inhibition was observed during catalysis, because the enone is rapidly displaced by additional aldehyde to return to acyl-hydride **2.3a** (step ***a***). The acyl-hydride concentration remains constant and is the observed resting state throughout the reaction, until all free aldehyde has been consumed. This is consistent with the 1st order behaviour observed in pre-catalyst and the overall *pseudo*-1st order kinetics of the reaction.

2.12. Mechanism of Acyl-Hydride Consumption

To understand the mechanism by which the acyl-hydride **2.3a** resting state is consumed at the end of productive hydroacylation (37–43 minutes), after all free aldehyde is consumed, the kinetics of the decay of acyl-hydride was studied. It was found to be a *pseudo*-first order process [k_{obs} = 3.8 (± 0.1) × 10^{-3} s^{-1}] (Figure 2.8).

Figure 2.8. Plot of ln [acyl-hydride (2.3a)] against time[a]

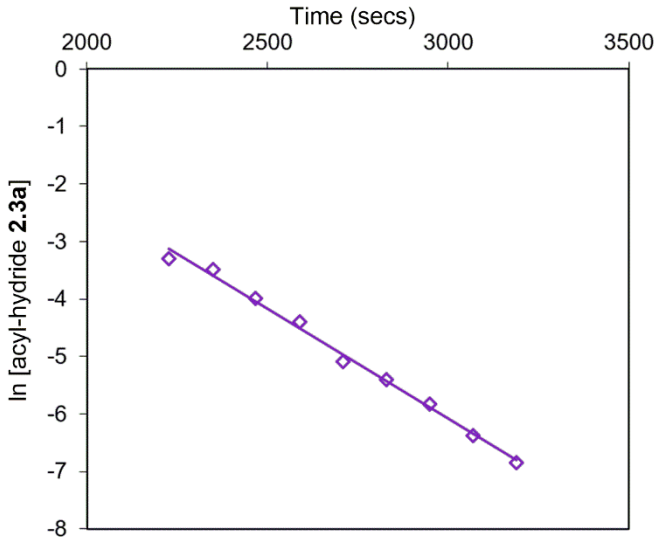

[a]gradient = 3.8 (± 0.1) × 10^{-3} s^{-1}

The process is *pseudo*-first order because there is an excess of 1-octyne (~6 eq) over this period, which allows the calculation of a reaction rate constant [k = 1.7 (± 0.4) x 10^{-2} $M^{-1}s^{-1}$] based on the average concentration of 1-octyne (0.22 M) over this time. When compared to the calculated rate constant [k = 1.6 (± 0.1) x 10^{-2} $M^{-1}s^{-1}$] for the overall hydroacylation process, based on the 1st order consumption of 1-octyne (Figure 2.5), it indicates that direct hydroacylation from intermediate **2.3a** (i.e. not reductive elimination to afford aldehyde or reductive decarbonylation) is the dominant

pathway for acyl-hydride consumption. This is in agreement with no free aldehyde being observed in solution over this period.

Further evidence for direct hydroacylation from the acyl-hydride being the dominant pathway for acyl-hydride consumption, after all free aldehyde is consumed, is that the absolute rate of hydroacylation [$rate_{obs}$ = 6 (± 1) x 10^{-5} Ms^{-1}] as estimated by measuring the gradient of enone **2.10a**/**2.10b** formation between 37-45 mins, matches the absolute rate of acyl-hydride **2.3a** consumption [$rate_{obs}$ = 7 (± 1) x 10^{-5} Ms^{-1}] over the same time period (Figure 2.9).

Figure 2.9. Plots of enones 2.10a/2.10b concentration (Graph A) and acyl-hydride 2.3a (Graph B) against time (37–43 minutes)[a]

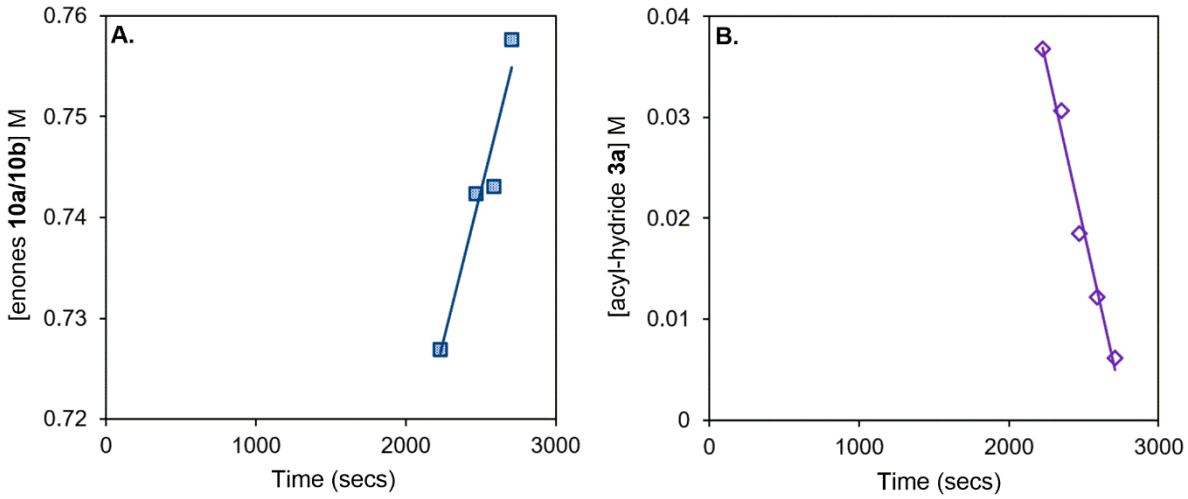

[a]Graph A: gradient = 7 (± 1) x 10^{-5} Ms^{-1}; Graph B: gradient = 6 (± 1) x 10^{-5} Ms^{-1}.

2.13. XantPhos Hydroacylation

Having studied the kinetics with DPEPhos we turned our attention the application of XantPhos as ligand. During the ligand optimisation for the hydroacylation of *β*-amido aldehydes, XantPhos afforded significantly reduced yields compared to DPEPhos. To investigate this, the reaction of isolated XantPhos acyl-hydride complex **2.5** (10 mol%) as catalyst with aldehyde **2.3c** (0.65 M), 1-octyne **2.9** (0.65 M) in acetone-d_6 at 55 ºC was monitored by ^{1}H NMR spectroscopy, using the $BAr^F{}_4$ anion as an internal reference (Figure 2.10).

After 24 h reaction time a 49% ^{1}H NMR yield of linear enone product **2.19** alongside no branched

Figure 2.10. Reaction profile with the acyl-hydride XantPhos catalyst 2.5

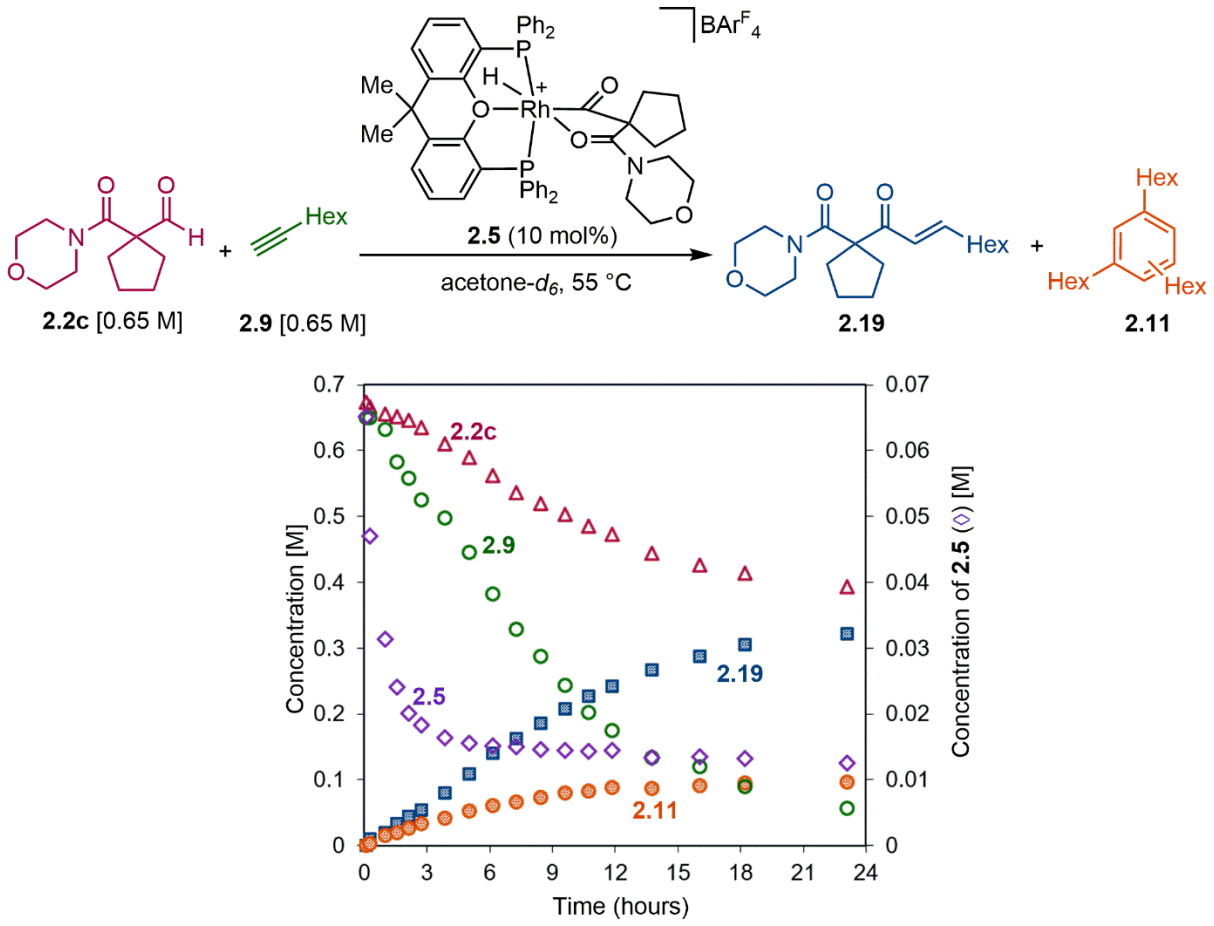

[a]Reaction profile as measured by ^{1}H NMR spectroscopy. Left axis: red △ = aldehyde **2.2c**, green ○ = 1-octyne **2.9**, blue ■ = enone **2.8a**, and orange ● = tri-*n*-hexylbenzenes **2.11**. Right axis: purple ◇ = acyl-hydride, **2.5**.

enone was measured, combined with a 44% yield of cyclotrimer products **2.11a**/**2.11b** (4.3 : 1, 1,2,4-tri-*n*-hexyl benzene : 1,3,5-tri-*n*-hexyl benzene). Analysis of the reaction profile revealed that the formation of both enone **2.19** (Figure 2.10, Filled Blue Squares) and tri-*n*-hexylbenzenes **2.11** (Figure 2.10, Filled Orange Circles) were competitive throughout the reaction. This meant that the rate of 1-octyne consumption (Figure 2.10, Green Circles) was significantly higher than aldehyde consumption (Figure 2.10, Red Triangles) with only 45% of aldehyde **2.3c** (including aldehyde bound to the pre-catalyst 2.10) being consumed after 24 h. The catalytic cyclotrimerisation of alkynes has previously been reported using the Rh(I) catalyst [Rh(*mer*-κ^3-$_{P,O,P}$-Xantphos)(η^2-PhCCPh)][BAr$^F_4$] **2.4** and this process is also competitive with alkyne carbothiolation using *β*-*S*-aldehydes.[30]

An induction period is observed for enone formation (0 – 3 h), which means acyl-hydride **2.5** is a

pre-catalyst to an active hydroacylation mechanistic pathway where acyl-hydride **2.5** is neither the catalytic resting state nor part of the mechanistic pathway. The picture is complicated further by competitive cyclotrimerisation, which will also have its own catalytic resting state species. Consistent with these observations, the concentration of acyl-hydride **2.5** (Figure 2.10, Purple Diamonds) reduces significantly during the same period (0 – 3 h), it then appears to reach a steady state and continues to reduce more slowly, consistent with the resting state of catalysis changing. Because a steady concentration of acyl-hydride remains, it suggests the acyl-hydride intermediate is in equilibrium with the two other formed resting states. It's also possible that acyl-hydride itself is the catalytic resting state of a separate and slower hydroacylation mechanistic pathway, that is simultaneously in operation. A mechanism consistent with these observations is shown in Scheme 2.16.

Starting from acyl-hydride pre-catalyst **2.5** two potential hydroacylation pathways are described: Pathway (i) – Hydroacylation where **2.5** it is an active intermediate (steps ***b***, ***c***, ***d***, ***a***): this starts with the coordination of 1-octyne to give complex **I**, followed by linear selective, irreversible hydride insertion to give alkenyl-acyl intermediate **II**. Reductive elimination of enone **2.19** will then provide a Rh(I) intermediate **III** and oxidative addition of aldehyde to re-form complex **2.5** completes the catalytic cycle; Pathway (ii) – Hydroacylation where **2.5** is not an active intermediate (steps ***e***, ***f***, ***c***, ***d***): from **2.5** a new catalytic species is formed, that avoids the turnover limiting step of pathway (i), this is proposed to be *fac*-acyl-hydride intermediate **IV**. Formation of **IV** can occur either directly from acyl-hydride **2.5** or by reversible oxidative addition of aldehyde *via* **III**. From *fac*-acyl-hydride **IV**, alkyne coordination forms the alkyne-bound complex **I**, from which the same sequence of linear selective, irreversible hydride insertion (***c***) and reductive elimination (***d***), forming complex **III** will occur. From complex **III** oxidative addition to directly form *fac*-acyl-hydride **IV** completes the catalytic cycle and avoids formation of *mer*-acyl-hydride **2.5**.

Because of the induction period in product formation, pathway (ii) must be faster than pathway (i), if pathway (i) is even in operation. This means the turnover limiting step of the proposed catalytic cycles are different. A scenario consistent with different turnover limiting steps is if in pathway (i) alkyne coordination from *mer*-acyl-hydride **2.5** to complex **I** (potentially *via* **IV**) is turnover limiting and slower than all the steps in pathway (ii), where the turnover limiting step is either alkyne coordination

Scheme 2.16. Hydroacylation mechanism with XantPhos

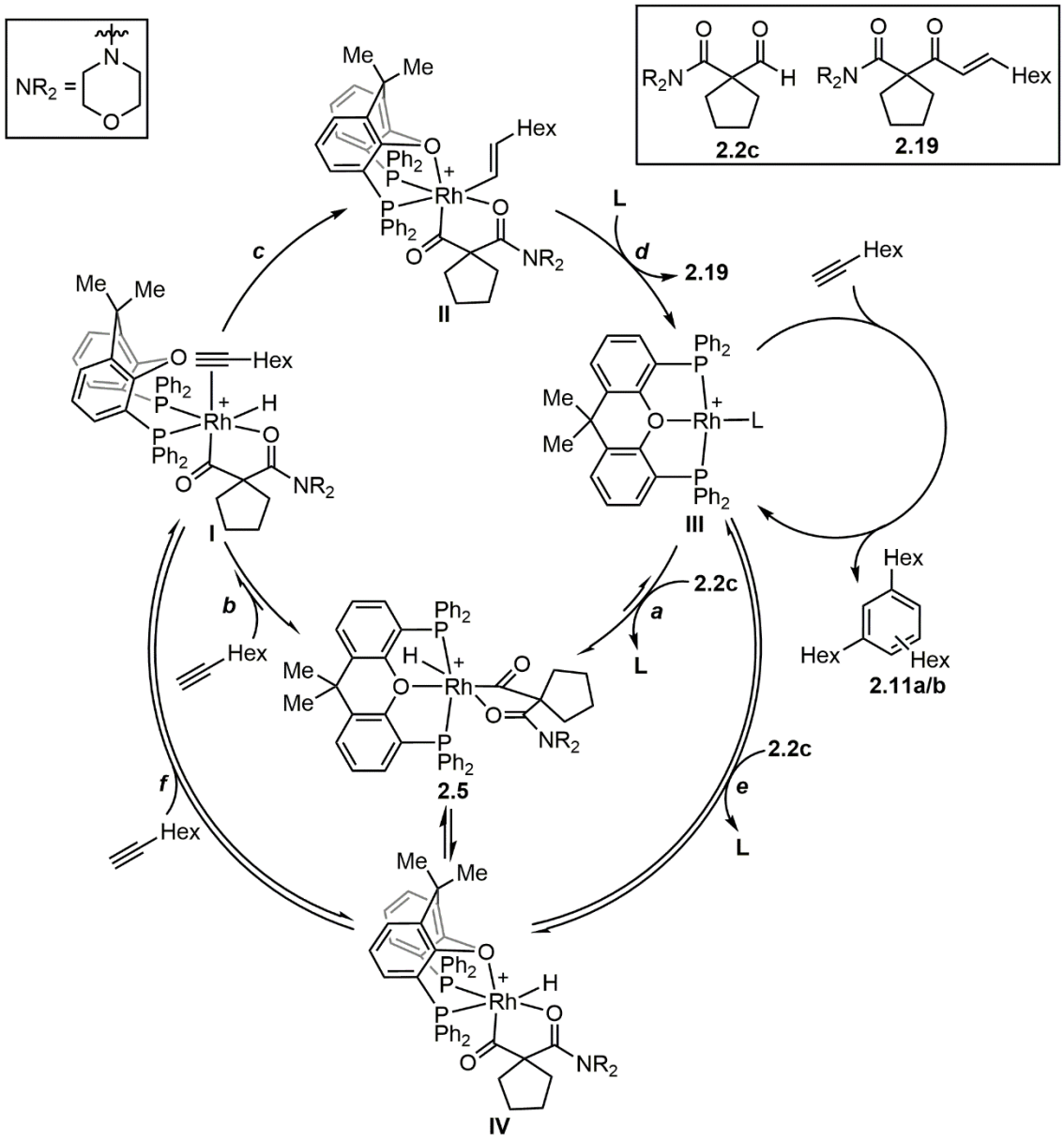

[a]BAr^F_4 anions omitted for clarity

(***f***), hydride insertion (***c***) or reductive elimination (***d***). Formation of **I** from *mer*-acyl-hydride **2.5** could be expected to have a high energy barrier due to the low kinetic flexibility of the XantPhos ligand, which hinders formation the κ^2-complex from *mer*-complex **2.5**. During the independent synthesis of *mer*-acyl-hydride **2.5** from [Rh(*mer*-κ^3-$_{P,O,P}$-XantPhos)(η^2-PhCCPh)][BAr^F_4] **2.5** and aldehyde **2.2c** not in the presence of alkyne (See Scheme 2.2), the initial product of oxidative addition is likely *fac*-acyl-hydride **IV**, which then rearranges to form the more stable *mer*-acyl-hydride **2.5**. In contrast, during

catalysis the *fac*-acyl-hydride **IV** is intercepted by alkyne to directly form complex **I**, before the rearrangement can occur.

The competing mechanistic pathway of the cyclotrimerisation reaction can occur from the so-formed Rh(I)-complex **III**, which can react with 1-octyne to form tri-*n*-hexylbenzene products. This may happen because all the steps leading up to the turnover limiting step of the hydroacylation, including oxidative addition, are reversible and that the rate of cyclotrimerisation is competitive with this turnover limiting step. Or that aldehyde oxidative addition and cyclotrimerisation are competitive irreversible reactions from intermediate **III**.

Overall there are significant differences between the XantPhos and DPEPhos systems. The catalysis is significantly slower with XantPhos, requiring extended reaction times at higher temperatures, a similar effect has been reported for *β*-*S*-aldehydes.[6] This could be due to the reduced propensity for the formation of κ^2-XantPhos intermediates compared to κ^2-DPEPhos intermediates.[31] κ^2-Intermediates are required for alkyne coordination and likely reductive elimination, if it proceeds *via* a 5-coordinate complex. Furthermore, with XantPhos and not DPEPhos, cyclotrimerisation is competitive with hydroacylation in the presence of free aldehyde. The mechanism of cyclotrimerisation with the DPEPhos catalytic system is explored further in Chapter 3.

2.14. Conclusions

Acyl-hydride complexes were synthesised from *β*-amido aldehydes and $\{Rh(DPEPhos)\}^+$ or $\{Rh(XantPhos)\}^+$ systems. Characterisation of an acyl-hydride complex by single X-ray diffraction revealed that the *β*-amido tethering group was coordinated to rhodium through a κ^1-oxygen interaction. The analogous DPEPhos-Rh-complexes of both tertiary and secondary *β*-amido aldehydes displayed similar characteristic NMR spectroscopic data and their rates of decarbonylation were studied. The secondary aldehyde acyl-hydride was found to undergo reductive decarbonylation significantly faster than the tertiary aldehyde acyl-hydride, with no decarbonylation being detected for the later, after an extended reaction time. This reactivity was rationalised by the reduced propensity for initial decarbonylation of the tertiary centre due formation of a less favourable tertiary M–C bond.

The kinetics of hydroacylation were studied with this stable catalyst system and the acyl-hydride was found to be the catalytic resting state until consumption of free aldehyde (i.e. not bound to rhodium as the acyl-hydride), while no decarbonylation was observed throughout the reaction. The reaction was found to be *pseudo*-first order, by analysis of alkyne consumption and by the initial rates method. The reaction was found to be zero order in aldehyde, first order in alkyne, first order in catalyst and no product inhibition was observed, which is consistent with aldehyde being incorporated in the reaction resting state. Stoichiometric reactions of the acyl-hydride complex indicated that aldehyde oxidative addition is fast and reversible on the reaction timescale but is strongly biased toward the acyl-hydride complex. The reaction of acyl-hydride with acetonitrile, formed an acetonitrile bound intermediate, consistent with alkyne binding during the catalytic cycle. Furthermore, product bound complex could be synthesised and was shown to be rapidly converted to acyl-hydride upon addition of aldehyde, consistent with no observed product inhibition during catalysis. A small KIE [1.5 (± 0.1)] was observed with formyl-deuterated aldehyde, which is consistent with hydride-insertion being the turnover limiting step of the reaction.

The resting state of the reaction changed when all free aldehyde was consumed, and the mechanism was determined to be direct alkyne hydroacylation from the remaining acyl-hydride, this was shown by comparing the kinetics of acyl-hydride consumption and hydroacylation product formation. As the resting state changed alkyne cyclotrimerisation to form tri-*n*-hexylbenzenes became a competitive side reaction. When the XantPhos catalyst system was used the rate of hydroacylation was significantly reduced and cyclotrimerisation became competitive in the presence of excess aldehyde indicating a significant shift in the reaction mechanism. The subtleties of these competing reactions with the DPEPhos catalyst are studied further in the following chapter.

2.15. References

1 J. Uddin, C. M. Morales, H. H. Maynard and C. R. Landis, *Organometallics*, 2006, **25**, 5566–5581.

2 T. J. Coxon, M. Fernández, J. Barwick-Silk, A. I. McKay, L. E. Britton, A. S. Weller and M. C. Willis, *J. Am. Chem. Soc.*, 2017, **139**, 10142–10149.

3 G. L. Moxham, H. E. Randell-Sly, S. K. Brayshaw, R. L. Woodward, A. S. Weller and M. C. Willis, *Angew. Chem. Int. Ed.*, 2006, **45**, 7618–7622.

4 G. L. Moxham, H. Randell-Sly, S. K. Brayshaw, A. S. Weller and M. C. Willis, *Chem. Eur. J.*, 2008, **14**, 8383–8397.

5 P. S. Pregosin, *NMR in Organometallic Chemistry*, Wiley VCH, 2012.

6 R. J. Pawley, G. L. Moxham, R. Dallanegra, A. B. Chaplin, S. K. Brayshaw, A. S. Weller and M. C. Willis, *Organometallics*, 2010, **29**, 1717–1728.

7 A. J. Sandee, L. A. van der Veen, J. N. H. Reek, P. C. J. Kamer, M. Lutz, A. L. Spek and P. W. N. M. van Leeuwen, *Angew. Chem. Int. Ed.*, 1999, **38**, 3231–3235.

8 G. L. Williams, C. M. Parks, C. R. Smith, H. Adams, A. Haynes, A. J. H. M. Meijer, G. J. Sunley and S. Gaemers, *Organometallics*, 2011, **30**, 6166–6179.

9 G. P. F. van Strijdonck, M. D. K. Boele, P. C. J. Kamer, J. G. de Vries and P. W. N. M. van Leeuwen, *Eur. J. Inorg. Chem.*, 1999, **1999**, 1073–1076.

10 L. J. Sewell, M. A. Huertos, M. E. Dickinson, A. S. Weller and G. C. Lloyd-Jones, *Inorg. Chem.*, 2013, **52**, 4509–4516.

11 I. Pernik, J. F. Hooper, A. B. Chaplin, A. S. Weller and M. C. Willis, *ACS Catal.*, 2012, **2**, 2779–2786.

12 A. Prades, M. Fernández, S. D. Pike, M. C. Willis and A. S. Weller, *Angew. Chem. Int. Ed.*, 2015, **54**, 8520–8524.

13 A. B. Chaplin, J. F. Hooper, A. S. Weller and M. C. Willis, *J. Am. Chem. Soc.*, 2012, **134**, 4885–4897.

14 S. H. Bergens and B. Bosnich, *J. Am. Chem. Soc.*, 1991, **113**, 958–967.

15 K. Tanaka, S. Qiao, M. To*bis*u, M. M.-C. Lo and G. C. Fu, *J. Am. Chem. Soc.*, 2000, **122**, 9870–9871.

16 W. Goertz, W. Keim, D. Vogt, U. Englert, M. D. K. Boele, L. A. van der Veen, P. C. J. Kamer and P. W. N. M. van Leeuwen, *J. Chem. Soc. Dalt. Trans.*, 1998, 2981–2988.

17 D. Pingen, T. Lebl, M. Lutz, G. S. Nichol, P. C. J. Kamer and D. Vogt, *Organometallics*, 2014, **33**, 2798–2805.

18 G. R. Fulmer, A. J. M. Miller, N. H. Sherden, H. E. Gottlieb, A. Nudelman, B. M. Stoltz, J. E. Bercaw and K. I. Goldberg, *Organometallics*, 2010, **29**, 2176–2179.

19 C.-C. Tsai, W.-C. Shih, C.-H. Fang, C.-Y. Li, T.-G. Ong and G. P. A. Yap, *J. Am. Chem. Soc.*, 2010, **132**, 11887–11889.

20 J. Yamaguchi, K. Muto and K. Itami, *Top. Curr. Chem.*, 2016, 1–33.

21 R. J. Pawley, M. A. Huertos, G. C. Lloyd-Jones, A. S. Weller and M. C. Willis, *Organometallics*, 2012, **31**, 5650–5659.

22 W. D. Jones, *Acc. Chem. Res.*, 2003, **36**, 140–146.

23 E. M. Simmons and J. F. Hartwig, *Angew. Chem. Int. Ed.*, 2012, **51**, 3066–3072.

24 P. Fristrup, M. Kreis, A. Palmelund, P.-O. Norrby and R. Madsen, *J. Am. Chem. Soc.*, 2008, **130**, 5206–5215.

25 K. G. M. Kou, D. N. Le and V. M. Dong, *J. Am. Chem. Soc.*, 2014, **136**, 9471–9476.

26 S. K. Murphy, A. Bruch and V. M. Dong, *Chem. Sci.*, 2015, **6**, 174–180.

27 R. Ghosh, X. Zhang, P. Achord, T. J. Emge, K. Krogh-Jespersen and A. S. Goldman, *J. Am. Chem. Soc.*, 2007, **129**, 853–866.

28 E. Zuidema, L. Escorihuela, T. Eichelsheim, J. J. Carbó, C. Bo, P. C. J. Kamer and P. W. N. M. van Leeuwen, *Chem. Eur. J.*, 2008, **14**, 1843–1853.

29 M. Arndt, K. S. M. Salih, A. Fromm, L. J. Goossen, F. Menges and G. Niedner-Schatteburg, *J. Am. Chem. Soc.*, 2011, **133**, 7428–7449.

30 J. F. Hooper, A. B. Chaplin, C. González-Rodríguez, A. L. Thompson, A. S. Weller and M. C. Willis, *J. Am. Chem. Soc.*, 2012, **134**, 2906–2909.

31 G. M. Adams and A. S. Weller, *Coord. Chem. Rev.*, 2018, **355**, 150–172.

Chapter 3: Cyclotrimerisation and Optimisation of Hydroacylation

3.1. Introduction

Metal catalysed processes are commonly used in the manufacturing-scale synthesis of active pharmaceutical ingredients.[1,2] In order to use these methodologies, they must not only enable important synthetic transformations, they must also be highly efficient in reagent stoichiometry and catalyst loading, particularly if precious metals and expensive ligands are being used. Having established that competitive cyclotrimerisation occurs at the end of hydroacylation catalysis, we sought to establish the mechanism of how these catalytic pathways interact. With the ultimate goal, to develop a method that is selective for hydroacylation using low catalyst loadings and equal stoichiometries of reagents.

This chapter discusses how the mechanism of 1-octyne cyclotrimerisation was elucidated, including the initial catalytic resting state and how the catalyst is transformed into a poorly active *α*-pyran complex. The mechanistic scenario for when the catalytic cycles becomes competitive is shown and this understanding is used to optimise the reaction selectivity, by reducing the catalyst loading. Further optimisation then demonstrated how this process can be efficiently performed on a 5-gram scale.

3.2. Alkyne Cyclotrimerisation and Catalytic Resting States

As shown in the previous chapter cyclotrimerisation of 1-octyne **3.1** to form tri-*n*-hexylbenzenes **3.3a**/**3.3b** becomes competitive at the later stages of hydroacylation catalysis, when no free aldehyde remains. To study this process in more detail, in the absence of aldehyde, 1-octyne [0.20 M] was reacted with catalyst [Rh(*cis*-κ^2-$_{P,P}$-DPEPhos)(acetone)$_2$][BAr$^F{}_4$] **3.2** (5 mol%, 0.01 M) in acetone at 25 °C. This slowly (12 h) gave a 66% ^{1}H NMR yield of tri-*n*-hexylbenzene products **3.3a**/**3.3b** in a 2 : 1 ratio respectively (Scheme 3.1).

As measured by *in situ* NMR spectroscopy, complex **3.2** is immediately consumed at the start of catalysis and after 5 minutes a new resting state is observed which is assigned to three isomers of the Rh(III)-metallacyclopentadiene[3,4] complex [Rh(*mer*-κ^3-$_{P,O,P}$-DPEPhos)(L)((CH)$_2$(C$_6$H$_{13}$))$_2$][BAr$^F{}_4$] **3.4a** (L = 1-octyne). Over 12 hours these resonances decreased in intensity, with concomitant increase in the

Scheme 3.1. Cyclotrimerisation catalysis[a]

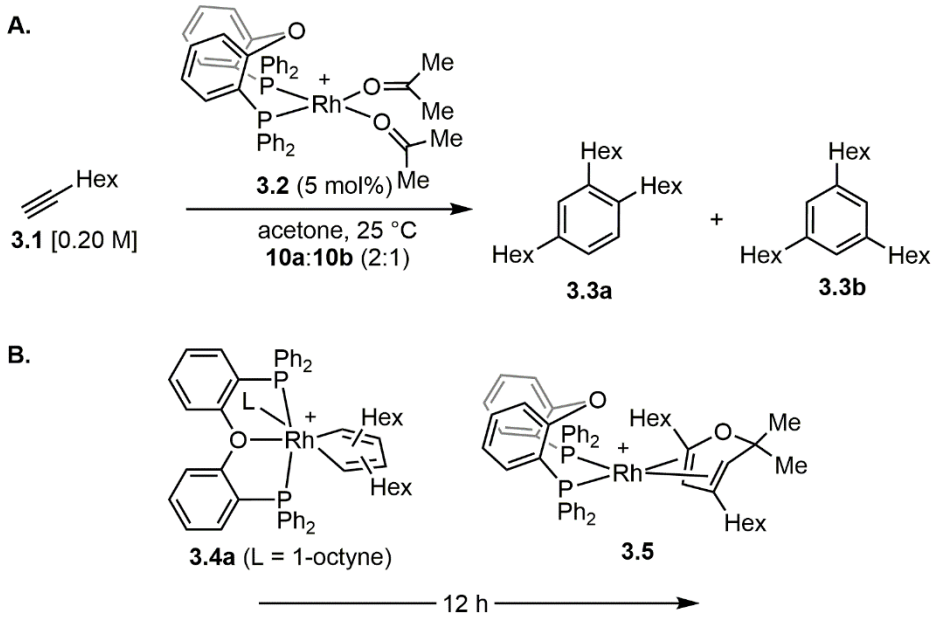

[a]BAr^F_4 anions omitted for clarity

concentration of a new species, characterized as the Rh(I)-*α*-pyran complex [Rh(*cis*–κ^2-$_{P,P}$-DPEPhos)(κ^2-2,2-methyl-4,6-*n*-hexyl-*α*-pyran)][BAr^F_4] **3.5**.

Metallacyclopentadiene complex **3.4** and its acetonitrile analogue were characterized *in situ* by $^{31}P\{^1H\}$ NMR spectroscopy and ESI-MS. The metallacyclopentadienes were formed by the addition of 1-octyne [0.20 M] to catalyst [Rh(*cis*-κ^2-$_{P,P}$-DPEPhos)(acetone)$_2$][BAr^F_4] **3.2** (5 mol%, 0.01 M) in acetone at 25 °C, the acetonitrile analogue was then formed by the addition of acetonitrile (2 eq.) to the same mixture after 5 minutes reaction time (Figure 3.1).

After 5 mins reaction time, before the addition of acetonitrile, a set of three overlapping broad doublets were observed in the $^{31}P\{^1H\}$ NMR spectrum at δ 23.9 [J_{RhP} = 125 Hz], δ 23.1 [J_{RhP} = 130 Hz] and δ 22.9 [J_{RhP} = 135 Hz]. These were assigned to three different isomers of the Rh(III) complex [Rh(*mer*-κ^3-$_{P,O,P}$-DPEPhos)(1-octyne)((CH)$_2$(C(C_6H_{13}))$_2$][BAr^F_4] **3.4a**. In the ^1H NMR spectrum, multiple peaks were observed between δ 5.64 and δ 5.29 (total integral = 2) which are assigned to the alkenyl groups of the metallacyclopentadiene. After the addition of 2 equivalents of acetonitrile, the alkenyl peaks shifted to δ 5.72 – δ 5.43 (total integral = 2) and in the $^{31}P\{^1H\}$ NMR spectrum the resonances became a sharper set of three doublets at δ 24.8 [J_{RhP} = 128 Hz], δ 22.7 [J_{RhP} = 127 Hz] and

Figure 3.1. $^{31}P\{^{1}H\}$ NMR spectra of cyclotrimerisation resting state after A) 5 mins B) Addition of acetonitrile (2 equivalents)[a]

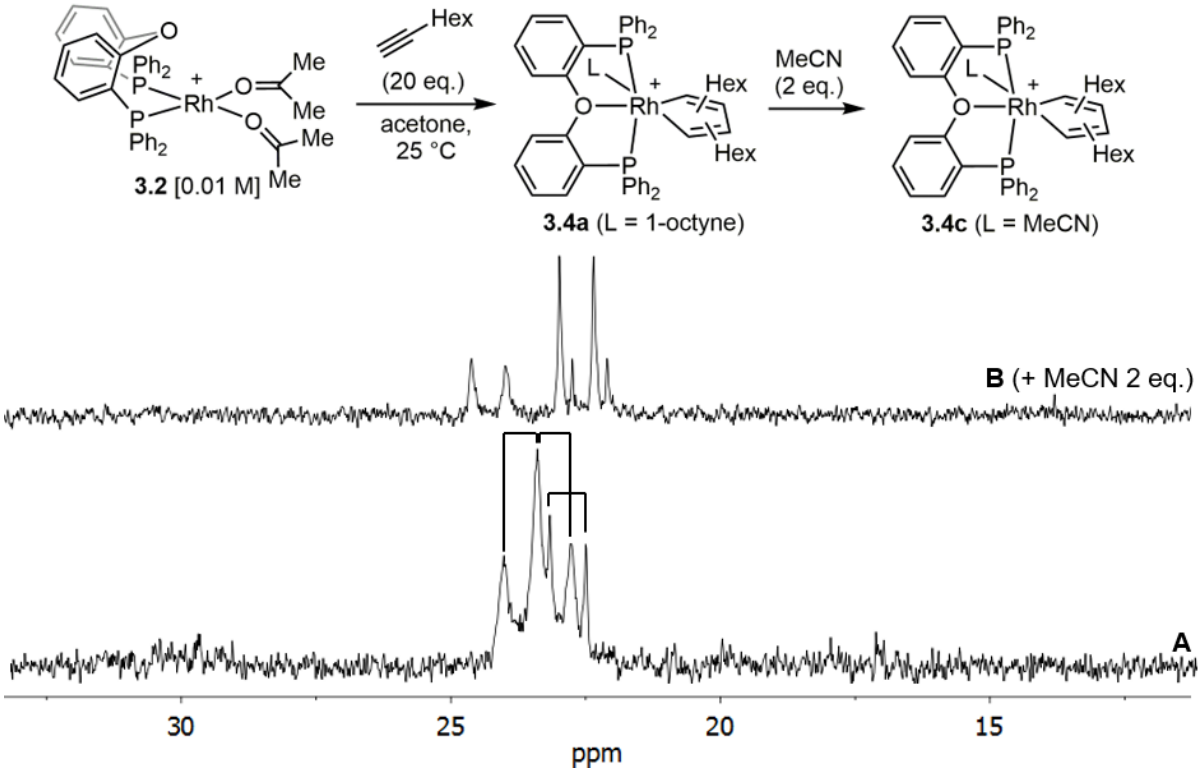

[a]BAr^{F}_{4} anions omitted for clarity

δ 22.4 [J_{RhP} = 130 Hz]. These observations are consistent with the formation of the Rh(III) complex [Rh(*mer*-κ^3-$_{P,O,P}$-DPEPhos)(NCMe)((CH)$_2$(C(C_6H_{13}))$_2$][BAr^{F}_{4}] **3.4c** (Figure 3.1).

In the ESI-MS, before addition of acetonitrile, a major peak at *m/z* = 861.29 is observed, which corresponds to and possesses the correct isotope pattern for a {Rh(DPEPhos)}$^+$ complex containing two 1-octyne fragments (Figure 3.2, A).

Two minor peaks at *m/z* = 919.33 and *m/z* = 971.40 were also observed, which are assigned as complexes **3.4b** (L = acetone) and **3.4a** (L = 1-octyne) respectively. After acetonitrile was added, the major peak remains unchanged and both minor peaks disappear and a signal at *m/z* = 902.31 is observed which is assigned as complex **3.4c** (L = acetonitrile) (Figure 3.2, B).

The collected data is consistent with the assignment of a 6 coordinate κ^3-DPEPhos metallacyclopentadiene complex possessing a labile ligand. Under ESI-MS conditions the labile ligand undergoes a low energy dissociation resulting in the major observed peak being a {Rh(DPEPhos)(1-octyne)$_2$}$^+$. In the $^{31}P\{^{1}H\}$ NMR spectrum sharp peaks are observed with added acetonitrile, but broad

Figure 3.2. ESI-MS of cyclotrimerisation resting state after A) 5 mins B) Addition of acetonitrile (2 equivalents)

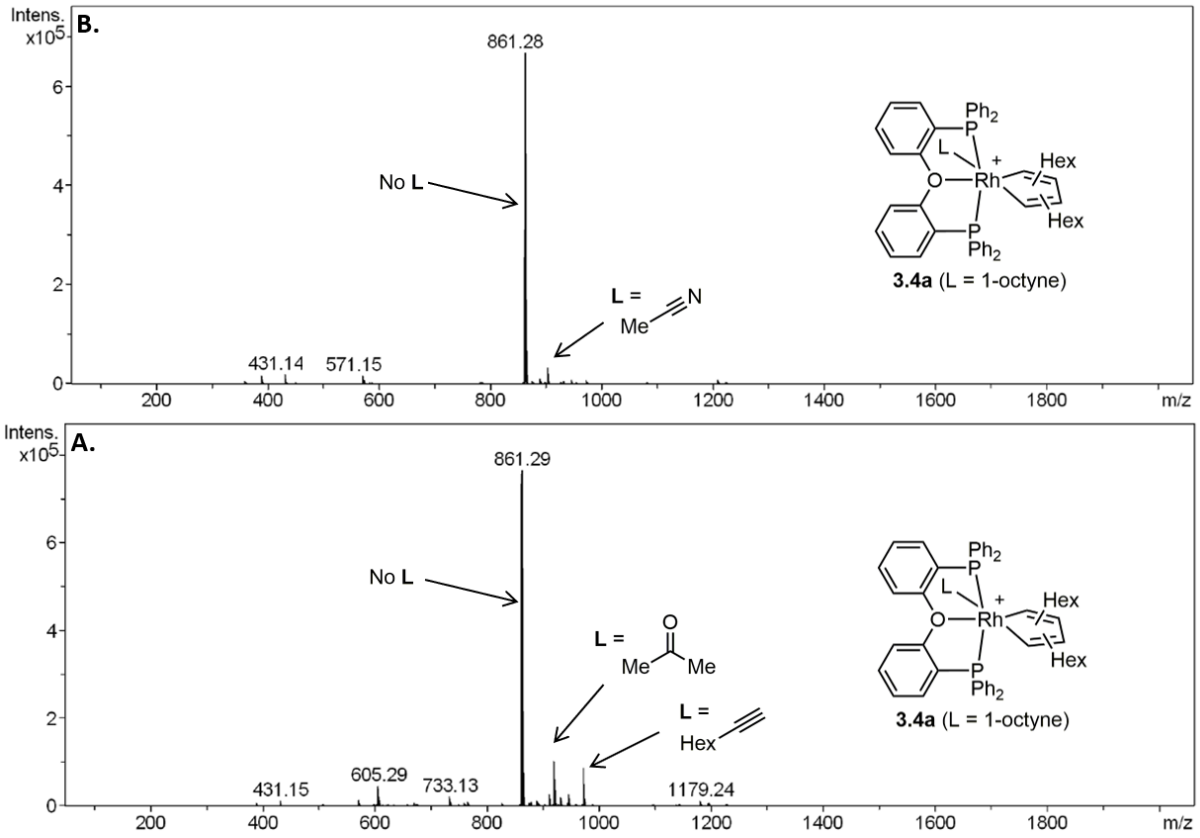

peaks are observed without, perhaps due to reversible dissociation of 1-octyne/acetone ligands under these conditions. Mechanistic studies (*vide infra*) are consistent with these complexes being acetone or 1-octyne bound complexes during catalysis and show that reversible dissociation of these ligands is in operation. The structural assignment also means that the high *trans* influence alkenyl ligands are *trans* to the low *trans* influence acetone and ether DPEPhos ligands.

The observation of closely related complexes in the $^{31}P\{^{1}H\}$ NMR spectrum is consistent with three isomers of the Rh(III)-metallacyclopentadiene complexes being present. We propose that they differ in the substitution pattern of the dienyl fragment but retain the core Rh(DPEPhos)$^{+}$ motif. $^{1}H/^{1}H$ COSY NMR experiments were used to characterize the isomers and suggest 2,4-, 3,4-, and 3,5-hexyl isomers are present. This is because no mutual $^{3}J_{HH}$ coupling between the alkenyl peaks was observed, which would only by expected in the 2,5-isomer (Figure 3.3).

Metallacyclopentadiene complexes such as **3.4** are well established as intermediates in alkyne cyclotrimerisation reactions and are formed by [2+2+2] oxidative-metallacyclisation.[4–8] The observation

Figure 3.3. Isomers of metallacyclopentadiene complex 3.4[a]

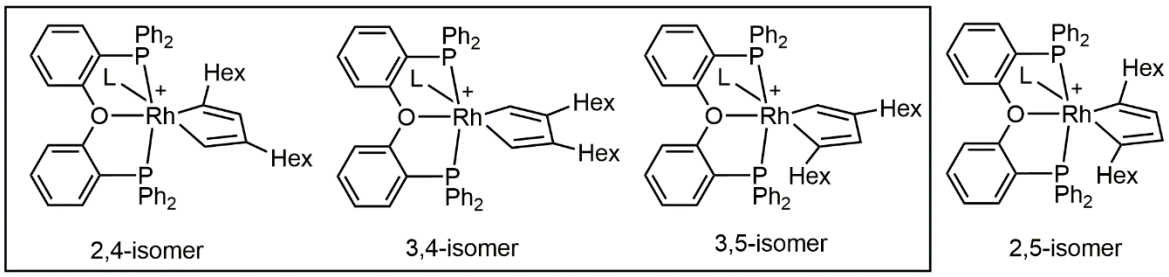

[a]BAr^F_4 anions omitted for clarity

of different metallacyclopentadiene isomers is consistent with multiple isomers of tri-*n*-hexylbenzenes being observed during catalysis, because the insertion of the third alkyne is dependent on the regiochemistry of the metallacyclopentadiene. The different metallacyclopentadiene isomers are formed because the alkynes can undergo the initial oxidative-metallacyclisation in a: ***a***) tail to tail, ***b***) head to tail or ***c***) head to head fashion (Figure 3.4).

Figure 3.4. Alkyne coordination for [2+2+2] oxidative-metallacyclisation[a]

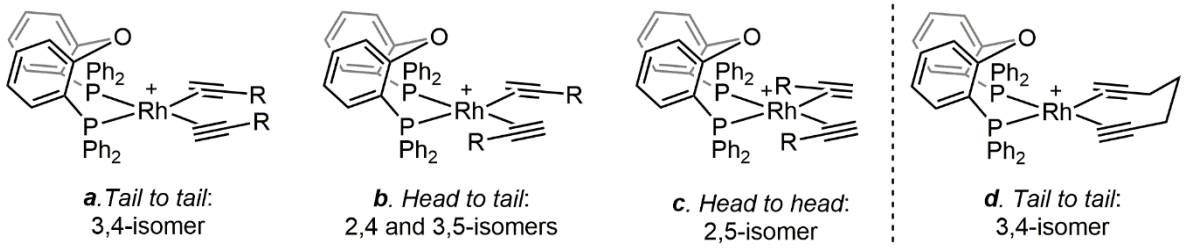

[a]BAr^F_4 anions omitted for clarity

The 2,5-metallacylopentadiene-isomer is not an observed resting state, which can be rationalised by the increased steric interactions in the transition state of metallacyclisation from the head to head alkyne bound complex (Figure 3.4, ***c***), where the alkyl groups point toward the DPEPhos ligand. Based on this understanding, it was predicted that only one isomer would be observed as the resting state for the cyclotrimerisation of the tethered diyne 1,6-heptadiyne **3.6**, because the tether will restrict the metallacyclisation to being only tail to tail (Figure 3.4, ***d***). To test this, the reaction of *bis*-acetone complex **3.2** with 20 equivalents of 1,6-heptadiyne, followed by the addition of 2 equivalents of acetonitrile, after 5 minutes reaction time, was monitored by $^{31}P\{^1H\}$ NMR spectroscopy and ESI-MS (Scheme 3.2).

Scheme 3.2. *In situ* formation of complex 3.7[a]

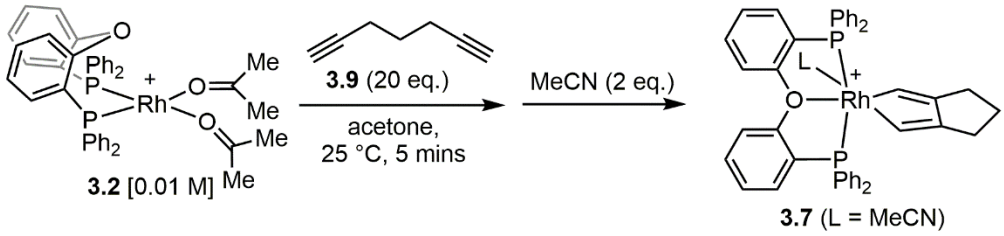

[a]BAr^F_4 anions omitted for clarity

In the $^{31}P\{^1H\}$ NMR a doublet at δ 25.6 [J_{RhP} = 125 Hz] was observed, indicating only one isomer of complex **3.7** is present in solution, with the chemical shift and coupling constant being similar to those observed for the 1-octyne cyclotrimerisation (See Figure 3.1). In the ESI-MS at 30 V, *m/z* = 733.13 and 774.16 were observed in a 7 : 1 ratio, which correspond to the cations $\{Rh(DPEPhos)(CH(CH_2)_3CH)\}^+$ and $\{Rh(DPEPhos)(CH(CH_2)_3CH)(NCMe)\}^+$ respectively. When the voltage of the spray was increased to 120 V, the *m/z* = 733.13 peak increased in intensity and the peak at *m/z* = 774.16 disappeared, indicating that the acetonitrile group in the complex is labile under ESI-MS conditions. These results are consistent with the assignment of the metallacyclopentadiene complexes being the resting state of 1-octyne cyclotrimerisation.

3.3. Characterisation of the *α*-Pyran Complex

The metallacyclopentadiene resting state is slowly converted to the *α*-pyran complex **3.5**, which became the only observed species after 12 hours of 1-octyne cyclotrimerisation (Scheme 3.1) The complex was isolated as a non-crystallisable oil using the $[Al(OC(CF_3)_3)_4]$ ($[AlO^F_4]$) anion,[9] and characterized by ^1H, $^{13}C\{^1H\}$, $^{31}P\{^1H\}$ NMR, nOeSY spectroscopy and ESI mass spectrometry, the nOeSY spectrum (0 – 4 ppm) is shown in Figure 3.5.

In the ESI-MS a major peak at *m*/z = 919.31 is observed, which corresponds to a $\{Rh(DPEPhos)\}^+$ complex containing two 1-octyne fragments and 1 acetone fragment. In the $^{31}P\{^1H\}$ NMR spectrum two doublet of doublets were observed at δ 20.7 [J_{RhP} = 209; J_{PP} = 31 Hz], δ 17.6 [J_{RhP} =169; J_{PP} = 31 Hz], indicating a single Rh(I) species with inequivalent *cis*-phosphines. In the ^1H NMR spectrum the signals indicated that only one isomer of coordinated *α*-pyran was present. The alkene peaks were observed as broad singlets at δ 3.85 and δ 2.76, which are shifted upfield compared unbound *α*-pyran (*vide infra*),

Figure 3.5. nOeSY correlation spectrum of *α*-pyran-complex

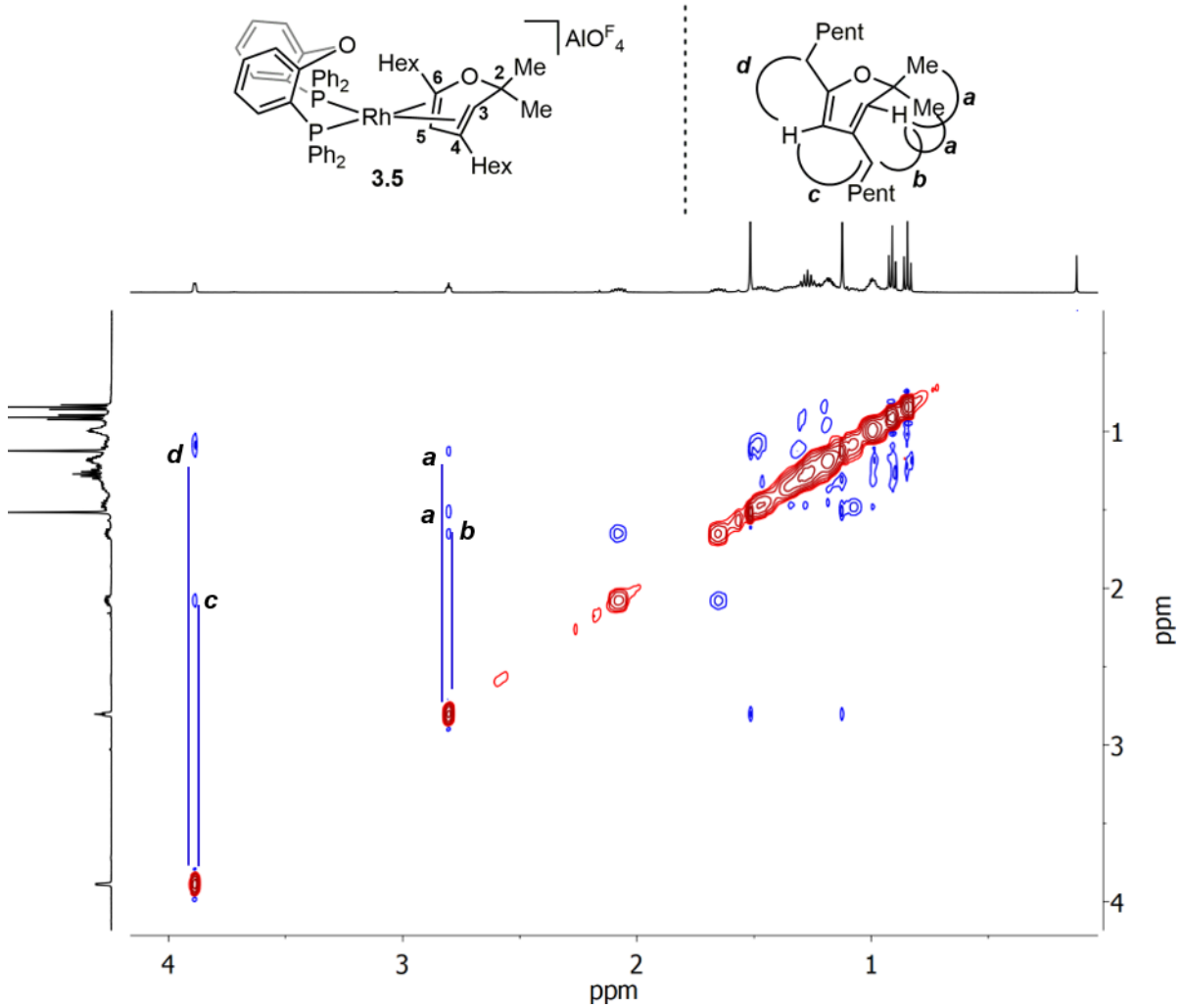

indicating that the alkenes are coordinated to the rhodium metal centre.[10] The methyl groups were observed as two distinct singlets at δ 1.48 and δ 1.08, indicating they are in different environments. Both sets of allylic protons are diastereotopic, due to being in a chiral environment, with one set observed as two doublet of doublet of doublets at δ 2.05 and δ 1.61 and the other as two partially obscured peaks at δ 1.45–1.39 and δ 1.07–1.00.

The stereochemistry of the α-pyran was assigned by nOeSY correlation spectroscopy (Figure 3.5), where the *gem*-2,2-dimethyl protons at δ 1.48 and δ 1.08 only show correlation between themselves and with the 3-postion alkene proton at δ 2.76 (Figure 3.5, ***a***). The 3-position alkene at δ 2.76 also correlates with the 4-position allylic CH_2-proton at δ 1.61 (Figure 3.5, ***b***). The other 4-position allylic CH_2-proton at δ 2.05 correlates with the 5-position alkene-proton at δ 3.85 (Figure 3.5, ***c***). The 5-position alkene-proton at δ 3.85 itself correlates to the 6-position allylic proton at δ 1.07–1.00 (Figure 3.5, ***d***). These

collected data are consistent with the assignment of a 2,2-dimethyl-4,6-di-*n*-hexyl-*α*-pyran. *α*-Pyran coordinated complexes with other metals have been previously reported,[11] and the catalytic hetero–cyclotrimerisation of diynes with ketones,[12–14] or aryl ethynyl ethers with ketones catalysed by Rh(I)-complexes,[15] to give *α*-pyrans is known.

Unbound *α*-Pyrans can exist in equilibrium with their valance isomer *cis*-dienones by retro-electrocyclisation (Figure 3.6).

Figure 3.6. Potential equilibrium of *α*-Pyran 3.8 with its *cis*-dienone valance isomer

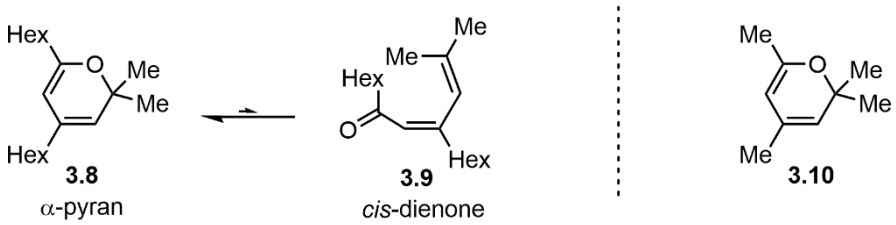

Unbound 2,2-disubstitued *α*-pyrans have been shown to strongly bias the equilibrium, in solution, towards the *α*-pyran valence isomer and the structurally related 2,2,4,6-tetramethyl-*α*-pyran **3.10** has been shown to exists exclusively as the *α*-pyran.[16,17] Evidence for the bound *α*-pyran valance isomer in complex **3.5** is found in the nOeSY correlation spectrum, were both methyl groups are correlated to the 3-position alkene, which would not be observed in the bound *cis*-dienone valance isomer, due to the sp^2 centre.

Formation of the *α*-pyran was confirmed by release of the free organic fragment by addition of 1 equivalent of triphenylphosphine to the *α*-pyran-complex **3.5** (Scheme 3.3).

Scheme 3.3. Addition of triphenylphosphine to pyran-complex 3.5[a]

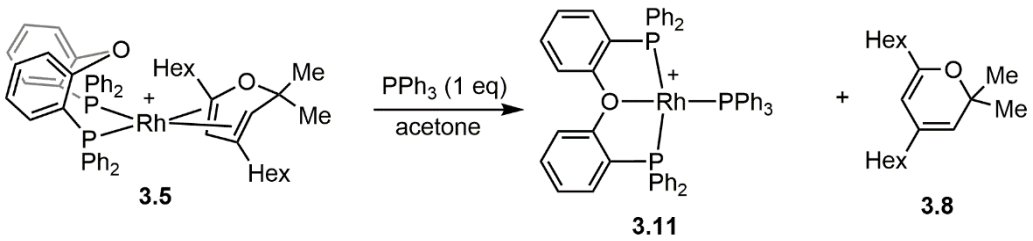

[a]BAr^F_4 anions omitted for clarity

Characterisation of the unbound *α*-pyran **3.8** by ^1H and $^{13}C\{^1H\}$ spectroscopy indicated that it exists

exclusively as the α-pyran isomer. In the ^{1}H NMR spectrum the α-pyran alkene peaks appeared as downfield shifted (compared to Rh-bound α-pyran **3.5**) singlets at δ 4.93 and δ 4.81. The allylic peaks were non-diastereotopic triplets at δ 2.03 and δ 1.96 and a single methyl environment at δ 1.29 was observed. These peaks correspond well with reported α-pyrans with related structures.[18–21]

The formed complex [Rh(*mer*-κ^3-$_{P,O,P}$-DPEPhos)(PPh_3)][BAr^F_4] **3.11** was independently synthesised by addition of 1 equivalent triphenylphosphine to the complex [Rh(*cis*-κ^2-$_{P,P}$-DPEPhos)(acetone)$_2$][BAr^F_4] **3.2** and was characterized by ^{1}H, ^{31}P{^{1}H} NMR spectroscopy and ESI-MS. In the ^{31}P{^{1}H} NMR spectrum the triphenylphosphine environment was observed as a doublet of triplets at δ 51.6 [J_{RhP} = 206 Hz; J_{PP} = 36 Hz] and the DPEPhos environment was observed as a doublet of doublets at δ 31.8 [J_{RhP} = 146 Hz; J_{PP} = 36 Hz], in a 1 : 2 ratio respectively. The small phosphine-phosphine coupling constants are consistent with the *mer*-geometry of the DPEPhos ligand, with the phosphine environments both *cis* to the triphenylphosphine ligand.

3.4. Kinetics and Mechanism of Cyclotrimerisation

Having established the catalytic resting states of cyclotrimerisation, the kinetics at the early stages of the reaction were interrogated by the initial rates method. The first 10% of 1-octyne consumption was measured by ^{1}H NMR spectroscopy using the BAr^F_4 anion as an internal standard. In this temporal regime no α-pyran-bound complex **3.5** was detected (Table 3.1 and Figure 3.7).

Table 3.1. Initial rates of Cyclotrimerisation

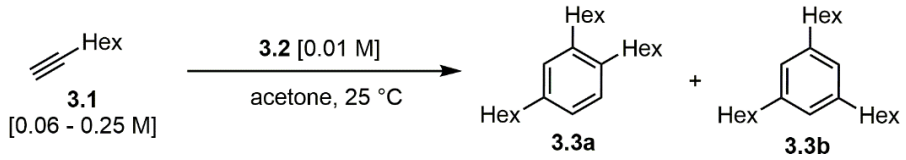

Entry	[1-octyne] M	[Rhodium cat.] M	Rate (10^{-5} Ms^{-1})
1	0.06	0.01	0.38 ± 0.01
2	0.08	0.01	0.44 ± 0.01
3	0.10	0.01	0.53 ± 0.04
4	0.18	0.01	1.03 ± 0.02
5	0.22	0.01	1.02 ± 0.02
6	0.25	0.01	1.04 ± 0.03

Figure 3.7. Cyclotrimerisation initial rates

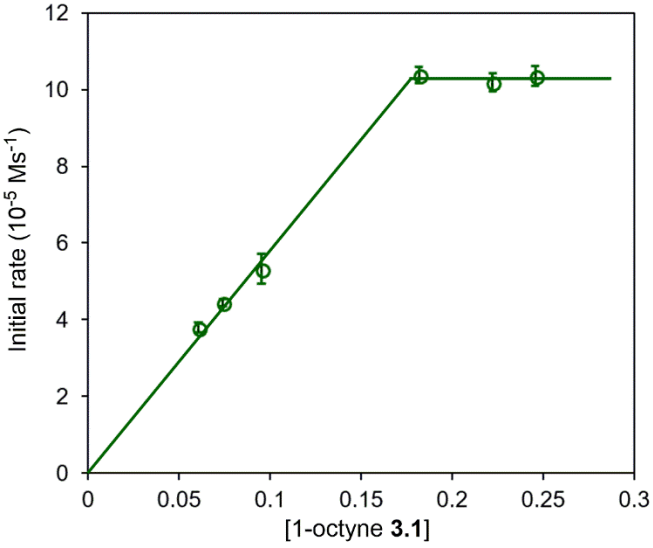

Variation of the concentration of 1-octyne **3.1** shows two distinct regimes in the order of 1-octyne: at lower concentrations [<0.15 M], first order behaviour is observed, which switches to zero order at higher concentrations [>0.15 M]. When combined with the observed resting of a metallacyclopentadiene **3.4** at the early stages of the reaction, a mechanism for cyclotrimerisation is proposed (Scheme 3.4).

Scheme 3.4. Cyclotrimerisation mechanism[a]

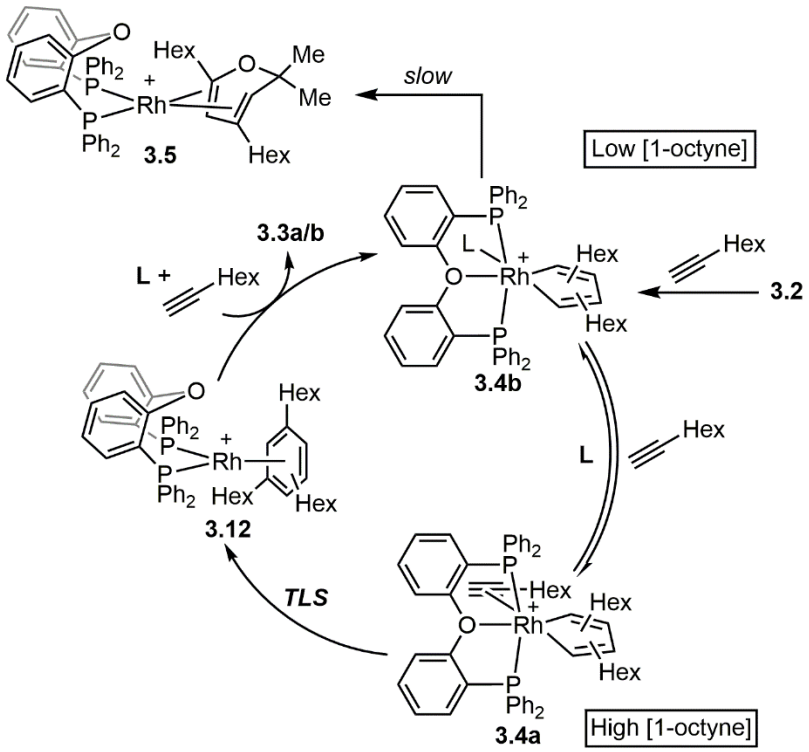

[a]BAr^F_4 anions omitted for clarity

Starting from *bis*-acetone complex **3.2**, coordination of 1-octyne and oxidative-metallacyclisation forms either metallacyclopentadiene **3.4a** or **3.4b** depending on the alkyne concentration. At higher concentrations of alkyne [>0.15 M], quasi-irreversible binding of the 1-octyne occurs, as indicated by the zero-order kinetics in alkyne, and metallacyclopentadiene **3.4a** (L = 1-octyne) is the catalytic resting state. At lower concentrations of alkyne [<0.15 M], binding of acetone becomes quasi-irreversible, as indicated by the first order kinetics in 1-octyne, and metallacyclopentadiene **3.4b** (L = acetone) becomes the catalytic resting sate.

From the alkyne bound metallacyclopentadiene **3.4a**, a turnover-limiting arene forming process gives the arene-bound complex **3.12**. Subsequent and rapid displacement of the arene from the metal centre by 1-octyne then reforms the, alkyne concentration dependant, metallacyclopentadiene resting state. Preliminary studies show that addition of tri-*n*-hexylbenzene **3.3a**/**3.3b** to *bis*-acetone complex **3.2**, results in an equilibrium mixture of 1 : 14 that strongly favours the *bis*-acetone complex **3.2**. This lability is likely due to the combined electronic and steric effects of the wide-bite angle DPEPhos.[22]

There are two commonly proposed mechanisms for arene formation from a metallacyclopentadiene: i) intramolecular [4+2] cycloaddition of the metallacyclopentadiene with alkyne followed by isomerisation; ii) insertion of coordinated alkyne followed by reductive elimination. Theoretical studies of Ir(I)-catalysed cyclotrimerisation have suggested that substituted alkynes favour the insertion mechanism, whereas the reaction of unsubstituted acetylene likely proceeds *via* an intramolecular [4+2] cycloaddition-type mechanism.[23,24] This may suggest an insertion-type mechanism is in operation for this Rh(I)-catalysed system.

The mechanism for the formation of the *α*-pyran complex **3.5**, which becomes the resting state of, and slows, cyclotrimerisation catalysis, may proceed *via* acetone bound metallacyclopentadiene **3.4b**. Due to the polarized nature of the acetone bond, this reaction would be expected to proceed by an insertion, reductive elimination-type reaction sequence *via* an alkenyl-alkoxide intermediate (alkenyl-alkoxide complexes have been isolated for other metals[25]). That the 4,6-hexyl-*α*-pyran-isomer is formed exclusively implies that, if in operation, one of the insertion/reductive elimination steps is selective, depending on the isomer of acetone bound metallacyclopentadiene **3.4** (Scheme 3.5).

Scheme 3.5. Mechanism of *α*–pyran formation from metallacyclopentadiene[a]

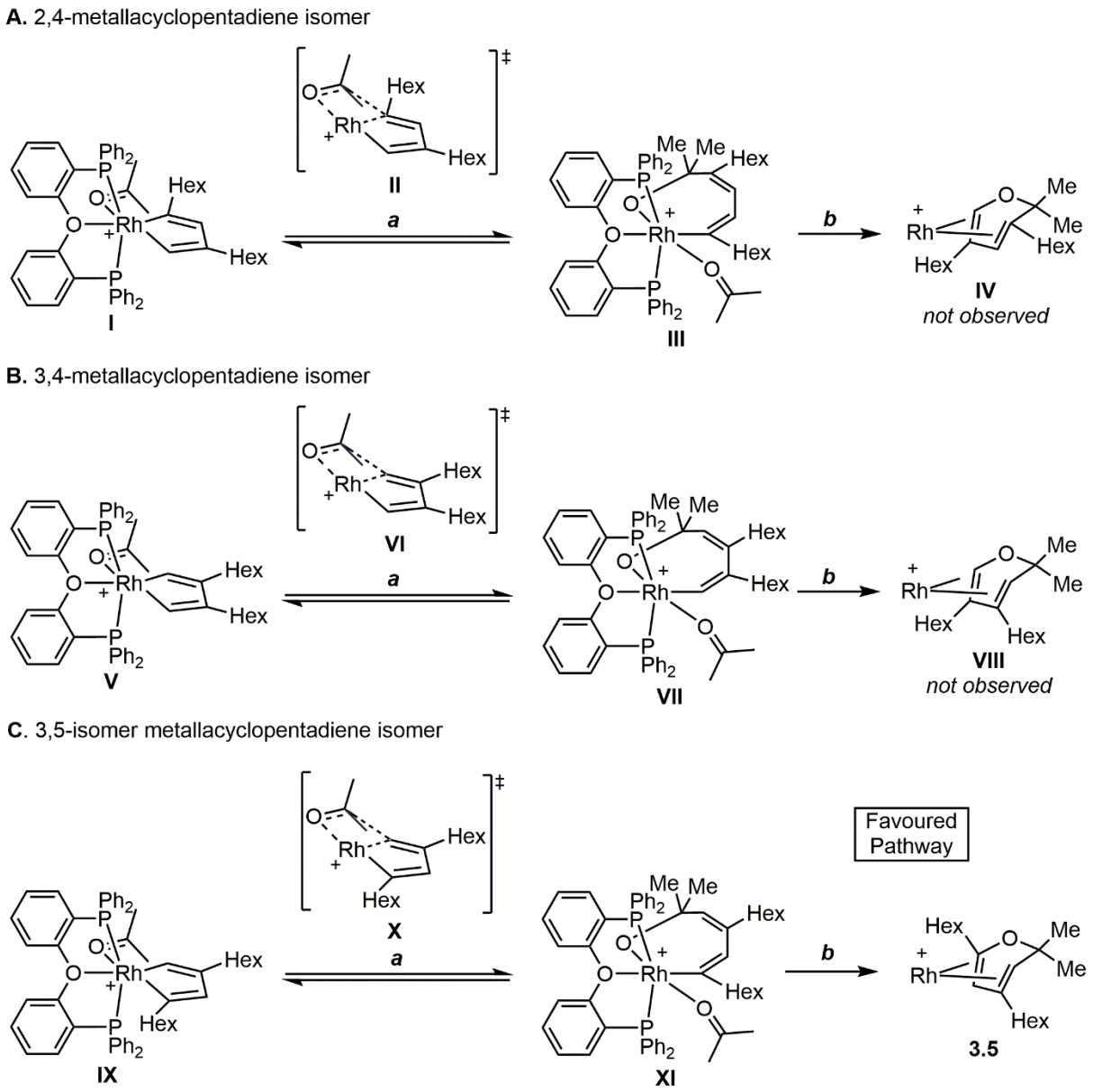

[a]BAr^F_4 anions omitted for clarity

Inspection of the three-acetone bound metallacyclopentadiene isomers (**I**, **V**, **IX**) and consideration of the migratory insertion and reductive coupling steps from them (***a*** and ***b***), indicates that the observed 4,6-hexyl-isomer of *α*–pyran complex **3.5** must come from the 3,5-metallacyclopentadiene isomer **IX**. From the proposed transition states of the insertion step from each isomer (**II**, **VI**, **X**), insertion from intermediates **V** and **IX** is expected to be favoured over **I**, due to the increased steric interactions in transition state **II** compared to **VI** and **X**, leading to *α*–pyran complex **IV** which is not observed.

Comparison of the three so-formed alkoxide-alkenyl intermediates (**VII**, **XI**) shows that reductive coupling from **VII** is between an alkoxide and an unsubstituted alkenyl group, whereas reductive coupling from intermediate **XI** is between an alkoxide and a hexyl-substituted alkenyl group. Because *α*–pyran complex **3.5** is the only observed isomer, we propose that reductive coupling from intermediate **XI** is more favourable than for **VII**. A potential reason for the increased rate of reductive elimination is the increased steric hinderance in **XI**, which promotes acetone ligand dissociation and therefore reductive elimination.[26] Because the transition sates (**VI** and **X**) for the migratory insertion step to form the alkenyl alkoxide intermediates **VII** and **XI** appear to be similar in energy, we propose that the migratory insertion step is reversible for both intermediates and that reductive coupling from **XI** is the rate limiting step. However, a reaction pathway that goes *via* κ^2/*fac*-DPEPhos intermediates cannot be ruled out, although no evidence for κ^2/*fac*-DPEPhos complexes have been observed.

3.5. Moving between catalytic cycles

Having established that *bis*-acetone complex **3.2** is a pre-catalyst for both hydroacylation and cyclotrimerisation. Combined with the observation that during hydroacylation catalysis (See Chapter 2, Figure 2.5) cyclotrimerisation becomes competitive with hydroacylation when no free aldehyde remains in solution. The link between the two cycles was investigated by monitoring the stoichiometric reactions of acyl hydride **3.13** in the presence and absence of excess aldehyde. The reactions of acyl hydride **3.13** (1 equivalent), 1-octyne (1 equivalent) with and without added aldehyde **3.14a** (1 equivalent), in acetone-d_6, were monitored by ^{1}H NMR spectroscopy using the $BAr^F{}_4$ anion as internal reference (Figure 3.8).

For the reaction with no added aldehyde, after 3 h, a 33% NMR yield of enones **3.15a** and **3.15b** and a 54% NMR yield of cyclotrimer products **3.3** was measured (Figure 3.8, A). In the ^{31}P{^{1}H} NMR spectrum a mixture of *bis*-acetone complex **3.2**, acyl hydride **3.13** and *α*-pyran-complex **3.5** was present in the relative ratio of 1 : 2 : 1 respectively. For the reaction with 1 equivalent of added aldehyde **3.14a**, a 97% ^{1}H NMR yield of enones **3.15a** and **3.15b** was observed with only traces of cyclotrimerisation detected, a dramatic shift in the reaction outcome (Figure 3.8, B). Accordingly, at the end of the reaction the only species observed in the ^{31}P{^{1}H} NMR spectrum was the acyl hydride complex **3.13**.

Figure 3.8. Stoichiometric reaction of acyl-hydride 3.13 and 1-octyne: A) 0 equivalents of aldehyde 3.14a; B) 1 equivalent of aldehyde 3.14a[a]

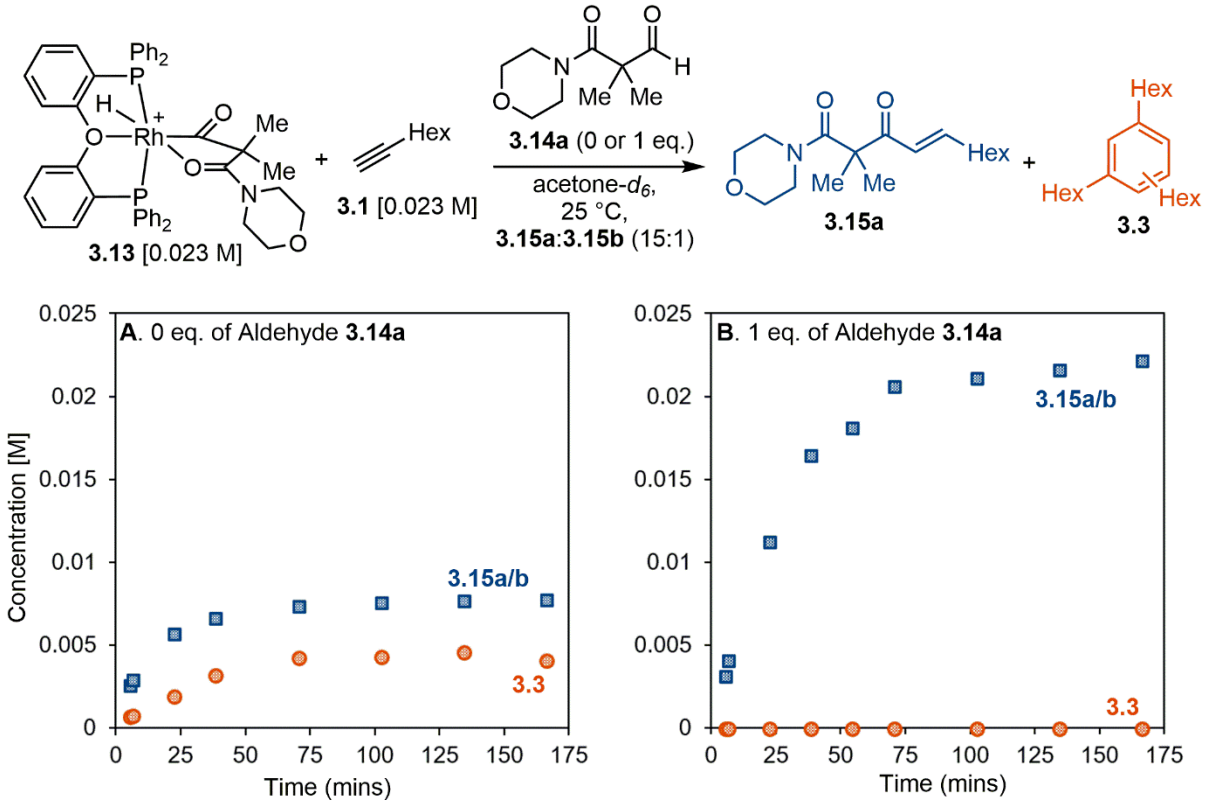

[a]Reaction profile as measured by ^{1}H NMR spectroscopy: ■ (enones **3.15a**/**3.15b**), ● (tri-*n*-hexylbenzenes **3.3a**/**3.3b**).

These experiments clearly demonstrate that cyclotrimerisation only becomes competitive when there is no free aldehyde present in solution because, as shown in Chapter 2, aldehyde binds *pseudo*-irreversibly to form acyl-hydride **3.13**. In catalysis, the point at which this happens will directly correlate to catalyst loading, as observed in the initial hydroacylation reaction using 5 mol% catalyst (See Chapter 2, Figure 2.5) where competitive cyclotrimerisation began at 94% yield of enones.

Having established the point at which cyclotrimerisation becomes competitive with hydroacylation, how the resting state changes after this point was analysed for the initial hydroacylation conditions. After 43 minutes, cyclotrimerisation became competitive and acyl-hydride **3.13** was consumed. Initially, the ^{31}P{^{1}H} NMR spectrum became broad and contained a mixture of the product bound complex **3.16** and the metallacyclopentadiene complex **3.4** (Scheme 3.6).

Scheme 3.6 Evolution of reaction resting state after acyl-hydride consumption[a]

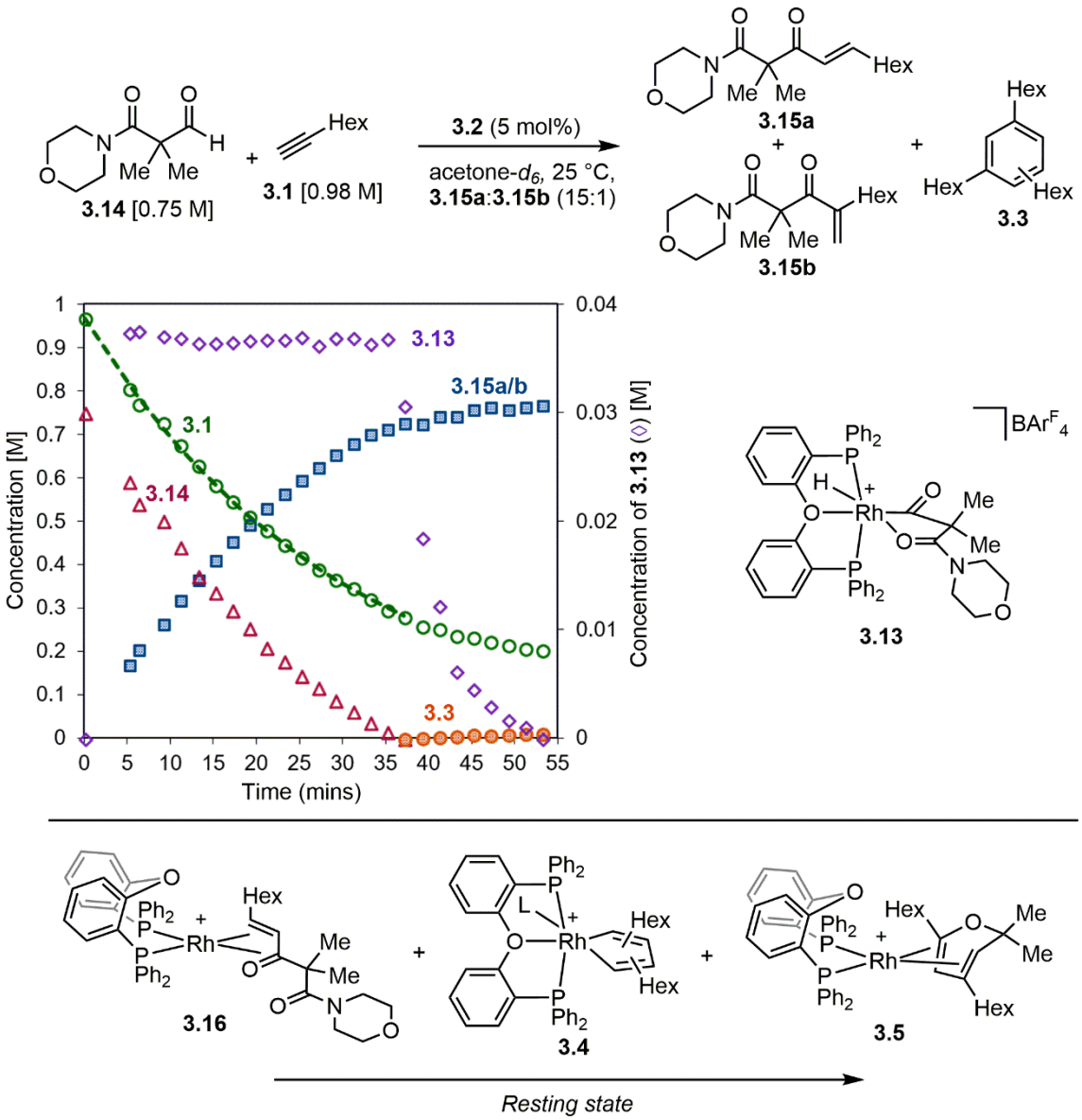

[a]BAr^F_4 anions omitted for clarity

After a 1 h reaction time and complete consumption of acyl-hydride a mixture of metallacyclopentadiene complex **3.4** and *α*-pyran complex **3.5** was observed, indicating the acyl-hydride complex is converted to cyclotrimerisation intermediates.

To confirm that product bound complex **3.16** can enter the cyclotrimerisation manifold, its reaction with 1-octyne **3.1** (20 equivalents, 0.20 M) in acetone-d_6 was performed at 25 ºC and then monitored periodically by ^{1}H and ^{31}P{^{1}H} NMR spectroscopy at 205 K, so to ensure the product bound complex appeared as sharp peaks by preventing fluxionality on the NMR timescale (Figure 3.9).

Figure 3.9. Monitoring of the addition of 1-octyne to product bound complex 3.16 by $^{31}P\{^{1}H\}$ NMR spectroscopy[a]

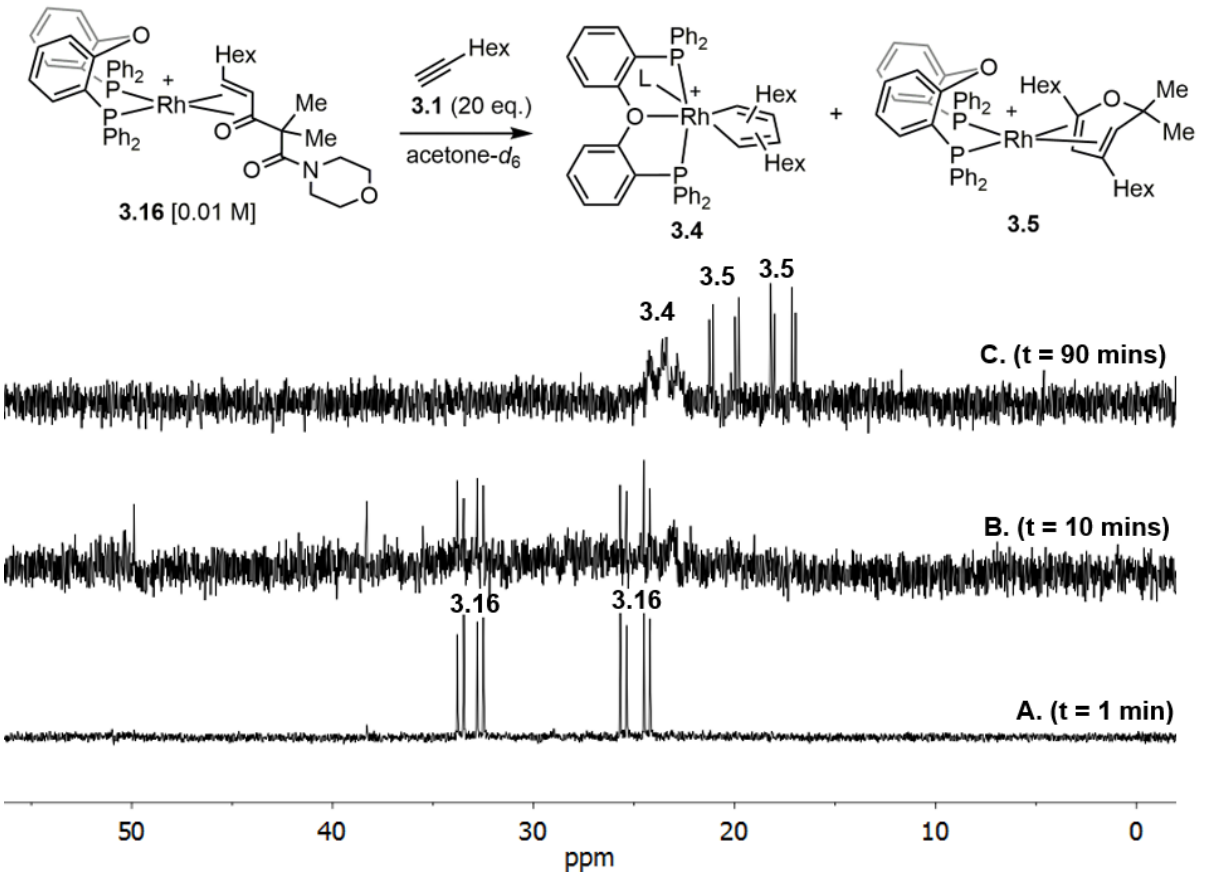

[a]BAr^{F}_{4} anions omitted for clarity

After 10 minutes, a mixture of product-bound complex **3.16** and metallacyclopentadiene complexes **3.4** were observed, which were subsequently converted to a mixture of metallacyclopentadiene complexes and *α*-pyran complex **3.5** after 90 minutes. The concomitant formation of tri-*n*-hexyl-benzenes **3.3** was confirmed by ^{1}H NMR spectroscopy, indicating cyclotrimerisation was in operation.

To then establish a complete mechanistic picture of the competing processes, the ability of different observed catalytic intermediates to move between reaction cycles was studied. The efficacy of the isolated *α*-pyran complex **3.5** in hydroacylation was investigated using similar conditions as for the initial hydroacylation reaction (Chapter 2, Figure 2.5), employing aldehyde **3.13** (0.75 M), 1-octyne **3.1** (1.5 M), catalyst **3.2** (0.038 M) at 25 ºC, and was monitored by ^{1}H NMR spectroscopy (Figure 3.10).

The reaction was considerably slower than the catalysis using *bis*-acetone pre-catalyst **3.2**, despite a higher concentration of alkyne (1.5 M compared to 0.98 M). The reaction took 80 minutes (compared

Figure 3.10. Hydroacylation reaction using *α*-pyran-complex 3.5 as catalyst

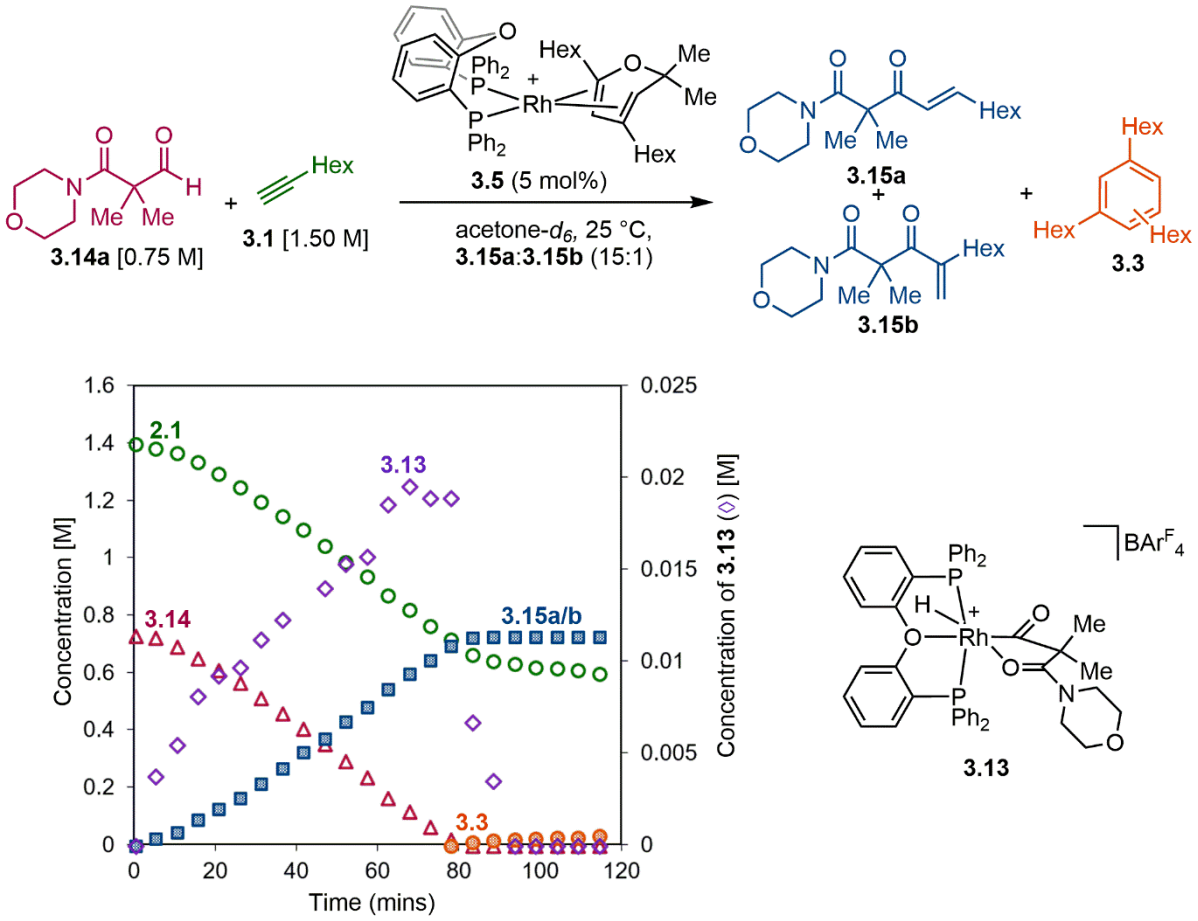

[a]Reaction profile as measured by ^{1}H NMR spectroscopy. Left axis: red △ = aldehyde **3.14a**, green ○ = 1-octyne **3.1**, blue ■ = enones **3.15a** and **3.15b**, and orange ● = tri-*n*-hexylbenzenes **3.3**. Right axis: purple ◇ = acyl-hydride, **3.13**.

to 45 minutes) to achieve full consumption of free aldehyde, at which point competitive cyclotrimerisation began. Monitoring the rhodium-speciation by ^{1}H NMR spectroscopy, revealed a slow conversion of the *α*-pyran-bound complex **3.5** to the acyl hydride **3.13**, with no other rhodium complexes being observed until full consumption of free aldehyde. This suggests that the *α*-pyran ligand is relatively strongly bound to the Rh(I)-centre, and its slow conversion to an active catalytic species slows the rate of hydroacylation. Once free aldehyde has been consumed (83 mins), similarly to the hydroacylation conditions with *bis*-acetone pre-catalyst **3.2** (See Figure 3.6), the concentration of acyl-hydride dramatically drops as cyclotrimerisation begins, until it approaches zero at 94 mins. This is due to formation of the metallacyclopentadiene resting state.

The ability for the metallacyclopentadiene resting **3.4** to then switch to hydroacylation reactivity was demonstrated by the addition of aldehyde **3.14a** (20 equivalents) to the metallacyclopentadiene **3.4a**

formed in the presence of excess alkyne (20 equivalents) (Scheme 3.7).

Scheme 3.7. Addition of aldehyde 3.14a to metallacyclopentadiene 3.4a[a]

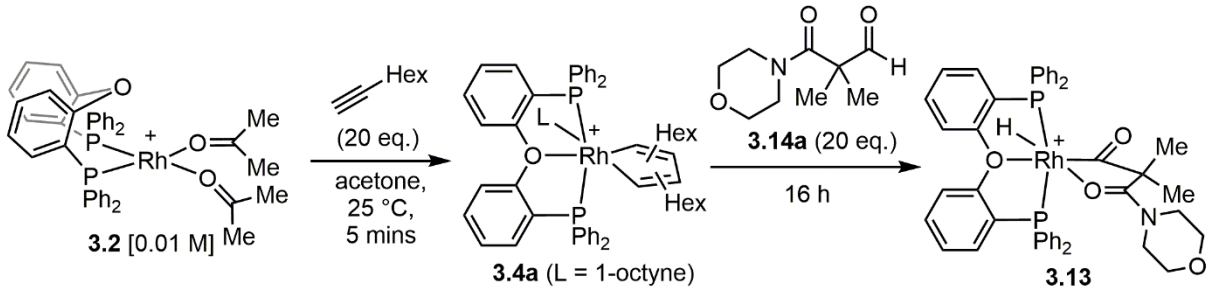

[a]BAr^F_4 anions omitted for clarity

This resulted in the slow formation of acyl-hydride **3.13** (ca. 16 h for full conversion), presumably *via* slow cyclotrimerisation to form tri-*n*-hexyl-benzene complex **3.12**, which then rapidly reacts with aldehyde. The slow conversion of cyclotrimerisation catalytic intermediates to hydroacylation catalysis was further exemplified by the catalytic recharging experiment with aldehyde **3.14a** [0.75 M], 1-octyne **3.1** [0.98 M], *bis*-acetone catalyst **3.2** in acetone-d_6 (5 mol%) at 25 ºC. After the hydroacylation reaction had reached completion (*ca*. 60 mins) the reaction mixture was recharged with aldehyde **3.14a** [0.75 M] and 1-octyne **3.1** [0.98 M] (Figure 3.11).

Figure 3.11. Hydroacylation recharging experiment with excess 1-octyne

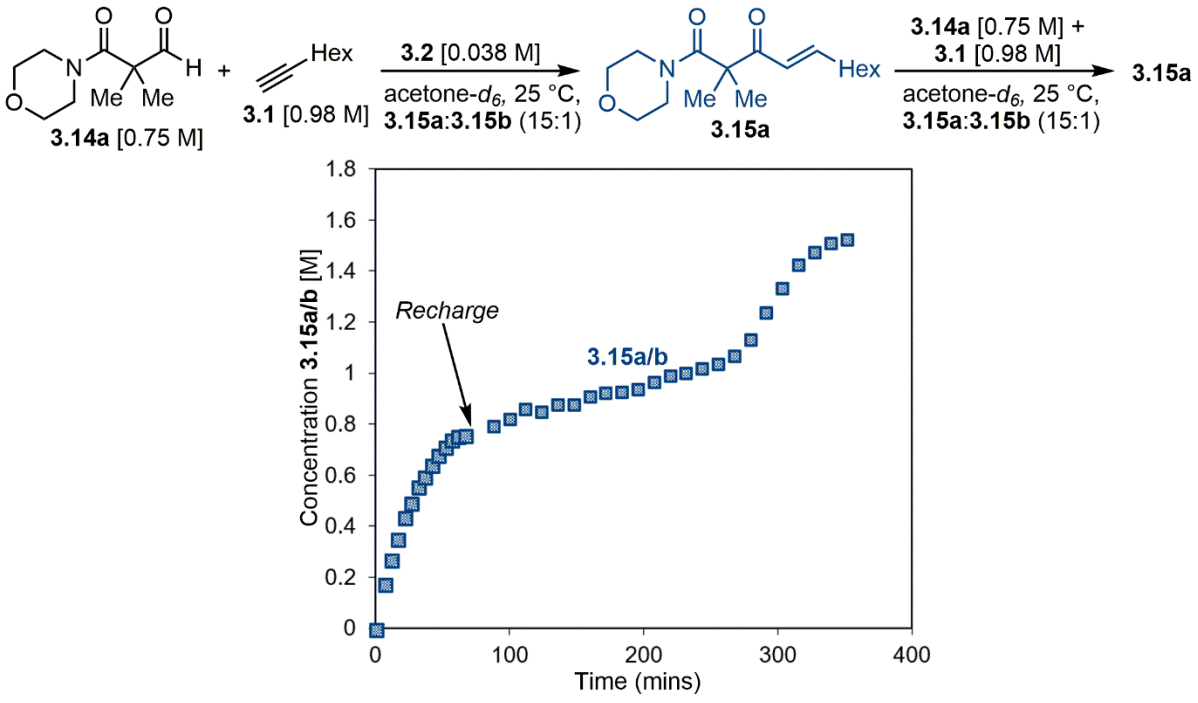

Before recharging the reaction, the catalyst speciation was probed by $^{31}P\{^{1}H\}$ NMR spectroscopy which indicated a mixture of metallacyclopentadiene complexes **3.4** and *α*-pyran complex **3.5** were present. This means acyl-hydride was completley consumed and that cyclotrimiersation was in operation, as confimed by the obsrvation of tri-*n*-hexylbenzenes **3.3** by ^{1}H NMR spectroscopy. After the second recharge a clear induction period is observed until 300 minutes, at which point the catalysis accelerates until it reaches competition. The induction period is a result of the slow conversion of metallacyclopentadiene **3.4** and *α*-pyran **3.5** complexes to the acyl-hydride, the resting state of hydroacylation catalysis.

3.6. Overall Mechanistic Landscape

Based on the mechanistic findings from both Chapter 2 and Chapter 3 an overall mechanistic picture for hydroacylation and cyclotrimerisation is presented (Scheme 3.8).

The resting state of hydroacylation (Cycle A) is acyl-hydride **3.13**, due to strong aldehyde binding, and the rate determining step is proposed to be hydride insertion. When the concentration of free aldehyde approaches zero, cyclotrimerisation (Cycle B) becomes competitive. At this point, when the remaining acyl hydride **3.13** turns over in hydroacylation, there is no aldehyde left to reform it and with free alkyne now effectively in excess, the resting state moves to the metallacyclopentadiene, (e.g. **3.4a**) *via* enone-bound complex **3.16**. Addition of aldehyde **3.14a** moves the resting state back to acyl-hydride **3.13**, albeit slowly.

The key deduction for the development of a selective hydroacylation reaction is that cyclotrimerisation becomes competitive when the concentration of free aldehyde approaches zero, with the remaining aldehyde being bound to rhodium as the acyl-hydride. Up to this point the reaction is completely selective for hydroacylation. This means that the catalyst loading determines the yield of enones, at the point cyclotrimerisation becomes competitive (i.e. at 5 mol% catalyst loading, cyclotrimerisation becomes competitive at 95% enone yield). Therefore, it was proposed that reducing catalyst loading would increase the selectivity for hydroacylation, by shifting the point at which cyclotrimerisation becomes competitive to higher yields of enone.

Scheme 3.8. Overall mechanistic landscape

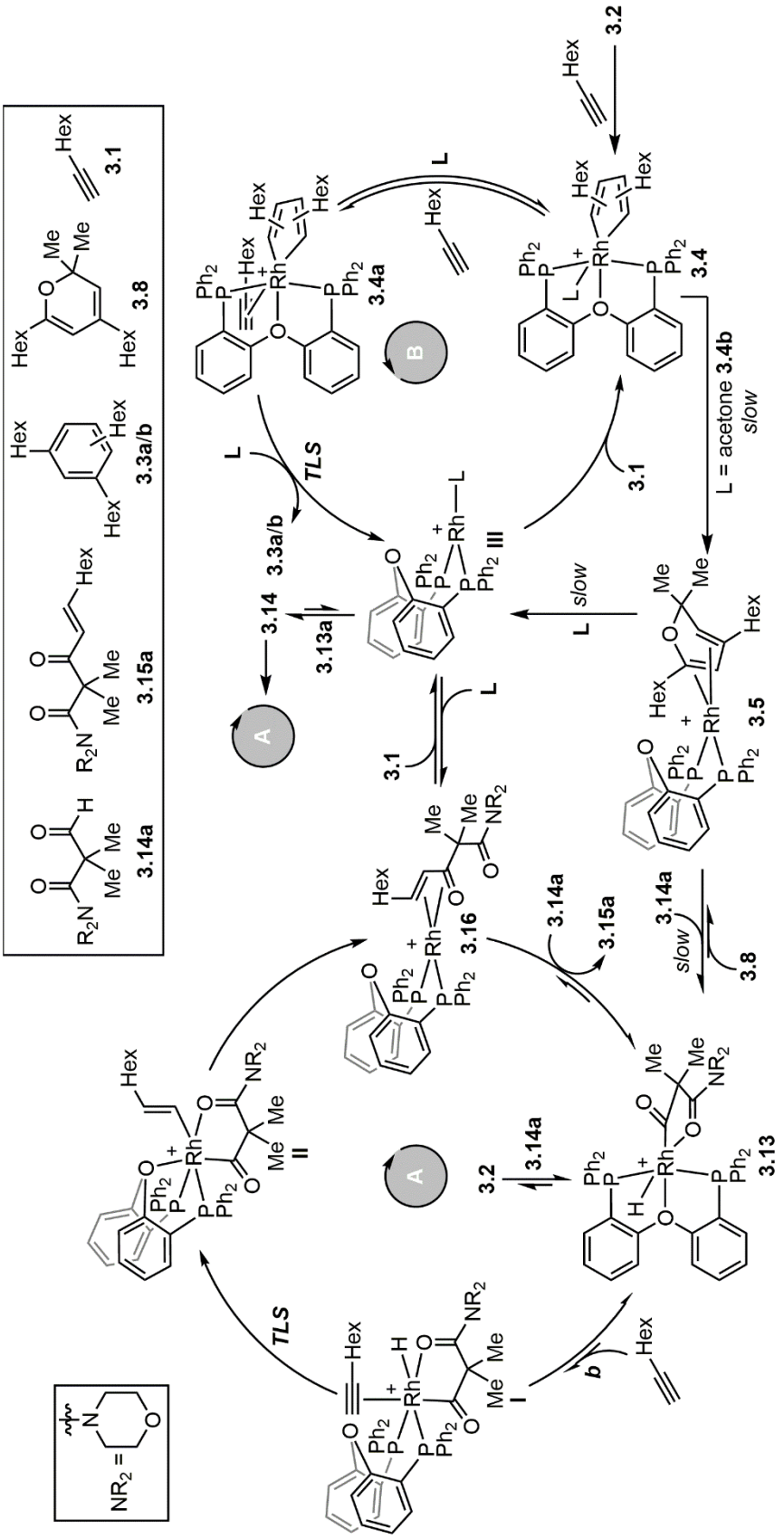

[a]BAr^F_4 anions omitted for clarity

3.7. Optimisation of Selectivity for Hydroacylation

We sought to use this understanding to optimize the hydroacylation reaction through altering the reagent stoichiometries and the catalyst loading (Table 3.2).

Table 3.2. Optimisation of reaction selectivity

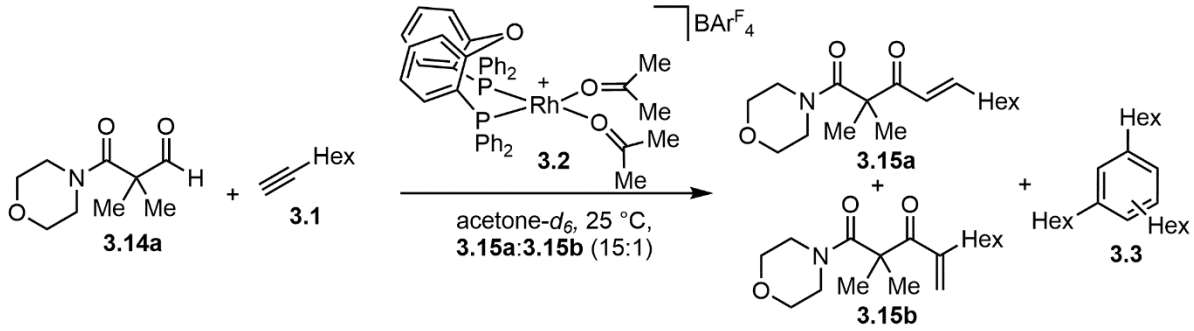

Entry	eq. 3.14**a**	eq. **3.1**	**3.2** (mol%)	**3.15a/b** (%)[a]	**3.3a/b** (%)[a]	Selectivity (%)[b]
1	1.0	1.3	5.0	>98	9	92
2	1.2	1.0	5.0	>98	0	100
3	1.0	1.0	20	96	4	96
4	1.0	1.0	2.5	>98	1	99
5	1.0	1.0	0.5	>98	0	100

[a][1]H NMR yield based on limiting reagent; [b]using 1,2,4,5-tetrachloro-3-nitrobenzene as an internal standard; [c][1]H NMR yield based on available alkyne, [d]% yield of **3.15a/3.15b** relative to **3.3a/b**.

Using the initial hydroacylation conditions with an excess of 1-octyne **3.1** (1.3 equivalents), a selectivity for hydroacylation of 92% was measured (Entry 1). Changing the reagent stoichiometries so that aldehyde was in excess (1.2 eq.) gave a selectivity of 100% for hydroacylation (Entry 2), this is due to there always being free aldehyde present in solution, resulting in the acyl-hydride resting state persisting until the full consumption of 1-octyne. However, due to the imbalance in stoichiometry, these conditions lead to a non-ideal atom economy in reagents.

At a more favourable 1 : 1 aldehyde to alkyne ratio and a catalyst loading of 20 mol% a selectivity of 96% was measured, with a hydroacylation yield of 96% (Entry 3). At 2.5 mol% loading of **3.2** a selectivity of 99% was measured (Entry 4), while at 0.5 mol% essentially 100% selectivity (Entry 5) is achieved using equimolar amounts of starting materials. This is a remarkable result, as the highest selectivity, and maximum atom-economy of products from reagents, occurs with the lowest catalyst loading and without excess of either substrate. The increased selectivity is due to the increased yield of

enone products **3.3** at the point when no free aldehyde remains in solution. This is the moment at which cyclotrimerisation becomes competitive and starts to form tri-*n*-hexylbenzenes from 1-octyne. This tipping point occurs at enone yields of 80%, 97.5% and 99.5% for catalyst loadings of 20 mol%, 2.5 mol% and 0.5 mol% respectively. This means that for the 0.5 mol% catalytic run only 0.5 mol% of alkyne was remaining when cyclotrimerisation became competitive with hydroacylation, leading to only traces of cyclotrimerisation being observed.

3.8. Optimisation of Hydroacylation for a Large-Scale Reaction

With such a robust, selective and efficient hydroacylation system in hand the opportunity to scale up to gram-quantities presented an exciting possibility. This work was performed during a placement at the process department of AstraZeneca in Macclesfield. It was decided that pyrrolidine aldehyde **3.14b** would be used as the coupling partner, as it is a solid at room temperature (unlike aldehyde **3.14a** which is an oil) making handling on scale easier. In order to access the aldehyde at the desired decagram scale, a route avoiding the previously optimized Raney nickel reduction of the corresponding α-amido-nitrile[27] was developed (Scheme 3.9).

Scheme 3.9. Synthetic routes to pyrrolidine aldehyde 3.14b

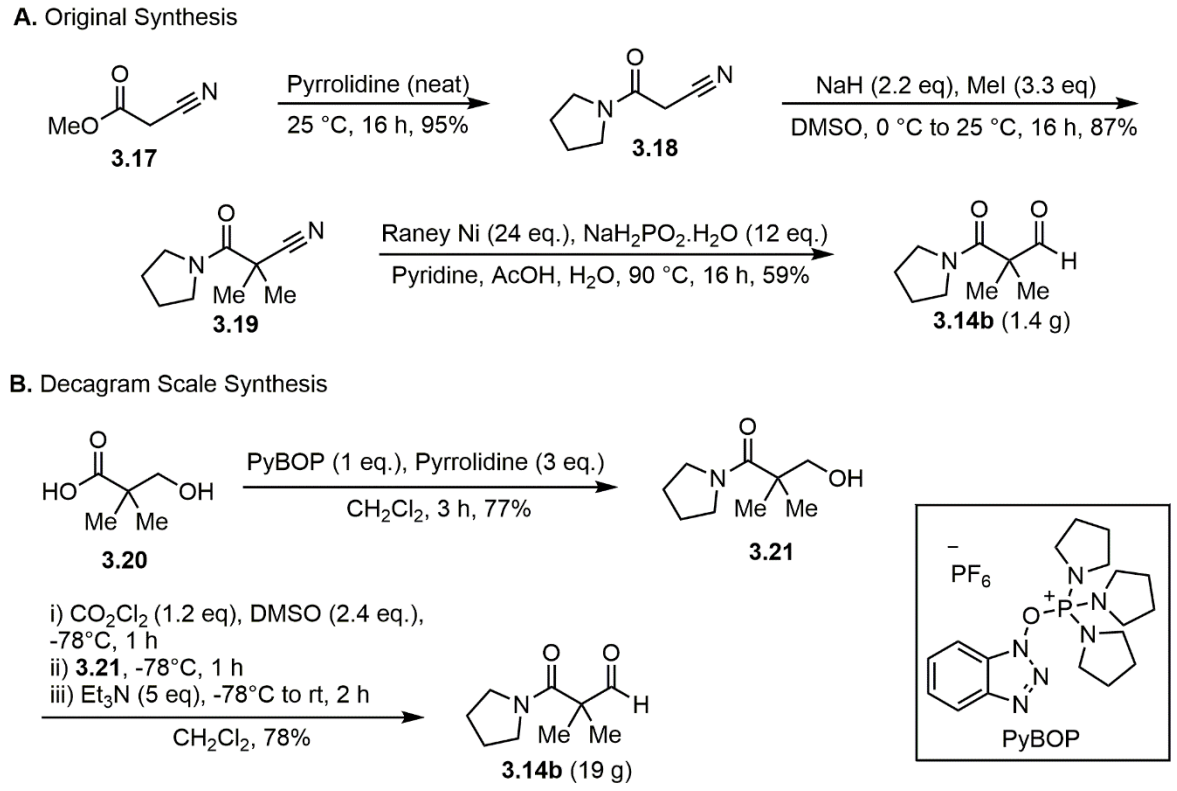

The first two steps of the original synthesis, amide formation followed by dimethylation with methyl iodide (Scheme 3.9, A), were high yielding and potentially scalable, however, it was desirable to avoid the use of large quantities of flammable Raney nickel and highly toxic pyridine as solvent.

The first step of the decagram scale synthesis was an amide coupling reaction, between pyrrolidine and 3-hydroxy-2,2-dimethylpropanoic acid **3.20** to afford pyrrolidine alcohol **3.21** in 77% yield (Scheme 3.9, B). The reaction was performed in a jacketed vessel (2 L) and the amide coupling partner benzotriazol-1-yl-oxytripyrrolidinophosphonium hexafluorophosphate (PyBOP) was added portionwise to the mixture of acid **3.21** and pyrrolidine to ensure the reaction temperature remained at 25 ºC. The next step was a Swern oxidation that was performed in a 1 L three necked round bottom flask, with appropriate scrubbing, which afforded the desired aldehyde in 78% yield (19 g).

At the AstraZeneca process department in Macclesfield, due to available equipment and safety considerations, is was not possible to generate the active catalyst *in situ* by hydrogenation, followed by purging the system back into an inert gas. Furthermore, there was no access to glove boxes in the laboratory. This meant a pre-catalyst that is active without hydrogenation and is also bench stable for significant periods of time was required. Initial studies revealed the previously reported Rh(I)-complex [Rh(*cis*-κ^2-$_{P,P}$-DPEPhos)(*o*-xylene)][BAr^F_4] **3.22** to be the perfect candidate.[28] Complete conversion to acyl-hydride **3.13** was immediately observed upon addition of aldehyde **3.13** to a solution of xylene complex **3.22** (0.01 M) in acetone. (Scheme 3.10).

Scheme 3.10. Addition of aldehyde 3.13 to an acetone solution of xylene complex 3.22[a]

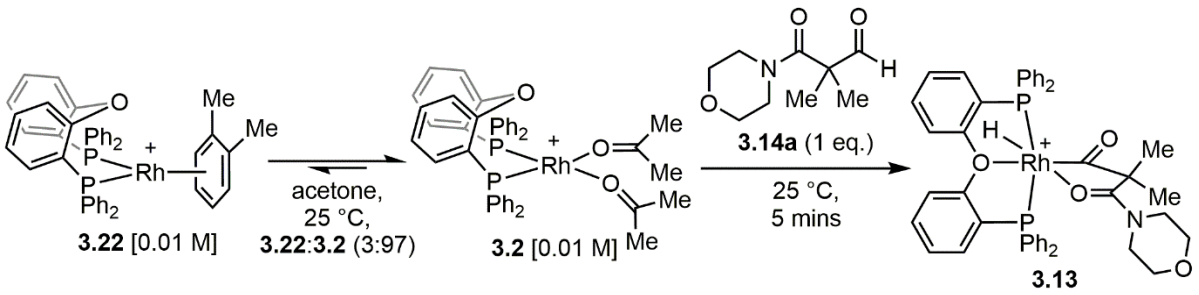

[a]BAr^F_4 anions omitted for clarity

This observation suggests that during catalysis using this pre-catalyst the acyl-hydride resting state **3.13** will be rapidly formed, and the reaction's kinetics will not be significantly altered. Before the

addition of aldehyde, the complex speciation was observed by $^{31}P\{^{1}H\}$ spectroscopy and revealed a 3 : 97 ratio of complexes **3.22** : **3.2**, demonstrating the lability of the *ortho*-xylene ligand in acetone solvent alone. The *ortho*-xylene complex **3.22** is bench stable for at least 6 months as observed by ^{1}H and $^{31}P\{^{1}H\}$ NMR spectroscopy.

A design of experiments (DoE) methodology was used for reaction time optimisation. A complemented 2D-design was used, with the variables being temperature and concentration. Each reaction was run on a 0.5 g scale, temperature was controlled using an integrity-10 temperature controller and the reaction was monitored by gas chromatography (GC) using dodecane as an internal standard (Table 3.3).

Table 3.3. Optimisation of hydroacylation conditions using a complemented 2D-DoE design

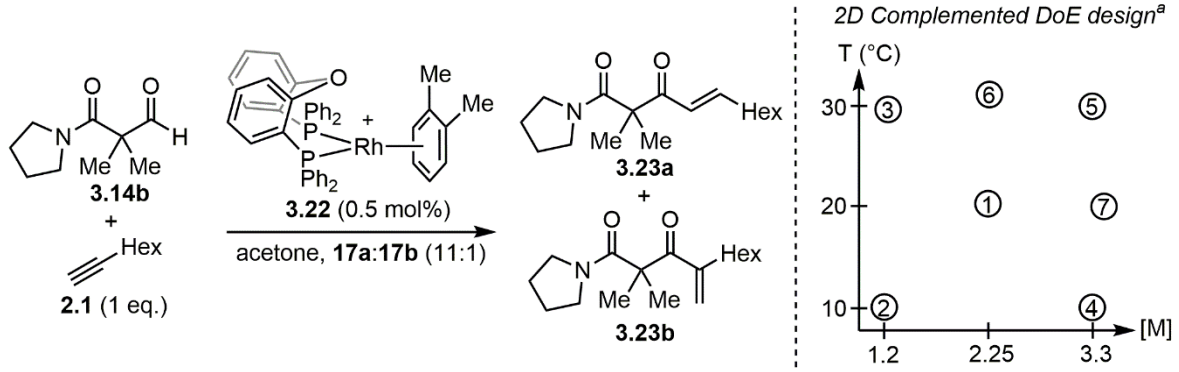

Entry	[**3.14b**] and [**3.1**] (M)	T (°C)	k_{obs} (10^{-3} molmin^{-1})	Time (h)[b]	Yield (%)[c]
1	2.25	20.0	7.9[d] (±0.8)[e]	10	> 98
2	1.20	10.0	1.7	38	> 98
3	1.20	30.0	14	7	> 98
4	3.30	10.0	3.8	20	> 98
5	3.30	30.0	22	3	> 98
6	2.25	31.5	20	3	> 98
7	3.46	20.0	9.3	7	> 98

[a]Each point and its associated number corresponds to an entry in the optimisation table (i.e. 1 = Entry 1) [b]Estimated from reaction profile; [c]^{1}H NMR yield using 1,2,4,5-tetrachloro-3-nitrobenzene as an internal standard; [d]Average of 3 runs; [e]Standard deviation of 3 runs.

A >98% yield and 100% selectivity was observed for all the examined conditions, demonstrating the efficacy of the catalyst system. The linear : branched ratio (11 : 1) showed little variation under the conditions tested and is reduced compared to the morpholine aldehyde **3.14a**. This is likely due to a

minor steric effect in the transition state of the selectivity determining (and rate limiting) hydride insertion. For all the reactions a pseudo-1st order rate law was obtained for the first two half-lives of aldehyde/alkyne consumption, allowing the calculation of k_{obs} and suggesting that the gross reaction mechanism is unchanged, as well as implying that the resting state of the reaction is the acyl-hydride (Figure 3.12).

Figure 3.12. Optimisation kinetics: Concentration of [3.14b] and [3.1] = 3.30 M; T = 30 ºC (Table 3.3, Entry 5)[a]

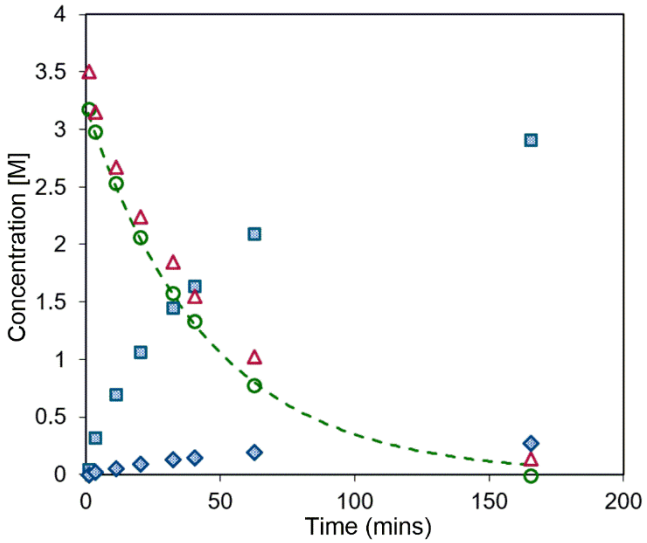

[a]Reaction profile as measured by ^{1}H NMR spectroscopy. Red △ = aldehyde **3.14a**, green ○ = 1-octyne 3.1, blue ■ = enone **3.15a**, blue ◆ = enone **3.15b**, dotted green line = first-order model for the consumption of 1-octyne **3.1**.

Both an increase in temperature and concentration, as expected, had a positive effect on the observed rate constant (k_{obs}), with temperature having a larger effect over the range studied. For the scale-up reaction the conditions of highest temperature and concentration where chosen to minimise reaction time (30 °C, 3.3 M). The reaction had a total volume of 10 ml and was therefore carried out in a 50 ml two-neck round bottom flask, under an atmosphere of nitrogen. The reaction was measured to be complete by GC after 3 hours. Simple precipitation of the catalyst from the reaction mixture by addition of heptane (250 ml) followed by filtration through a plug of silica resulted in a 97% (8.3 g) isolated yield of **3.5a**/**3.5b** (11 : 1) with >98% ^{1}H NMR purity, as measured by adding an internal standard to isolated material (Scheme 3.11).

Scheme 3.11. Hydroacylation scale up reaction

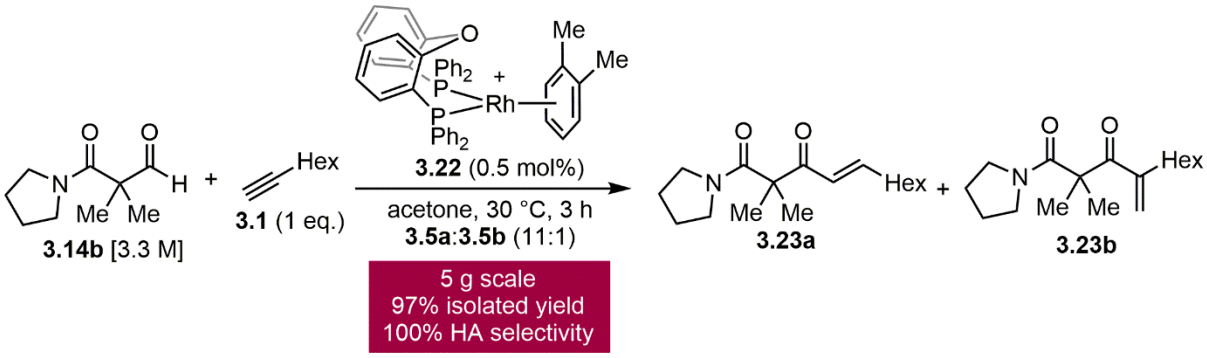

Having optimized the reaction for large scale we sought to quantify its efficiency. The Process Mass Intensity (PMI)[29] is the ratio of the total input mass in a process (including catalysts and solvents) compared to the mass of isolated product. A desirable PMI is one that approaches 1, which can only be attained in a 100% yielding, atom-efficient reaction, that uses no solvent or catalyst. The optimized hydroacylation reaction possesses many of these desirable attributes, including a 1 : 1 ratio of aldehyde to alkyne, low catalyst loadings, and high yields/selectivity, which allow for simple purification that avoids column chromatography. This is in addition to the modest temperature and short reaction times. For these optimised conditions we estimate a PMI = 30. This metric can be compared with an equivalent hydroacylation process reported for similar substrates and catalysts, for which we estimate to have a PMI = 330, an order of magnitude difference.[27] These procedures use lower substrate concentrations, have lower isolated yields and require column chromatography, increasing the amount of solvent used. Our optimized conditions were also tested at lower catalyst loadings (0.1 mol%) under otherwise identical conditions but on a smaller scale (0.5 g) and afforded a 91% isolated yield of enones **3.23** after 24 h, further demonstrating the stability of the catalytic system.

3.9. Conclusions

The cyclotrimerisation reaction of 1-octyne to form tri-*n*-hexylbenzenes was shown to be catalysed by the Rh(I) *bis*-acetone complex. The initial resting state of the reaction is three isomers of the Rh(III) metallacyclopentadiene complex [Rh(*mer*-κ^3-$_{P,O,P}$-DPEPhos)(L)((CH)$_2$(C(C$_6$H$_{13}$))$_2$][BAr$^F{}_4$] with a labile monodentate ligand (L = acetone/1-octyne). The different isomers are formed by the different alkyne regiochemistry in the oxidative-metallacyclisation step, which determines the regiochemistry of the

hexyl groups in the metallacyclopentadiene backbone. This assignment was supported by the complex formed from the reaction of 1,6-heptadiyne, where only one isomer of the metallacyclopentadiene was observed. This is because, due to the tether between the alkynes, only one regioisomer can be formed by the oxidative-metallacyclisation of 1,6-heptadiyene with the Rh(I)-fragment.

The kinetics of the cyclotrimerisation, as studied by initial rates, indicated that two distinct order regimes in 1-octyne were in operation. At lower concentrations of 1-octyne, first order behaviour was observed; and at higher concentration of 1-octyne, zero order behaviour was observed. These results are consistent with the labile monodentate ligand, that is bound to the metallacyclopentadiene complex, being acetone in the low 1-octyne concentration regime and being 1-octyne in the high concentration regime. From the 1-ocytne-bound complex, a mechanistic sequence occurs to afford tri-*n*-hexylbenzene product. Addition of acetonitrile to the metallacyclopentadiene resulted in the formation of an acetonitrile bound complex, formed by displacing the labile monodentate ligand.

During cyclotrimerisation the resting slowly changed to an α-pyran complex, which is proposed to be formed by a formal [2+2+2] cycloaddition between 1-octyne and acetone solvent. The α-pyran complex is likely formed from the acetone bound metallacyclopentadiene complex, by a similar mechanism as for tri-*n*-hexylbenzenes. Interestingly, only one isomer of the α-pyran was observed, which was assigned based on nOeSY correlations. The α-pyran complex eventually becomes the resting state of cyclotrimerisation, this is because the α-pyran is a relatively strongly bound ligand owing to its two alkene groups. The effects of this binding were observed when the complex was employed as a pre-catalyst for hydroacylation where the catalysis was slow, due to slow transformation of the α-pyran complex to the acyl-hydride resting state. Further experiments which probed the ability for different catalytic intermediates to move between hydroacylation and cyclotrimerisation catalysis were carried out, which facilitated the proposal of a comprehensive mechanistic picture, of both catalytic cycles and their interplay.

The stoichiometric reaction of acyl-hydride with 1-ocytne, in the presence and absence of added aldehyde, revealed that cyclotrimerisation only becomes competitive with hydroacylation when no free aldehyde remains in solution. This result corroborated with the reaction profile observed in the

hydroacylation reaction with excess 1-octyne. With this understanding, optimisation of the hydroacylation was carried out. It was found that, when using a 1 : 1 stoichiometry of aldehyde and alkyne, a decrease in catalyst loading led to an increase in selectivity for hydroacylation. As catalyst loading is reduced, the yield of enone increases at the point where no free aldehyde remains, and therefore more alkyne is consumed at the point when cyclotrimerisation becomes competitive: i.e. at 5 mol% catalyst loading this tipping point occurs at 95% enone yield, whereas at 0.5 mol% catalyst loading this occurs at 99.5% enone yield. This is means, in the latter case, that only 0.5 mol% of alkyne is remaining at the point when hydroacylation and cyclotrimerisation become competitive and therefore no cyclotrimerisation products were detected.

The conditions were further optimized for a large-scale reaction, by increasing the reaction temperature and concentration. This lead to a highly efficient reaction, with a calculated process mass intensity an order of magnitude lower that the for the originally reported hydroacylation conditions. The key features that lead to this improvement where the: low catalyst loading, high reagent concentrations and, most importantly, the high selectivity for hydroacylation at equal reagent stoichiometry, which allowed for simple purification of the product. This result was achieved on the foundation of detailed mechanistic knowledge, illustrating that mechanistic understanding can be as, if not more useful, than screening for reaction optimisation.

3.10 References

1 C. A. Busacca, D. R. Fandrick, J. J. Song and C. H. Senanayake, *Adv. Synth. Catal.*, 2011, **353**, 1825–1864.

2 C. S. Wei, E. M. Simmons, Y. Hsaio and M. D. Eastgate, *Top. Catal.*, 2017, **60**, 620–630.

3 A. Steffen, R. M. Ward, M. G. Tay, R. M. Edkins, F. Seeler, M. van Leeuwen, L.-O. Pålsson, A. Beeby, A. S. Batsanov, J. A. K. Howard and T. B. Marder, *Chem. Eur. J.*, 2014, **20**, 3652–3666.

4 W. Ma, C. Yu, T. Chen, L. Xu, W.-X. Zhang and Z. Xi, *Chem. Soc. Rev.*, 2017, **46**, 1160–1192.

5 D. R. McAlister, J. E. Bercaw and R. G. Bergman, *J. Am. Chem. Soc.*, 1977, **99**, 1666–1668.

6 N. Agenet, V. Gandon, V. K. Peter C., M. Malacria and C. Aubert, *J. Am. Chem. Soc.*, 2007, **129**, 8860–8871.

7 W. H. Monillas, J. F. Young, G. P. A. Yap and K. H. Theopold, *Dalt. Trans.*, 2013, **42**, 9198–9210.

8 K. Yamamoto, H. Nagae, H. Tsurugi and K. Mashima, *Dalt. Trans.*, 2016, **45**, 17072–17081.

9 I. Krossing, *Chem. Eur. J.*, 2001, **7**, 490–502.

10 P. S. Pregosin, *NMR in Organometallic Chemistry*, Wiley VCH, 2012.

11 S. Hansson, J. F. Miller and L. S. Liebeskind, *J. Am. Chem. Soc.*, 1990, **112**, 9660–9661.

12 K. Tsuchikama, Y. Yoshinami and T. Shibata, *Synlett*, 2007, 1395–1398.

13 K. Tanaka, Y. Otake, H. Sagae, K. Noguchi and M. Hirano, *Angew. Chem. Int. Ed.*, 2008, **47**, 1312–1316.

14 T. N. Tekavec and J. Louie, *J. Org. Chem.*, 2008, **73**, 2641–2648.

15 Y. Miyauchi, M. Kobayashi and K. Tanaka, *Angew. Chem. Int. Ed.*, 2011, **50**, 10922–10926.

16 E. N. Marvell, G. Caple, T. A. Gosink and G. Zimmer, *J. Am. Chem. Soc.*, 1966, **88**, 619–620.

17 M. A. Duperrier and J. Dreux, *Tetrahedron Lett.*, 1970, **11**, 3127–3130.

18 G. Büchi and N. C. Yang, *J. Am. Chem. Soc.*, 1957, **79**, 2318–2323.

19 T. A. Gosink, *J. Org. Chem.*, 1974, **39**, 1942–1944.

20 E. N. Marvell and T. A. Gosink, *J. Org. Chem.*, 1972, **37**, 3036–3037.

21 E. N. Marvell, T. Chadwick, G. Caple, T. Gosink and G. Zimmer, *J. Org. Chem.*, 1972, **37**, 2992–2997.

22 S. D. Pike, I. Pernik, R. Theron, J. S. McIndoe and A. S. Weller, *J. Organomet. Chem.*, 2015, **784**, 75–83.

23 M. Paneque, M. L. Poveda, N. Rendón and K. Mereiter, *J. Am. Chem. Soc.*, 2004, **126**, 1610–1611.

24 A. A. Dahy and N. Koga, *Organometallics*, 2015, **34**, 4965–4974.

25 L. Xu, Y.-C. Wang, J. Wei, Y. Wang, Z. Wang, W.-X. Zhang and Z. Xi, *Chem. Eur. J.*, 2015, **21**, 6686–6689.

26 R. Ghosh, T. J. Emge, K. Krogh-Jespersen and A. S. Goldman, *J. Am. Chem. Soc.*, 2008, **130**, 11317–11327.

27 T. J. Coxon, M. Fernández, J. Barwick-Silk, A. I. McKay, L. E. Britton, A. S. Weller and M. C. Willis, *J. Am. Chem. Soc.*, 2017, **139**, 10142–10149.

28 J. F. Hooper, A. B. Chaplin, C. González-Rodríguez, A. L. Thompson, A. S. Weller and M. C. Willis, *J. Am. Chem. Soc.*, 2012, **134**, 2906–2909.

29 C. Jimenez-Gonzalez, C. S. Ponder, Q. B. Broxterman and J. B. Manley, *Org. Process Res. Dev.*, 2011, **15**, 912–917.

Chapter 4: Non-tethered Aldehyde Hydroacylation of Acrylates

4.1. Introduction

For hydroacylation to become a general methodology in organic synthesis the substrate scope needs to be extended beyond tethered aldehydes. Having studied the mechanism of *β*-amido aldehyde hydroacylation and established the key role that *α*-aldehyde substitution has on reactivity, we sought to develop an intermolecular hydroacylation using non-tethered aldehydes.

This chapter discusses how the studies of the coordination chemistry of Rh(I)-*β*-amido ketone complexes led to the discovery of a non-tethered aldehyde hydroacylation (Tishchenko) reaction in weakly coordinating fluoroarene solvents. This methodology was then extended to the development of a selective intermolecular non-tethered aldehyde hydroacylation of acrylates, promoted by wide bite-angle *bis*-phosphine ligands. Most notably, the first example of a non-tethered quaternary aldehyde hydroacylation is reported.

4.2. Synthesis of a Rh(I)-*β*-Amido Ketone Complex

The studies began by looking at the coordination chemistry of Rh(I)-*β*-amido ketone complexes with the small bite-angle *bis*-phosphine *bis*(dicyclohexylphosphino)methane (dcpm). This was the only ligand that catalysed the *alkene* hydroacylation with *β*-amido aldehydes. The elementary steps of this hydroacylation were probed, including the synthesis of an analogue of a product-bound complex, a potential intermediate in the catalytic cycle (Scheme 4.1).

β-amido ketone **4.3** was used as an analogue of hydroacylation product and was synthesised in 2 steps (Scheme 4.2). The first step of the synthesis was an amide coupling reaction between ethyl acetoacetate and morpholine catalysed by 4-dimethylaminopyridine to give 1-morpholinobutane-1,3-dione **4.5** in 88% yield. The second step was a dialkylation with 1,4-dibromobutane using K_2CO_3 as base and 1-butyl-3-methylimidazolium tetrafluoroborate ([BMIM]BF_4) as a phase transfer catalyst,[1] to give *β*-amido ketone **4.3** in 22% yield.

Scheme 4.1 A. Alkene hydroacylation with dcpm; B. Potential catalytic intermediate; C. product analogue

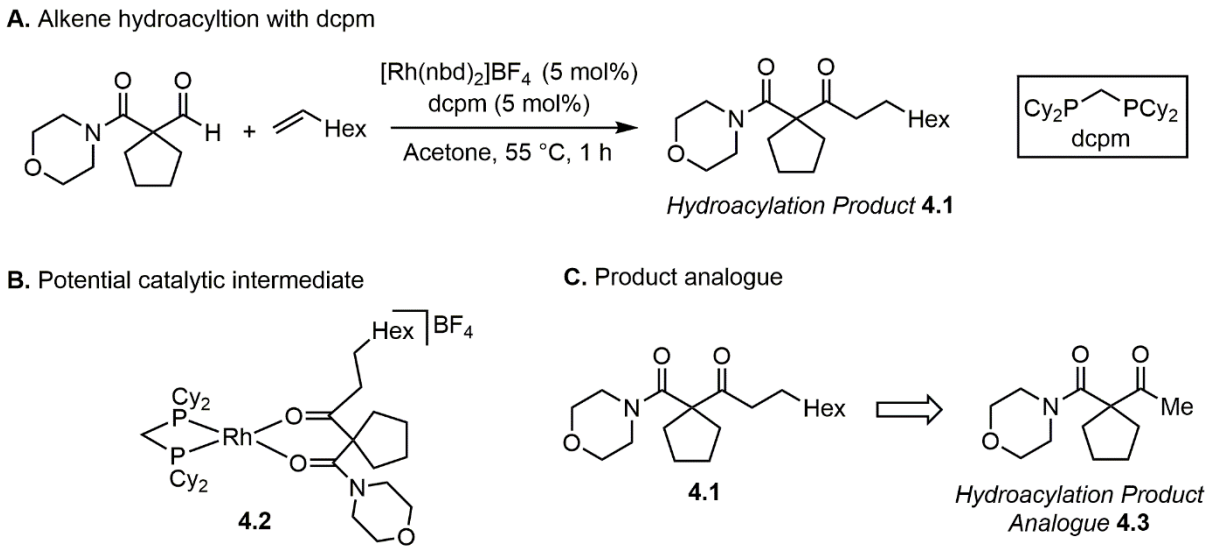

Scheme 4.2. Synthesis of *β*-amido-methyl ketone 4.3

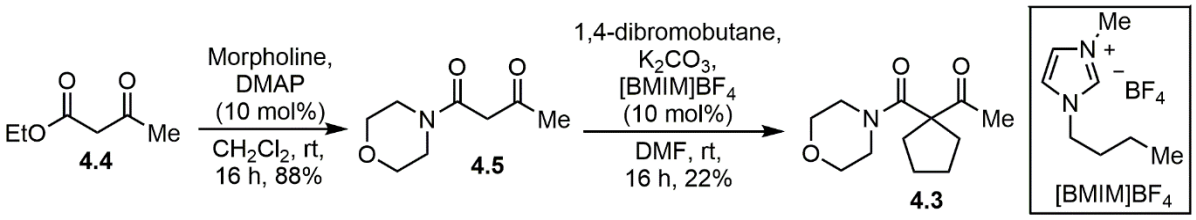

Addition of *β*-amido ketone **4.3** (10 eq.) to either $[Rh(Cy_2PCH_2PCy_2)(acetone)_2][BAr^F{}_4]$ **4.6** in acetone solvent or $[Rh(Cy_2PCH_2PCy_2)(\eta^6\text{-}1,2\text{-}C_6H_4F_2)][BAr^F{}_4]$ 4.7 in 1,2-difluorobenzene solvent resulted in no reaction (Scheme 4.3).

Scheme 4.3. Addition of *β*-amido-methyl-ketone 4.3 to complexes 4.6 and 4.7[a]

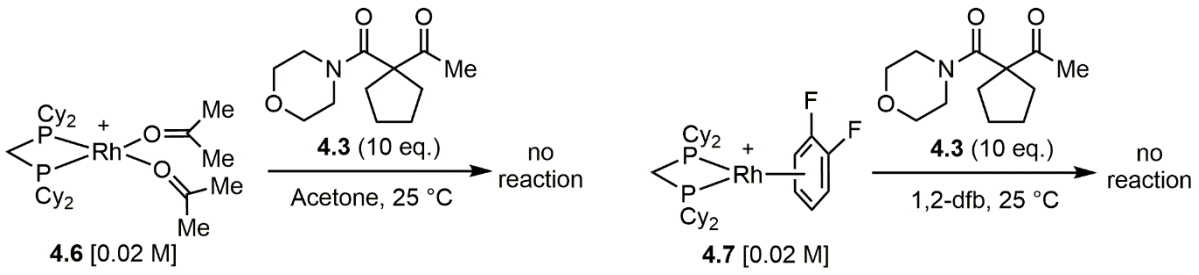

[a]$BAr^F{}_4$ anion omitted for clarity

To test whether this was due to solvent outcompeting coordination of the methyl-ketone **4.3**, reactions using the more weakly coordinating solvent pentafluorobenzene (C_6F_5H) were carried out. Increased

fluorine substitution of fluoroarenes has been established to decrease the strength of their binding to rhodium-*bis*-phosphine complexes.[2,3] Both the dcpm rhodium complexes [Rh($Cy_2PCH_2PCy_2$)(nbd)][BAr^F_4] **4.8a** and [Rh($Cy_2PCH_2PCy_2$)(nbd)][AlO^F_4] **4.8b** were hydrogenated in pentafluorobenzene (0.10 M) under H_2 (4 atm) to form their corresponding active species (Scheme 4.4).

Scheme 4.4. Hydrogenation of [Rh(dcpm)(nbd)]X complexes in pentafluorobenzene (a. X = BAr^F_4, b. X = AlO^F_4)

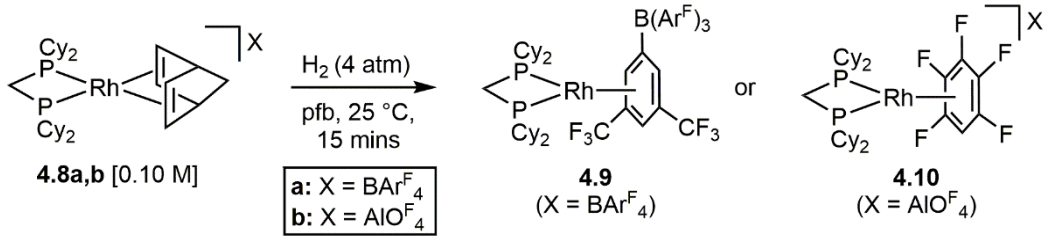

Hydrogenation of [Rh($Cy_2PCH_2PCy_2$)(nbd)][BAr^F_4] **4.8a** resulted in the formation of the zwitterionic complex [Rh($Cy_2PCH_2PCy_2$)(η^6-($C_6H_3(CF_3)_2$)B($C_6H_3(CF_3)_2)_3$)] **4.9** where one of the aryl groups of the BAr^F_4 is η^6-cordinated to the rhodium centre. In the $^{31}P\{^1H\}$NMR spectrum a doublet at δ –16.8 [J_{RhP} = 171 Hz] was observed, and in the ^1H NMR spectrum broad singlets were observed for the coordinated aryl-group in a 2 : 1 ratio at δ 6.98 and δ 6.84. These signals were observed in an overall 1 : 3 ratio with the un-coordinated BAr^F_3 signals at δ 7.72 and δ 7.56. The same effect was observed in the previously reported *bis*(dicyclohexylphosphino)ethane (dcpe) [Rh($Cy_2PCH_2CH_2PCy_2$)(η^6-($C_6H_3(CF_3)_2$)B($C_6H_3(CF_3)_2)_3$)] analogue of this complex.[3]

Hydrogenation using the same reaction conditions with the corresponding Krossing anion complex [Rh($Cy_2PCH_2PCy_2$)(nbd)][AlO^F_4] **4.8b** (OF_4 = $OC(CF_3)_3)_4$), formed the pentafluorobenzene bound complex [Rh($Cy_2PCH_2PCy_2$)(η^6-C_6F_5H)][AlO^F_4] **4.10** (Scheme 4.4) as indicated by the doublet observed in the $^{31}P\{^1H\}$ NMR at δ –11.4 [J_{RhP} = 164 Hz].

Methyl-ketone **4.3** (10 eq.) was then subsequently added to the *in situ* formed complexes **4.9** and **4.10** in anticipation of substitution of the weakly bound η^6-ligands (Scheme 4.5).

No reaction was observed with the BAr^F_4 coordinated complex **4.9**, indicating the β-amido ketone is too weak a ligand to displace the coordinated BAr^F_4. In contrast, the pentafluorobenzene complex **4.10**

Scheme 4.5. Addition of *β*-amido-methyl-ketone 4.3 to complexes 4.9 and 4.10

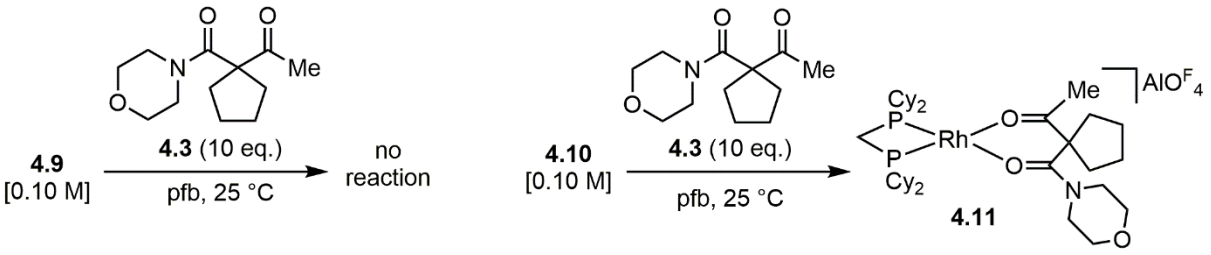

reacted to form a new complex on time of mixing, as indicated by the formation of a major (*ca* 90%) broad doublet at δ –1.20 [J_{RhP} = 181 Hz] in the $^{31}P\{^{1}H\}$ NMR spectrum along with other unidentified species (Figure 4.1).

Figure 4.1. $^{31}P\{^{1}H\}$ NMR spectra of A) pentafluorobenzene complex 4.10; B) 5 minutes after the addition of *β*-amido-methyl-ketone 4.3

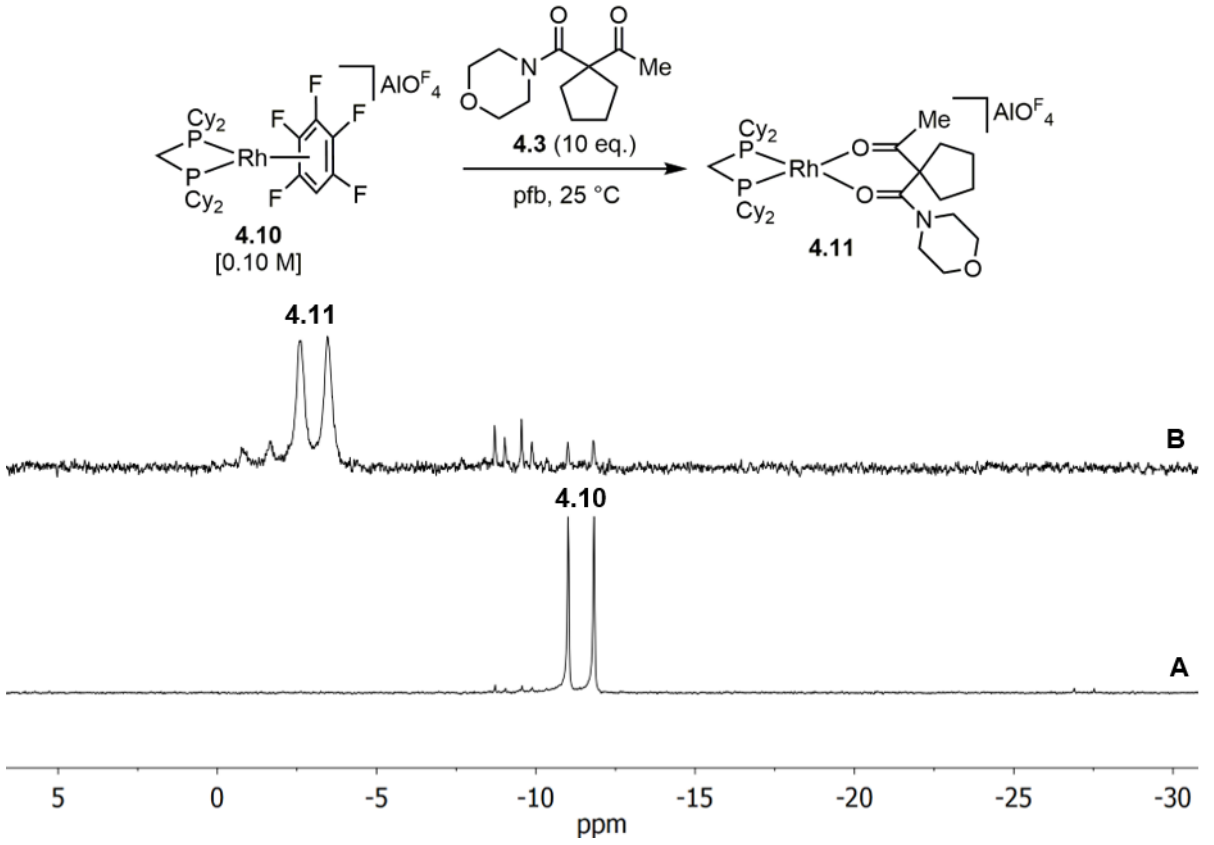

The new complex is tentatively assigned as the *β*-amido ketone-bound complex $[Rh(Cy_2PCH_2PCy_2)(\kappa^2\text{-}_{O,O}\text{-}(CH_3COC\{CH_2\}_4CO\{NC_4H_8O\}))][AlO^{F}{}_4]$ **4.11**. A broad doublet is observed in the $^{31}P\{^{1}H\}$ NMR spectrum; however, if square planar, complex **4.11** would be expected to have inequivalent ^{31}P environments. This could be due to a fluxional process involving de-coordination of

the *β*-amido ketone ligand. Because of the relatively high freezing point of the pentafluorobenzene (272 K), the fluxionality was not probed by VT NMR spectroscopy. Attempts at isolating the complex unfortunately led to immediate decomposition.

Based on the observed coordinating ability of the *β*-amido ketone ligand and the mechanistic studies of alkyne hydroacylation with *β*-amido aldehydes in Chapter 2, combined with the previously reported studies of the Rh-catalysed alkene hydroacylation with *β*-*S*-aldehydes,[4] a potential mechanism for alkene hydroacylation is shown in Scheme 4.6.

Scheme 4.6. Potential hydroacylation mechanism with *β*-amido aldehydes and alkenes

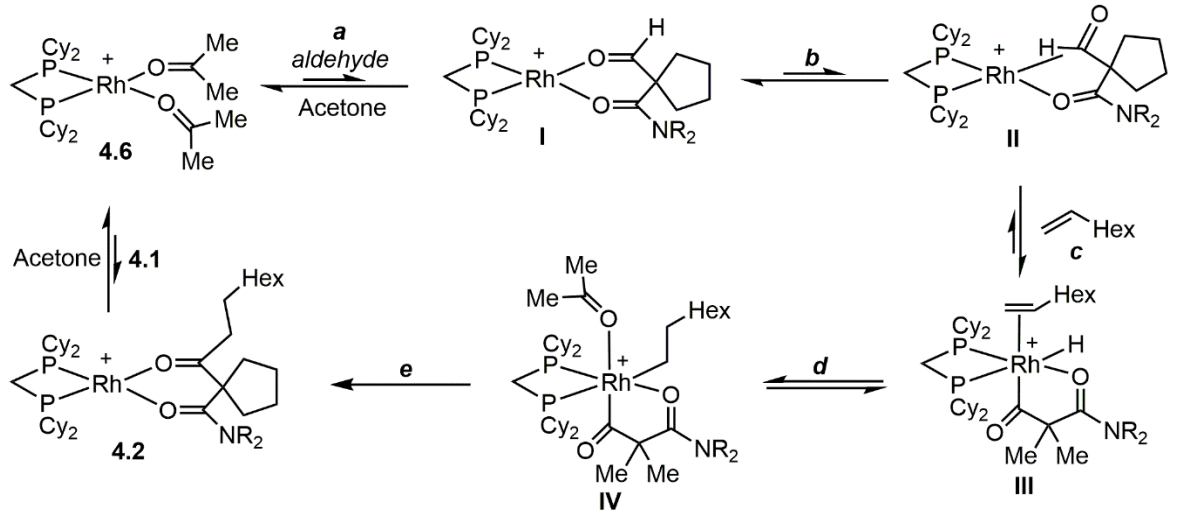

a. Ligand substitution; ***b***. σ-complex formation; ***c***. Oxidative cleavage; ***d***. Hydride insertion; ***e***. Reductive coupling

Starting from the *bis*-acetone complex **4.6**, aldehyde will bind to form complex **I**. This complex will then rearrange to form the C–H agostic aldehyde complex **II**, which after subsequent C–H activation will form an acyl-hydride complex **III**.[5–7] When an alkene is coordinated (as shown in complex **III**), reversible hydride insertion into the alkene will then form the acyl-alkenyl intermediate **IV**, which after reductive bond formation will form the *β*-amido ketone complex **4.2**. This ligand will then be displaced to reform the *bis*-acetone complex **4.6**, completing the catalytic cycle

As previously shown, when the *β*-amido ketone analogue **4.3** is added to the *bis*-acetone complex **4.6** no *β*-amido ketone binding was observed, indicating the equilibrium between the *β*-amido ketone complex **4.2** and *bis*-acetone complex **4.6** lies predominately to the side of **4.6**. Consequently, due to their structurally similarity, the coordination ability of *β*-amido aldehyde in complex **I** would be

expected to be similar to the coordination ability of *β*-amido ketone product. This means the pre-equilibrium to form aldehyde-bound complex **I** will also lie heavily toward the *bis*-acetone complex **4.6**.

When the weak binding of *β*-amido aldehydes to Rh(I)-complexes is taken into the context of non-tethered aldehydes, where no hydroacylation reactivity is observed under similar catalytic conditions,[2] the pre-equilibrium of aldehyde binding would be expected to be shifted even further toward the *bis*-acetone complex. This is because non-tethered aldehydes do no possess the benefit of the chelation effect, from a more strongly coordinating group (i.e. a *β*-amido group) (Scheme 4.7).

Scheme 4.7. Comparison of pre-equilibria with a non-tethered aldehyde

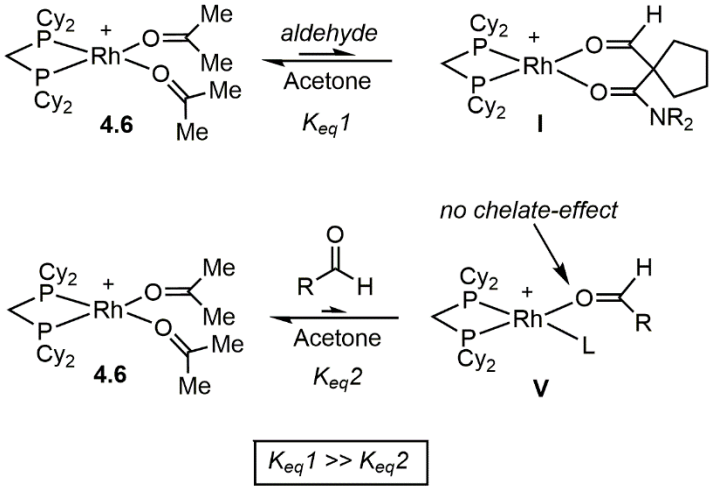

This postulation led to the study of the reactivity of non-tethered aldehydes with Rh(I)-dcpm complexes in non-coordinating solvents in combination with the weakly coordinating Krossing anion. It was anticipated that by promoting the equilibrium toward aldehyde-bound complexes hydroacylation reactivity would be observed.

4.3. Tishchenko Reaction of Non-Tethered Aldehydes

The aldehyde selected to test for reactivity in non-coordinating polyfluorinated benzenes was cyclohexanecarboxaldehyde. This was chosen because using a tertiary aldehyde could help slow reductive decarbonylation compared to the often employed aromatic or secondary aliphatic aldehydes. The reaction of cyclohexanecarboxaldehyde **4.12** with 5 mol% of *in situ* formed $[Rh(Cy_2PCH_2PCy_2)(\eta^6\text{-}C_6F_5H)][AlO^F{}_4]$ **4.10**, in pentafluorobenzene, resulted in complete consumption

of starting material and formation of the Tishchenko ester product **4.13** within 5 minutes at 25 ºC (Scheme 4.8).

Scheme 4.8. Tishchenko reaction of cyclohexanecarboxaldehyde 4.12 with {Rh($Cy_2PCH_2PCy_2$)}-complexes in polyfluorinated-benzenes

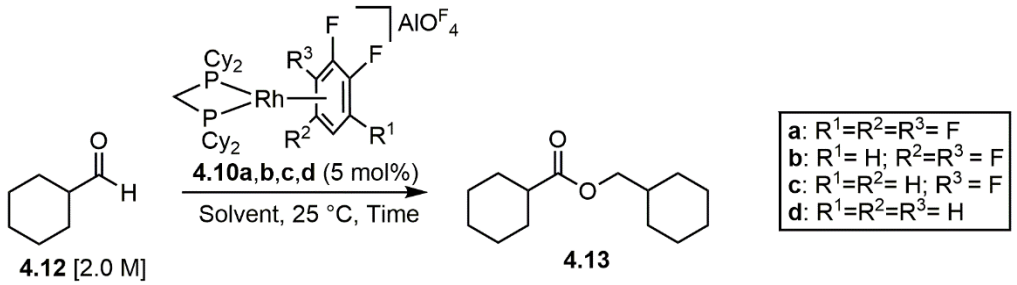

Catalyst	Solvent	Time (mins)[a]	TOF (Mmin^{-1})
a	pentafluorobenzene	<5	>0.4
b	1,2,3,4-tetrafluorobenzene	<5	>0.4
c	1,2,3-trifluorobenzene	80	0.03
d	1,2-difluorobenzene	600	0.003

[a]Time until full consumption of cyclohexanecarboxaldehyde **4.12** as indicated by periodic monitoring by ^{1}H NMR spectroscopy, ester **4.13** was the only product observed by ^{1}H NMR spectroscopy for all reactions.

The ester product was isolated in 91% yield after purification by column chromatography. To test whether the co-ordination of the solvent had any effect on reactivity the reaction was repeated with *in situ* formed [Rh($Cy_2PCH_2PCy_2$)(η^6-fluoroarene)][AlO$^F_4$] complexes (where fluoroarene = 1,2,3,4-tetrafluorobenzene **4.10b**, 1,2,3-trifluorobenzene **4.10c**, 1,2-difluorobenzene **4.10d**) in conjunction with the corresponding fluoroarene as solvent. The reactions were monitored periodically by ^{1}H NMR spectroscopy and in all cases aldehyde **4.12** was eventually consumed and ester **4.13** was the only observed product. There was a significant decrease in rate with decreased fluorine substitution, with the reaction using 1,2-difluorbenzene coordinated catalyst **4.10d** in 1,2-difluorobenzene requiring 600 mins to go to completion compared to <5 mins for the 1,2,3,4-tetrafluorobenzene system. This indicates that more coordinating solvents slow reactivity, which we propose to be due to reducing the pre-equilibrium concentration of Rh(I)-bound aldehyde.

The mechanism of the Tishchenko reaction was not probed any further, both aldehyde oxidative addition-type mechanisms[8,9] and oxidative cyclisation-type mechanisms[10] have been proposed for transition metal-catalysed Tishchenko reactions. The mechanistic studies performed on Rh(I)-*bis*-phosphine-catalysed Tishchenko reactions, which include an intramolecular reaction[11] and

intermolecular reactions using tethered[12] and non-tethered[13] aldehydes have all been proposed to go *via* oxidative addition-type pathways. Based on these reports an oxidative addition mechanism is proposed for the non-tethered aldehyde hydroacylation (Scheme 4.9).

Scheme 4.9. Proposed mechanism for Tishchenko reaction

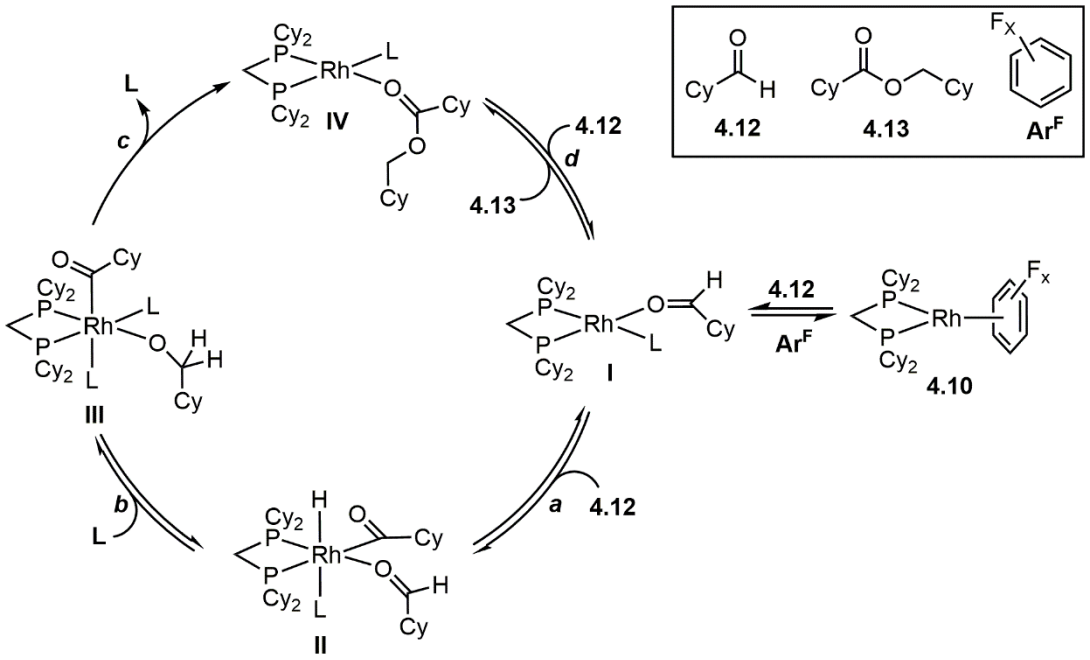

From the fluoroarene pre-catalyst **4.10** a pre-equilibrium with the κ^1-aldehyde bound complex **I** is established, which will be solvent dependant, with more highly fluorinated solvents favouring the aldehyde-bound complex. Oxidative addition will form the acyl-hydride complex **II**, which with coordinated aldehyde will undergo hydride insertion to produce acyl-alkoxide complex **III**. Reductive elimination of this complex will afford the ester bound product **IV**, which will be in equilibrium with complexes **I** and **4.10**, completing the catalytic cycle.

4.4. Discovery of Acrylate Hydroacylation with Non-Tethered Aldehydes

If, as proposed, an aldehyde oxidative addition-type pathway is in operation, interception of the acyl-hydride intermediate with an alkene/alkyne could lead to hydroacylation reactivity. This opportunity was explored by the screening the reaction of alkenes/alkynes with aldehyde **4.12** [0.7 M] and $[Rh(Cy_2PCH_2PCy_2)(\eta^6\text{-}C_6F_5H)][AlO^F{}_4]$ **4.10a** (10 mol%) in pentafluorobenzene. Initial reactions

carried out at 25 ºC gave low conversions of starting material, so further screening was carried out at 75 ºC with a 16 h reaction time (Table 4.1).

Table 4.1. Screening for hydroacylation reactivity of alkenes/alkynes

Entry	Alkene/alkyne	Eq.	Reaction outcome
1	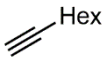 **4.14**	1.0	*Some alkyne decomposition*
2	 **4.15**	1.0	*Some alkyne decomposition*
3	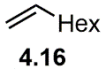 **4.16**	3.0	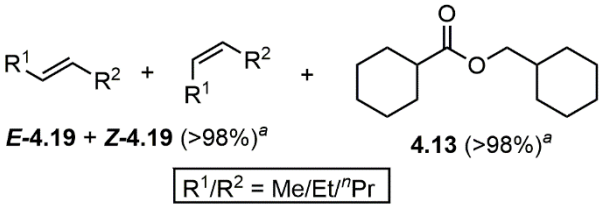 ***E*-4.19 + *Z*-4.19** (>98%)[a] **4.13** (>98%)[a] R^1/R^2 = Me/Et/^{n}Pr
4	 **4.17**	3.0	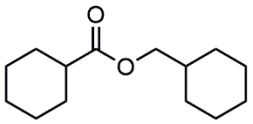 **4.13** (>98%)[a]
5	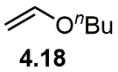 **4.18**	3.0	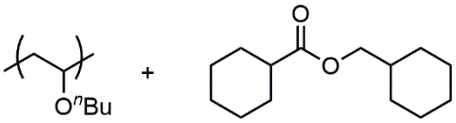 **4.20** **4.13** (69%)[a]

[a]^{1}H NMR yields using 1,2,4,5-tetrachloro-3-nitrobenzene (TCNB) as a standard.

The reactions using alkynes 1-octyne **4.14** (Table 4.1, Entry 1) and phenylacetylene **4.15** (Table 4.1, Entry 2) resulted in no reaction of the aldehyde and limited consumption of each alkyne to an unidentified mixture of products. Upon addition of alkyne a black precipitate is observed, which suggests colloidal Rh(0) is formed.[14] A potential mechanism for the formation of colloidal Rh(0) is a Glaser-type oxidative coupling of two alkynes with concomitant loss of H_2.[15]

The reactivity of alkenes was then studied, in the anticipation they would not promote the formation of colloidal Rh(0). In the reaction of 1-octene **2.16**, full consumption of both 1-octene and aldehyde **4.12**

was observed and the reaction solution remained dark red throughout, indicating no colloidal Rh(0) was formed (Table 4.1, Entry 3). The alkene had been isomerised to a mixture of internal octenes ***E*-4.19**, ***Z*-4.19** (>98%) as indicated by the broad alkene signals between δ 5.5–5.3 in the ^{1}H NMR spectrum and the aldehyde had been converted to Tishchenko product **4.13** (>98%). This result indicated that two separate Rh-catalysed reactions of each reaction component had occurred, an aldehyde Tishchenko reaction and an alkene isomerization. The order of the two processes was not probed, although due to the stronger binding of alkenes compared to aldehydes, the isomerization reaction could be expected to proceed at a faster rate. The mechanism of the alkene isomerization will likely be a Rh(I)-mediated allyl mechanism as proposed for the {Rh(DPEPhos}$^{+}$ alkene isomerization in Chapter 2 (See Scheme 2.8).

In order to prevent alkene isomerisation, non-isomerisable alkenes were next studied. However, in the reaction of norbornene **4.17** full conversion of aldehyde to Tishchenko product was also observed, alongside some norbornene decomposition (Table 4.1, Entry 4). In the reaction of *n*-butyl vinyl ether **4.18** both starting materials were fully consumed (Table 4.1, Entry 5). The main products observed were poly-*n*-butyl vinyl ether, as indicated by the broad set of ethereal peaks between δ 3.65–3.25,[16] and Tishchenko product **4.13** (69%). Unpublished work in the group has shown that [Rh($Cy_2PCH_2CH_2PCy_2$)(η^6-1,2-$C_6H_4F_2$)][BAr^F_4] is an effective catalyst for methyl vinyl-ether polymerisation.[17]

In all the reactions of non-tethered aldehyde **4.12** with the alkyne/alkene substrates discussed thus far, no desired hydroacylation reactivity has been observed. This is in contrast to the effiecint alkene/alkyne hydroacylation observed for all the trialled substrates in combination with β-S-substituted aldehydes, catalysed by the Rh(I)-complex [Rh($Cy_2PCH_2PCy_2$)$(MeCN)_2$][BAr^F_4].[4] This can be rationalised by the differences in the resting state of the reactions. With β-S-substituted aldehydes the resting state starts as a Rh(III) κ^2-aldehyde-bound acyl-hydride complex, which then becomes a Rh(I)-κ^2-product-bound complex as the reaction proceeds.[18,19] These resting states persist due to the strong coordination of the β-S-tether and prevent alternative reactivity of the alkenes/alkynes, such as alkene isomerization. Interestingly, no Tishchenko reactivity was observed with the [Rh($Cy_2PCH_2PCy_2$)$(MeCN)_2$][BAr^F_4] catalyst system in the reactions of β-S-tether aldehydes with alkene/alkynes, indicating the β-S-tether must also play a role in preventing further aldehyde coordination/reactivity.

Finally, acrylates were trialled with aldehyde **4.12**, they have previously been shown to possess significant hydroacylation reactivity with *β*-S-substituted aldehydes and the alkene position is non-isomerisable. Reactivity was observed using the unoptimized conditions of aldehyde **4.12** (0.7 M), *n*-butyl acrylate **4.21** (3.0 equivalents) with *in situ* formed catalyst [Rh($Cy_2PCH_2PCy_2$)(η^6-C_6F_5H)][$AlO^F{}_4$] **4.10a** in pentafluorobenzene and with the preformed catalyst **4.10d** [Rh($Cy_2PCH_2PCy_2$)(η^6-1,2-$C_6H_4F_2$)][$AlO^F{}_4$] **4.10d** (10 mol%) in 1,2-difluorobenzene at 75 ºC, with both catalyst systems giving similar yields (Scheme 4.10).

Scheme 4.10. Acrylate hydroacylation reactivity with complex 4.10d

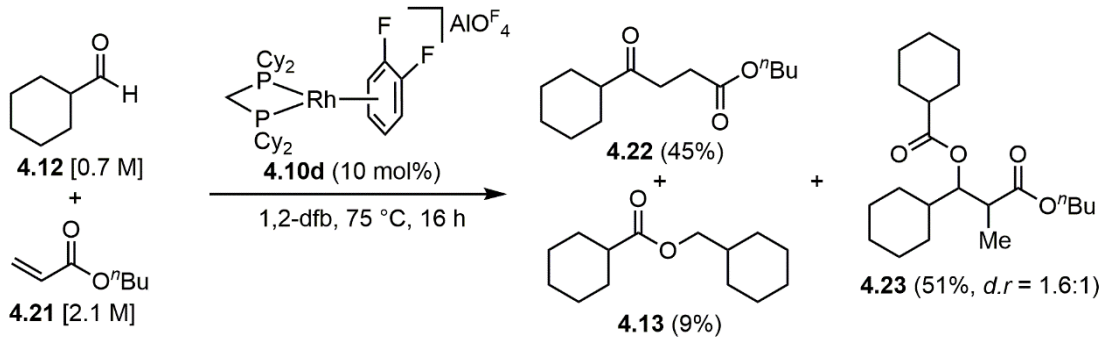

Three products were observed: *γ*-ketoester **4.22**, formed by alkene hydroacylation between aldehyde **4.12** and acrylate **4.21**; Tishchenko product **4.13**; and reductive-aldol-hydroacylation product **4.23** formed as a mixture of diastereomers. Changing the reaction solvent to 1,2-diflurobenzene from pentafluorobenzene did not affect the reaction outcome significantly, which is likely due to acrylate outcompeting both 1,2-diflurobenzene and pentafluorobenzene to bind to Rh(I)-under the employed reaction conditions.

A Rh-catalysed hydroacylation of methacrylate and a secondary untethered aldehyde to afford an analogous methyl-*γ*-ketoester has been previously reported by Tanaka and co-workers (See Chapter 1).[20] However, only a moderate yield (43%) was reported with 10 mol% of the {Rh(dppb)}$^+$ (dppb = 1,4-*bis*(diphenylphosphino)butane) catalyst and methacrylate was used as solvent (the exact conditions were not reported). Significantly better yields were reported using the structurally related *N*,*N*-dialkylacrylamides as an alkene, supporting their postulation that amide co-ordination plays a crucial role in reactivity (See Chapter 1).

Reductive-aldol-hydroacylation products such as **4.23** were not reported in the acrylamide system but have previously been observed in the rhodium catalysed reaction between *β*-S-substituted aldehydes and a range of Michael acceptors.[21,22] Interestingly, it was found that switching the ligand from dcpe to DPEPhos resulted in a complete selectivity switch to alkene hydroacylation from reductive-aldol-hydroacylation with acrylate esters.[22]

4.5. Rh-DPEPhos-Catalysed Acrylate Hydroacylation with Non-Tethered Aldehydes

Inspired by the previous studies showing that using DPEPhos as the ligand provided selectivity for alkene hydroacylation, a brief ligand screen was undertaken (a more detailed ligand screen is discussed later, Table 4.7). To carry out the ligand screen, the Rh(I)-complex $[Rh(nbd)_2]AlO^F{}_4$ was used as the rhodium source. The active pre-catalyst was generated in the reaction flask by adding the solvent to a mixture of the rhodium complex and ligand, which forms the Rh(I)-complex $\{Rh(nbd)(ligand)\}^+$; followed by hydrogenation of nbd and repurging of the system back into inert gas.

The best result from the ligand screen, using the conditions of aldehyde **4.12** (0.7 M), *n*-butyl acrylate **4.21** (3 equivalents) in 1,2-difluorobenzene at 75 ºC for 16 h, was the combination of $[Rh(nbd)_2]AlO^F{}_4$ **4.24** (10 mol%) and DPEPhos **4.25** (10 mol%). This afforded the *γ*-ketoester **4.22** in 58% yield, with no Tishchenko or reductive-aldol-hydroacylation being observed (Scheme 4.11).

Scheme 4.11. Initial conditions for the Rh-DPEPhos catalysed acrylate hydroacylation

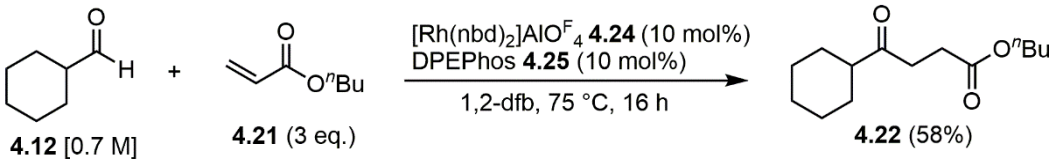

Having established that DPEPhos provides perfect selectivity for the desired *γ*-ketoester, the reaction was optimized for ^{1}H NMR yield using the $[Rh(nbd)_2]AlO^F{}_4$ **4.24** (5 mol%), DPEPhos **4.25** (5 mol %) catalyst system, in 1,2-diflourobenzene with a 16 h reaction time, nitromethane was used as an external ^{1}H NMR standard (Table 4.2).

It was found that increasing the equivalents of acrylate **4.21** significantly increased yield. 1, 1.5 and 3 equivalents afforded 19%, 37% and 65% yield respectively (Table 4.2, Entries 1–3). A small effect was

Table 4.2. Optimization of reagent concentration, stoichiometry and reaction temperature in the Rh-DPEPhos catalysed acrylate hydroacylation

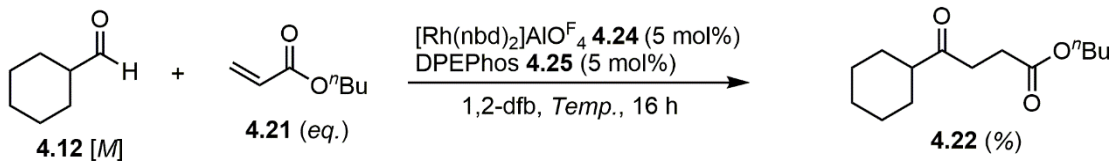

Entry	[**4.12**] (M)[a]	Eq. of **4.21**	Temp. (ºC)	**4.22** (%)[b]
1	1.2	**1.0**	90	19
2	1.2	**1.5**	90	37
3	1.2	**3.0**	90	65
4	**0.7**	3.0	90	58
5	**2.3**[c]	3.0	90	51
6	1.2	3.0	**100**	67
7	1.2	3.0	**110**	75
8	1.2	3.0	**120**	74

[a]Concentration of aldehyde **4.12** using total starting volume of reagents and solvent; [b]^{1}H NMR yield using nitromethane as a standard; [c]No 1,2-difluorobenzene added.

observed with increased concentration with 0.7 M and 1.2 M giving yields of 58% and 65% respectively (Table 4.2, Entries 3–4), a decrease in yield (51%) was observed when using conditions without 1,2-diflourobenzene (2.3 M, Table 4.2, Entry 5). Over the range tested, 110 ºC was the optimal reaction temperature providing a 75% yield (Table 4.2, Entries 3 and 6–8). Because yield increases significantly with alkene concentration, but not overall reaction concentration, we suggest that alkene is likely preventing deleterious reductive decarbonylation by quasi-irreversible coordination to the acyl-hydride. This effect has been previously reported in alkene hydroacylation with β-S-aldehydes.[4]

Using the optimized conditions of aldehyde **4.12** (1.2 M), acrylate **4.21** (3 equivalents) with 1,2-difluorobenzene as solvent at 110 ºC the effect of the counterion was then studied (Table 4.3).

Under conditions using $[Rh(nbd)_2]BF_4$ (5 mol%) and DPEPhos **4.25** (5 mol%) only a 23% ^{1}H NMR yield of γ-ketoester **4.22** was observed (Table 4.3, Entry 2). The low yield was likely caused by the poor solubility of the BF_4 catalyst system under the employed conditions, a precipitate was observed throughout the reaction. Using $[Rh(nbd)_2]BAr^F{}_4$ (5 mol%) and DPEPhos **4.25** (5 mol%) a 55% yield of γ-ketoester **4.22** was observed (Table 4.3, Entry 3), a significant decrease compared to the yield for

Table 4.3. The effect of the counterion in the Rh-DPEPhos catalysed acrylate hydroacylation

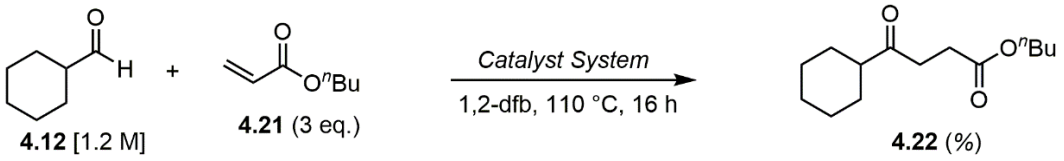

Entry	Catalyst System	**4.22** (%)[a]
1	$[Rh(nbd)_2]AlO^F{}_4$ (5 mol%), DPEPhos (5 mol%)	75
2	$[Rh(nbd)_2]BF_4$ (5 mol%), DPEPhos (5 mol%)	23
3	$[Rh(nbd)_2]BAr^F{}_4$ (5 mol%), DPEPhos (5 mol%)	55
4	[Rh(DPEPhos)(*o*-xylene)]$BAr^F{}_4$ (5 mol%)	65

[a]^{1}H NMR yield using nitromethane as a standard.

the $AlO^F{}_4$ catalyst system (75%, Table 4.3, Entry 1). Finally, the pre-catalyst [Rh(*cis*-κ^2-$_{P,P}$-DPEPhos)(η^6-*o*-xylene)]$BAr^F{}_4$ (5 mol%) was used, giving a 65% yield of γ-ketoester **4.22** (Table 4.3, Entry 4). These results show that $AlO^F{}_4$ is the optimal counterion for this reaction system.

4.6. Reaction scope of Acrylate Hydroacylation of Non-Tethered Aldehydes

Having established the optimized conditions when using DPEPhos as ligand, the aldehyde substrate scope was explored with a 30 h reaction time (Table 4.4).

Table 4.4. Preliminary aldehyde scope in acrylate hydroacylation

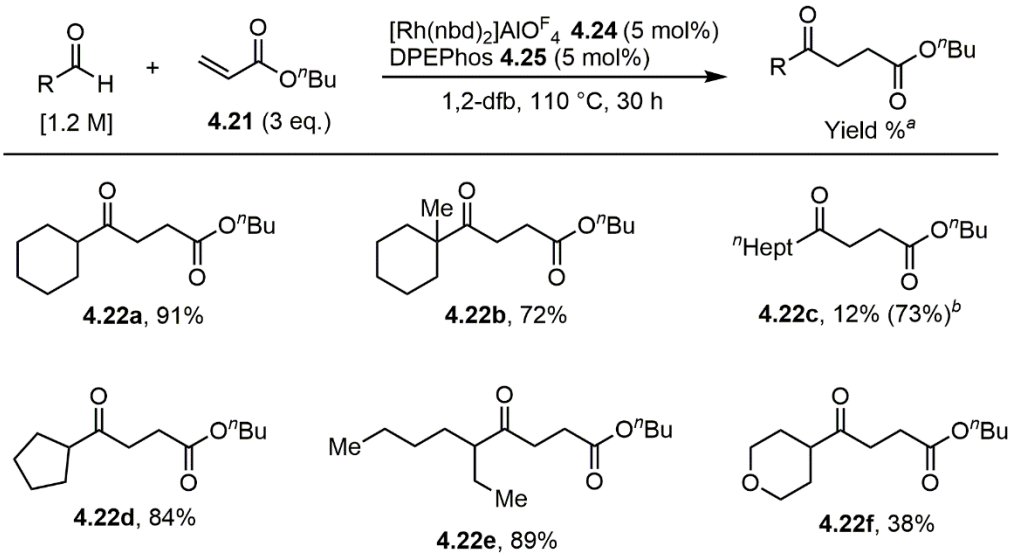

[a]Isolated yield; [b]isolated yield using $[Rh(nbd)_2]AlO^F{}_4$ (10 mol%) and dppb (10 mol %).

When using the standard substrate cyclohexanecarboxaldehyde **4.12** the γ-ketoester **4.22a** was isolated

in 91% yield after column chromatography. The quaternary aldehyde 1-methylcyclohexane-1-carboxaldehyde also performed well, affording *γ*-ketoester **4.22b** in 72% yield, to our knowledge this is the first example of a non-tethered quaternary aldehyde intermolecular hydroacylation reaction.

In the reaction of secondary aldehyde *n*-octanal only a 12% isolated yield of product **4.22c** was observed, the ^{1}H NMR spectrum of the crude reaction mixture indicated a significant amount of unreacted aldehyde remained, suggesting catalyst decomposition may have caused the low yield. A potential reason for the reduced product yield with a secondary aldehyde compared to both tertiary and quaternary aldehydes is the increased propensity for less substituted aldehydes to undergo reductive decarbonylation (See Chapter 2). It was discovered that using dppb as a ligand provided higher yields of secondary *γ*-ketoester **4.22c**, and when used at 10 mol% in combination with 10% of $[Rh(nbd)_2]AlO^F_4$ **4.24** the *γ*-ketoester **4.22c** was isolated in 73% yield. Interestingly, in Tanaka's acrylamide system using a $\{Rh(I)dppb\}^+$ catalyst, secondary and tertiary aldehydes performed well, perhaps suggesting the amide tethering group helps prevent decarbonylation compared to the ester group.

Using the standard conditions, the tertiary aldehydes cyclopentanecarboxaldehyde and 2-ethylhexanal provided good isolated yields of the *γ*-ketoester **4.22d** (84%) and **4.22e** (89%) respectively. However, under the same conditions using tetrahydro-2*H*-pyran-4-carboxaldehyde only a 38% isolated yield of *γ*-ketoesters **4.22f** was observed, the reduced yield may be caused by coordination of the ethereal oxygen to rhodium. Several aldehydes that were trialled afforded only traces of or no desired product (Table 4.5).

Aldehydes **4.26**–**4.31** all provided no hydroacylation reactivity. For substrates **4.26**–**4.29**, this can be explained by their increased propensity to reductive decarbonylation, due to forming more favourable M–C bonds after decarbonylation when compared to *n*-heptanal. In contrast, tertiary aldehydes **4.29** and **4.30** would be expected to form less favourable M–C bonds after decarbonylation when compared to *n*-heptanal. Their lack of reactivity may be due to possessing electron rich aromatic rings that compete for coordination to the rhodium metal centre, arene ligands have been previously shown to be poisonous in Rh(I)-catalysis.[23,24] In Tanaka's $\{Rh(I)\text{-}dppb\}^+$ acrylamide system, aromatic aldehydes such as

Table 4.5. Unsuccessful aldehydes in the acrylate hydroacylation

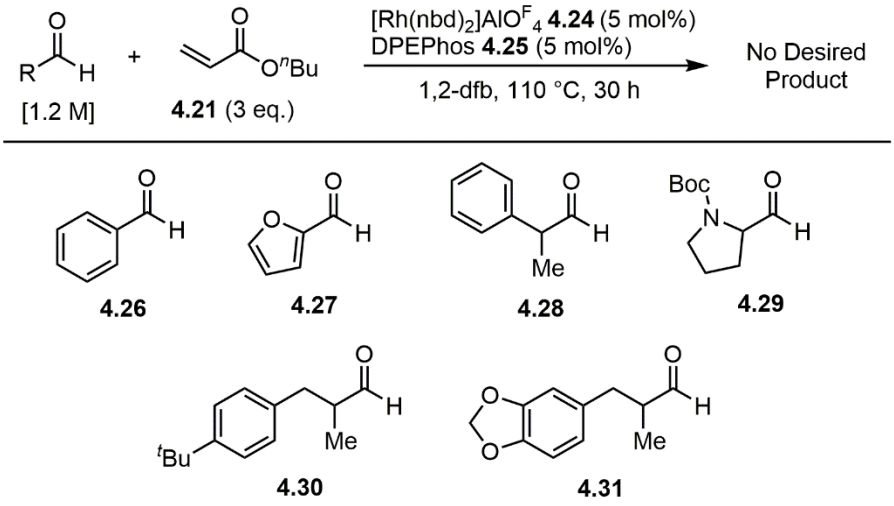

benzaldehyde and secondary aldehydes with remote aromatic groups provided high yields of hydroacylation products.[20] Suggesting that not only is reductive decarbonylation supressed with acrylamides, they may also prevent deleterious binding of aromatic groups. Having assessed the preliminary aldehyde scope, the scope of acrylate was studied next (Table 4.6).

Table 4.6. Preliminary acrylate screen

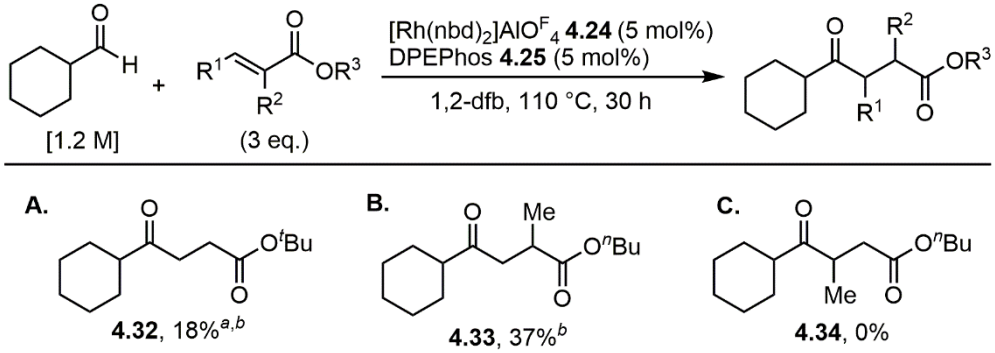

[a]Reaction temperature 90 ºC instead of 110 ºC; [b] NMR yield using nitromethane as a standard.

The reaction with *t*-butyl acrylate resulted in a poor 18% ^{1}H NMR yield of product **4.32** (Table 4.6, **A**), with the reaction being performed at 90 ºC due to evaporation of the substrate. In the reaction of *n*-butyl methyl methacrylate only a in 37% ^{1}H NMR yield of *γ*-ketoester **4.33** was observed (Table 4.6, **B**), while the acrylate ethyl (*E*)-2-crotonate did not afford any hydroacylation product. These two results are in contrast to the high yields reported when the corresponding substituted acrylamides were employed in Tanaka's system.[20] This could be explained by differences in the rate of reductive

decarbonylation for acrylamide compared to acrylates. The increased substitution of the alkene is most likely to hinder the hydride insertion step, potentially making it rate-limting.[19] At the start of catalysis, this would lead to an increase in the equilibrium concentration of acyl-hydride which can undergo deleterious reductive decarbonylation. If acrylamides, as proposed by Tanaka, decrease the rate of reductive decarbonylation compared to acrylates, this may lead to the significant difference in their reactivities with substituted alkenes.

4.7. Evaluation of Ligand effects in Acrylate Hydroacylation of Non-Tethered Aldehydes

Having found that dppb performed better than DPEPhos in the reaction of *n*-octanal under the optimized conditions, during the substrate scope, ligands were then rescreened for reactivity (Table 4.7).

Table 4.7. Ligand screen for the non-tethered aldehyde hydroacylation with acrylates

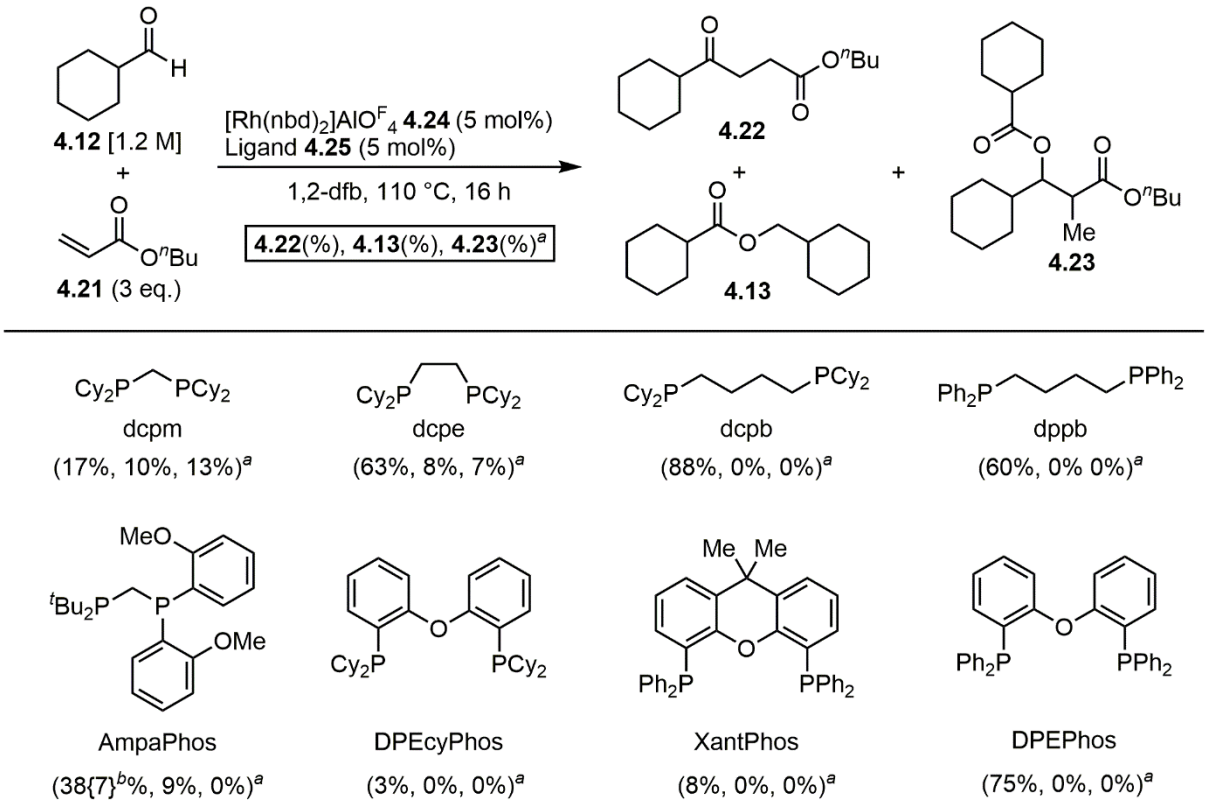

[a]^{1}H NMR yield of (**4.22**, **4.13**, **4.23**) using nitromethane as a standard; [b]Yield of branched hydroacylation product in parenthesis.

A clear trend was observed for increased selectivity and ^{1}H NMR yield for γ-ketoester **4.22** with increasing ligand bite-angle (Table 4.7: dcpm, dcpe and dcpb). The yield of γ-ketoester **4.22** decreased when the substituent on the phosphine was changed from cyclohexyl to phenyl, with dcpb giving 88%

yield and dppb giving 60% yield (Table 4.7: dcpb, dppb). When the unsymmetrical small bite-angle ligand AmpaPhos was used, moderate yields (38%) of γ-ketoester **4.22** alongside the branched hydroacylation product (7%) and Tishchenko ester **4.13** (9%) were observed (Table 4.7: AmpaPhos); AmpaPhos has previously been shown to increase branched selectivity in alkyne hydroacylation.[25]

Further screening of POP-type ligands DPE(cy)Phos and Xantphos resulted in greatly reduced yields, 3% and 8% respectively, compared to 75% for DPEPhos (Table 4.7: DPE(cy)Phos, Xantphos, DPEPhos).[26] DPEPhos possesses greater flexibility than XantPhos, allowing it to switch between *mer* and *fac*/κ^2 arrangements more readily.[26] DPE(cy)Phos has been speculated to also have reduced flexibility compared to DPEPhos due to the steric constraints of the cyclohexyl groups in *fac*/κ^2-arrangement.[28] The significant difference in reactivity between the ligands could be due to the requirement of a *fac*/κ^2-coordinated complex during the catalytic cycle, which is more easily accessed by DPEPhos than XantPhos or DPE(cy)Phos. Overall, the ligand screen indicated that dcpb performs better than DPEPhos in under the optimized conditions for the model reaction and therefore should be used to re-examine the aldehyde substrate scope.

4.8. *In situ* synthesis of a potential Rh(I)DPEPhos acrylate-bound complex

The catalyst speciation with DPEPhos as ligand was briefly explored by attempting to synthesise a methacrylate-bound Rh(I)-DPEPhos complex. The reactions were performed in high pressure NMR spectroscopy tubes, which necessitated the hydrogenation to be performed by freeze-pump-thawing, rather than by bubbling H_2 gas through the solution, as is done for catalysis. Hydrogenation of [Rh(*cis*-κ^2-$_{P,P}$-DPEPhos)(nbd)][BAr^F_4] **4.37** (0.02 M) in 1,2-difluorobenzene, under 4 atm of hydrogen, at 25 ºC, resulted in an initial colour change from orange to dark red after 2 minutes. The solution became darker still after periodic and vigorous shaking for 30 minutes, a similar set of colour changes are observed under catalytic hydrogenation conditions, but within 3 minutes hydrogenation time. The formed complex is tentatively assigned as [Rh(*fac*-κ^3-$_{P,O,P}$-DPEPhos)(H)(μ-H)$_2$]$_2$[BAr^F_4]$_2$ **4.35** which remined stable after being placed under argon (Figure 4.2).

The hydrogenation was followed by $^{31}P\{^1H\}$ NMR spectroscopy and after 1 minute (Figure 4.2, A) a further species was observed as a doublet in the $^{31}P\{^1H\}$ NMR spectrum at δ 30.8 [J_{RhP} = 215 Hz)] in

Figure 4.2. $^{31}P\{^{1}H\}$ NMR spectra of the hydrogenation of nbd complex 4.35 after A) 1 min; B) After 10 mins; C) After 30 mins [a]

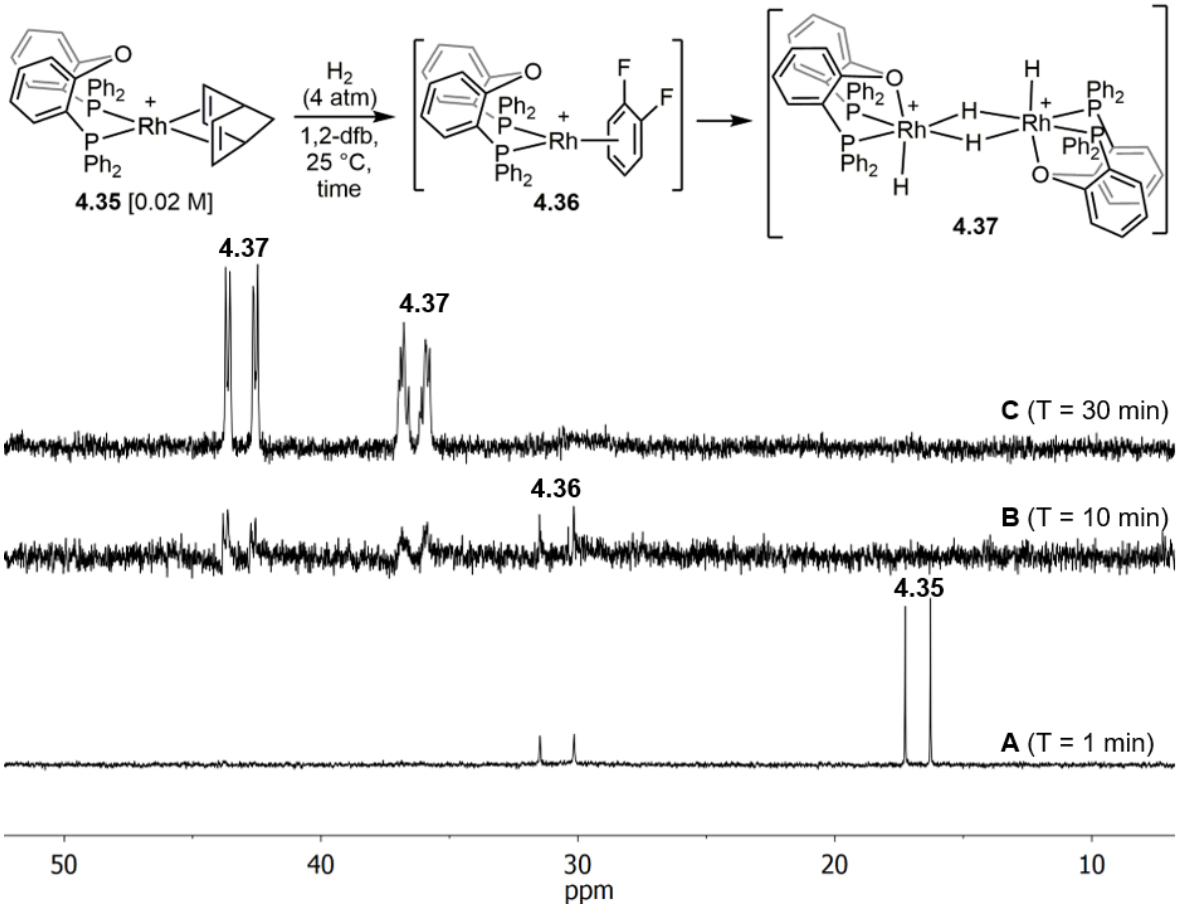

[a]BAr^{F}_{4} anions omitted for clarity

1 : 3 ratio with nbd complex **4.35**. The complex is tentatively assigned as [Rh(*cis*-κ^2-$_{P,P}$-DPEPhos)(η^6-1,2-$C_6H_4F_2$)][BAr^{F}_{4}] **4.36**, the structurally related complex [Rh(*cis*-κ^2-$_{P,P}$-DPEPhos)(η^6-*o*-xylene)][BAr^{F}_{4}] has been previously characterised and possesses a similar doublet in the $^{31}P\{^{1}H\}$ NMR spectrum at δ 32.6 [J_{RhP} = 216 Hz].

After 10 minutes (Figure 4.2, B): all the nbd complex was consumed, some of 1,2-difluorobenzene complex **4.36** remained and complex **4.37** started to form. After 30 minutes complex **4.37** became the only species present in the $^{31}P\{^{1}H\}$ NMR spectrum (Figure 4.2, C). Which displayed a doublet of doublets at δ 43.1 [J_{RhP} = 173 Hz, J_{PP} = 27 Hz] and a doublet with second order coupling at δ 36.4, indicating that the phosphorous atoms are in two different environments. In the hydride region of the ^{1}H NMR spectrum two signals were observed as a 1 : 1 ratio, with a complex multiplet at δ –10.9 and a broad apparent triplet at δ –15.6 [J_{PH} = 34.0 Hz, J_{PH} = 34.0 Hz]. These chemical shifts and coupling

patterns are consistent with the signals corresponding to bridging and terminal hydrides respectively (Figure 4.3).

Figure 4.3. Hydride Region of the ^{1}H NMR Spectrum of Intermediate 4.37

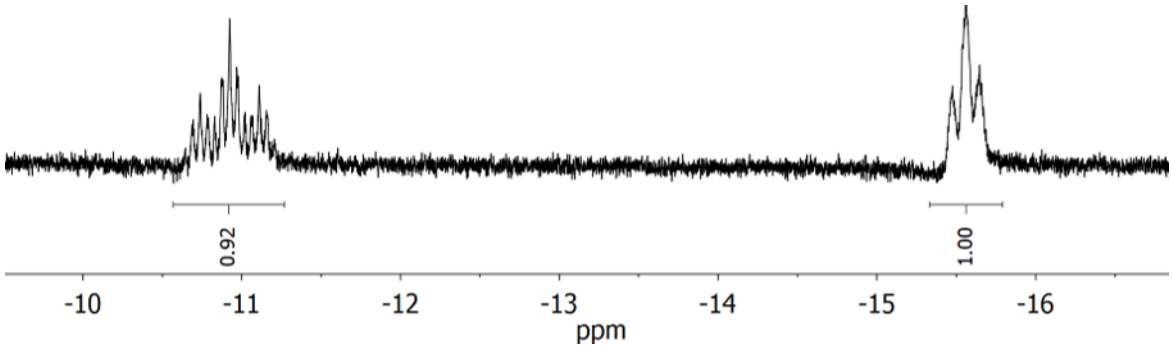

The observed chemical shifts are similar to those reported for the hydride-bridged dimer complex $[(PPh_3)_2RhH(\mu\text{-}H)(\mu\text{-}Cl)_2HRh(PPh_3)_2][CB_{11}H_6I_6]$ (δ –11.0 for the bridging hydride and at δ -16.5 for terminal hydrides).[29] The bridging hydride signal at δ –10.9 in the ^{1}H NMR spectrum of complex **4.37** can be modelled as an AA'BB'XX' spin system [J = 74 Hz, 74 Hz, 19 Hz, 19 Hz, 19 Hz, 19 Hz] (Figure 4.4).

Figure 4.4. A) Simulated AA'BB'XX' spin system; B) Actual ^{1}H NMR Spectrum

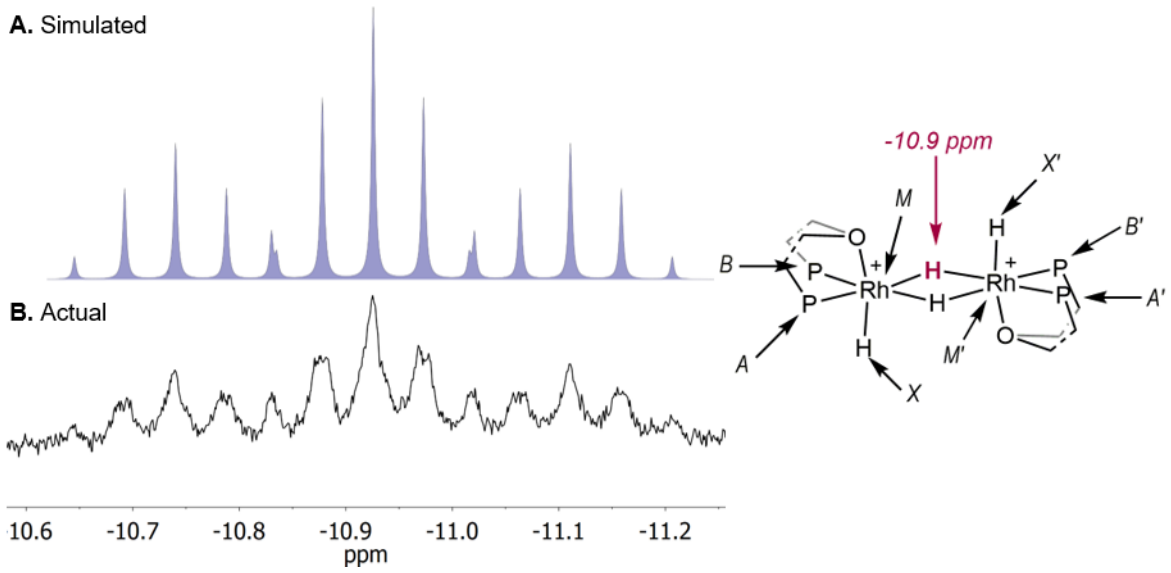

The large coupling constant (74 Hz) is assigned as the *trans*-coupling to two phosphines in similar environments (A and A'), a similarly large *trans*-phosphine coupling constant (75 Hz) is observed in the $[(PPh_3)_2RhH(\mu\text{-}H)(\mu\text{-}Cl)_2HRh(PPh_3)_2][CB_{11}H_6Y_6]$ complex.[29] The 4 smaller coupling constants (19 Hz)

are assigned as coupling to two *cis*-phosphines in similar environments (B and B') and the two rhodium atoms (X and X'). Close inspection of the hydride signal reveals that a small, poorly resolved, coupling is also present, this is attributed to coupling with the *cis*-hydrides.

For the terminal and axial hydride with a chemical shift of δ –16.5 the coupling constants (34 Hz) are consistent with coupling to two *cis*-phosphines in similar environments and small unresolved couplings with rhodium and the *cis*-hydrides. This data is consistent with the assignment of a κ^3-DPEPhos intermediate with axial-terminal hydrides and equatorial-bridging hydrides. The related Ir(III)-complex [Ir(*fac*-κ^3-$_{P,O,P}$-XantPhos)(H)(μ-H)$_2$][BAr$^F{}_4$]$_2$ has been previously synthesised in an analogous manner and has been shown to have the same hydride regiochemistry by single crystal X-ray diffraction.[30] In this iridium complex a small *cis*-hydride hydride coupling constant of 3 Hz was observed, consistent with the poorly resolved coupling in the spectrum of the Rh(III)-bridged hydride complex **4.37**.

In the Ir(III)-complex [Ir(*fac*-κ^3-$_{P,O,P}$-XantPhos)(H)(μ-H)$_2$][BAr$^F{}_4$]$_2$ only one phosphine environment was observed compared to the two environments in the Rh(III)-bridged hydride complex **4.37**. This can be rationalised by puckering of the DPEPhos backbone, which removes the C_2-symmetry in the complex. This is indicative of the phosphorus atoms being in subtly different environments, however, the difference is small, meaning that the coupling constants observed in the hydride region of the ^{1}H spectrum are measured as being the same. Rhodium complexes with a coordinated κ^3-DPEPhos often exhibit this puckering whereas κ^3-XantPhos ligands do not, this is exemplified in the previously reported x-ray diffraction structures of the Rh(I)-complexes [Rh(*fac*-κ^3-$_{P,O,P}$-DPEPhos){PCyp$_2$(η^2-C$_5$H$_7$)}][BAr$^F{}_4$] Rh(III)-bridged hydride complex **4.38a** and [Rh(*fac*-κ^3-$_{P,O,P}$-XantPhos){PCyp$_2$(η^2-C$_5$H$_7$)}][BAr$^F{}_4$] Rh(III)-bridged hydride complex **4.38b** (Figure 4.5).[31]

Clear puckering is observed for DPEPhos whereas the dimethyl bridge of the XantPhos ligand (C3, Figure 4.5) forces symmetry in the ligand backbone. For DPEPhos-complex **4.38a** only one phosphorous enviroment is observed in the ^{31}P NMR spectrum, due to a fluxional process on the NMR timescale. We suggest that this fluxional process is inhibited for the Rh(III)-bridged hydride complex **4.37**, resulting in the two observed phosphorous environments.

Figure 4.5. Single crystal x-ray diffraction structures of [Rh(*fac*-κ^3-$_{P,O,P}$-DPEPhos){PCyp$_2$(η^2-C$_5$H$_7$)}][BAr$^F_4$] 4.38a and [Rh(*fac*-κ^3-$_{P,O,P}$-XantPhos){PCyp$_2$(η^2-C$_5$H$_7$)}][BAr$^F_4$] 4.38b[a]

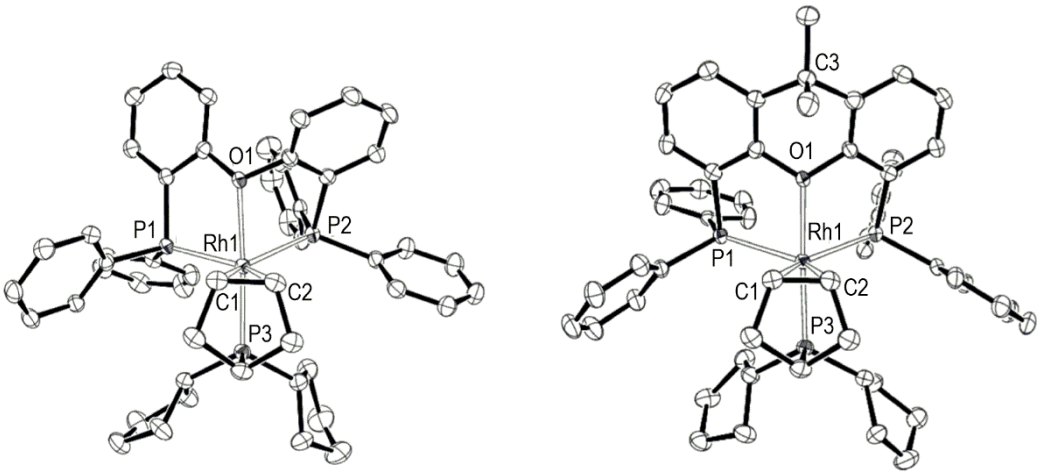

4.38a - {Rh(*fac*-κ^3-$_{P,O,P}$-DPEPhos)}$^+$ **4.38b** - {Rh(*fac*-κ^3-$_{P,O,P}$-XantPhos)}$^+$

[a] Structures taken from reference 31, [BAr$^F_4$] anions omitted for clarity.

With the intention of synthesising a methyl acrylate coordinated Rh-complex, methyl acrylate **4.39** (20 eq.) was then added to the *in situ* formed Rh(III)-bridged hydride complex **4.37**. The reaction mixture was left to stand for 16 h until complete consumption of **4.37** was observed, alongside formation of a new species that is tentatively assigned as the Rh(I)-complex [Rh(*cis*-κ^2-$_{P,P}$-DPEPhos)(methacrylate)][BAr$^F_4$] **4.40** (Figure 4.6).

No hydride signals were observed in the ^{1}H NMR spectrum and in the ^{31}P{^{1}H} NMR spectrum two sets of doublet of doublets were observed at δ 41.5 [J_{RhP} = 171 Hz, J_{PP} = 21 Hz] and δ 8.2 [J_{RhP} = 98 Hz, J_{PP} = 21 Hz]. The small phosphine-phosphine coupling constant (21 Hz) is characteristic of a Rh(I)-complex with *cis* phosphines in different environments, the large difference in rhodium-phosphine coupling constants indicates the *trans* ligands are distinct in nature. The phosphine with the smaller coupling constant (98 Hz) is proposed to be *trans* to the alkene. The rhodium-phosphine coupling constant is remarkably small for a Rh(I)-complex, although in the square based pyramidal Rh(I)-methyl vinyl ketone (MVK) complex [Rh(PMe$_3$)$_4$(MVK)][BPh$_4$] with an axial PMe$_3$ group, the phosphine *trans* to the alkene has a Rh–P coupling constant of 119 Hz.[32] The phosphine with the larger coupling constant (171 Hz) is proposed to be *trans* to the ester group, the Rh–P coupling constant in the Rh(I)-complex [Rh(*cis*-κ^2-$_{P,P}$-DPEPhos)(acetone)$_2$][BAr$^F_4$] is 204 Hz, where both phosphorus atoms are *trans* to κ^1-$_O$-acetone ligands.[33]

Figure 4.6. Addition of methacrylate to [Rh(*fac*-κ^3-$_{P,O,P}$-DPEPhos)(H)(μ-H)$_2$]$_2$[BAr$^F{}_4$]$_2$, ^{31}P{^{1}H} NMR spectra: A) T = 0 B) T = 16 h

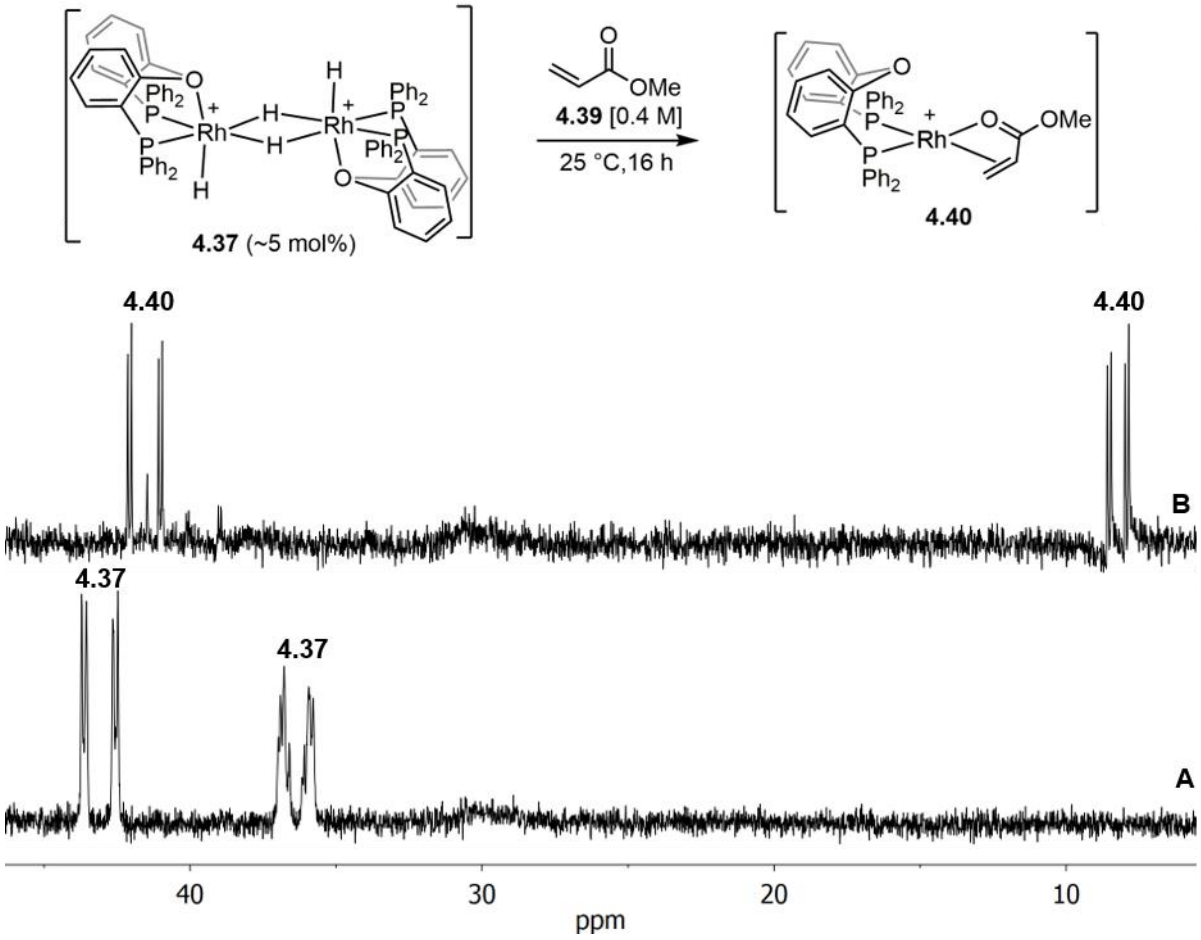

The formation of the acrylate bound complex **4.40** is proposed to proceed *via* hydrogenation of an equivalent of methacrylate. Consistent with this postulation are the two new methyl-ester environments observed in the ^{1}H NMR spectrum after 16 h, one is proposed to be the hydrogenated ester product, the other the coordinated acrylate. Furthermore, no free H_2 was observed in the ^{1}H NMR spectrum, ruling out a ligand substitution reaction with H_2.

After the hydrogenation step, the presence of the methacrylate complex and no 1,2-difluorobenene complex indicates that methacrylate outcompetes 1,2-diflourobenzene for coordination to rhodium. The concentration of acrylate (0.4 M) is much lower than in the optimized hydroacylation conditions (3.6 M), which indicates that acrylate is the most strongly coordinating ligand (compared to solvent and aldehyde) at the start of catalysis. For the other ligand systems, the position of this equilibrium will be strongly influenced by the ligand bite-angle, previous studies have shown that wider bite-angle ligands disfavour η^6-coordination of the fluorobenzene.[2,34]

4.9. Plausible Mechanisms in the Reactions of Non-Tethered Aldehydes

Considering these studies of the non-tethered aldehyde hydroacylation with methacrylate, a plausible mechanistic scenario is presented, focussing on the effect on reactivity with variation of the *bis*-phosphine ligand (Scheme 4.12).

Scheme 4.12. Plausible mechanisms for hydroacylation (Cycle A), reductive reductive-aldol-hydroacylation (Cycle B) and Tishchenko reaction (Cycle C)

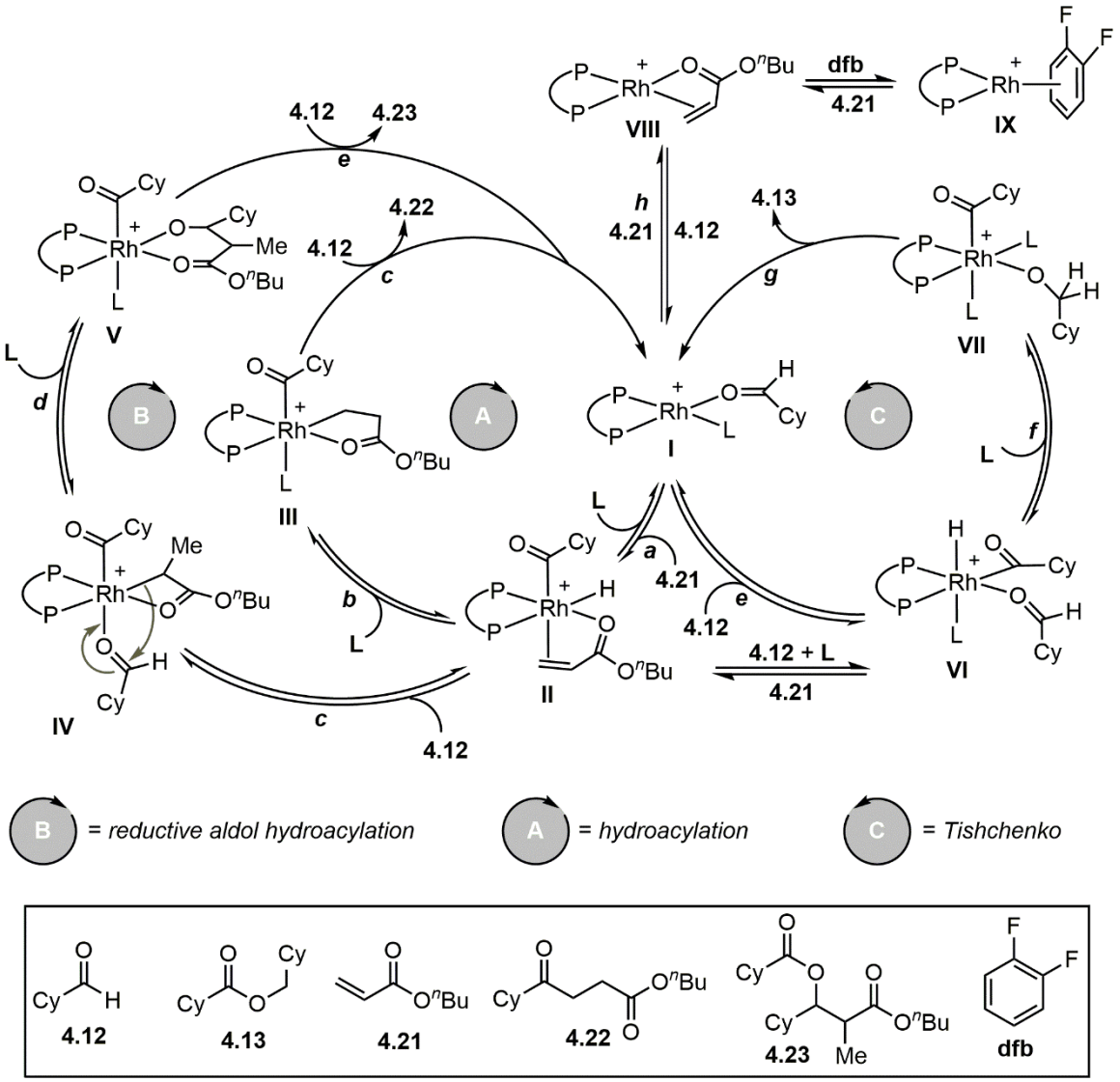

The hydroacylation (Cycle A) and reductive-aldol-hydroacylation (Cycle B) are likely to proceed by similar mechanisms to those proposed for *β*-S-aldehydes,[21,35] with differences due to there being an absence of an aldehyde-tethering group, which are discussed here-in.

Hydroacylation (Cycle A): Before addition of aldehyde a ligand dependant equilibrium will be set up

between 1,2-difluorobenzene bound complex **IX** and acrylate bound complex **VIII**. Productive catalysis will start with oxidative addition from a Rh(I)-aldehyde bound intermediate **I** to form the Rh(III)-acyl-hydride intermediate **II**, which for productive hydroacylation pathways will likely have an κ^2-bound acrylate. Due to the chelation effect, the acrylate will be relatively strongly bound and may help prevent reductive decarbonylation, as is proposed for Tanaka's acrylamide hydroacylation reaction.[20] The effect of having a tertiary acyl-hydride will also help prevent reductive decarbonylation in this system. For hydroacylation from intermediate **II** (Cycle A), likely reversible hydride insertion to form linear acyl-alkyl intermediate **III** will be followed by likely irreversible reductive elimination to form γ-ketoester **4.22** and complex **I**.

Reductive-aldol-hydroacylation (Cycle B): From acyl-hydride intermediate **II** likely reversible branched hydride insertion from Rh(III)-acyl-hydride **II** will form the Rh(III)-acyl-enolate intermediate **IV**. This Rh-enolate will then undergo an aldol reaction with a further equivalent of co-ordinated aldehyde to form Rh(III)-acyl-alkoxide complex **V**, this aldol reaction may also be reversible. From this intermediate irreversible-reductive C–O bond formation followed by ligand substitution will then afford diester **4.23**.

Tishchenko reaction (Cycle C): As discussed earlier (Scheme 4.9), the mechansim will begin with aldehyde oxidative addition *via* complex **I** to give a Rh(III)-acyl-hydride complex **VI**, which can undergo hydride insertion to a second equivalent of bound aldehyde to form a Rh(III)-acyl-alkoxide complex **VII**, reductive elimination will then liberate ester **4.13** and reform aldehyde bound complex **I**.

There are several possible reasons for the observed increase in selectivity for acrylate hydroacylation, over reductive-aldol-hydroacylation, with increasing ligand bite-angle: i) There may be a preference for linear over branched hydride insertion, although hydride insertion with simple alkenes (e.g. 1-octene) is usually fast and reversible;[4,19] ii) The aldol reaction to form Rh(III)-acyl-alkoxide **V** becomes slow; iii) ester reductive elimination from **V** becomes relatively slow or iv) reductive elimination to form γ-ketoester **4.22** from Rh(III)acyl-alkyl complex **III** becomes relatively fast.

As the natural bite-angle[36] of the ligand increases the accessible molecular surface of the ligand becomes smaller, which may disfavour additional aldehyde approach or the aldol reaction itself, which

would prevent reductive-aldol-hydroacylation. Interestingly, rates of reductive elimination have been shown to increase with small bite-angle ligands,[37] which could mean dcpm promotes the potentially challenging ester bond forming reductive elimination. Reductive elimination of methanol has been shown to have a higher barrier that reductive elimination of methane from Rh(III) complexes,[38] which may suggest that reductive elimination to form esters is also more challenging than ketone formation.

Hydroacylation being favoured over Tishchenko reaction with increased bite-angle could be due to an increased preference for acrylate binding in Rh(III)-acyl-hydride **II** compared to aldehyde binding in Rh(III)-acyl-hydride **VI**, or due to the relative rates of hydride insertion or reduction elimination for the subsequently formed intermediates in the respective cycles. Interestingly, increasing ligand bite-angle increases the selectivity for the Tishchenko reaction in the hydroacylation reactions of β-S-aldehydes and methacrylate.[12]

The effect of ligand bite-angle on reaction selectivity could be understood better by studying the kinetics of the Tishchenko reaction, providing information on whether the increased bite-angle slows down the Tishchenko reaction or potentially accelerates the acrylate hydroacylation reaction. Identification of the resting states of the reaction, and the kinetic order in reagents, would help elucidate the effect further. Further information could be found by performing deuterium labelling studies and measuring a KIE. Potentially providing information on whether hydride insertion to the acrylate is reversible.

4.10. Conclusions

An acrylate hydroacylation for non-tethered aliphatic aldehydes has been developed utilising wide bite-angle *bis*-phosphine ligands (DPEPhos, dcpb). Tertiary and quaternary aldehydes perform particularly well and the first example of a non-tethered-quaternary aldehyde intermolecular hydroacylation is reported. Secondary aldehydes perform less well, this is proposed to be due to faster rates of reductive decarbonylation for less substituted aldehydes. Interestingly, aromatic aldehydes also do not work in the reaction, including tertiary aldehydes with more remote aromatic rings, suggesting that the presence of aromatic groups can also inhibit catalysis.

The dppb ligand was shown to perform much better than DPEPhos for secondary aldehydes and a ligand screen under the optimized DPEPhos conditions revealed dcpb to be marginally better in tertiary aldehyde hydroacylation. The improvement in yield using these conditions suggests that re-evaluating the aldehyde and acrylate scope with dcpb may provide better results. This could also be extended to re-evaluating different non-isomerisable alkenes such as norbornadiene and vinyltrimethylsilane.

The use of wide bite-angle ligands increased the selectivity for hydroacylation over the side reactions of reductive-aldol-hydroacylation and the Tishchenko reaction. The mechanistic detail for this observation is not clear and mechanistic studies to probe this were suggested. Initial studies of the {Rh(dcpm)}$^+$ catalysed Tishchenko reaction showed that reaction rate significantly increased with increased fluorine substitution of the fluoroarene solvent. This was rationalised by the increased concentration of Rh(I)-aldehyde-bound complexes, facilitating aldehyde oxidative addition. The effect of solvent was less pronounced in the acrylate hydroacylation because, as was demonstrated for {Rh(DPEPhos)}$^+$ ligand system, acrylate likely becomes more strongly coordinating than 1,2-difluorobenzene.

Overall, the development of non-tethered aldehyde hydroacylation catalysed by rhodium remains a substantial challenge, due to the significant effect the aldehyde-tether plays on the reaction equilibrium, including preventing side reactions of the alkene/alkyne coupling partner. A catalyst system in which a 3-coordinate Rh(I)-complex undergoes selective aldehyde oxidative addition, to form a 5-coordinate acyl-hydride intermediate, instead of reacting with alkene/alkyne can be envisaged as a principle for catalyst design. The so-formed acyl-hydride complex would need to be stable to decarbonylation and/or then be able to undergo alkene/alkyne coordination, followed by hydride insertion and reductive elimination for a productive hydroacylation reaction.

4.11. References

1 S. Muthusamy and B. Gnanaprakasam, *Tetrahedron Lett.*, 2005, **46**, 635–638.

2 S. D. Pike, I. Pernik, R. Theron, J. S. McIndoe and A. S. Weller, *J. Organomet. Chem.*, 2015, **784**, 75–83.

3 A. L. Colebatch, A. I. McKay, N. A. Beattie, S. A. Macgregor and A. S. Weller, *Eur. J. Inorg. Chem.*, 2017, 4533–4540.

4 A. B. Chaplin, J. F. Hooper, A. S. Weller and M. C. Willis, *J. Am. Chem. Soc.*, 2012, **134**, 4885–4897.

5 D. P. Fairlie and B. Bosnich, *Organometallics*, 1988, **7**, 946–954.

6 I. F. D. Hyatt, H. K. Anderson, A. T. Morehead and A. L. Sargent, *Organometallics*, 2008, **27**, 135–147.

7 K. E. McPherson, L. J. Bartolotti, A. T. Morehead and A. L. Sargent, *Organometallics*, 2016, **35**, 1861–1865.

8 H. Yu, A. D. Schlüter and B. Zhang, *Helv. Chim. Acta*, 2012, **95**, 2399–2410.

9 T. Li, B.-H. Xu, D.-P. Zhu, Y.-F. Wang and S.-J. Zhang, *Org. Chem. Front.*, 2018, **5**, 1933–1939.

10 Y. Hoshimoto, M. Ohashi and S. Ogoshi, *J. Am. Chem. Soc.*, 2011, **133**, 4668–4671.

11 Z. Shen, P. K. Dornan, H. A. Khan, T. K. Woo and V. M. Dong, *J. Am. Chem. Soc.*, 2009, **131**, 1077–1091.

12 R. J. Pawley, G. L. Moxham, R. Dallanegra, A. B. Chaplin, S. K. Brayshaw, A. S. Weller and M. C. Willis, *Organometallics*, 2010, **29**, 1717–1728.

13 K. G. M. Kou, D. N. Le and V. M. Dong, *J. Am. Chem. Soc.*, 2014, **136**, 9471–9476.

14 T. J. Clark, G. R. Whittell and I. Manners, *Inorg. Chem.*, 2007, **46**, 7522–7527.

15 P. Siemsen, R. C. Livingston and F. Diederich, *Angew. Chem. Int. Ed.*, 2000, **39**, 2632–2657.

16 S. Kéki, M. Nagy, G. Deák and M. Zsuga, *J. Phys. Chem. B*, 2001, **105**, 9896–9901.

17 H. G. Garwood, A. J. Buckvic and A. S. Weller, *Unpublished Results*.

18 I. Pernik, J. F. Hooper, A. B. Chaplin, A. S. Weller and M. C. Willis, *ACS Catal.*, 2012, **2**, 2779–2786.

19 A. Prades, M. Fernández, S. D. Pike, M. C. Willis and A. S. Weller, *Angew. Chem. Int. Ed.*, 2015, **54**, 8520–8524.

20 K. Tanaka, Y. Shibata, T. Suda, Y. Hagiwara and M. Hirano, *Org. Lett.*, 2007, **9**, 1215–1218.

21 M. C. Willis and R. L. Woodward, *J. Am. Chem. Soc.*, 2005, **127**, 18012–18013.

22 J. D. Osborne and M. C. Willis, *Chem. Commun.*, 2008, **0**, 5025–5027.

23 D. Heller, H.-J. Drexler, A. Spannenberg, B. Heller, J. You and W. Baumann, *Angew. Chem. Int. Ed.*, 2002, **41**, 777–780.

24 A. Meißner, H.-J. Drexler, S. Keller, C. Selle, V. Ratovelomanana-Vidal and D. Heller, *Eur. J. Inorg. Chem.*, 2014, 4836–4842.

25 T. J. Coxon, M. Fernández, J. Barwick-Silk, A. I. McKay, L. E. Britton, A. S. Weller and M. C. Willis, *J. Am. Chem. Soc.*, 2017, **139**, 10142–10149.

26 G. M. Adams and A. S. Weller, *Coord. Chem. Rev.*, 2018, **355**, 150–172.

27 R. J. Pawley, M. A. Huertos, G. C. Lloyd-Jones, A. S. Weller and M. C. Willis, *Organometallics*, 2012, **31**, 5650–5659.

28 C. Holzapfel and T. Bredenkamp, *ChemCatChem*, 2015, **7**, 2598–2606.

29 A. Rifat, N. J. Patmore, M. F. Mahon and A. S. Weller, *Organometallics*, 2002, **21**, 2856.

30 A. J. Pontiggia, A. B. Chaplin and A. S. Weller, *J. Organomet. Chem.*, 2011, **696**, 2870–2876.

31 R. Dallanegra, A. B. Chaplin and A. S. Weller, *Organometallics*, 2012, **31**, 2720–2728.

32 I. P. Kovalev, Y. N. Kolmogorov, Y. A. Strelenko, A. V. Ignatenko, M. G. Vinogradov and G. I. Nikishin, *J. Organomet. Chem.*, 1990, **385**, 173–184.

33 G. L. Moxham, H. Randell-Sly, S. K. Brayshaw, A. S. Weller and M. C. Willis, *Chem. Eur. J.*, 2008, **14**, 8383–8397.

34 A. Kumar, I. K. Priest, T. N. Hooper and A. S. Weller, *Dalt. Trans.*, 2016, **45**, 6183–6195.

35 G. L. Moxham, H. E. Randell-Sly, S. K. Brayshaw, R. L. Woodward, A. S. Weller and M. C. Willis, *Angew. Chem. Int. Ed.*, 2006, **45**, 7618–7622.

36 K. Angermund, W. Baumann, E. Dinjus, R. Fornika, H. Görls, M. Kessler, C. Krüger, W. Leitner and F. Lutz, *Chem. Eur. J.*, 1997, **3**, 755–764.

37 S. M. Reid, J. T. Mague and M. J. Fink, *J. Am. Chem. Soc.*, 2001, **123**, 4081–4082.

38 J. Yuwen, Y. Jiao, W. W. Brennessel and W. D. Jones, *Inorg. Chem.*, 2016, **55**, 9482–9491.

Chapter 5: Conclusions

Mechanistic Studies of *β*-Amido Aldehyde Hydroacylation: The mechanistic studies of the reaction of a *β*-amido aldehyde substrate with 1-octyne, catalysed by the Rh(I)-complex [Rh(*cis*-κ^2-$_{P,P}$-DPEPhos)(acetone)$_2$][BAr$^F_4$] was described. An acyl-hydride complex, formed by oxidative addition of the aldehyde, was shown to be a stable and persistent resting state in the hydroacylation reaction. Tertiary *α*-substitution of the aldehyde was shown to be crucial in preventing reductive decarbonylation of the acyl-hydride complex. Stoichiometric reactions of the isolated acyl-hydride complex indicate that oxidative addition of the aldehyde is fast and reversible, with the equilibrium being strongly biased toward the acyl-hydride. Initial rate, kinetic isotope effect and deuterium labelling studies suggested that hydride insertion is the turnover-limiting step as well as being selectivity determining for linear/branched products. The mechanism of acyl-hydride consumption toward the end of catalysis, when all free aldehyde is consumed, is shown to proceed by continued hydroacylation. The kinetics of the less active pre-catalyst [Rh(*mer*-κ^3-$_{P,O,P}$-XantPhos)(H)(COC{(C$_4$H$_8$)}CO{NC$_4$H$_8$O})][BAr$^F_4$] were briefly explored.

Cyclotrimerisation and Optimisation of Hydroacylation: Further stoichiometric studies with acyl-hydride showed that, toward the end of the hydroacylation reaction, cyclotrimerisation becomes a competitive side-reaction when all free aldehyde is consumed. The mechanism of the cyclotrimerisation reaction was explored with the pre-catalyst [Rh(*cis*-κ^2-$_{P,P}$-DPEPhos)(acetone)$_2$][BAr$^F_4$], in the absence of aldehyde. The initial resting state of the reaction is shown to be a metallacyclopentadiene complex, which is slowly converted to an *α*-pyran complex, formed by a cycloaddition reaction of 1-octyne and acetone. The understanding that cyclotrimerisation becomes competitive when all free aldehyde is consumed was then used to optimize the hydroacylation conditions, with low catalyst loadings and equal stoichiometries providing the highest yield and selectivity for hydroacylation. Further optimization of reaction concentration and temperature led to the development of conditions that afforded a 97% isolated yield of hydroacylation products, with 100% selectivity for hydroacylation.

Non-tethered Aldehyde Hydroacylation of Acrylates: A Tishchenko reaction of the non-tethered aldehyde, cyclohexanecarboxaldehyde, catalysed by [Rh(Cy$_2$PCH$_2$PCy$_2$)(η^6-fluoroarene)][AlO$^F_4$]

complexes in weakly coordinating fluoroarene solvents was discovered. The rate of reaction was shown to increase with increased fluorine substitution of the fluoroarene solvent. It was then shown that in the reaction of cyclohexanecarboxaldehyde with *n*-butyl acrylate, that increasing ligand bite-angle promoted selective hydroacylation reaction over Tishchenko and reductive-aldol-hydroacylation reactions. The optimized reaction conditions used the {Rh(*bis*-phoshine)}$^{+}$ catalyst system, with wide-bite angle DPEPhos or dppb as the *bis*-phoshine ligand. Good yields of ketone products were obtained with secondary α-substituted aldehydes and the first example of a non-tethered tertiary α-substituted aldehyde hydroacylation was reported.

Chapter 6: Experimental

6.1. General Information

6.1.1. Work carried out at The University of Oxford

All work was performed at The University of Oxford unless stated otherwise after the section heading. All manipulations were performed under an atmosphere of argon, using Schlenk and glove box techniques. A high vacuum pump which pulled between *ca*. 1.0 x 10^{-2} – 1.0 x 10^{-3} mbar was used for vacuum/argon cycles. Glassware was oven dried at 130 °C overnight and flamed under vacuum prior to use. Pentane and CH_2Cl_2 was dried using a Grubbs-type solvent purification system (MBraun SPS-800) and were degassed by successive freeze-pump-thaw cycles. Acetonitrile was purchased dry over molecular sieves, degassed by successive freeze-pump-thaw cycles and stored over fresh molecular sieves. Acetone and acetone-d_6 were dried over boric anhydride for 12 h, vacuum distilled and degassed by successive freeze-pump-thaw cycles. 1,2-difluorobenzene 1,2,3-trifluorobenzene, 1,2,3,4-tetrafluorobeznene and pentafluorobenzene were purchased from Fluorochem, pre-treated with alumina, dried with CaH_2, vacuum distilled, freeze-pump-thawed into argon and stored over 3 Å molecular sieves. 1-octyne and 1,6-heptadiyne were dried over $NaBH_4$, vacuum distilled and degassed by successive freeze-pump-thaw cycles. 1-octene was distilled, degassed by successive freeze-pump-thaw cycles and stored over molecular sieves. All other alkenes and alkynes were distilled directly and freeze-pump-thawed into argon. Sodium acetate was dried under vacuum at 60 °C for 72 h. D_2O, acetic acid-d_4, prydine-d_5, and hypophosphorous acid-d_3 (50% weight in D_2O) were all immediately transferred to a dry argon filled Young's flask upon opening. All purchased aldehydes were distilled and freeze-pump-thawed into argon. [Rh(*cis*-κ^2-$_{P,P}$-DPEPhos)(nbd)][BAr^F_4],[1] 2,2-dimethyl-3-oxo-3-morpholino-3-propanenitrile,[1] 2,2-dimethyl-3-morpholino-3-oxopropanal,[1] 2-methyl-3-morpholino-3-oxopropanal,[1] 2,2-cyclopentane-3-morpholino-3-oxopropanal,[1] [Rh(*mer*-κ^3-$_{P,O,P}$-XantPhos)(η^2-PhCCPh)],[2] ^{2}H-1-octyne,[3] [Rh(AmpaPhos)(C_6H_5F)][BAr^F_4] (AmpaPhos = ^{t}Bu$_2$PCH$_2$P(*o*-C_6H_4OMe)$_2$)$_2$),[4] [Rh(*cis*-κ^2-$_{P,P}$-DPEPhos)(η^6-*o*-xylene)][BAr^F_4],[5] Li[Al(OC(CF_3)$_3$)$_4$],[6] [Rh($Cy_2PCH_2PCy_2$)(η^6-1,2-dfb)][AlO^F_4],[7] [Rh($Cy_2PCH_2PCy_2$)(nbd)][AlO^F_4],[7]

$[Rh(Cy_2PCH_2PCy_2)(nbd)][BAr^F{}_4]$,[8] $[Rh(nbd)_2]AlO^F{}_4$,[9] $[Rh(nbd)_2]BAr^F{}_4$,[9] $[Rh(nbd)_2]BF_4$,[9] and 1-morpholinobutane-1,3-dione[10] were prepared using literature methods. NMR spectra were recorded on Bruker DPX 400 MHz, Bruker DRX 400 MHz and Bruker AVC 500 MHz spectrometers. Chemical shifts are quoted in ppm and coupling constants in Hz with the multiplicities of the spectra reported as following: s, singlet; d, doublet; t, triplet; q, quartet; m, multiplet; br, broad. ESI-MS of inorganic cations were recorded on a Bruker MicroOTOF instrument. GC-MS were recorded on a Waters GCT ToF mass spectrometer. Low resolution ESI mass spectra were recorded on a Waters LCT Premier spectrometer. High resolution ESI mass spectrometry of organic compounds were recorded on a Brucker Daltronics microTOF (ESI) spectrometer by the internal service at the Department of Organic Chemistry, University of Oxford. Infra-red spectra were recorded as thin films on a Bruker Tensor 27 FT-IR spectrometer. Microanalyses were performed at University of London by Stephen Boyer.

6.1.2. Work carried out at AstraZeneca

Synthetic manipulations were carried out at AstraZeneca, Pharmaceutical Sciences, Silk Road Business Park, Macclesfield SK10 2NA, U.K, with full characterization being performed at Oxford University using the instruments stated above. Reactions were performed under inert atmosphere of nitrogen gas, which was passed through a Drierite® drying tube before use. House vacuum which pulled to *ca*. 20-30 mbar was used for vacuum/N_2 cycles. Unless otherwise stated, all reactions used dry N_2 degassed solvents as purchased from Sigma-Aldrich Chemical Co. Ltd or Acros Organics Ltd. Reactions were monitored by TLC using aluminium backed silica plates. Plates were visualized under ultraviolet light and/or by staining with $KMnO_4$. Reagents were purchased from Sigma-Aldrich Chemical Co. Ltd., Acros Organics Ltd., AlfaAesar, Strem Chemicals Inc., or Fluorochem Ltd., and were used as supplied unless otherwise stated. Flash chromatography was carried out using matrix 60 silica. 1-octyne was distilled, bubbled degassed with N_2 prior to use. GC analysis was performed using the Agilent 6890N network GC system. Column: Restsek Rxi® - 55il MS, 20 m, 180 μm diameter, 0.36 μm thickness, front injector: 250 ºC, 11.2 psi initial pressure, 2.5 $mlmin^{-1}$ flow, FID detector. Initial temp 80 °C, hold for 1 min; Heat at 45 $ºCmin^{-1}$ until 300 ºC, hold for 6 mins.

6.2. Mechanistic Studies of *β*-Amido Aldehyde Hydroacylation

6.2.1. Inorganic Synthesis

General Procedure A: *in situ* generation of [Rh(*cis*-κ^2-$_{P,P}$-DPEPhos)(acetone)$_2$][BAr$^F_4$] 2.1

A high-pressure NMR tube with a controlled atmosphere valve was charged with [Rh(*cis*-κ^2-$_{P,P}$-DPEPhos)(nbd)][BAr$^F_4$] (23.4 mg, 0.0147 mmol). Acetone (300 μl) was added and the solution was freeze-pump-thawed into an atmosphere of H_2 (4 atm). After vigorous shaking, the NMR tube was left to stand for 15 minutes after which the solution was freeze-pumped-thawed into an atmosphere of argon (1 atm). This quantitatively forms the previously reported [Rh(*cis*-κ^2-$_{P,P}$-DPEPhos)(acetone)$_2$][BAr$^F_4$] **2.1**[11] complex as indicated by $^{31}P\{^1H\}$ NMR spectroscopy.

[Rh(*mer*-κ^3-$_{P,O,P}$-DPEPhos)(H)(COC{(CH$_3$)$_2$}CO{NC$_4$H$_8$O})][BAr$^F_4$] 2.3a

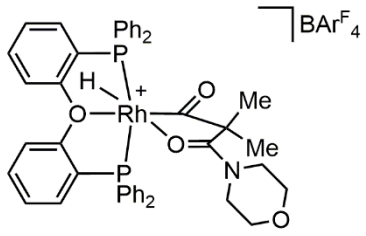

Using General Procedure A, [Rh(*cis*-κ^2-$_{P,P}$-DPEPhos)(acetone)$_2$][BAr$^F_4$] was generated *in situ* from a solution of [Rh(*cis*-κ^2-$_{P,P}$-DPEPhos)(nbd)][BAr$^F_4$] (23.4 mg, 0.014 mmol) in acetone (300 μl). To this was added a stock solution of 2,2-dimethyl-3-morpholino-3-oxopropanal **2.2a** (2.6 mg, 0.014 mmol) in acetone (200 μl). A colour change from red to pale yellow was observed upon mixing, the solution was allowed to stand for 5 mins, monitoring by ^{31}P NMR spectroscopy indicated full conversion to product. The solvent was then removed *in vacuo* and the residue was re-dissolved in CH_2Cl_2 and an oil was formed by the addition of pentane. The solvent was filtered and the residue was washed with pentane (3 x 3 ml) before concentration *in vacuo*.

^{1}H NMR (400 MHz, Acetone-d_6) δ 8.18 (app. q, J_{PH} = 6.5 Hz, J_{HH} = 6.5 Hz, 4H, ArH), 7.85-7.80 (m, 2H, ArH), 7.79 (s, 8H, BAr$^F_4$), 7.77-7.65 (m, 12H, ArH, BAr$^F_4$), 7.65-7.49 (m, 8H, ArH), 7.40 (t, J_{HH} = 7.5 Hz, 2H, ArH), 7.33 (app. q, J_{PH} = 6.0 Hz, J_{HH} = 6.0 Hz, 4H, ArH), 3.51-3.41 (m, 6H, NCH_2, OCH_2), 3.30-3.26 (m, 2H, OCH_2), 0.74 (s, 6H, CH_3), –14.55 (dt, J_{RhH} = 27.5, J_{PH} = 9.5 Hz, 1H, Rh*H*); **$^{31}P\{^1H\}$**

NMR (162 MHz, Acetone-d_6) δ 25.2 (d, J_{RhP} = 129 Hz); Selected **^{13}C{^{1}H} NMR** (126 MHz, Acetone-d_6) δ 224.7 (dt, *J*(RhC) = 37.0, *J*(PC) = 6.0 Hz, 1H, Rh*C*); **ESI-MS** (CH_2Cl_2, 60 °C, 4.5 kV): *m/z* = 826.17 (calculated 826.16).

[Rh(*mer*-κ^3-$_{P,O,P}$-DPEPhos)(^{2}H)(COC{$(CH_3)_2$}CO{NC_4H_8O})][BAr^F_4] 2.3a-*d_1*

Synthesised using same procedure as 2.3a but with 2,2-dimethyl-3-morpholino-3-oxopropan-^{2}H-al 2.2a-*d_1* (2.6 mg, 0.014 mmol).

^{1}H NMR (400 MHz, Acetone-d_6) δ 8.18 (app. q, J_{PH} = 6.5 Hz, J_{HH} = 6.5 Hz, 4H, ArH), 7.85-7.80 (m, 2H, ArH), 7.79 (s, 8H, BAr^F_4), 7.77-7.65 (m, 12H, ArH, BAr^F_4), 7.65-7.49 (m, 8H, ArH), 7.40 (t, J_{HH} = 7.5 Hz, 2H, ArH), 7.33 (app. q, J_{PH} = 6.0 Hz, J_{HH} = 6.0 Hz, 4H, ArH), 3.51-3.41 (m, 6H, NCH_2, OCH_2), 3.30-3.26 (m, 2H, OCH_2), 0.74 (s, 6H, CH_3); **^{31}P{^{1}H} NMR** (162 MHz, Acetone-d_6) δ 25.2 (d, J_{RhP} = 129 Hz); Selected **^{13}C{^{1}H} NMR** (126 MHz, Acetone-d_6) δ 224.7 (dt, *J*(RhC) = 37.0, *J*(PC) = 6.0 Hz, 1H, Rh*C*); **ESI-MS** (CH_2Cl_2, 60 °C, 4.5 kV): *m/z* = 826.17 (calculated 826.17).

[Rh(*mer*-κ^3-$_{P,O,P}$-DPEPhos)(H)(COC{(CH_3)(H)}CO{NC_4H_8O})][BAr^F_4] 2.3b

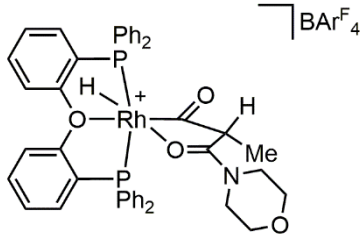

Using General Procedure A, [Rh(*cis*-κ^2-$_{P,P}$-DPEPhos)(acetone)$_2$][BAr^F_4] was generated *in situ* from a solution of [Rh(*cis*-κ^2-$_{P,P}$-DPEPhos)(nbd)][BAr^F_4] (26.7 mg, 0.016 mmol) in acetone (250 µl). To this was added a stock solution of 2-methyl-3-morpholino-3-oxopropanal **2.2b** (2.8 mg, 0.016 mmol) in acetone (280 µl). A colour change from red to pale yellow was observed upon mixing, the solution was allowed to stand for 5 mins, monitoring by ^{31}P NMR spectroscopy indicated full conversion to product. The solvent was then removed *in vacuo* and the residue was re-dissolved in CH_2Cl_2 and an oil was formed by the addition of pentane. The solvent was filtered, and the residue was washed with pentane (3 x 5 ml) before concentration *in vacuo*.

^{1}H NMR (400 MHz, Acetone-d_6) δ 8.21 (ddd, J_{PH} = 12.5, J_{HH} = 7.0, J_{HH} = 2.0 Hz, 2H, ArH), 8.05 (dd, J_{PH} = 12.5, J_{HH} = 7.5 Hz, 2H, ArH), 7.93 (dd, J_{HH} = 8.0, J_{PH} = 5.0 Hz, 1H, ArH), 7.85-7.46 (m, 30H, BAr^F_4, ArH), 7.40 (dd, J_{PH} = 12.0, J_{HH} = 7.0 Hz, 2H, ArH), 7.31 (t, J_{HH} = 7.5 Hz, 1H, ArH), 7.22 (dd, J_{PH} = 12.0, J_{HH} = 7.0 Hz, 2H, ArH), 3.69-3.61 (ddd, J_{HH} = 11.5 Hz, J_{HH} = 5.0 Hz, J_{HH} = 3.0 Hz, 1H, NCH_2), 3.52-3.31 (m, 5H, NCH_2, OCH_2, C(CH_3)(CO)(CO)(H)) 3.23 (ddd, J = 14.0, 8.0, 3.0 Hz, 1H, OCH_2), 2.86-2.77 (m, 2H, OCH_2), 0.49 (d, J_{HH} = 7.5 Hz, 3H, CH_3), –14.9 (app. dt, 29.0 Hz, 9.0 Hz, 1H, RhH); **^{31}P{^{1}H} NMR** (162 MHz, Acetone-d_6) δ 31.3 (dd, J_{PP} = 319, J_{RhP} = 129 Hz), 22.9 (dd, J_{PP} = 319, J_{RhP} = 129 Hz); Selected **^{13}C{^{1}H} NMR** (126 MHz, Acetone-d_6) δ 220.3 (app. dt, J(RhC) = 35.0, J(PC) = 5.5 Hz, 1H, RhC); **ESI-MS** (CH_2Cl_2, 60 °C, 4.5 kV): m/z = 812.16 (calculated 812.16).

[Rh(*mer*-κ^3-$_{P,O,P}$-DPEPhos)(H)(COC{C_4H_8}CO{NC_4H_8O})][BAr^F_4] 2.3c

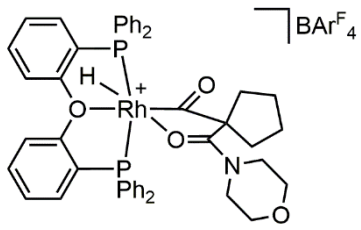

Using General Procedure A, [Rh(*cis*-κ^2-$_{P,P}$-DPEPhos)(acetone)$_2$][BAr^F_4] was generated *in situ* from a solution of [Rh(*cis*-κ^2-$_{P,P}$-DPEPhos)(nbd)][BAr^F_4] (15.0 mg, 0.0094 mmol) in acetone (300 µl). To this was added a stock solution of 1-(morpholine-4-carbonyl)cyclopentane-1-carbaldehyde **2.2c** (2.0 mg, 0.0094 mmol) in acetone (200 µl). A colour change from red to pale yellow was observed upon mixing, the solution was allowed to stand for 5 mins, monitoring by ^{31}P NMR spectroscopy indicated full conversion to product. The solvent was then removed *in vacuo* and the residue was re-dissolved in CH_2Cl_2 and an oil was formed by the addition of pentane. The solvent was filtered and the residue was washed with pentane (3 x 3 ml) before concentration *in vacuo*.

^{1}H NMR (400 MHz, Acetone-d_6) δ 8.18 (app. q, J_{PH} = 6.5 Hz, J_{HH} = 6.5 Hz, 4H, ArH), 7.85-7.80 (m, 2H, ArH), 7.79 (s, 8H, BAr^F_4), 7.76-7.66 (m, 12H, ArH, BAr^F_4), 7.65-7.54 (m, 8H, ArH), 7.40 (t, J_{HH} = 7.5 Hz, 2H), 7.29 (app. q, J_{PH} = 5.5 Hz, J_{HH} = 6.0 Hz, 4H), 3.50 (app. t, J_{HH} = 5.0 Hz, 2H, OCH_2), 3.43 (app. t, J_{HH} = 5.0 Hz, 2H, OCH_2), 3.27 (app. t, J_{HH} = 5.0 Hz, 2H, NCH_2), 3.22 (app. t, J_{HH} = 5.0 Hz, 2H, NCH_2), 1.72-1.61 (m, 4H, C(CH_2)$_2$, 1.47-1.37 (m, 2H, CCH_2CH_2), 1.25-1.14 (m, 2H, CCH_2CH_2), –14.49

(dt, J_{RhH} = 27.5, J_{PH} = 9.5 Hz, 1H, Rh*H*); **^{31}P{^{1}H} NMR** (162 MHz, Acetone-d_6) δ 26.6 (d, J_{RhP} = 129 Hz); Selected **^{13}C{^{1}H} NMR** (126 MHz, Acetone-d_6) δ 225.1 (dt, *J*(RhC) = 36.0 Hz, *J*(PC) = 5.5 Hz); **ESI-MS** (CH_2Cl_2, 60 °C, 4.5 kV): *m/z* = 852.20 (calculated 852.19).

[Rh(*mer*-κ^3-$_{P,O,P}$-XantPhos)(H)(COC{(C_4H_8)}CO{NC_4H_8O})][BAr^F_4] 2.5

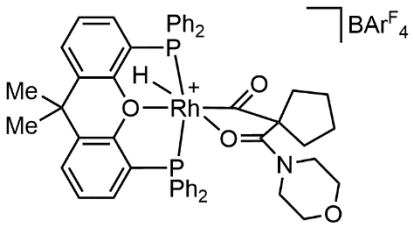

To a stirred solution of [Rh(*mer*-κ^3-$_{P,O,P}$-XantPhos)(η^2-PhCCPh)] (200 mg, 0.114 mmol) in acetone (1.5 ml) was added a solution of aldehyde **2.2c** (26.5 mg, 0.125 mmol) in acetone (1.5 ml). The solution was stirred for 5 mins in which time the colour change from red to light yellow was observed. The solvent was removed *in vacuo*, and the residue was re-dissolved in 1,2-flourobenzene and a precipitate was formed by the addition of pentane and sonication. The filtrate was filtered off and the solid was washed with pentane (3 x 10 ml). The product was recrystallized from 1,2-diflourobenzene/pentane by diffusion to yield light yellow crystals (170 mg, 75%).

^{1}H NMR (500 MHz, Acetone-d_6) δ 8.26 (app q, J_{PH} = 6.5 Hz, J_{HH} = 6.5 Hz, 4H, ArH), 8.01 (dd, J_{HH} = 8.0 Hz, J_{HH} = 1.5 Hz, 2H, ArH), 7.82-7.78 (m, 8H, BAr^F_4) 7.75-7.66 (m, 12H, ArH, BAr^F_4), 7.62-7.53 (m, 6H, ArH), 7.51 (t, J_{HH} = 8.0 Hz, 2H, ArH), 7.27 (app q, J_{PH} = 6.0 Hz, J_{HH} = 6.0 Hz, 4H, ArH), 3.52-3.47 (m, 2H, OCH_2), 3.42-3.36 (m, 4H, OCH_2, NCH_2), 3.14-3.08 (m, 2H, NCH_2), 1.84 (s, 3H, CH_3), 1.81 (s, 3H, CH_3), 1.74-1.56 (m, 4H, C(CH_2)$_2$), 1.47 (dt, J_{HH} = 12.5, J_{HH} = 6.0 Hz, 2H, CCH_2CH_2), 0.95 (dt, J_{HH} = 14.5, J_{HH} = 7.5 Hz, 2H, CCH_2CH_2), –14.74 (dt, J_{RhH} = 27.0, J_{PH} = 9.5 Hz, 1H, Rh*H*); **^{31}P NMR** (162 MHz, Acetone-d_6) δ 29.0 (d, J_{RhP} = 128 Hz); Selected **^{13}C{^{1}H} NMR** (126 MHz, Acetone-d_6) δ 224.0 (dt, *J*(RhC) = 37.0 Hz, *J*(PC) = 6.0 Hz); **Anal.** Calculated for $C_{82}H_{61}BF_{24}NO_4P_2Rh$ (1756.02 gmol^{-1}): C, 56.09 H, 3.50; Found: C, 55.94, H 3.39; **ESI-MS** (CH_2Cl_2, 60 °C, 4.5 kV): *m/z* = 892.20 (calculated 892.22).

[Rh(*cis*-κ^2-$_{P,P}$-DPEPhos)$(MeCN)_2$][BAr^F_4] 2.13

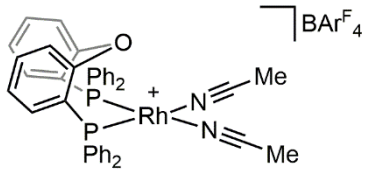

A high-pressure NMR tube with a controlled atmosphere valve was charged with [Rh(*cis*-$\kappa^2_{P,P}$-DPEPhos)(nbd)][BAr$^F_4$] (15.0 mg, 0.0094 mmol). Acetonitrile (400 μl) was added and the solution was freeze-pump-thawed into an atmosphere of H_2 (4 atm). After vigorous shaking the NMR tube was left to stand for 15 minutes after which the solution was freeze-pumped-thawed into an atmosphere of argon (1 atm), monitoring by ^{31}P NMR spectroscopy indicated full conversion to product. The solvent was then removed *in vacuo*.

^{1}H NMR (400 MHz, Methylene Chloride-d_2) δ 7.73 (s, 8H, BAr$^F_4$), 7.58-7.48 (m, 12H, ArH, BAr$^F_4$), 7.42-7.22 (m, 12H, ArH), 7.17-7.06 (m, 2H, ArH), 6.87 (d, J_{HH} = 8.0 Hz, 2H, ArH), 6.82 (t, J_{HH} = 7.5 Hz, 2H, ArH), 6.66-6.56 (m, 2H, ArH), 1.66 (s, 6H, NCH_3); **^{31}P{^{1}H} NMR** (162 MHz, Methylene Chloride-d_2) δ 34.3 (d, J_{RhP} = 181 Hz); **ESI-MS** (1,2-difluorobenzene, 60 °C, 4.5 kV): *m/z* = 682.10 (calculated 682.09 for [Rh(DPEPhos)(MeCN)]$^+$.

[Rh(*cis*-κ^2-$_{P,P}$-DPEPhos)(2.10a)][BAr$^F_4$] 2.15

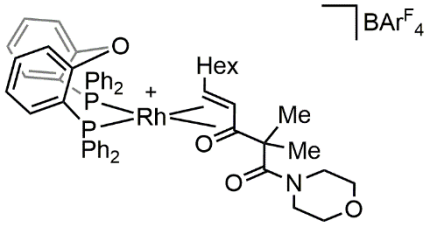

Using General Procedure A, [Rh(*cis*-κ^2-$_{P,P}$-DPEPhos)(acetone)$_2$][BAr$^F_4$] was generated *in situ* from a solution of [Rh(*cis*-κ^2-$_{P,P}$-DPEPhos)(nbd)][BAr$^F_4$] (25.0 mg, 0.016 mmol) in acetone (200 μl). To this was added a stock solution of **2.10a** (20.0 mg, 0.067 mmol) in acetone (200 μl). The solution was allowed to stand for 20 mins, monitoring by ^{31}P NMR spectroscopy indicated full conversion to product. The solvent was then removed *in vacuo* and the residue was re-dissolved in CH_2Cl_2 and an oil was formed by the addition of pentane. The solvent was filtered and the residue was washed with pentane (3 x 10 ml) before concentration *in vacuo*.

^{1}H NMR (500 MHz, Methylene Chloride-d_2) at 190 K: δ 8.12 (dd, J_{PH} = 14.5, J_{HH} = 6.5 Hz, 1H, ArH), 8.04 (dd, J_{PH} = 12.0, J_{HH} = 6.5 Hz, 1H, ArH), 7.71 (s, 8H, BAr^{F}_4), 7.62-7.30 (m, 19H, ArH, BAr^{F}_4), 7.15 (t, J_{HH} = 7.5 Hz, 1H, ArH), 7.07-6.98 (m, 3H, ArH), 6.94 (t, J_{HH} = 8.0 Hz, 1H, ArH), 6.73 (t, J_{HH} = 7.5 Hz, 1H, ArH), 6.55 (dd, J_{HH} = 8.0, J_{PH} = 5.0 Hz, 1H, ArH), 6.50 (t, J_{HH} = 7.5 Hz, 1H, ArH), 6.34 (dd, J_{PH} = 11.5, J_{HH} = 8.0 Hz, 1H, ArH), 6.23 (m, 2H, ArH) 5.10 (app. t, J_{PH} = 7.5, J_{HH} = 7.5 Hz, 1H, C(O)C*H*), 3.90-3.25 (m, 8H, OCH_2, NCH_2), 2.34 (app. p, J_{PH} = 7.5, J_{HH} = 7.5, J_{HH} = 7.5 Hz, 1H, CH_2C*H*), 1.55 (s, 3H, C(CH_3)CH_3), 1.04-0.90 (m, CH_2, 2H), 0.85-0.54 (m, CH_2, CH_2CH_3, C(CH_3)CH_3, 12H), 0.50-0.40 (m, 2H, CHCH_2); **^{31}P{^{1}H} NMR** at 190 K (202 MHz, Methylene Chloride-d_2) δ 33.0 (dd, J_{RhP} = 160, J_{PP} = 50 Hz), 25.0 (dd, J_{RhP} = 190, J_{PP} = 50 Hz); **^{31}P{^{1}H} NMR** at 298 K (202 MHz, Methylene Chloride-d_2) δ 33.0 (br, d), 25.0 (br, d); **ESI-MS** (1,2-difluorobenzene, 60 °C, 4.5 kV): *m/z* = 936.27 (calculated 936.28).

6.2.2. Inorganic Reactions

Decarbonylation reaction

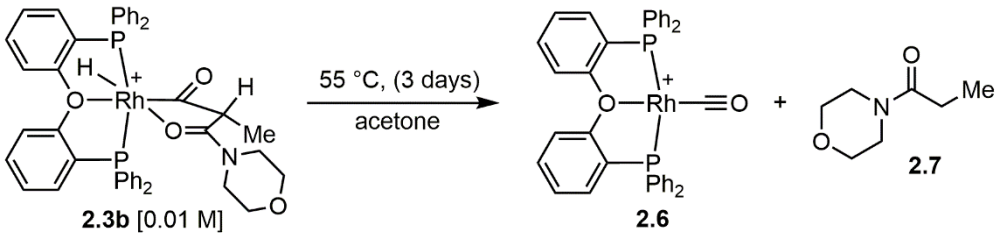

[a] BAr^{F}_4 anion omitted for clarity

In a Young's NMR tube, a solution of **2.3b** (6.7 mg, 0.0040 mmol) in acetone-d_6 (400 µl) was heated at 55 °C for 3 days and was periodically monitored by ^{31}P{^{1}H} and ^{1}H NMR spectroscopy. After full conversion to **2.6** the mixture was precipitated into pentane (5 ml) and washed with pentane (2 x 3 ml) before concentration *in vacuo*.

Precipitate **2.6**: **^{1}H NMR** (400 MHz, Acetone-d_6) δ 7.89-7.35 (m, 40H, ArH, BAr^{F}_4); **^{31}P{^{1}H} NMR** (162 MHz, Acetone-d_6) δ 35.0 (d, J_{RhP} = 124 Hz); **ESI-MS** (1,2-difluorobenzene, 60 °C, 4.5 kV): *m/z* = 669.07 (calculated 669.06); **IR** (film cm^{-1}) 2017 (CO).

Filtrate **2.7**: **^{1}H NMR** (400 MHz, Acetone-d_6) 3.66-3.55 (m, 4H, NCH_2), 3.53-3.45 (m, 4H, OCH_2), 2.33 (q, J_{HH} = 7.5 Hz, 2H, COCH_2), 1.04 (t, J_{HH} = 7.5 Hz, 3H, CH_2CH_3); **LRMS (ESI$^+$)** m/z 144.2 $[M+H]^+$.

Reversibility of oxidative addition

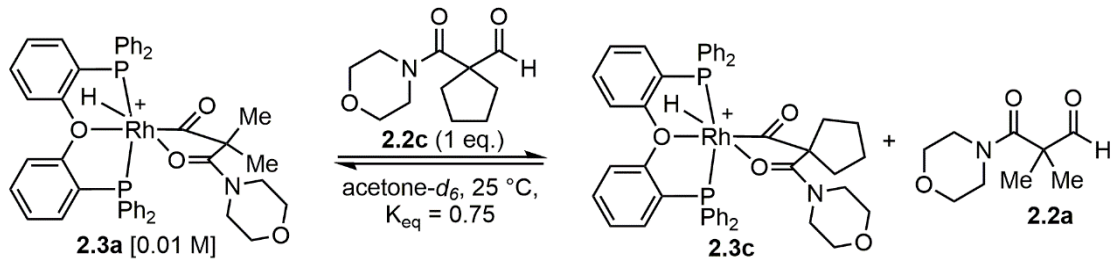

[a]BAr^F_4 anion omitted for clarity

Using General Procedure A, [Rh(*cis*-κ^2-$_{P,P}$-DPEPhos)(acetone)$_2$][BAr^F_4] was generated *in situ* from a solution of [Rh(*cis*-κ^2-$_{P,P}$-DPEPhos)(nbd)][BAr^F_4] (5.6 mg, 0.0035 mmol) in acetone-d_6 (100 µl). To this a stock solution of aldehyde **2.2a** (0.7 mg, 0.0035 mmol) in acetone-d_6 (150 µl) was added, the mixture was vigorously shaken and allowed to stand for 5 mins. Then a stock solution of aldehyde **2.2c** (0.8 mg, 0.0035 mmol) in acetone-d_6 (100 µl) was added the mixture was vigorously shaken then immediately monitored by ^{1}H and ^{31}P{^{1}H} NMR spectroscopy. By which time a mixture of **2.3a**, **2.3c**, **2.2a** and **2.2c** was observed, in a ratio of 1.3 : 1.0 of **2.3a**/**2.2c** : **2.3c**/**2.2a**.

Addition of MeCN to acyl hydride 2.3a

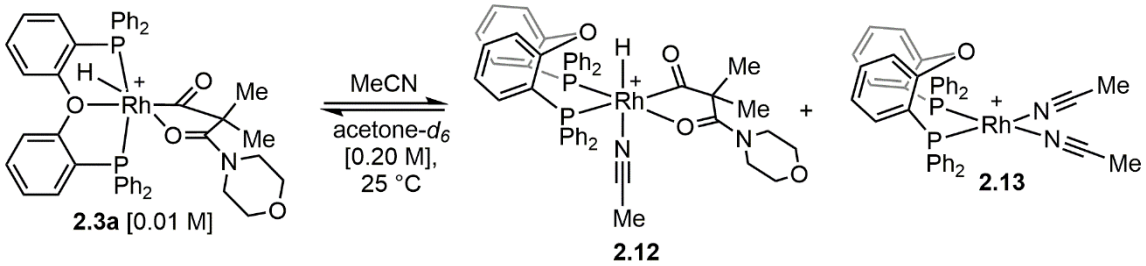

[a]BAr^F_4 anion omitted for clarity

In three separate NMR tubes to a 0.005 M solution of [Rh(*mer*-κ^3-$_{P,O,P}$-DPEPhos)(H)(COC{$(CH_3)_2$}CO{NC_4H_8O})][BAr^F_4] in acetone-d_6 (170 µl) was added: Reaction **A**, a stock solution of MeCN (3.6 µl, 0.068 mmol) in acetone-d_6 (170 µl), the mixture was then vigorously shaken; Reaction **B**, a stock solution of MeCN (3.6 µl, 0.068 mmol) and aldehyde **2.2a** (12.6

mg, 0.068 mmol) in acetone-d_6 (170 µl) and the mixture was vigorously shaken and Reaction **C**, a stock solution of MeCN (35.6 µl, 0.680 mmol) and aldehyde **2.2a** (12.6 mg, 0.068 mmol) in acetone-d_6 (170 µl) and the mixture was vigorously shaken.

Selected NMR spectroscopy data for **2.12**: **^{1}H NMR** (400 MHz, Acetone-d_6) –15.83 (app. td, J_{RhH} = 20.0, J_{PH} = 20.0, J_{PH} = 8.0 Hz, 1H, Rh*H*); **^{1}H{^{31}P} NMR** (400 MHz, Acetone-d_6) –15.83 (d, J_{RhH} = 20.0, 1H, Rh*H*); **^{31}P{^{1}H} NMR** (162 MHz, Acetone-d_6) δ 45.6 (dd, J_{RhP} = 174, J_{PP} = 7 Hz), 11.8 (dd, J_{RhP} = 67, J_{PP} = 7 Hz).

Addition of alkene to ^{2}H-acyl hydride

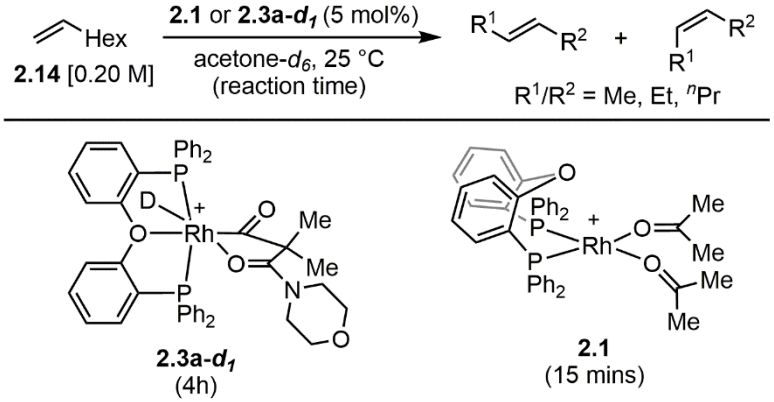

[a]BAr^F_4 anion omitted for clarity

Using General Procedure A, [Rh(*cis*-$\kappa^2_{P,P}$-DPEPhos)(acetone)$_2$][BAr^F_4] was generated *in situ* from a solution of [Rh(*cis*-$\kappa^2_{P,P}$-DPEPhos)(nbd)][BAr^F_4] (5.6 mg, 0.0035 mmol) in acetone-d_6 (100 µl). To this a solution of aldehyde **2.3-d_1** (0.7 mg, 0.0035 mmol) in acetone-d_6 (250 µl) was added, the mixture was vigorously shaken and allowed to stand for 5 mins. Then 1-octene (11 µl, 0.070 mmol) was added and the mixture was vigorously shaken then allowed to stand and was periodically monitored by NMR spectroscopy over 16h.

Using General Procedure A, [Rh(*cis*-$\kappa^2_{P,P}$-DPEPhos)(acetone)$_2$][BAr^F_4] was generated *in situ* from a solution of [Rh(*cis*-$\kappa^2_{P,P}$-DPEPhos)(nbd)][BAr^F_4] (5.6 mg, 0.0035 mmol) in acetone-d_6 (100 µl). To this acetone-d_6 (250 µl) was added, followed by 1-octene (11 µl, 0.070 mmol). The mixture was vigorously shaken then allowed to stand and was periodically monitored by NMR spectroscopy over 16h.

Addition of aldehyde 2.2a to product bound complex 2.15

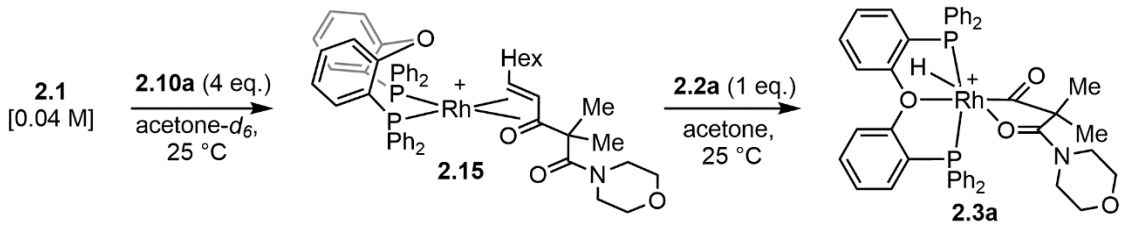

[a]BAr^F_4 anion omitted for clarity

Using General Procedure A, [Rh(*cis*-κ^2-$_{P,P}$-DPEPhos)(acetone)$_2$][BAr^F_4] was generated *in situ* from a solution of [Rh(*cis*-κ^2-$_{P,P}$-DPEPhos)(nbd)][BAr^F_4] (7.8 mg, 0.0049 mmol) in acetone-d_6 (100 µl). A solution of product (15 mg, 0.049 mmol) in acetone-d_6 (100 µl) was added and the mixture was shaken, a colour change from red to orange was observed. To this was added a solution of aldehyde **2.2a** (1.0 mg, 0.0054 mmol) in acetone-d_6 (100 µl), after vigorous shaking a colour change to pale yellow occurred and full conversion to the acyl-hydride **2.3a** was indicated by $^{31}P\{^1H\}$ NMR spectroscopy.

6.2.3. Organic Synthesis

2,2-dimethyl-3-morpholino-3-oxopropan-^{2}H-al 2.2a-d_1

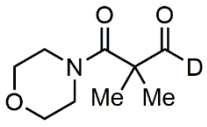

A Raney® nickel solution in D_2O was prepared by adding Raney nickel (200 mg, 3.5 mmol) in water to an argon filled Young's flask, the mixture was filtered and washed with D_2O (3 x 2 ml) before being concentrated and co-evaporated in D_2O (2 ml) to dryness. To a separate Schleck charged with 2,2-dimethyl-3-oxo-3-morpholino-3-propanenitrile (50 mg, 0.28 mmol) and sodium acetate (271 mg, 3.3 mmol), D_2O (600 µl), acetic acid-d_4 (600 µl), prydine-d_5 (1.2 ml) and hypophosphorous acid-d_3 50% wt in D_2O (290 µl) were added simultaneously. This mixture was transferred to the Raney® nickel by cannula and washed with D_2O (2 ml), the Young's flask was sealed and the mixture was heated at 90 °C for 16 h. After cooling, the mixture was extracted in to CH_2Cl_2 (50 ml) and washed with sat. $NaHCO_{3(aq)}$ solution (10 ml), $HCl_{(aq)}$ solution (6M, 10 ml) and brine (10 ml). After drying over $MgSO_4$,

the crude was concentrated in *vacuo* and purified by flash column chromatography (EtOAc) and isolated (25 mg, 50%) as a colourless oil.

^{1}H NMR (400 MHz, Chloroform-*d*) δ 3.74-3.16 (m, 8H, NCH_2, OCH_2), 1.33 (s, CH_3 6H); **^{13}C{^{1}H} NMR** (101 MHz, Chloroform-*d*) δ 199.45 (t, J(C^{2}H) = 17.0 Hz), 169.82, 66.67 (t, J(C^{2}H) = 3.0 Hz), 53.76, 45.91 (br), 43.80 (br), 20.42; **^{2}H NMR** (61 MHz, Chloroform/Chloroform-*d*) δ 9.63 (s); **IR** (film cm^{-1}) 2980, 2930, 1712, 1639, 1463, 1425, 1387, 1362, 1301, 1273, 129, 1186, 1154, 1116, 1063, 1035, 964, 847; **LRMS (ESI^{+})** m/z 187.2 [M+H]$^{+}$; **HRMS (ESI^{+})** m/z 187.11871 (187.11875 calculated for $C_9H_{15}{}^{2}HNO_3$ [M+H]$^{+}$).

Hydroacylation: General Procedure B

Using General Procedure A, [Rh(*cis*-κ^2-$_{P,P}$-DPEPhos)(acetone)$_2$][BAr$^{F}{}_4$] was generated *in situ* from a solution of [Rh(*cis*-κ^2-$_{P,P}$-DPEPhos)(nbd)][BAr$^{F}{}_4$] (5.4 mg, 0.0034 mmol) in acetone (100 μl), to this was added a stock solution of aldehyde **2.2a** (12.6 mg, 0.068 mmol) in acetone (150 μl) followed by 100 μl of a stock solution of 1-octyne (9 μl, 0.062 mmol) and acetone (91 μl), the mixture was vigorously shaken and allowed stand until reaction went to completion as indicated by ^{1}H NMR spectroscopy. Product was isolated by column chromatography (EtOAc/Heptane 5 : 5) from the reaction mixture.

(*E*)-2,2-dimethyl-1-morpholinoundec-4-ene-1,3-dione 2.10a

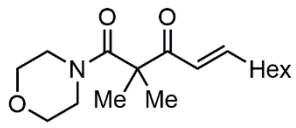

Following General Procedure B with [Rh(*cis*-κ^2-$_{P,P}$-DPEPhos)(nbd)][BAr$^{F}{}_4$] (5.4 mg, 0.0034 mmol), aldehyde **2.2a** (12.6 mg, 0.068 mmol), 1-octyne (9 μl, 0.062 mmol) in acetone (341 μl). Product was isolated by column chromatography (16.8 mg, 92%).

^{1}H NMR (400 MHz, Chloroform-*d*) δ 7.05 (dt, J = 15.0, 7.0 Hz, 1H, CH_2CH), 6.21 (d, J = 15.0 Hz, 1H, CH_2CHCH), 3.72-3.43 (m, 6H, NCH_2, OCH_2), 3.26-3.09 (m, 2H, NCH_2), 2.20 (app. q, J = 7.0 Hz, 2H, CHCH_2), 1.48-1.39 (m, 2H, $CHCH_2CH_2$), 1.35 (s, 6H, C(CH_3)$_2$), 1.33-1.21 (m, 6H, CH_2), 0.87 (t, J = 6.5 Hz, 3H, CH_2CH_3); **^{13}C{^{1}H} NMR** (101 MHz, Chloroform-*d*) δ 199.18, 171.58, 150.39, 125.35, 67.02 (br), 66.30 (br), 54.53, 46.52 (br), 43.25 (br), 32.59, 31.63, 29.00, 28.16, 23.14, 22.66, 14.17; **IR**

(film cm^{-1}) 2957, 2927, 2856, 2360, 2341, 1693, 1641, 1625, 1460, 1421, 1361, 1299, 1273, 1247, 1183, 1117, 1073, 1030; **LRMS (ESI$^+$)** m/z 296.2 $[M+H]^+$; **HRMS (ESI$^+$)** m/z 296.22207 (296.22202 calculated for $C_{17}H_{30}NO_3$ $[M+H]^+$).

(*E*)-2,2-dimethyl-1-morpholinoundec-4-ene-5-^{2}H-1,3-dione 2.10c

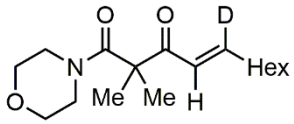

Following General Procedure B with [Rh(*cis*-κ^2-$_{P,P}$-DPEPhos)(nbd)][BAr^F_4] (5.4 mg, 0.0034 mmol), aldehyde **2.2a-*d*$_1$** (12.6 mg, 0.068 mmol), 1-octyne (9 µl, 0.062 mmol) in acetone-d_6 (341 µl). Product was isolated by column chromatography (16.1 mg, 87%).

^{1}H NMR (400 MHz, Chloroform-*d*) δ 6.21 (s, 1H, CH_2CHCH), 3.72-3.43 (m, 6H, NCH_2, OCH_2), 3.25-3.08 (m, 2H, NCH_2), 2.21 (t, J = 7.0 Hz, 2H, $CHCH_2$), 1.48-1.39 (m, 2H, $CHCH_2CH_2$), 1.37 (s, 6H, $C(CH_3)_2$), 1.31-1.20 (m, 6H, CH_2), 0.88 (t, J = 6.5 Hz, 3H, CH_2CH_3); **^{13}C{^{1}H} NMR** (126 MHz, Chloroform-*d*) δ 199.23, 171.64, 150.09 (t, $J(C^2H)$ = 23.0 Hz), 125.30, 67.02 (br), 66.27 (br), 54.57, 46.55 (br), 43.27 (br), 32.50, 31.66, 29.03, 28.16, 23.18, 22.68, 14.19; **IR** (film cm^{-1}) 2958, 2926, 2856, 2361, 2337, 1726, 1690, 1641, 1614, 1462, 1423, 1356, 1299, 1276, 1249, 1181, 1119, 1028; **LRMS (ESI$^+$)** m/z 319.2 $[M+Na]^+$; **HRMS (ESI$^+$)** m/z 297.22842 (297.22830 calculated for $C_{17}H_{30}NO_3$ $[M+H]^+$).

(*E*)-2,2-dimethyl-1-morpholinoundec-4-ene-4-^{2}H-1,3-dione 2.10e

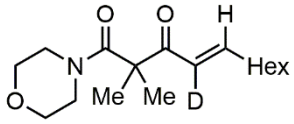

Following General Procedure B with [Rh(*cis*-κ^2-$_{P,P}$-DPEPhos)(nbd)][BAr^F_4] (5.4 mg, 0.0034 mmol), aldehyde **2.2a** (12.6 mg, 0.068 mmol), ^{2}H-1-octyne (9 µl, 0.062 mmol) in acetone-d_6 (341 µl). Product was isolated by column chromatography (16.1 mg, 87%).

^{1}H NMR (400 MHz, Chloroform-*d*) δ 7.06 (t, J = 7.0 Hz, 1H, CH_2CH), 3.74-3.43 (m, 6H, NCH_2, OCH_2), 3.26-3.11 (m, 2H, NCH_2), 2.21 (app. q, J = 7.0 Hz, 2H, $CHCH_2$), 1.48-1.39 (m, 2H,

$CHCH_2CH_2$), 1.37 (s, 6H, $C(CH_3)_2$), 1.31-1.20 (m, 6H, CH_2), 0.88 (t, J = 6.5 Hz, 3H, CH_2CH_3); **$^{13}C\{^1H\}$ NMR** (126 MHz, Chloroform-*d*) δ 199.19, 171.63, 150.32, 125.08 (t, $J(C^2H)$ = 24.0 Hz), 67.05 (br), 66.30 (br), 54.56, 46.53 (br), 43.24 (br), 32.57, 31.66, 29.02, 28.18, 23.17, 22.68, 14.18; **IR** (film cm^{-1}) 2962, 2927, 2857, 2361, 2337, 1726, 1687, 1641, 1617, 1462, 1422, 1383, 1271, 1253, 1181, 1157, 1119, 1036; **LRMS (ESI^+)** m/z 319.2 $[M+Na]^+$; **HRMS (ESI^+)** m/z 297.22824 (297.22830 calculated for $C_{17}H_{30}NO_3$ $[M+H]^+$).

2,2-dimethyl-4-methylene-1-morpholinodecane-1,3-dione 2.10a/b

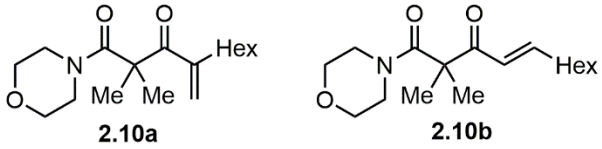

A microwave vial was charged with $[Rh(AmpaPhos)(C_6H_5F)][BAr^F_4]$ (14.7 mg, 0.05 mmol) and aldehyde **2.2a** (37mg, 0.20 mmol), the vial was backfilled three times and placed on an ice bath before addition of acetone (100 µl) and 1-octyne (35 µl, 0.24 mmol). The mixture was stirred at 0 °C for 16 h before direct purification by column chromatography (EtOAc/Heptane 5 : 5) affording a mixture 1 : 1 mixture of **2.10a** and **2.10b** (51 mg, 88%). **2.10b** was characterized as a mixture.

^1H NMR (400 MHz, Chloroform-*d*), *Denotes peaks corresponding to **2.10b**, δ 7.05 (dt, J = 15.0, 7.0 Hz, 1H, CH_2CH), 6.21 (d, J = 15.0, 1H, CH_2CHCH), 5.94* (s, 1H, $(CO)C(CH_2)$), 5.81* (s, 1H, $((CO)C(CH_2)$), 3.74-3.42* (m, 12H, NCH_2, OCH_2), 3.28-3.07* (m, 4H, NCH_2), 2.27-2.11* (m, 4H, $CHCH_2$, $(CO)(CH_2)C(CH_2*)$), 1.48-1.39* (m, 4H, CH_2), 1.40* (s, 6H, $C(CH_3)_2$), 1.35 (s, 6H, $C(CH_3)_2$), 1.32-1.21* (m, 12H, CH_2), 0.87* (t, J = 6.5 Hz, 6H, CH_2CH_3); **$^{13}C\{^1H\}$ NMR** (126 MHz, Chloroform-*d*), only peaks corresponding to **2.10b** are reported, δ 202.07, 173.01, 146.38, 126.00, 66.87 (br), 66.24 (br), 53.66, 46.31 (br), 43.16 (br), 32.33, 31.74, 29.22, 28.70, 25.74, 22.71, 14.20; **LRMS (ESI^+)** m/z 296.2 $[M+H]^+$.

6.2.4. Kinetics

Monitoring of full reaction profile with DPEPhos (Figure 2.5)

Using General Procedure A, [Rh(*cis*-κ^2-$_{P,P}$-DPEPhos)(acetone)$_2$][BAr^F_4] was generated *in situ* from a solution of [Rh(*cis*-κ^2-$_{P,P}$-DPEPhos)(nbd)][BAr^F_4] (18.6 mg, 0.0116 mmol) in acetone-d_6 (100 μl), to this was added a stock solution of aldehyde **2.2a** (43 mg, 0.23 mmol) in acetone-d_6 (150 μl). Then a solution of 1-octyne (44 μl, 0.30 mmol) and acetone (60 μl) was added carefully ensuring no mixing, the mixture was then immediately frozen in liquid nitrogen. The sample was thawed and shaken vigorously before being inserted to the NMR probe at 298 K. The sample was locked and shimmed before running a ^{1}H NMR multi_zgvd run with a fixed 2 min delay until the reaction had proceeded to completion. The data was analysed by using the BAr^F_4 resonance at δ 7.79 as an internal reference and measuring the integral of the aldehyde resonance at δ 9.66, the alkene resonances at δ 6.28 (linear) δ 5.91 (branched), the 1-octyne resonance at δ 2.18, the cyclotrimer resonance at δ 2.05 and the hydride resonance at δ –14.53.

Initial rates (Table 2.1 and Figure 2.6): General Procedure C

Using General Procedure A, [Rh(*cis*-κ^2-$_{P,P}$-DPEPhos)(acetone)$_2$][BAr^F_4] was generated *in situ* from a solution of [Rh(*cis*-κ^2-$_{P,P}$-DPEPhos)(nbd)][BAr^F_4] (5.4 mg, 0.0034 mmol) in acetone-d_6 (100 μl), to this was added a stock solution of aldehyde **2.2a** (12.6 mg, 0.068 mmol) in acetone-d_6 (150 μl). Then 100 μl of a stock solution of 1-octyne (4.5 μl, 0.031 mmol) and acetone (95.5 μl) was added carefully ensuring no mixing, the mixture was then immediately frozen in liquid nitrogen. The sample was thawed and shaken vigorously before being inserted to the NMR probe at 298 K. The sample was locked and shimmed before running a ^{1}H NMR multi_zgvd run with a fixed sec delay (30 – 60 secs). The data was analysed by using the BAr^F_4 resonance as an internal reference and measuring the integral of the enone **2.10a** resonance at δ 6.28.

Kinetic isotope effects

The reactions were run in parallel using the initial rates General Procedure C. The data was analysed by using the BAr^F_4 resonance as an internal reference and measuring the integral of the 1-octyne resonance at δ 2.18:

^{2}H-aldehyde: [Rh(*cis*-κ^2-$_{P,P}$-DPEPhos)(nbd)][BAr^F_4] (5.4 mg, 0.0034 mmol), **2a-*d*$_1$** (12.6 mg, 0.068 mmol), 1-octyne (9 µl, 0.062 mmol) in acetone-d_6 (341 µl).

^{2}H-1-octyne: [Rh(*cis*-κ^2-$_{P,P}$-DPEPhos)(nbd)][BAr^F_4] (5.4 mg, 0.0034 mmol), aldehyde **2.2a** (12.6 mg, 0.068 mmol), ^{2}H-1-octyne (9 µl, 0.062 mmol) in acetone-d_6 (341 µl).

Monitoring of full reaction profile with XantPhos (Figure F2.10)

In a glove box an NMR tube with a controlled atmosphere valve was charged with [Rh(*mer*-κ^3-$_{P,O,P}$-XantPhos)(H)(COC{C_4H_8}CO{C_4H_8N})] **2.5** (40.7 mg, 0.0232 mmol). Outside of the glove box, under an inert atmosphere, to the NMR tube was added a solution of aldehyde **2.2c** (44.1 mg, 0.209 mmol) in acetone (310 µl) followed by 1-octyne (34 µl, 0.232 mmol) ensuring no mixing, the mixture was then immediately frozen in liquid nitrogen. The sample was thawed and shaken vigorously before being inserted to the NMR probe at 298 K. The sample was locked and shimmed before running a ^{1}H NMR multi_zgvd run with a fixed 2 min delay until the reaction had proceeded to completion. The data was analysed by using the BAr^F_4 resonance at δ 7.79 as an internal reference and measuring the integral of the aldehyde resonance at δ 9.66, the alkene resonances at δ 6.34 (linear) the 1-octyne resonance at δ 2.18, the cyclotrimer resonance at δ 2.05 and the hydride resonance at δ –14.74.

6.3. Cyclotrimerisation and Optimisation of Hydroacylation

6.3.1 Inorganic Synthesis

[Rh(*cis*-κ^2-$_{P,P}$-DPEPhos)(κ^2-2,2-methyl-4,6-*n*-hexyl-α-pyran)][Al(OC(CF_3)$_3$)$_4$]

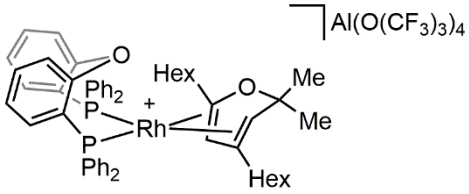

Using General Procedure A, [Rh(*cis*-κ^2-$_{P,P}$-DPEPhos)(acetone)$_2$][Al(OC(CF_3)$_3$)$_4$] was generated *in situ* from a solution of [Rh(*cis*-κ^2-$_{P,P}$-DPEPhos)(nbd)][Al(OC(CF_3)$_3$)$_4$] (15.0 mg, 0.0088 mmol) in acetone (350 µl). To this was added 1-octyne (27 µl, 0.018 mmol), an immediate colour change from red to pale yellow was observed upon mixing. The solution was allowed to stand for 24 h after which the solution

turned a deep red colour, monitoring by ^{31}P NMR spectroscopy indicated full conversion to product. The solvent was then removed *in vacuo* and the residue was re-dissolved in CH_2Cl_2 and an oil was formed by the addition of pentane. The solvent was filtered and the residue was washed with pentane (3 x 5 ml) before concentration *in vacuo*.

^{1}H NMR (400 MHz, Methylene Chloride-d_2) δ 7.67 (dd, J_{PH} = 12.0 Hz, J_{HH} = 8.5 Hz, 2H, ArH), 7.57-7.42 (m, 12H, ArH), 7.29-7.08 (m, 10H, ArH), 7.03 (t, J_{HH} = 9.0 Hz, 1H, ArH), 6.70 (t, J_{HH} = 7.5, 1H, ArH), 6.64 (t, J_{HH} = 8.5 Hz, 1H, ArH), 6.57 (dd, J_{HH} = 8.0, J_{HH} = 5.0, 1H, ArH), 3.85 (d, J = 3.5 Hz, 1H, C(O)(CH$_3$)$_2$(C*H*)), 2.79-2.68 (m, 1H, C(O)(CH$_2$)(C*H*)), 2.04 (ddd, J_{HH} = 13.0, J_{HH} = 9.0, J_{HH} = 6.0 Hz, 1H, CH_2), 1.61 (ddd, J_{HH} = 13.0, J_{HH} = 9.0, J_{HH} = 6.0 Hz, 1H, CH_2), 1.48 (s, 3H, CCH_3), 1.45-1.40 (m, 1H CH_2), 1.34-1.13 (m, 13H, CH_2), 1.08 (s, 3H, CCH_3), 1.00-0.91 (m, 4H, CH_2), 0.87 (t, J = 7.2 Hz, 3H, CH$_2$CH_3), 0.80 (t, J = 7.3 Hz, 3H, CH$_2$CH_3); **^{31}P{^{1}H} NMR** (162 MHz, Methylene Chloride-d_2) δ 20.8 (dd, J_{PP} = 209 Hz, J_{PP} = 31 Hz), 17.6 (dd, J = 169 Hz, J_{PP} = 31 Hz); **^{13}C{^{1}H} NMR** (126 MHz, Methylene Chloride-d_2) δ 158.50 (d, J = 7.9 Hz), 157.95 (d, J = 8.6 Hz), 155.27, 135.56-135.45 (m), 135.40, 134.23, 133.78 (d, J = 13.1 Hz), 133.53 (d, J = 10.9 Hz), 132.97 (d, J = 11.4 Hz), 132.72, 132.10, 131.45-131.24 (m), 131.01, 130.95 (d, J = 2.4 Hz), 130.84, 130.68, 130.30, 128.86 (d, J = 2.9 Hz), 128.78, 128.41 (d, J = 10.1 Hz), 128.30 (d, J = 10.8 Hz), 125.82 (d, J = 6.1 Hz), 125.26, 124.96, 124.06 (d, J = 6.9 Hz), 123.89 (d, J = 4.5 Hz), 122.09, 121.22 (q, J = 292.3, 291.3 Hz), 117.63 (d, J = 4.0 Hz), 101.59 (d, J = 8.1 Hz), 80.40, 80.37, 78.05 (ddd, J = 23.4, 10.6, 3.3 Hz), 73.07 (dd, J = 7.0, 4.7 Hz), 36.11, 35.71, 31.29, 30.88, 29.78, 29.37, 29.31, 28.79, 28.20, 27.55, 27.53, 22.41, 22.23, 13.73, 13.64; **ESI-MS** (CH_2Cl_2, 60 °C, 4.5 kV): *m/z* = 919.32 (calculated 919.33); Comparable ^{1}H, and ^{31}P{^{1}H} and ESI-MS data was measured with the BAr^F_4 analogue [Rh(*cis*-$\kappa^2_{P,P}$-DPEPhos)(κ^2-2,2-methyl-4,6-*n*-hexyl-α-pyran)][BAr^F_4].

6.3.2. Inorganic Reactions

Catalyst speciation during cyclotrimerization

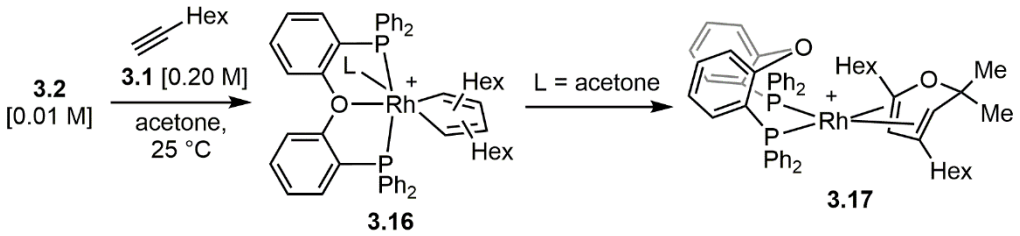

[a]BAr^F_4 anion omitted for clarity

Using General Procedure A, [Rh(*cis*-κ^2-$_{P,P}$-DPEPhos)(acetone)$_2$][BAr^F_4] was generated *in situ* from a solution of [Rh(*cis*-κ^2-$_{P,P}$-DPEPhos)(nbd)][BAr^F_4] (5.6 mg, 0.0035 mmol) in acetone-d_6 (250 µl). A stock solution of 1-octyne (14 µl, 0.098 mmol) in acetone-d_6 (100 µl) was added carefully to ensure minimal mixing after which the solution was frozen in liquid nitrogen. After thawing and vigorous mixing, periodic monitoring by NMR spectroscopy was undertaken.

Cyclotrimerization resting state studies

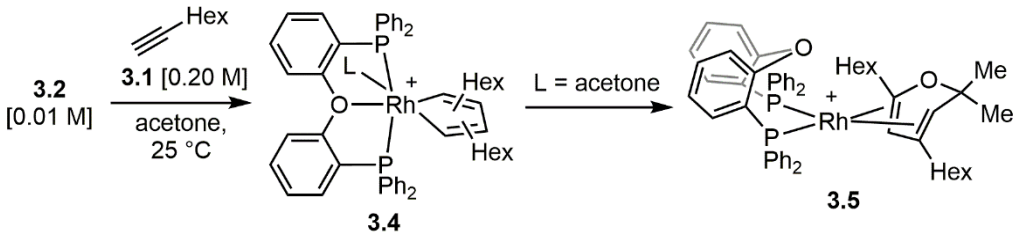

[a]BAr^F_4 anion omitted for clarity

Using General Procedure A, [Rh(*cis*-κ^2-$_{P,P}$-DPEPhos)(acetone)$_2$][BAr^F_4] was generated *in situ* from a solution of [Rh(*cis*-κ^2-$_{P,P}$-DPEPhos)(nbd)][BAr^F_4] (5.6 mg, 0.0035 mmol) in acetone-d_6 (250 µl). A stock solution of 1-octyne (14 µl, 0.098 mmol) in acetone-d_6 (100 µl) was added, after mixing the reaction was monitored by ^{1}H and ^{31}P{^{1}H} NMR spectroscopy, which indicated full conversion to **2.8a**. After 5 mins MeCN (1 µl) was added, before monitoring again by ^{1}H and ^{31}P{^{1}H} NMR spectroscopy which indicated full conversion to **2.8c**.

Selected NMR spectroscopy data for **2.8a**: **^{1}H NMR** (400 MHz, Acetone-d_6) δ 5.64 (br), 5.58 (br), 5.29 (br) sum integrate to 2H relative to BAr^F_4; **^{31}P{^{1}H} NMR** (162 MHz, Acetone-d_6) δ 23.9 (d, J_{RhP} =

125 Hz), 23.1 (d, J_{RhP} = 129 Hz), 22.9 (d, J_{RhP} = 134 Hz); **ESI-MS** (1,2-difluorobenzene, 60 °C, 4.5 kV): *m/z* = 861.29 (calculated 861.29).

Selected NMR spectroscopy data for **2.8c**: **^{1}H NMR** (400 MHz, Acetone-d_6) δ 5.72 (m), 5.64 (m), 5.52 (br), 5.43 (br) sum integrate to 2H relative to BAr^{F}_{4}; **^{31}P{^{1}H} NMR** (162 MHz, Acetone-d_6) δ 24.3 (d, J_{RhP} = 129 Hz), 22.7 (d, J_{RhP} = 129 Hz), 22.4 (d, J_{RhP} = 131 Hz); **ESI-MS** (1,2-difluorobenzene, 60 °C, 4.5 kV): *m/z* = 861.28 (calculated 861.29).

Cyclotrimerization resting state studies with 1,6-heptadiyne

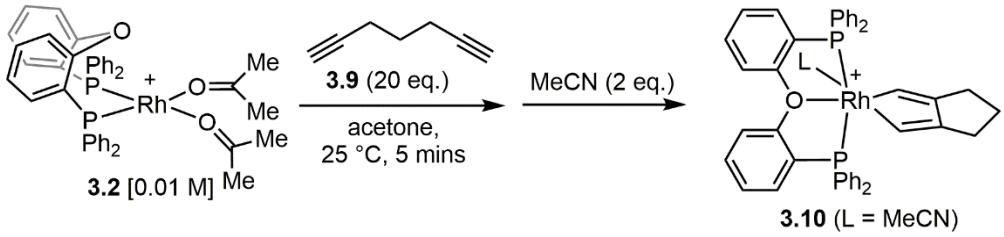

[a]BAr^{F}_{4} anion omitted for clarity

Using General Procedure A, [Rh(*cis*-κ^2-$_{P,P}$-DPEPhos)(acetone)$_2$][BAr^{F}_{4}] was generated *in situ* from a solution of [Rh(*cis*-κ^2-$_{P,P}$-DPEPhos)(nbd)][BAr^{F}_{4}] (5.6 mg, 0.0035 mmol) in acetone-d_6 (250 µl). A stock solution of 1,6-heptadiyne (11 µl, 0.098 mmol) in acetone-d_6 (100 µl) was added, after mixing and standing for 5 mins MeCN (1 µl) was added, before monitoring by ^{1}H and ^{31}P{^{1}H} NMR spectroscopy.

Addition of triphenylphosphine to *α*-pyran complex 3.4

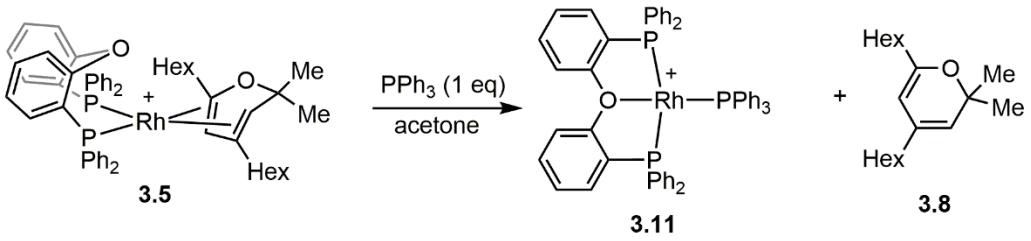

[a]BAr^{F}_{4} anion omitted for clarity

The reaction was carried out in a Young's flask. Using General Procedure A, [Rh(*cis*-κ^2-$_{P,P}$-DPEPhos)(acetone)$_2$][BAr^{F}_{4}] was generated *in situ* from a solution of [Rh(*cis*-κ^2-$_{P,P}$-DPEPhos)(nbd)][BAr^{F}_{4}] (108 mg, 0.068 mmol) in acetone-d_6 (6 ml). To this was added 1-octyne (200 µl, 1.36 mmol) an immediate colour change from red to pale yellow was observed upon

mixing, the solution was allowed to stand for 24 h after which the solution turned a deep red colour. The solvent was removed *in vacuo* and the residue was re-dissolved in CH_2Cl_2 and an oil was formed by the addition of pentane. The solvent was filtered and the residue was washed with pentane (3 x 15 ml) before concentration *in vacuo*. The residue was taken up in acetone-d_6 (500 µl) and a stock solution of triphenylphosphine (28.8 mg, 0.11 mmol) in acetone-d_6 (500 µl) was added, the mixture was stirred for 5 mins before characterization as a mixture.

Data for α-pyran **3.8**: **^{1}H NMR** (400 MHz, Acetone-d_6) δ 4.93 (s, 1H, C*H*), 4.81 (s, 1H, C*H*), 2.03 (t, J = 7.5 Hz, 2H, CHCH_2), 1.96 (t, J = 7.5 Hz, 2H, CHCH_2), 1.47-1.18 (m, 22H, CH_2, C(CH_3)), 0.93-0.80 (m, 6H); **^{13}C{^{1}H} NMR** (101 MHz, Acetone-d_6) δ 155.88 ((O)*C*(CH_2)(CH)), 118.5 (*C*(CH_2(CH)(CH)), 117.55 (C*H*), 99.29 (C*H*), 76.85 (O*C*(CH_3)$_2$(CH)), 34.91 (CH*C*H_2), 34.47 (CH*C*H_2), 32.40 (*C*H_2), 28.76 (*C*H_2), 27.71 (*C*H_2), 27.28 (C(*C*H_3)$_2$(CH)), 23.28 (*C*H_2), 14.34 (CH_2*C*H_3); **LRMS (ESI$^+$)** m/z 279.2 $[M+H]^+$ **HRMS (ESI$^+$)** m/z 279.26822 (279.26824 calculated for $C_{19}H_{35}O$ $[M+H]^+$).

[Rh(*mer*-κ^3-$_{P,O,P}$-DPEPhos)(PPh_3)][BAr^F_4] was also independently synthesised and characterized. Using General Procedure A, [Rh(*cis*-κ^2-$_{P,P}$-DPEPhos)(acetone)$_2$][BAr^F_4] was generated *in situ* from a solution of [Rh(*cis*-κ^2-$_{P,P}$-DPEPhos)(nbd)][BAr^F_4] (16.0 mg, 0.010 mmol) in acetone-d_6 (300 µl). To this a stock solution of triphenylphosphine (26.2 mg, 0.10 mmol) in acetone-d_6 (200 µl) was added, the mixture was vigorously shaken and allowed to stand for 5 mins after which full conversion was observed by ^{31}P NMR spectroscopy, the solvent was then removed *in vacuo*. The residue was re-dissolved in CH_2Cl_2 and an oil was formed by the addition of pentane. The solvent was filtered and the residue was washed with pentane (3 x 5 ml) before concentration *in vacuo*.

^{1}H NMR (400 MHz, Methylene Chloride-d_2) δ 7.80-7.75 (s, 8H, BAr^F_4), 7.58 (s, 4H), 7.56-7.09 (m, 37H), 6.98 (t, J_{HH} = 7.8 Hz, 6H); **^{31}P{^{1}H} NMR** (162 MHz, Methylene Chloride-d_2) δ 51.8 (dt, J_{RhP} = 206 Hz, J_{PP} = 35 Hz, 1P, *P*Ph_3), 31.83 (dd, J_{RhP} = 146 Hz, J_{PP} = 35 Hz, 2P DPEPhos-*P*); **ESI-MS** (1,2-difluorobenzene, 60 °C, 4.5 kV): *m/z* = 903.15 (calculated 903.16).

Addition of 1-octyne to product bound complex 3.16

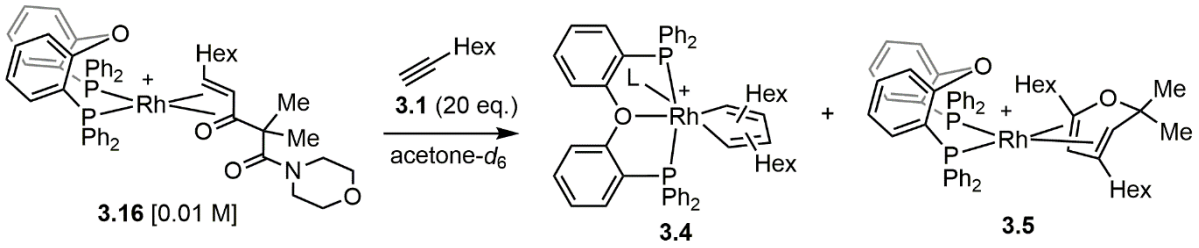

[a]BAr^F_4 anion omitted for clarity

Using General Procedure A, [Rh(*cis*-κ^2-$_{P,P}$-DPEPhos)(acetone)$_2$][BAr^F_4] was generated *in situ* from a solution of [Rh(*cis*-κ^2-$_{P,P}$-DPEPhos)(nbd)][BAr^F_4] (7.8 mg, 0.0049 mmol) in acetone-d_6 (200 µl). A solution of product (30 mg, 0.098 mmol) in acetone-d_6 (200 µl) was added and the mixture was shaken, a colour change from red to orange was observed. A stock solution of 1-octyne (14 µl, 0.098 mmol) in acetone-d_6 (100 µl) was added carefully to ensure minimal mixing after which the solution was frozen in liquid nitrogen. After thawing and vigorous mixing, the reaction was monitored by NMR spectroscopy.

Addition of aldehyde to 3.14a to metallacyclopentadiene 2.8a

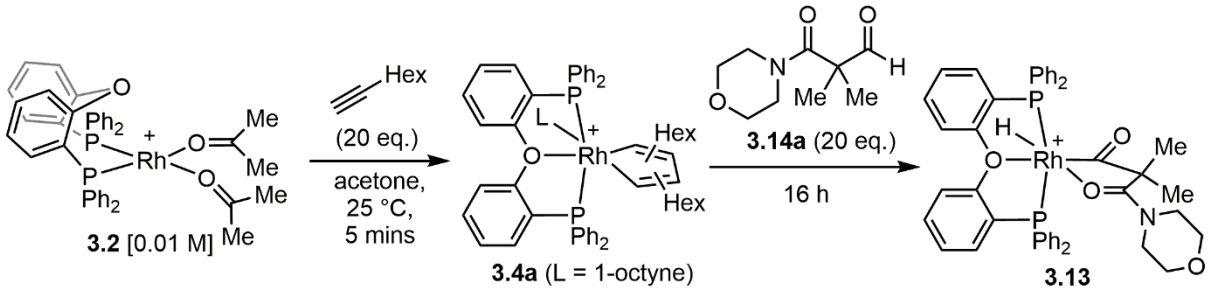

[a]BAr^F_4 anion omitted for clarity

Using General Procedure A, [Rh(*cis*-κ^2-$_{P,P}$-DPEPhos)(acetone)$_2$][BAr^F_4] was generated *in situ* from a solution of [Rh(*cis*-κ^2-$_{P,P}$-DPEPhos)(nbd)][BAr^F_4] (7.8 mg, 0.0049 mmol) in acetone-d_6 (200 µl). A stock solution of 1-octyne (14 µl, 0.098 mmol) in acetone-d_6 (200 µl) was added and the mixture was mixed vigorously. Then a stock solution of aldehyde **3.14a** (18.0 mg, 0.098 mmol) in acetone-d_6 (100 µl) was added; the mixture was vigorously shaken and monitored by $^{31}P\{^1H\}$ NMR spectroscopy.

Addition of aldehyde 3.14a to xylene complex 3.22

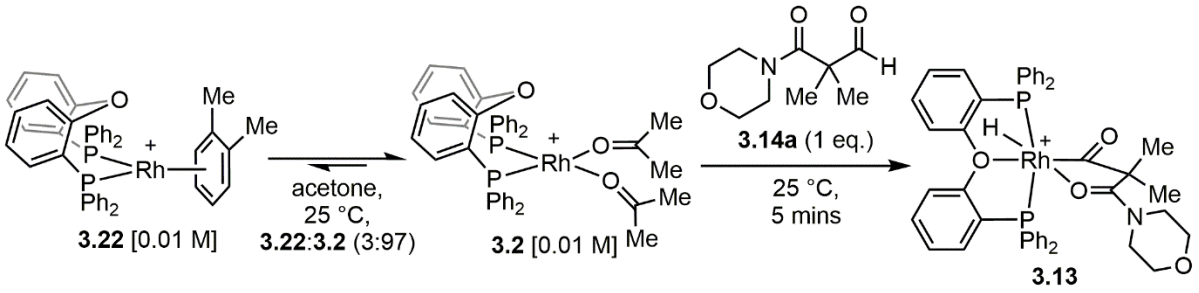

[a]BAr^F_4 anions omitted for clarity

A high-pressure NMR tube with a controlled atmosphere valve was charged with [Rh(*cis*-κ^2-$_{P,P}$-DPEPhos)(η^6-*o*-xylene)][BAr^F_4] (6.0 mg, 0.0035 mmol) and acetone (350 μl) was added. The solution was monitored by ^{1}H and ^{31}P{^{1}H} NMR spectroscopy before a stock solution of aldehyde **3.14a** (0.62 mg, 0.0035 mmol) in acetone-d_6 (100 μl) was added; the mixture was vigorously shaken and allowed to stand at room temperature for 5 minutes.

6.3.3. Organic Synthesis and Scale up (work carried out at AstraZeneca)

3-hydroxy-2,2-dimethyl-1-(pyrrolidin-1-yl)propan-1-one 3.21

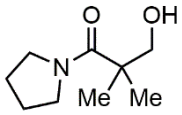

Hydroxypivalic acid (17.0 g, 144 mmol) was added to a 1 L 3 necked round bottom flask connected to a Shlenck line, fitted with a thermometer and a bubbler. The flask was backfilled with N_2 three times before addition of CH_2Cl_2 (360 ml), Et_3N (60 ml, 432 mmol) and pyrrolidine (36 ml, 432 mmol). PyBOP® (75 g, 144 mmol) was added portionwise under a gentle flow of nitrogen over 2 h ensuring the temperature remained below 25 °C, the mixture was stirred for a further 1 h. The mixture was washed with an aqueous sat. $NaHCO_3$ solution (100 ml) and an aqueous sat. NH_4Cl solution (100 ml) and then concentrated in *vacuo* (to *ca.* 50 ml DCM, ensuring any residual HOBt is not concentrated to dryness). To this was added MeOH (100 ml) and 20% wt K_2CO_3 water solution (500 ml) and the resultant solution was stirred for 2 h before extraction with CH_2Cl_2 (3 x 300 ml). After drying over $MgSO_4$, the crude was

concentrated in *vacuo* and purified by flash column chromatography (EtOAc) and isolated (17.9 g, 77%) as a low melting white solid.

^{1}H NMR (400 MHz, Chloroform-*d*) δ 3.94 (t, *J* = 6.5 Hz, 1H, O*H*), 3.62-3.40 (m, 6H, OCH_2, NCH_2), 2.02-1.71 (m, 4H), 1.21 (s, 6H); **^{13}C{^{1}H} NMR** (101 MHz, Chloroform-*d*) δ 176.66, 72.52, 48.03-48.01 (m), 43.19, 27.01, 22.99, 21.01; **IR** (film cm^{-1}) 3427, 2970, 2877, 1725, 1593, 1472, 1416, 1340, 1262, 1184, 1157, 1056, 1020; **HRMS (Methane CI^{+})** 172.1331 m/z (172.1332 calculated for $C_9H_{18}NO_2$ $[M+H]^{+}$).

2,2-dimethyl-3-pyrrolidino-3-oxopropanal 3.14b

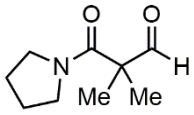

To a nitrogen flushed 1 L 3 necked round bottom flask connected to a Shlenck line, fitted with a thermometer and bubbler was added CH_2Cl_2 (120 ml) and oxalyl chloride (10.2 ml, 121 mmol), the flask was cooled to –78 ºC. In a separate degassed flask DMSO (17.2 ml, 242 mmol) was added to CH_2Cl_2 (120 ml), this mixture was added dropwise to the oxalyl chloride solution by cannula ensuring the temperature of the solution did not exceed –65 °C. After addition, the mixture was stirred for a further 5 mins at –78 °C. In a separate degassed flask, alcohol **3.21** (17.9 g, 110 mmol) was dissolved in CH_2Cl_2 (260 ml), this solution was then added dropwise to the reaction mixture by cannula, ensuring the temperature of the solution did not exceed –65 °C. During the addition the bubbler was connected to an aqueous $NaHCO_3$ scrubbing solution, after the addition was complete the mixture was stirred for a further 30 mins at –78 °C. Then dry Et_3N (76.3 ml, 550 mmol) was added dropwise by cannula, ensuring the temperature of the solution did not exceed –70 °C. During the addition the bubbler was connected to an aqueous NaOCl scrubbing solution. After the addition was complete the solution was allowed to warm to room temperature. The solution was washed with an aqueous HCl solution (2M, 100 ml) and an aqueous sat. $NaHCO_3$ solution (100 ml) and an aqueous sat. brine solution (100 ml). After drying over $MgSO_4$, the crude was concentrated in *vacuo* and purified by flash column chromatography (EtOAc/Heptane 5:5) and isolated (13.7 g, 81%) as a low melting white solid.

^{1}H NMR (500 MHz, Chloroform-*d*) δ 9.62 (s, 1H, C*H*O), 3.51 (t, *J* = 6.5 Hz, 2H, NC*H*$_2$), 3.27 (t, *J* = 6.5 Hz, 2H, NC*H*$_2$), 1.89 (app. p, *J* = 6.5 Hz, 2H, CH$_2$C*H*$_2$), 1.82 (app. p, *J* = 6.5 Hz, 2H, CH$_2$C*H*$_2$), 1.34 (s, 6H); **^{13}C{^{1}H} NMR** (101 MHz, Chloroform-*d*) δ 200.01, 169.64, 54.69, 47.51, 46.65, 26.70, 23.32, 19.52; **LRMS (ESI$^+$)** m/z 170.1; data consistent with that previously reported.[1]

(*E*)-2,2-dimethyl-1-(pyrrolidin-1-yl)undec-4-ene-1,3-dione 3.23a (5 gram-scale reaction)

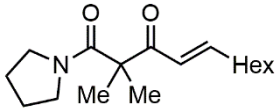

To a nitrogen filled 2 neck round bottom flask fitted with a reflux condenser and charged with [Rh(*cis*-κ^2-$_{P,P}$-DPEPhos)(η^6-*o*-xylene)][BAr$^F{}_4$] (490 mg, 0.305 mmol) and aldehyde **3.14b** (5.16 g, 30.5 mmol) was added acetone (5 ml) and 1-octyne (4.5 ml, 30.5 mmol). The mixture was heated to 30 °C for 2 h before precipitation of catalyst with pentane (300 ml), filtration through a silica plug and concentration in *vacuo* to afford product (8.3 g, 97%).

^{1}H NMR (400 MHz, Chloroform-*d*) δ 7.00 (dt, *J* = 15.0, 7.0 Hz, 1H, CH$_2$C*H*), 6.20 (d, *J* = 15.0 Hz, 1H, CH$_2$CHC*H*), 3.49 (t, *J* = 6.5 Hz, 2H, NC*H*$_2$), 3.12 (t, *J* = 6.0 Hz, 3H, NC*H*$_2$), 2.15 (app. q, *J* = 7.0 Hz, CHC*H*$_2$) 1.81-1.72 (m, 4H, NCH$_2$C*H*$_2$), 1.44-1.32 (m, 2H, CHCH$_2$C*H*$_2$), 1.33 (s, 6H, C(C*H*$_3$)$_2$) 1.28-1.20 (m, 6H, C*H*$_2$), 0.85 (t, *J* = 6.5 Hz, 3H, CH$_2$C*H*$_3$); **^{13}C{^{1}H} NMR** (101 MHz, Chloroform-*d*) δ 199.08, 171.22, 149.44, 125.60, 55.04, 47.47, 46.47, 32.50, 31.62, 28.88, 28.14, 26.66, 23.48, 22.64, 22.24, 14.14; **IR** (film cm^{-1}) 2977, 2888, 2857, 1720, 1628, 1464, 1463, 1385, 1253, 1153, 1075, 816; **LRMS (ESI$^+$)** m/z 280.2 [M+H]$^+$; **HRMS (ESI$^+$)** m/z 302.20930 (302.20905) calculated for $C_{17}H_{29}NO_2Na$ [M+Na]$^+$).

6.3.4. Kinetics

Initial rates (Table 3.1 and Figure 3.7): example cyclotrimerization procedure

Using General Procedure A, [Rh(*cis*-κ^2-$_{P,P}$-DPEPhos)(acetone)$_2$][BAr$^F{}_4$] was generated *in situ* from a solution of [Rh(*cis*-κ^2-$_{P,P}$-DPEPhos)(nbd)][BAr$^F{}_4$] (5.4 mg, 0.0034 mmol) in acetone-d_6 (100 µl), to this acetone-d_6 (150 µl) was aded. Then 100 µl of a stock solution of 1-octyne (9 µl, 0.034 mmol) and acetone (90 µl) was added carefully ensuring no mixing, the mixture was then immediately frozen in liquid

nitrogen. The sample was thawed and shaken vigorously before being inserted to the NMR probe at 298 K. The sample was locked and shimmed before running a ^{1}H NMR multi_zgvd run with a fixed 60 s delay. The data was analysed by using the BAr^{F}_{4} resonance as an internal reference and measuring the integral of the alkyne resonance at δ 2.18.

Stoichiometric reaction of acyl-hydride 3.13a (Figure 3.8)

In two separate NMR tubes containing a solution of acyl hydride **3.13a** (13.4 mg, 0.0079 mmol) in acetone-d_6 (175 µl) was added:

Reaction **A**: acetone-d_6 (75 µl) followed by a stock solution of 1-octyne (1.3 µl, 0.008 mmol) in acetone-d_6 (100 µl).

Reaction **B**: a stock solution of aldehyde **3.14a** (0.8 mg, 0.0085 mmol) in acetone-d_6 (75 µl) followed by a stock solution of 1-octyne (1.3 µl, 0.008 mmol) in acetone-d_6 (100 µl).

Both reactions were shaken vigorously before being inserted into the NMR probe at 298 K. The sample was locked and shimmed before running a ^{1}H NMR multi_zgvd run with a fixed 10 mins delay until the reaction had proceeded to completion. The data was analysed by using the BAr^{F}_{4} resonance as an internal reference and measuring the integral of the alkene resonance at δ 6.28, alkyne resonance at δ 2.18 and the cyclotrimer resonance at δ 2.05.

Hydroacylation reaction using α-pyran-complex 3.4 as catalyst (Figure 3.10)

To an NMR tube charged with [Rh(*cis*-κ^{2}-$_{P,P}$-DPEPhos)($\kappa^{2}_{C,C}$-2,2-methyl-4,6-*n*-hexyl-α-pyran)][BAr^{F}_{4}] **3.4** (20.8 mg, 0.0116 mmol) in acetone-d_6 (100 µl), was added a stock solution of aldehyde **3.14a** (43 mg, 0.23 mmol) in acetone-d_6 (150 µl). Then a solution of 1-octyne (68 µl, 0.46 mmol) and acetone (60 µl) was added carefully ensuring no mixing, the mixture was then immediately frozen in liquid nitrogen. The sample was thawed and shaken vigorously before being inserted to the NMR probe at 298 K. The sample was locked and shimmed before running a ^{1}H NMR multi_zgvd run with a fixed delay until the reaction had proceeded to completion. The data was analysed by using the BAr^{F}_{4} resonance as an internal reference and measuring the integral of the aldehyde resonance at δ 9.66, the alkene resonances at δ 6.28 (linear) δ 5.92 (branched), the alkyne resonance at δ 2.18, the cyclotrimer

resonance at δ 2.05 and the hydride resonance at δ –14.53.

Hydroacylation recharging experiment with 1-octyne (Figure 3.11)

Using General Procedure A, [Rh(*cis*-κ^2-$_{P,P}$-DPEPhos)(acetone)$_2$][BAr^F_4] was generated *in situ* from a solution of [Rh(*cis*-κ^2-$_{P,P}$-DPEPhos)(nbd)][BAr^F_4] (18.6 mg, 0.012 mmol) in acetone-d_6 (160 µl), to this was added a stock solution of aldehyde **3.14a** (43.0 mg, 0.23 mmol) in acetone-d_6 (150 µl) and 1-octyne (45 µl, 0.302 mmol). The sample was shaken vigorously before being inserted to the NMR probe at 298 K. The sample was locked and shimmed before running a ^{1}H NMR multi_zgvd run with a fixed 5 min delay until the reaction had proceeded to completion. Then a solution of aldehyde **3.14a** (43.0 mg, 0.232 mmol) in acetone-d_6 (100 µl) and 1-octyne (45 µl, 0.302 mmol) was added and the reaction was again monitored until completion. The data was analysed by using the BAr^F_4 resonance as an internal reference and measuring the integral of the alkene resonances at δ 6.28 (linear), δ 5.92 (branched) and alkyne resonance at δ 2.18 and the cyclotrimer resonance at δ 2.05.

6.3.5. Kinetics (work carried out at AstraZeneca)

Example Procedure (Table 3.3, Entry 2)

A nitrogen filled integrity-10® thin tube fitted with a rubber septum and connected to a low N_2 flow was charged with [Rh(*cis*-κ^2-$_{P,P}$-DPEPhos)(η^6-*o*-xylene)][BAr^F_4] (9.6 mg, 0.006 mmol) and aldehyde **3.14b** (203 mg, 1.20 mmol). To this dodecane (27 µl, 0.12 mmol) and acetone (796 µl) were added. The mixture was cooled to 10 °C using an integrity-10® heating block, then 1-octyne (177 µl, 1.20 mmol) was added. The reaction was sampled periodically and progress was measured by GC. GC samples were dissolved in acetonitrile to ensure catalysis ceased. Aldehyde, 1-octyne and products were calibrated for GC independently.

Figure 6.1. Optimisation profiles from Table 3.3 (See Figure 3.12 for Entry 5)

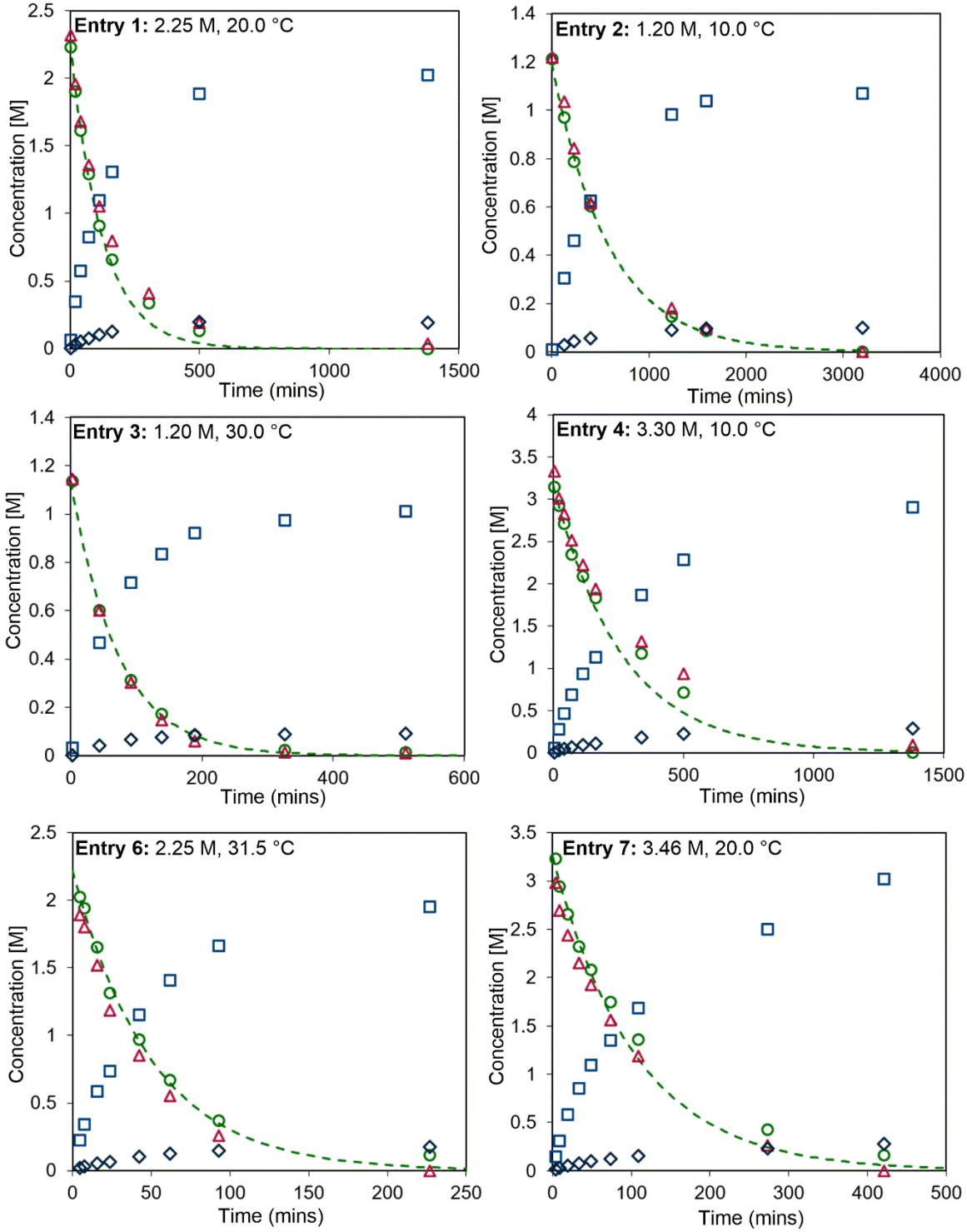

[a]Reaction profile as measured by ^{1}H NMR spectroscopy. Red △ = aldehyde **3.14a**, green ○ = 1-octyne 3.1, blue ■ = enone **3.15a**, blue ◆ = enone **3.15b**, dotted green line = first-order model for the consumption of 1-octyne **3.1**.

6.4. Non-tethered Aldehyde Hydroacylation with Acrylates

6.4.1. Inorganic Reactions

General Procedure D: Addition of *β*-amido-methyl-ketone to {Rh(dcpm)}$^+$ complexes

For reactions in Schemes **4.3**, **4.4** and **4.5**: A high-pressure NMR tube with a controlled atmosphere valve was charged with [Rh(*cis*-κ^2-$_{P,P}$-dcpm)(nbd)][X] (X = BAr^F_4 or AlO^F_4) (0.0108 mmol), then solvent (300 μl) was added and the solution was freeze-pump-thawed into an atmosphere of H_2 (4 atm). After vigorous shaking, the NMR tube was left to stand for 15 minutes after which the solution was freeze-pumped-thawed into an atmosphere of argon (1 atm). A stock solution of *β*-amido-methyl-ketone **4.3** (2.48 mg, 0.011 mmol) in solvent (200 μl) was added and the reaction mixture shaken vigorously before being monitored by $^{31}P\{^1H\}$ NMR spectroscopy.

Synthesis of a potential Rh(I)DPEPhos acrylate-bound complex

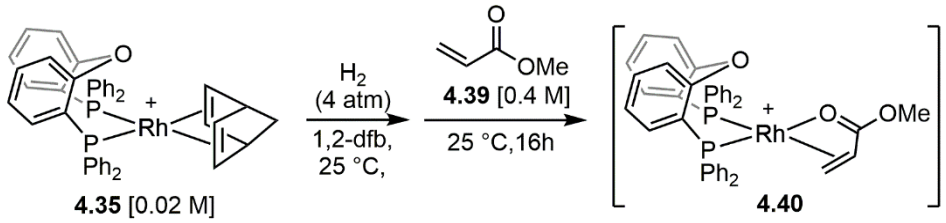

[a]BAr^F_4 anion omitted for clarity

A high-pressure NMR tube with a controlled atmosphere valve was charged with [Rh(*cis*-κ^2-$_{P,P}$-DPEPhos)(nbd)][BAr^F_4] (13.0 mg, 0.008 mmol). 1,2-difluorobenzene (400 μl) was added and the solution was freeze-pump-thawed into an atmosphere of H_2 (4 atm). After vigorous shaking, the NMR tube was left to stand for 30 minutes after which the solution was freeze-pumped-thawed into an atmosphere of argon (1 atm). The product of hydrogenation was characterised by ^1H and $^{31}P\{^1H\}$ NMR spectroscopy (see Figure 4.2). To this solution methacrylate (15 μl, 0.16 mmol) was added and the reaction mixture shaken vigorously before being monitored by $^{31}P\{^1H\}$ NMR spectroscopy.

6.4.2. Organic Reactions

Tishchenko reaction of cyclohexanecarboxaldehyde

A high-pressure NMR tube with a controlled atmosphere valve was charged with [Rh(*cis*-κ^2-$_{P,P}$-dcpm)(nbd)][AlO^F_4] (55 mg, 0.035 mmol), solvent (350 µl) was added and the solution was freeze-pump-thawed into an atmosphere of H_2 (4 atm). After vigorous shaking, the NMR tube was left to stand for 15 minutes after which the solution was freeze-pumped-thawed into an atmosphere of argon (1 atm). A stock solution of cyclohexanecarboxaldehyde **4.12** (85 µl, 0.70 mmol) was added and the reaction mixture shaken vigorously before being monitored by ^{1}H NMR spectroscopy.

6.4.3. Organic Synthesis

1-(1-(morpholine-4-carbonyl)cyclopentyl)ethan-1-one 4.3

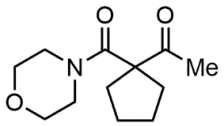

To a two necked round bottom flask (50 ml) charged with morpholinobutane-1,3-dione (900 mg, 4.0 mmol) and K_2CO_3 (1.38 g, 10.0 mmol) was added DMF (10 ml) followed by 1,4-dibromobutane (526 µl, 4.40 mmol). The mixture was stirred and cooled to 0 ºC on an ice water bath and [BMIM]BF_4 (75 µl, 0.40 mmol) was added dropwise. The mixture was warmed to room temperature and stirred for 16 h. The reaction was then filtered and washed with Et_2O (50 ml), to the filtrate water (50 ml) was added, which was then extracted with Et_2O (3 × 30 ml). The organic layers were combined and washed with brine (30 ml), dried over $MgSO_4$, filtered and concentrated *in vacuo*. The crude was purified by silica gel chromatography (EtOAc/Petrol 6 : 4) affording the product as a colourless oil (170 mg, 21%).

^{1}H NMR (400 MHz, Chloroform-*d*) δ 3.70-3.56 (br m, 4H, NCH_2, OCH_2), 3.56-3.47 (br m, 2H, OCH_2), 3.25-3.17 (br m, 2H, NCH_2), 2.19-2.09 (m, 2H, CCH_2), 2.11 (s, 3H, CH_3), 2.09-1.99 (m, 2H, CCH_2), 1.58 (m, 4H CCH_2CH_2); **^{13}C{^{1}H} NMR** (101 MHz, Chloroform-*d*) δ 206.03 (CH_3C(O)), 170.97 (N*C*(O)), 67.27 (C(O)*C*), 66.92 (br s, OCH_2), 66.27 (br s, OCH_2), 46.18 (s, NCH_2), 43.24 (s, NCH_2), 33.65 (CCH_2), 26.25 (CCH_2CH_2), 26.17 (CH_3); **IR** (film cm^{-1}) 2958, 2862, 1708, 1639, 1453,1421,1359,

1301, 1273, 1242, 1181, 1156, 1116, 1069, 1021; **LRMS** (ESI^+) m/z 226.2 [M+H]; **HRMS** (ESI^+) m/z 226.14379 (226.14377 calculated for $C_{12}H_{20}O_3N$).

General Procedure E: Acrylate Hydroacylation

A round bottom microwave vial (10 ml) was charged with $[Rh(nbd)_2]$Krossing (20.1 mg, 0.016 mmol) and DPEPhos (8.6 mg, 0.016 mmol). The vial was then sealed with a microwave cap with a rubber septa. The vial was vacuum-backfilled three times before 1,2-difluorobenzene (300 µl) was added. The resultant solution was stirred for 5 minutes until it became bright red and all solids were dissolved. The solution was then gently bubbled with hydrogen gas for 5 minutes after which the solution turned dark red. The solution was then blown dry with argon for 20 minutes, until an oily residue remained. Under an argon pressure 1,2-difluorobenzene (80 µl), *n*-butyl acrylate (140 µl, 0.96 mmol) and aldehyde (0.32 mmol) were added sequentially. After removing the argon flow, the vial lid was covered with three layers of parafilm before being placed in a preheated (110 °C) oil bath. The solution was placed level with the oil and the mixture was stirred (180 rpm) for 30 h. The mixture was evaporated and purified directly by silica gel chromatography.

Butyl 4-cyclohexyl-4-oxobutanoate 4.22a

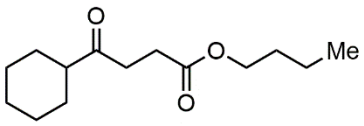

Using General Procedure E with *n*-butyl acrylate (140 µl, 0.96 mmol) and cyclohexanecarboxaldehyde (39 µl, 0.32 mmol). The crude was purified by silica gel chromatography (Petrol/Et_2O 8 : 2) affording the product as a colourless oil (69 mg, 91%).

^{1}H NMR (400 MHz, Chloroform-*d*) δ 4.05 (t, *J* = 6.5 Hz, 2H, OCH_2), 2.73 (t, *J* = 6.5 Hz, 2H, C(O)CH_2), 2.55 (t, *J* = 6.5 Hz, 2H, C(O)CH_2), 2.36 (tt, *J* = 11.5, 3.5 Hz, 1H, C*H*), 1.89-1.82 (m, 2H, CHCH_2), 1.80-1.72 (m, 2H, $CHCH_2CH_2$), 1.70-1.53 (m, 3H, $CHCH_2CH_2CH_2$, OCH_2CH_2), 1.41-1.12 (m, 7H, CHCH_2, $CHCH_2CH_2$, $CHCH_2CH_2CH_2$, CH_3CH_2), 0.91 (t, *J* = 6.5 Hz, 3H, CH_3); **13C{^{1}H} NMR** (101 MHz, Chloroform-d) δ 212.18 (CH*C*O), 173.14 (*C*$(O)_2$), 64.61 (OCH_2), 50.84 (*C*H), 35.14 ($C(O)CH_2$), 30.74 (OCH_2CH_2), 28.59 ($CHCH_2$), 28.06 ($C(O)CH_2$), 25.96 ($CHCH_2CH_2$), 25.75

($CHCH_2CH_2CH_2$), 19.23 (CH_3CH_2), 13.83 (CH_3); **IR** (film cm^{-1}) 2958, 2931, 2856, 1735, 1712, 1450, 1409, 1392, 1363, 1349, 1316, 1262, 1205, 1184, 1167, 1144, 1098, 1029, 997; **LRMS** (ESI^+) m/z 263.2 [M+Na]; **HRMS** (ESI^+) m/z 263.16146 (263.16177 calculated for $C_{14}H_{24}O_3Na$).

Butyl 4-(1-methylcyclohexyl)-4-oxobutanoate 4.22b

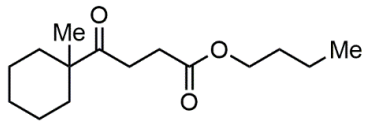

Using General Procedure E with *n*-butyl acrylate (140 µl, 0.96 mmol) and 1-methylcyclohexane-1-carboxaldehyde (42 µl, 0.32 mmol). The crude was purified by silica gel chromatography (Petrol/Et_2O 8:2) affording the product as a colourless oil (58 mg, 72%).

^{1}H NMR (400 MHz, Chloroform-*d*) δ 4.06 (t, J = 6.5 Hz, 2H, OCH_2), 2.78 (t, J = 6.5 Hz, 2H, $C(O)CH_2$), 2.55 (t, J = 6.5 Hz, 2H, $C(O)CH_2$), 1.96 (m, 2H, CH_3CCH_2), 1.66-1.47 (m, 4H, OCH_2CH_2, $CH_3CCH_2CH_2$), 1.46-1.22 (m, 8H, CH_3CH_2, CH_3CCH_2, $CH_3CCH_2CH_2$,, $CH_3CCH_2CH_2CH_2$), 1.09 (s, 3H, CCH_3), 0.91 (t, J = 7.5 Hz, 3H, CH_2CH_3); **^{13}C NMR{^{1}H}** (101 MHz, Chloroform-d) δ 213.93 (CCO), 173.28 ($C(O)_2$), 64.57 (OCH_2), 48.08 (CH_3C), 34.81 (CH_3CCH_2), 31.66 ($C(O)CH_2$), 30.78 (OCH_2CH_2), 28.23 ($C(O)CH_2$), 25.93 ($CH_3CCH_2CH_2CH_2$), 25.18 (CCH_3), 23.00 ($CH_3CCH_2CH_2$), 19.24 (CH_3CH_2), 13.83 (CH_2CH_3); **IR** (film cm^{-1}) 2971, 2927, 2864, 1734, 1714, 1454, 1397, 1364, 1349, 1256, 1999, 1194, 1164, 1140, 1101, 1029; **LRMS** (ESI^+) m/z 277.2 [M+Na]; **HRMS** (ESI^+) m/z 255.19556 (255.19547 calculated for $C_{15}H_{27}O_3$).

Butyl 4-oxoundecanoate 4.22c

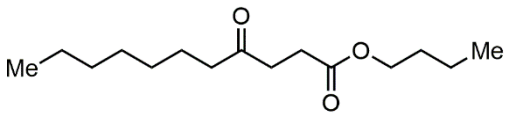

Using General Procedure E with *n*-butyl acrylate (140 µl, 0.96 mmol) and *n*-octanal (33 µl, 0.32 mmol). But with $Rh(nbd)_2$]Krossing (40.2 mg, 0.032 mmol) and dcpb (13.6 mg, 0.032 mmol) instead of DPEPhos. The crude was purified by silica gel chromatography (Petrol/Et_2O 9 : 1) affording the product as a colourless oil (58 mg, 71%).

^{1}H NMR (400 MHz, Chloroform-*d*) δ 4.06 (t, *J* = 6.5 Hz, 2H, C(O)OC*H*$_2$), 2.70 (t, *J* = 6.5 Hz, 2H, C(O)C*H*$_2$), 2.57 (t, *J* = 6.5 Hz, 2H, C(O)C*H*$_2$), 2.43 (t, *J* = 7.5 Hz, 2H, C(O)$_2$CH$_2$CH$_2$C(O)C*H*$_2$), 1.65-1.53 (m, 4H, C(O)OCH$_2$C*H*$_2$, C(O)$_2$CH$_2$CH$_2$C(O)CH$_2$C*H*$_2$), 1.37 (app. sextet, *J* = 7.5 Hz, 2H, C(O)OCH$_2$CH$_2$C*H*$_2$), 1.32-1.20 (m, 8H, C*H*$_2$), 0.92 (t, *J* = 7.5 Hz, 3H, C(O)OCH$_2$CH$_2$CH$_2$C*H*$_3$), 0.87 (t, *J* = 7.0 Hz, 3H, CH$_2$CH$_2$CH$_2$CH$_2$C*H*$_3$); **^{13}C {^{1}H} NMR** (101 MHz, Chloroform-*d*) δ 209.29 (CH$_2$*C*OCH$_2$), 173.06 (*C*(O)$_2$), 64.67 (C(O)O*C*H$_2$), 42.98 (C(O)$_2$CH$_2$CH$_2$C(O)*C*H$_2$), 37.19 (C(O)*C*H$_2$), 31.81 (*C*H$_2$), 30.78 (C(O)OCH$_2$*C*H$_2$), 29.31 (*C*H$_2$), 29.19 (*C*H$_2$), 28.15 (C(O)*C*H$_2$), 23.97 (C(O)$_2$CH$_2$CH$_2$C(O)CH$_2$*C*H$_2$), 22.74 (*C*H$_2$), 19.25 (C(O)OCH$_2$CH$_2$*C*H$_2$), 14.19 (CH$_2$CH$_2$CH$_2$CH$_2$*C*H$_3$), 13.83 (C(O)OCH$_2$CH$_2$CH$_2$*C*H$_3$); **IR** (film cm^{-1}) 2985, 2929, 2872, 2857, 1736, 1717, 1465, 1411, 1393, 1356, 1246, 1181, 1128, 1086; **LRMS** (ESI$^+$) m/z 279.2 [M+Na]; **HRMS** (ESI$^+$) m/z 279.19349 (279.19307 calculated for $C_{15}H_{28}O_3Na$).

Butyl 4-cyclopentyl-4-oxobutanoate 4.22d

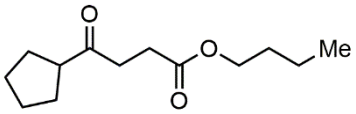

Using General Procedure E with *n*-butyl acrylate (140 µl, 0.96 mmol) and cyclopentanecarboxaldehyde (34 µl, 0.32 mmol). The crude was purified by silica gel chromatography (Petrol/EtOAc 9.5 : 0.5) affording the product as a colourless oil (61 mg, 84%).

^{1}H NMR (400 MHz, Chloroform-*d*) δ 4.05 (t, *J* = 6.5 Hz, 2H, OC*H*$_2$), 2.89 (p, *J* = 8.0 Hz, 1H, C*H*), 2.75 (t, *J* = 6.5 Hz, 2H, C(O)C*H*$_2$), 2.56 (t, *J* = 6.5 Hz, 2H, C(O)C*H*$_2$), 1.89-1.50 (m, 10H, OCH$_2$C*H*$_2$, CHC*H*$_2$, CHCH$_2$C*H*$_2$), 1.41-1.30 (m, 2H, CH$_3$C*H*$_2$), 0.91 (t, *J* = 7.5 Hz, 3H, CH$_3$); **^{13}C{^{1}H} NMR** (101 MHz, Chloroform-*d*) δ 211.29 (CH*C*O), 173.13 (*C*(O)$_2$), 64.61 (O*C*H$_2$), 51.40 (*C*H), 36.25 (C(O)*C*H$_2$), 30.74 (OCH$_2$*C*H$_2$), 28.98 (CH*C*H$_2$), 28.15 (C(O)*C*H$_2$), 26.11 (CHCH$_2$*C*H$_2$), 19.23 (CH$_3$*C*H$_2$), 13.83 (*C*H$_3$); **IR** (film cm^{-1}) 2958, 2871, 1735, 1712, 1454, 1409, 1393, 1355, 1304, 1235, 1204, 1173, 1104, 1072, 1021, 965, 946, 893, 841; **LRMS** (ESI$^+$) m/z 249.2 [M+Na]; **HRMS** (ESI$^+$) m/z 249.14617 (249.14612 calculated for $C_{13}H_{22}O_3Na$).

Butyl 5-ethyl-4-oxononanoate 4.22e

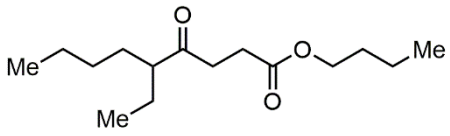

Using General Procedure E with *n*-butyl acrylate (140 µl, 0.96 mmol) and 2-ethylhexanal (48 µl, 0.32 mmol). The crude was purified by silica gel chromatography (Petrol/EtOAc 9.5 : 0.5) affording the product as a colourless oil (73 mg, 89%).

^{1}H NMR (400 MHz, Chloroform-*d*) δ 4.05 (t, *J* = 6.5 Hz, 2H, OC*H*$_2$) 2.71 (t, *J* = 6.5 Hz, 2H, C(O)C*H*$_2$), 2.54 (t, *J* = 6.5 Hz, 2H, C(O)C*H*$_2$), 2.39 (app. tt, *J* = 8.0, 5.5 Hz, 1H, C*H*), 1.66-1.53 (m, 4H, OCH$_2$C*H*$_2$, CHC*H*$_2$CH$_2$), 1.51-1.13 (m, 8H, OCH$_2$CH$_2$C*H*$_2$, CHC*H*$_2$CH$_3$, CHCH$_2$C*H*$_2$, CHCH$_2$CH$_2$C*H*$_2$), 0.90 (t, *J* = 7.5 Hz, 3H, OCH$_2$CH$_2$CH$_2$C*H*$_3$), 0.88-0.80 (m, 6H, CHCH$_2$C*H*$_3$, CHCH$_2$CH$_2$CH$_2$C*H*$_3$); **^{13}C{^{1}H} NMR** (101 MHz, Chloroform-*d*) δ 212.83 (CH*C*O), 173.05 (*C*(O)$_2$), 64.58 (O*C*H$_2$), 53.85 (*C*H), 36.97 (C(O)*C*H$_2$), 31.15 (CH*C*H$_2$CH$_3$), 30.74 (OCH$_2$*C*H$_2$), 29.71 (CHCH$_2$CH$_2$*C*H$_2$), 27.88 (C(O)*C*H$_2$), 24.84 (CH*C*H$_2$CH$_2$), 22.91 (CHCH$_2$*C*H$_2$), 19.21 (OCH$_2$CH$_2$*C*H$_2$), 14.02 (*C*H$_3$), 13.81 (*C*H$_3$), 11.91 CHCH$_2$*C*H$_3$); **IR** (film cm^{-1}) 2960, 2932, 2874, 1736, 1712, 1461, 1382, 1359, 1305, 1238, 1202, 1167, 1119, 1082, 1023, 965, 942, 841, 736; **LRMS** (ESI^{+}) m/z 279.2 [M+Na]; **HRMS** (ESI^{+}) m/z 279.19307 (279.19307 calculated for $C_{15}H_{28}O_3Na$).

Butyl 4-oxo-4-(tetrahydro-2H-pyran-4-yl)butanoate 4.22f

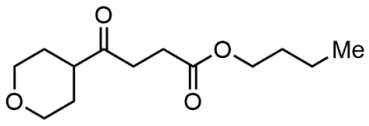

Using General Procedure E, *n*-butyl acrylate (140 µl, 0.96 mmol) and tetrahydro-2H-pyran-4-carboxaldehyde (33 µl, 0.32 mmol). The crude was purified by silica gel chromatography (Petrol/EtOAc 9 : 1) affording the product as a colourless oil (31 mg, 38%).

^{1}H NMR (400 MHz, Chloroform-*d*) δ 4.06 (t, *J* = 6.5 Hz, 2H, C(O)OC*H*$_2$), 4.00 (app. dt, *J* = 11.5, 3.0 Hz, 2H, C*H*$_2$OC*H*$_2$), 3.43 (app. td, *J* = 11.5, 3.0 Hz, 2H, C*H*$_2$OC*H*$_2$), 2.75 (t, *J* = 6.5 Hz, 2H, C(O)C*H*$_2$), 2.60 (m, 3H, C*H*, C(O)C*H*$_2$), 1.84-1.65 (m, 4H, CHC*H*$_2$), 1.64-1.54 (m, 2H, C(O)OCH$_2$C*H*$_2$), 1.37 (app.

sextet, *J* = 7.5 Hz, 2H, CH_3CH_2), 0.92 (t, *J* = 7.5 Hz, 3H, CH_3); **^{13}C {^{1}H} NMR** (101 MHz, Chloroform-*d*) δ 210.12 (CHCO), 172.99 ($C(O)_2$), 67.37 (CH_2OCH_2), 64.74 ($C(O)OCH_2$), 47.66 (CH), 34.87 ($C(O)CH_2$), 30.77 ($C(O)OCH_2CH_2$), 28.28 ($C(O)CH_2$), 28.02 ($CHCH_2$), 19.24 (CH_3CH_2), 13.83 (CH_3); **IR** (film cm^{-1}) 2958, 2873, 2848, 1733, 1711, 1466, 1388, 1350, 1324, 1302, 1258, 1240, 1204, 1173, 1149, 1115, 1092, 1069. 1018, 984; **LRMS** (ESI^{+}) m/z 265.1 [M+Na]; **HRMS** (ESI^{+}) m/z 265.14095 (265.14103 calculated for $C_{13}H_{22}O_4Na$).

6.5. References

1 T. J. Coxon, M. Fernández, J. Barwick-Silk, A. I. McKay, L. E. Britton, A. S. Weller and M. C. Willis, *J. Am. Chem. Soc.*, 2017, **139**, 10142–10149.

2 P. Ren, S. D. Pike, I. Pernik, A. S. Weller and M. C. Willis, *Organometallics*, 2015, **34**, 711–723.

3 A. Lumbroso, P. Koschker, N. R. Vautravers and B. Breit, *J. Am. Chem. Soc.*, 2011, **133**, 2386–2389.

4 A. Prades, M. Fernández, S. D. Pike, M. C. Willis and A. S. Weller, *Angew. Chem. Int. Ed.*, 2015, **54**, 8520–8524.

5 J. F. Hooper, A. B. Chaplin, C. González-Rodríguez, A. L. Thompson, A. S. Weller and M. C. Willis, *J. Am. Chem. Soc.*, 2012, **134**, 2906–2909.

6 I. Krossing, *Chem. Eur. J.*, 2001, **7**, 490–502.

7 A. L. Colebatch, A. I. McKay, N. A. Beattie, S. A. Macgregor and A. S. Weller, *Eur. J. Inorg. Chem.*, 2017, 4533–4540.

8 A. B. Chaplin, J. F. Hooper, A. S. Weller and M. C. Willis, *J. Am. Chem. Soc.*, 2012, **134**, 4885–4897.

9 R. R. Schrock and J. A. Osborn, *Inorg. Chem.*, 1970, **9**, 2339–2343.

10 C. Allais, F. Liéby-Muller, T. Constantieux and J. Rodriguez, *Adv. Synth. Catal.*, 2012, **354**, 2537–2544.

11 G. L. Moxham, H. E. Randell-Sly, S. K. Brayshaw, R. L. Woodward, A. S. Weller and M. C. Willis, *Angew. Chem. Int. Ed.*, 2006, **45**, 7618–7622.

6.6. NMR Spectra for Inorganic Compounds

[Rh(*mer*-κ^3-$_{P,O,P}$-DPEPhos)(H)(COC{$(CH_3)_2$}CO{NC_4H_8O})][BAr^F_4] 2.3a: ^{1}H NMR (400 MHz, Acetone-d_6)

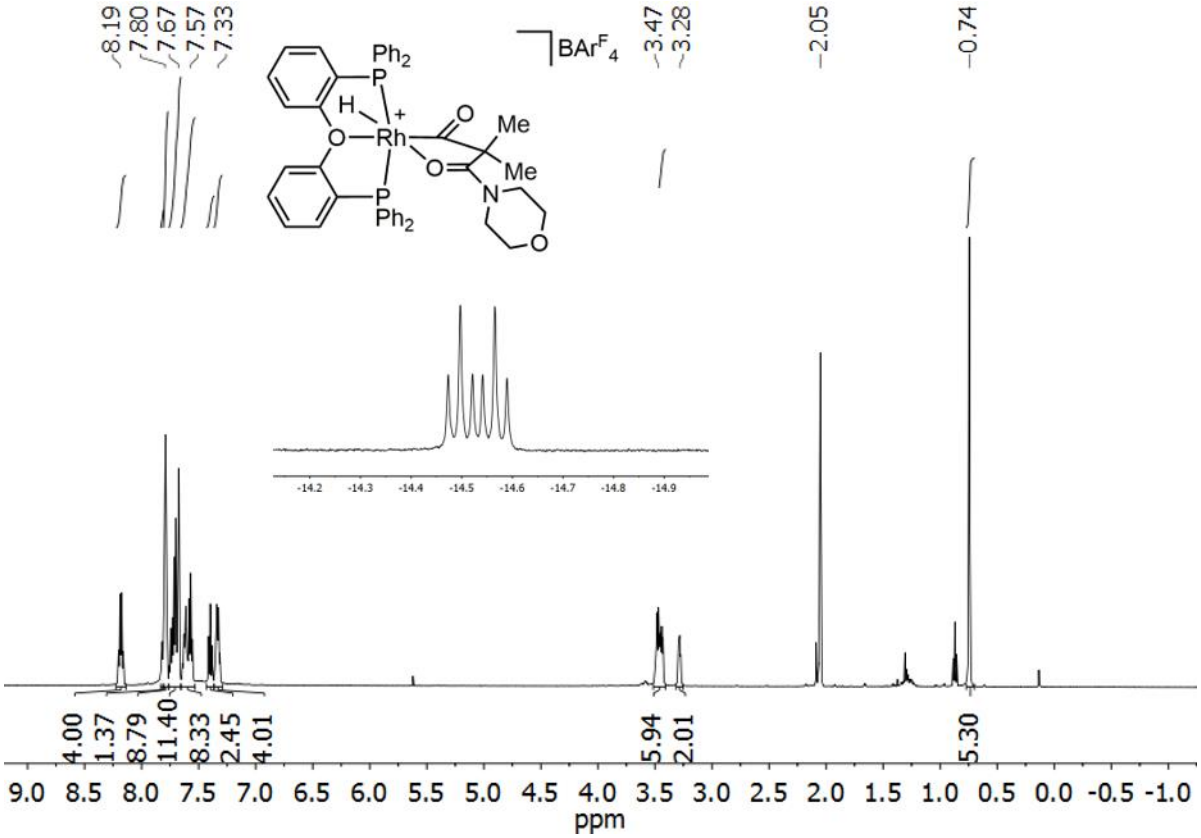

[Rh(*mer*-κ^3-$_{P,O,P}$-DPEPhos)(H)(COC{(CH_3)(H)}CO{NC_4H_8O})][BAr^F_4] 2.3b: ^{1}H NMR (400 MHz, Acetone-d_6)

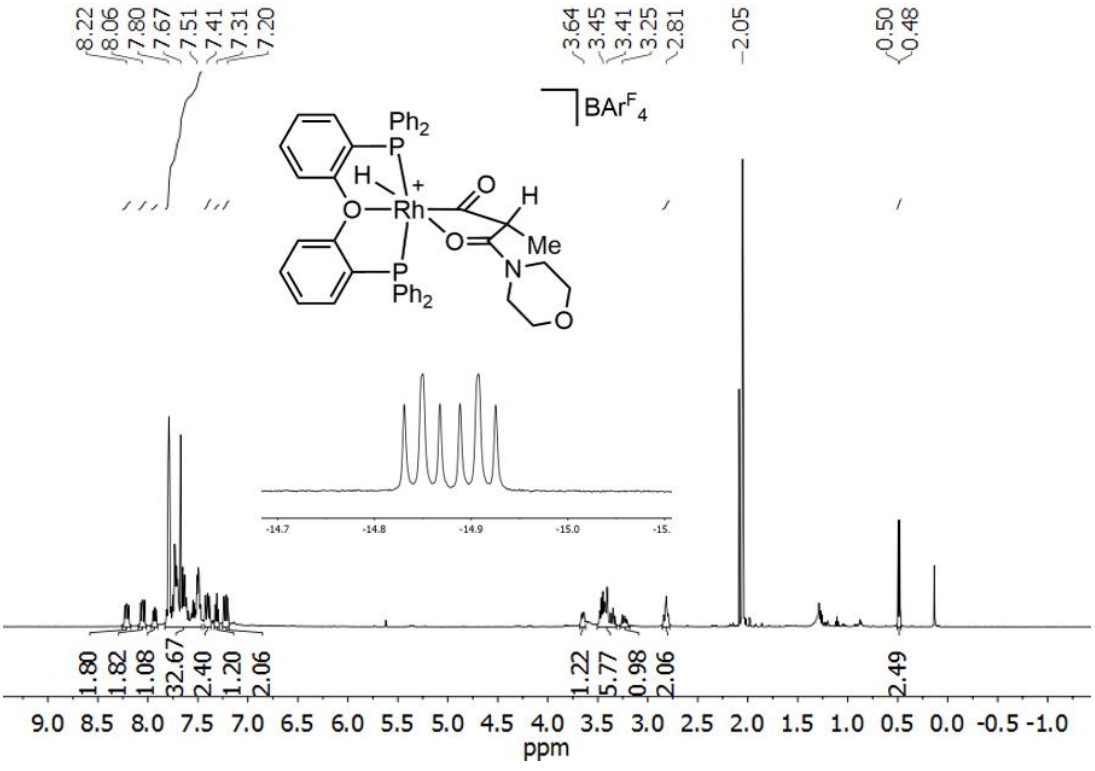

[Rh(*mer*-κ^3-$_{P,O,P}$-DPEPhos)(H)(COC{C_4H_8}CO{NC_4H_8O})][BAr^F_4] 2.3c: ^{1}H NMR (400 MHz, Acetone-d_6)

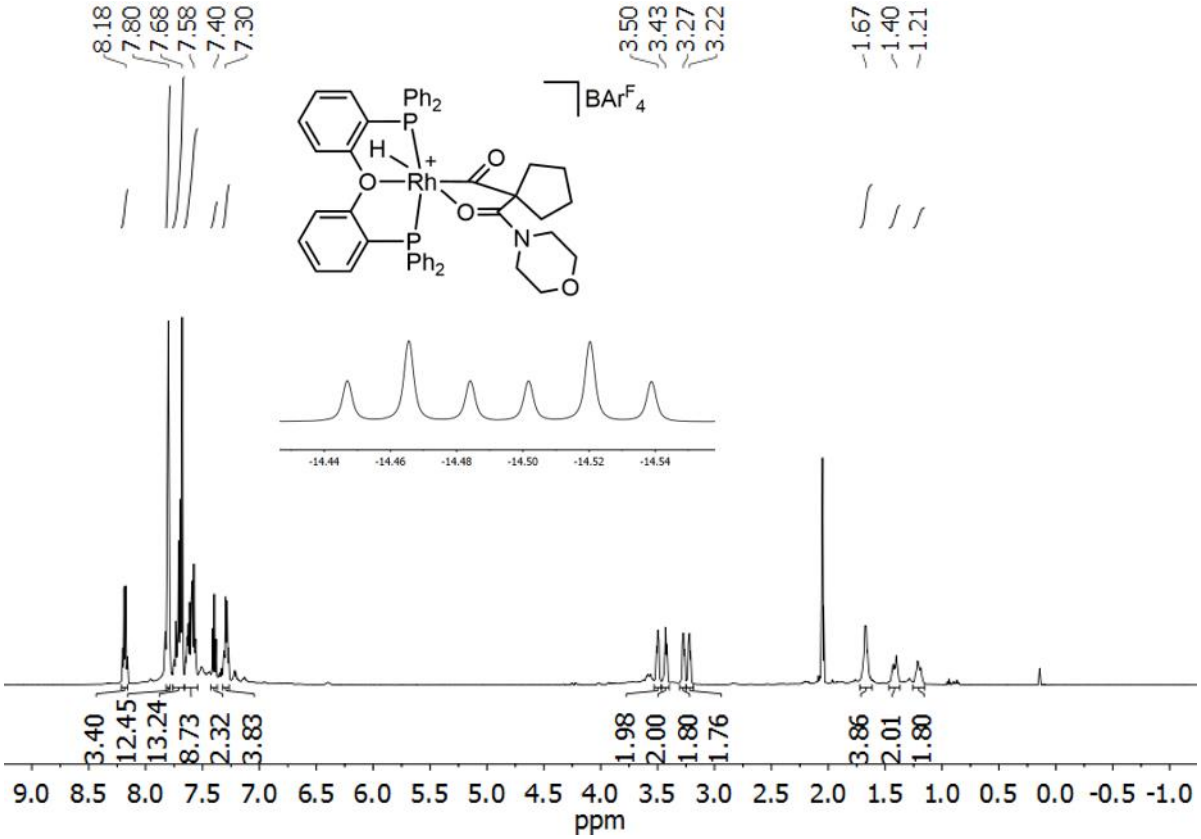

[Rh(*mer*-κ^3-$_{P,O,P}$-XantPhos)(H)(COC{(C_4H_8)}CO{NC_4H_8O})][BAr^F_4] 2.5: ^{1}H NMR (400 MHz, Acetone-d_6)

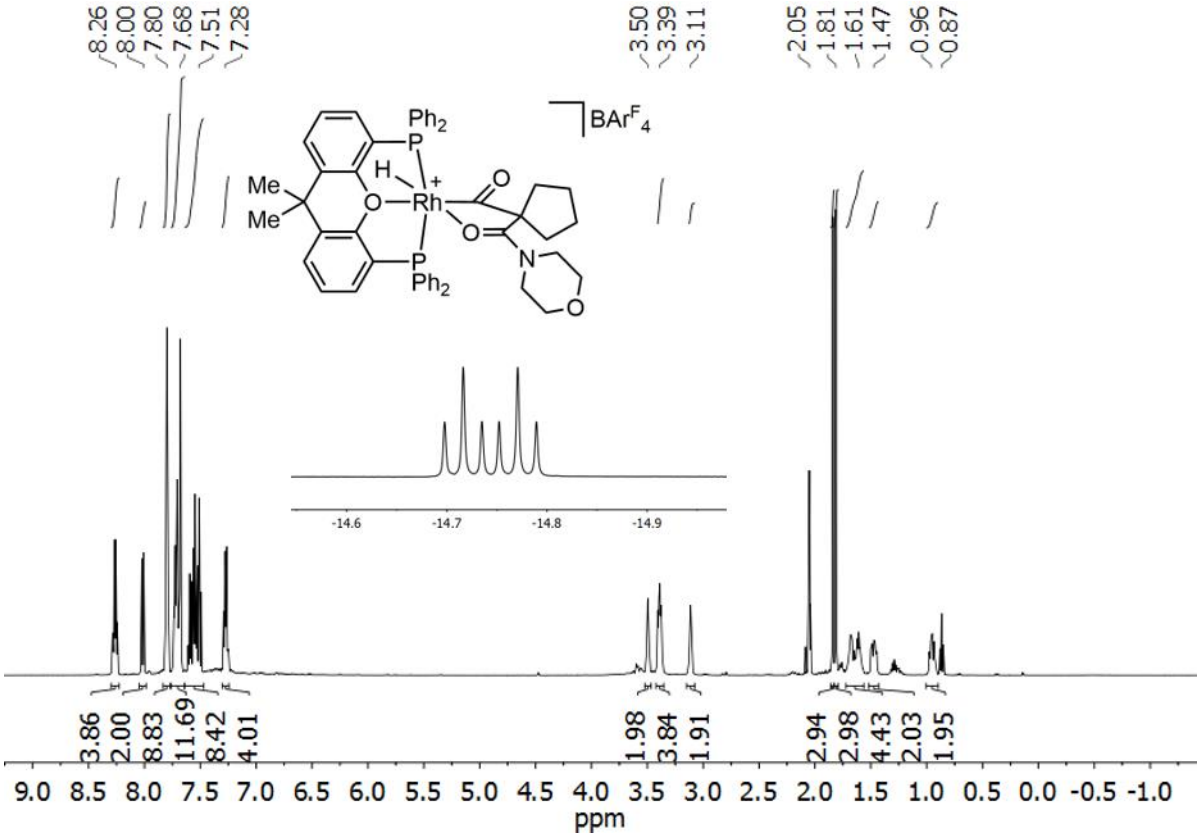

[Rh(*cis*-κ^2-$_{P,P}$-DPEPhos)(MeCN)$_2$][BAr$^F{}_4$] 2.13: ^{1}H NMR (400 MHz, CD_2Cl_2)

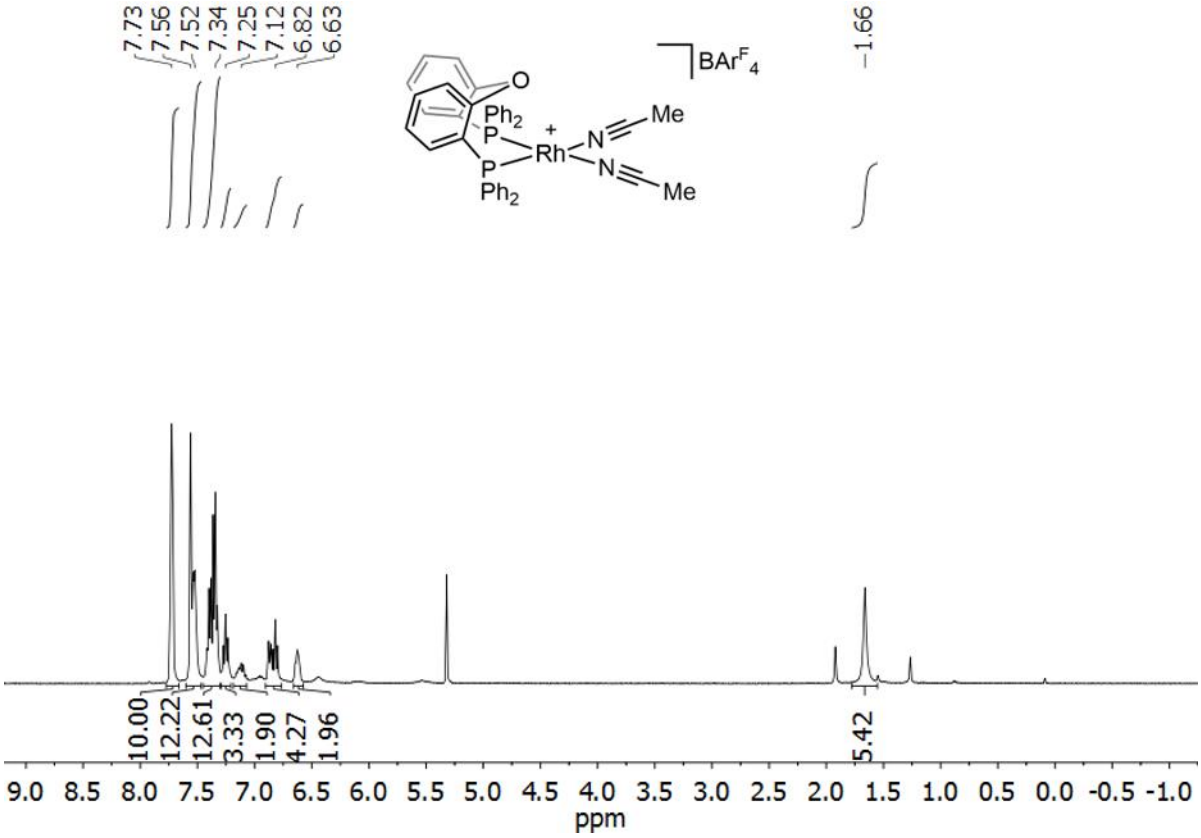

[Rh(*cis*-κ^2-$_{P,P}$-DPEPhos)(M2.10a)][BAr$^F{}_4$] 2.15: ^{1}H NMR (400 MHz, CD_2Cl_2)

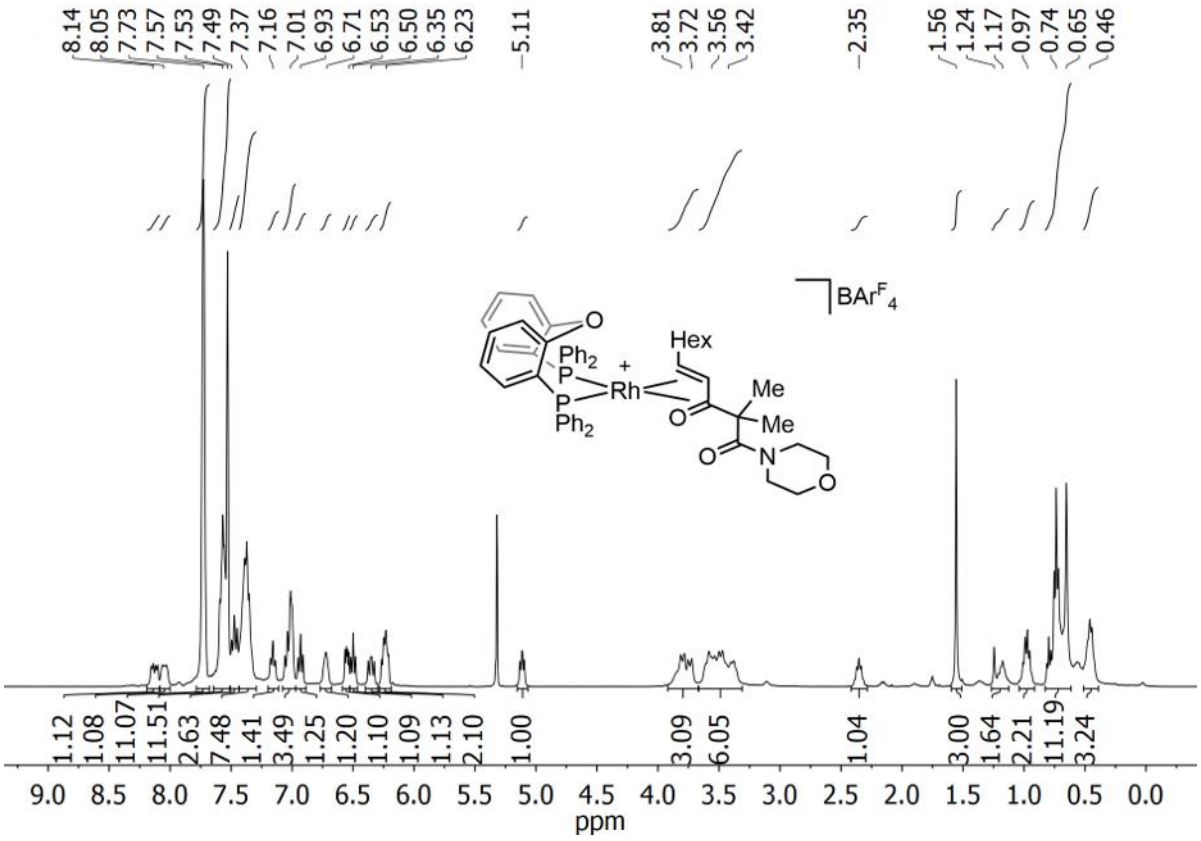

[Rh(*cis*-κ^2-P,P-DPEPhos)(κ^2-2,2-methyl-4,6-*n*-hexyl-α-pyran)][Al(OC(CF_3)$_3$)$_4$] : ^{1}H NMR (400 MHz, CD_2Cl_2)

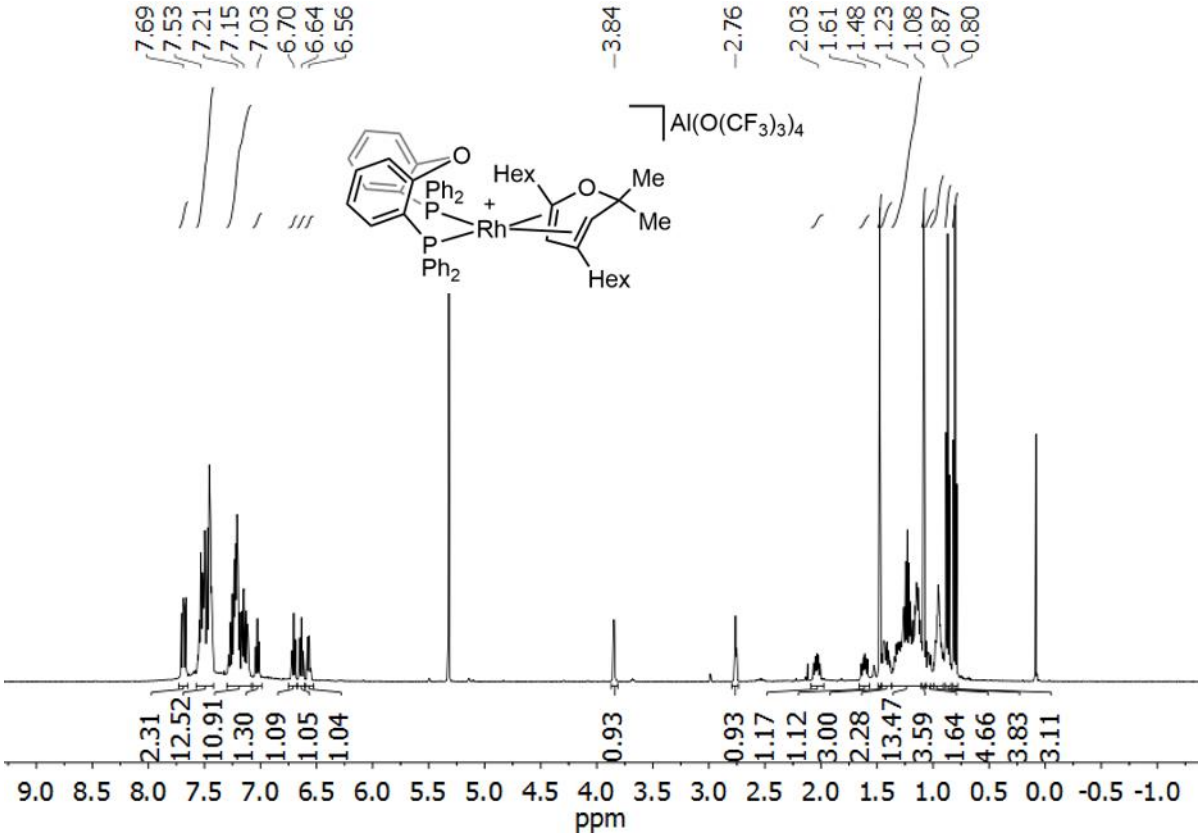

6.7. NMR Spectra for Organic Compounds

2,2-dimethyl-3-morpholino-3-oxopropan-^{2}H-al 2.2a-*d*$_1$: ^{1}H NMR (400 MHz, $CDCl_3$)

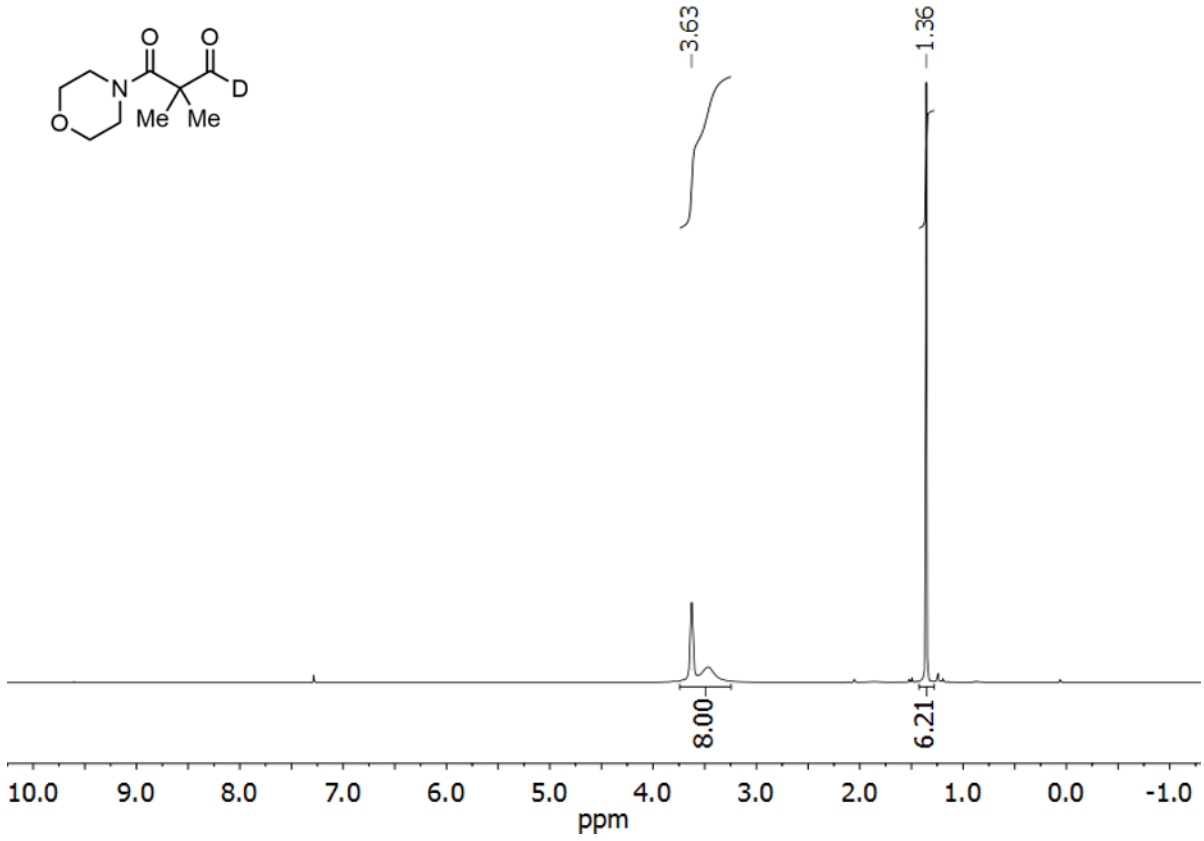

2,2-dimethyl-3-morpholino-3-oxopropan-^{2}H-al 2.2a-*d*$_1$: ^{13}C{^{1}H} NMR (400 MHz, $CDCl_3$)

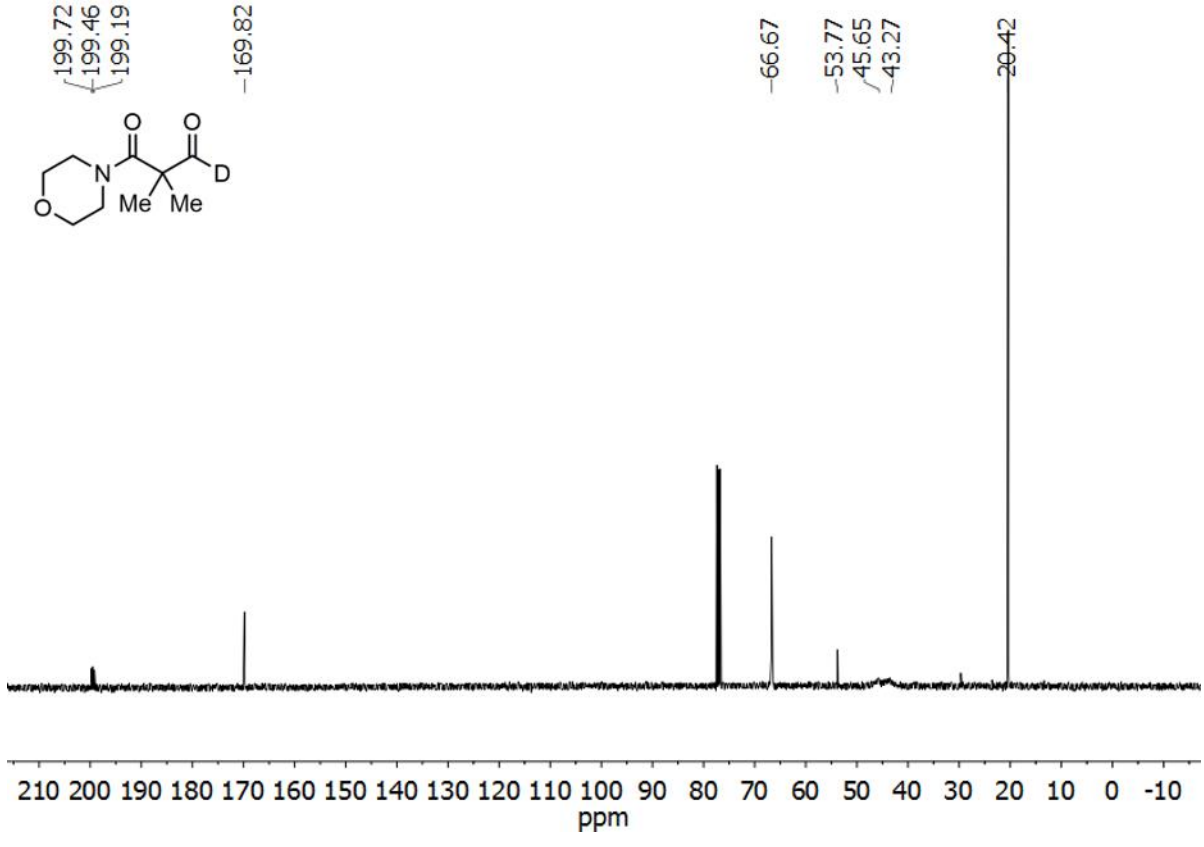

(*E*)-2,2-dimethyl-1-morpholinoundec-4-ene-5-^{2}H-1,3-dione 2.10c: ^{1}H NMR (400 MHz, $CDCl_3$)

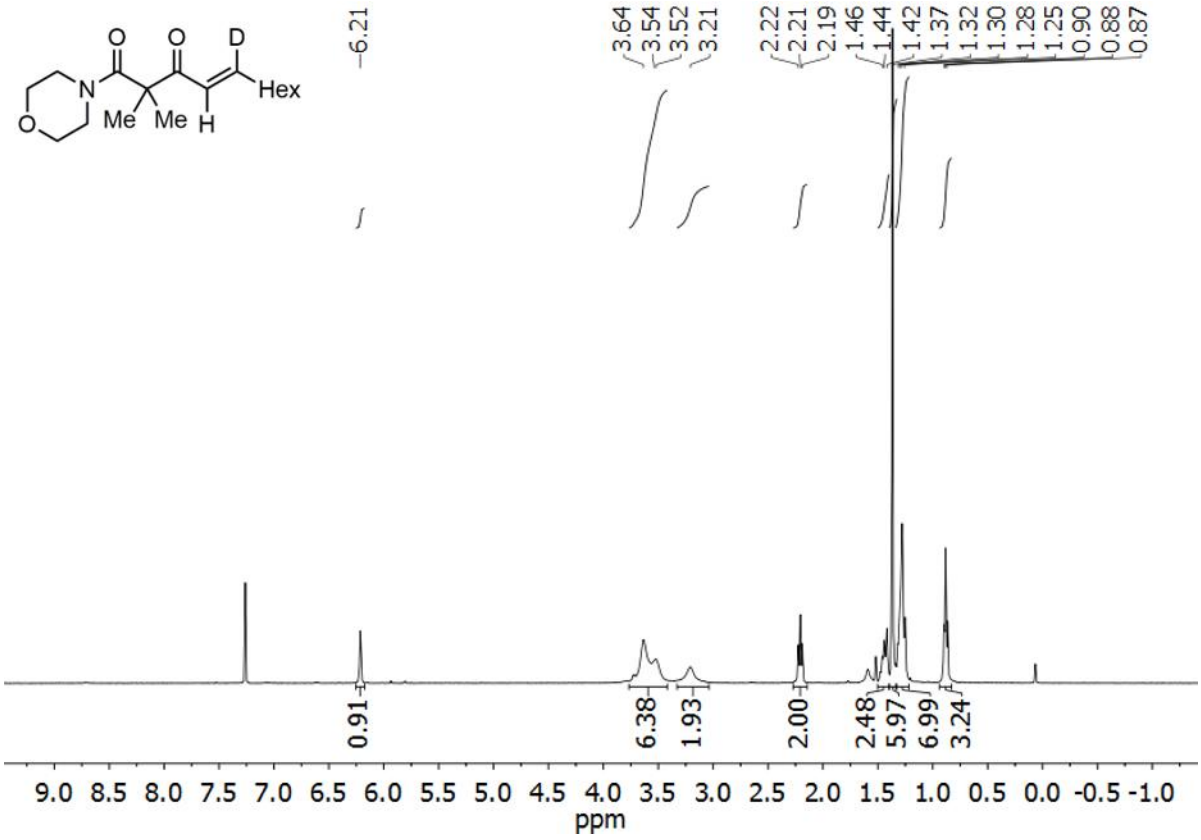

(*E*)-2,2-dimethyl-1-morpholinoundec-4-ene-5-^{2}H-1,3-dione 2.10c: ^{13}C{^{1}H} NMR (400 MHz, $CDCl_3$)

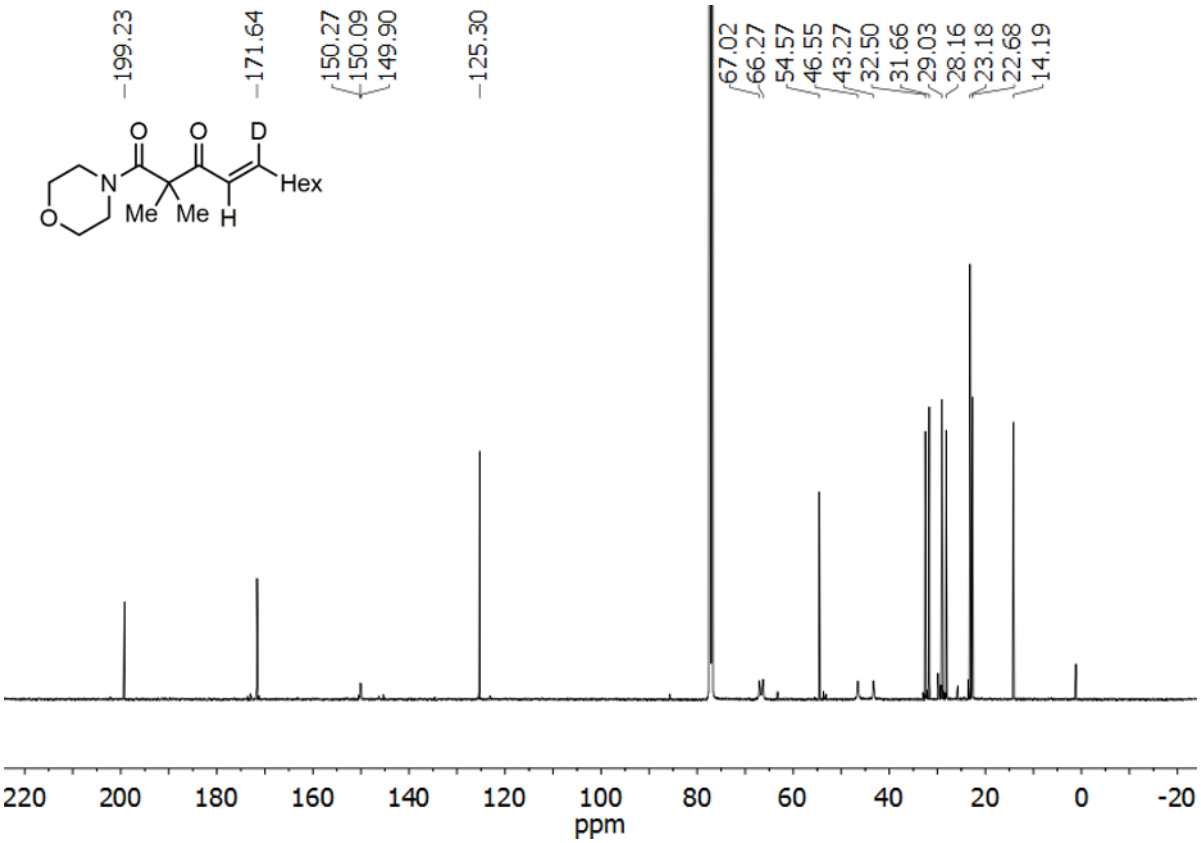

(*E*)-2,2-dimethyl-1-morpholinoundec-4-ene-4-^{2}H-1,3-dione 2.10e: ^{1}H NMR (400 MHz, $CDCl_3$)

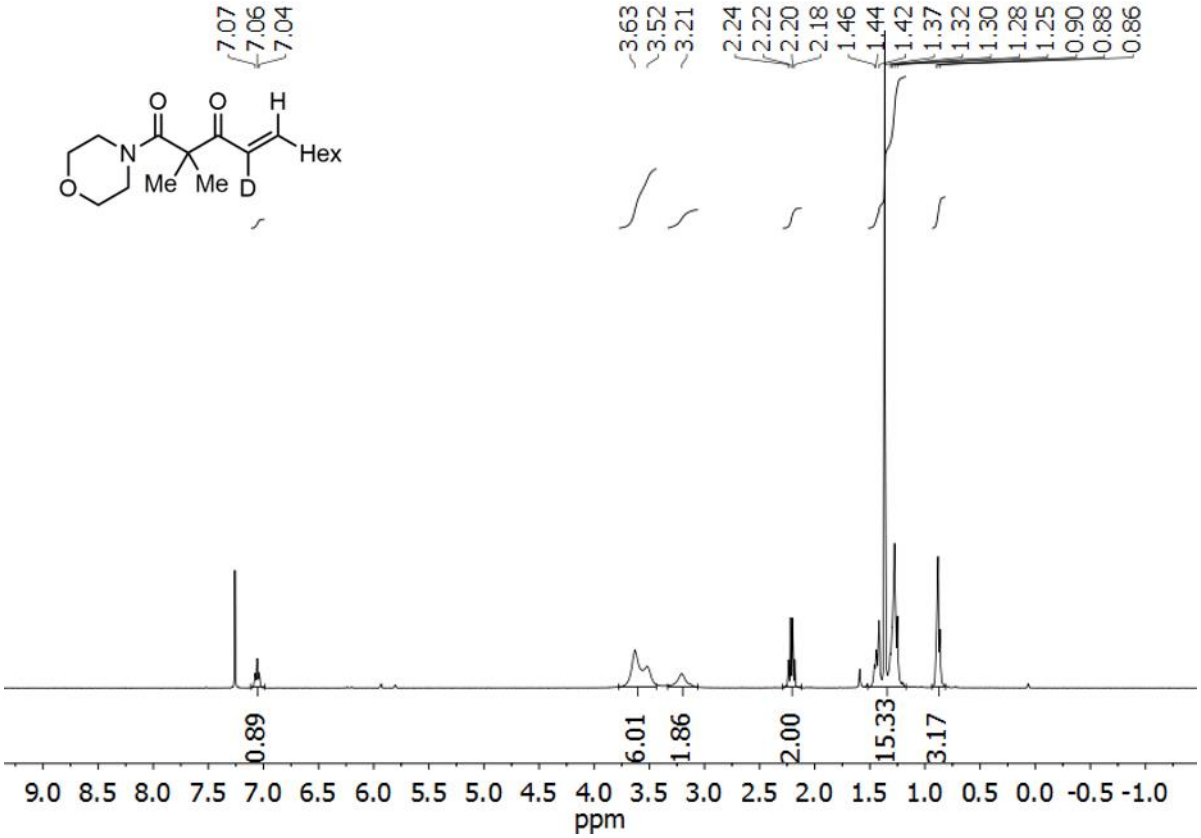

(*E*)-2,2-dimethyl-1-morpholinoundec-4-ene-4-^{2}H-1,3-dione 2.10e: ^{13}C{^{1}H} NMR (400 MHz, $CDCl_3$)

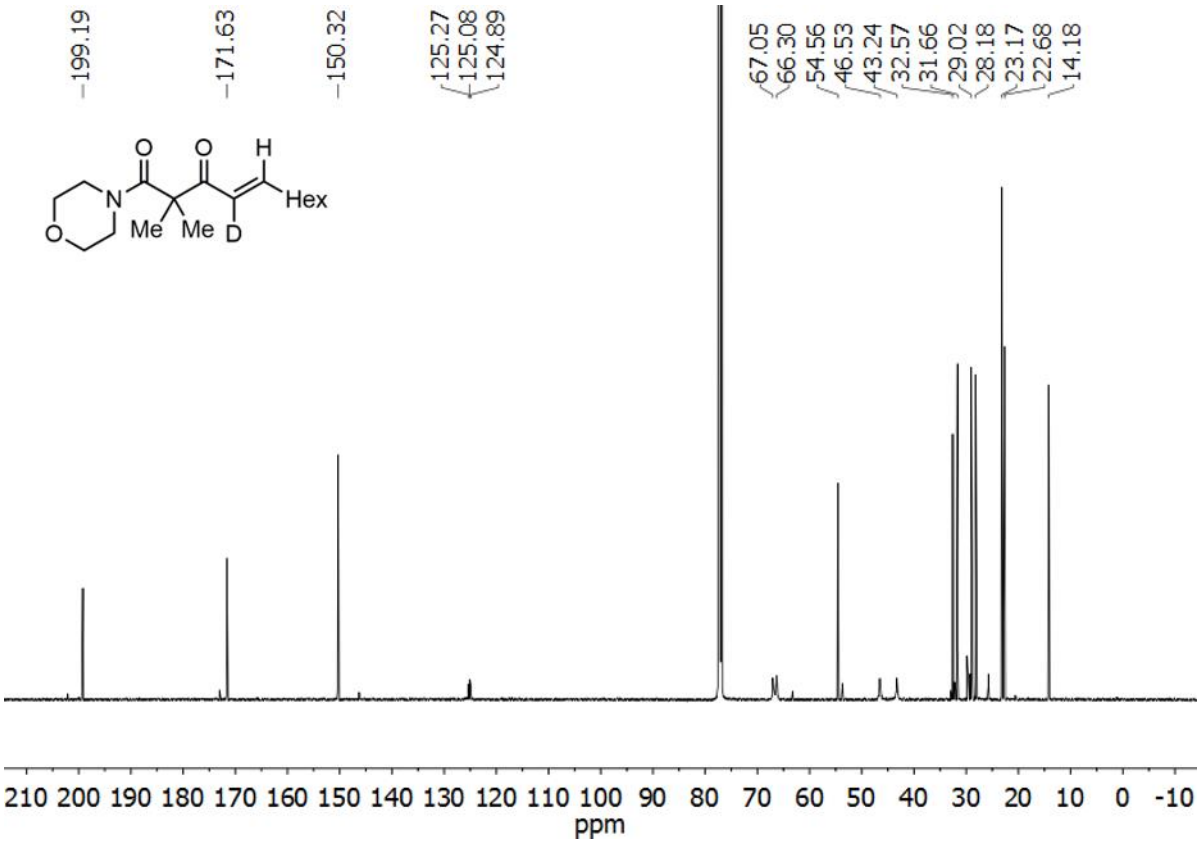

2,2-dimethyl-4-methylene-1-morpholinodecane-1,3-dione 2.10a/b: ^{1}H NMR (400 MHz, $CDCl_3$)

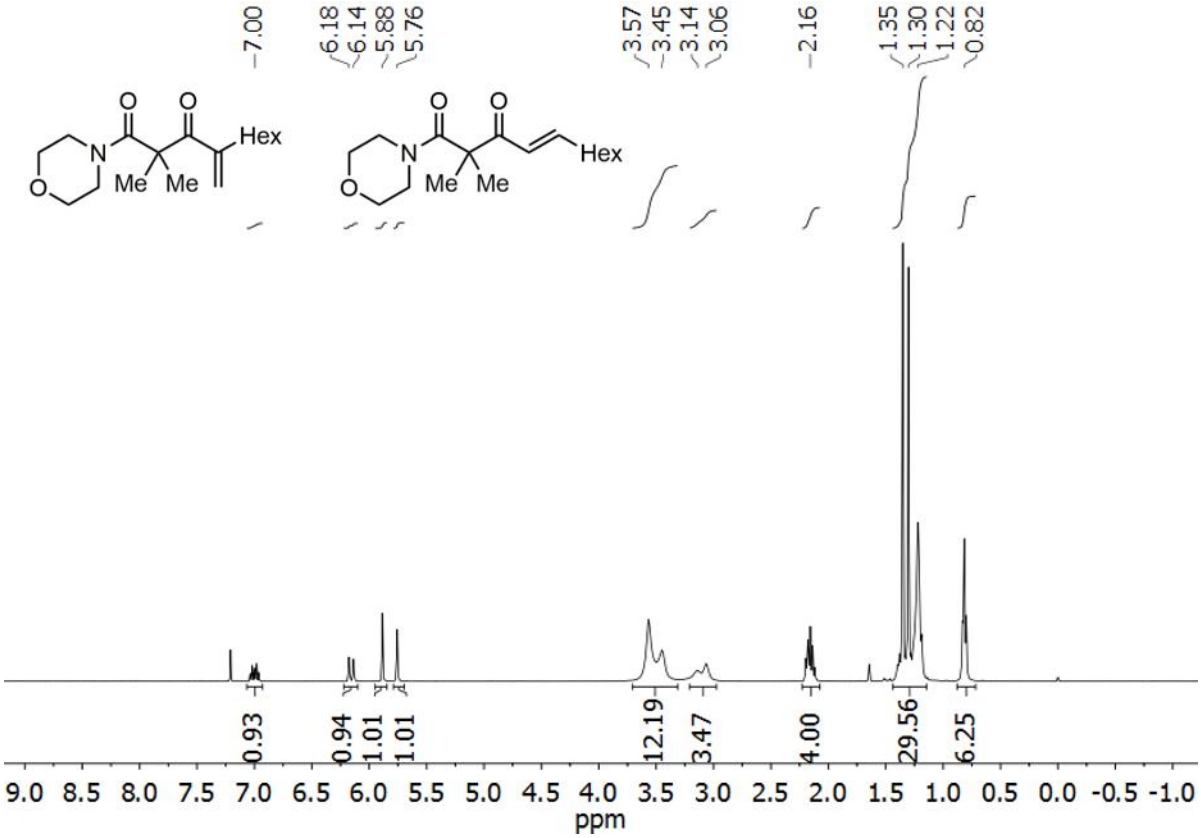

2,2-dimethyl-4-methylene-1-morpholinodecane-1,3-dione 2.10a/b: $^{13}C\{^{1}H\}$ NMR (400 MHz, $CDCl_3$)

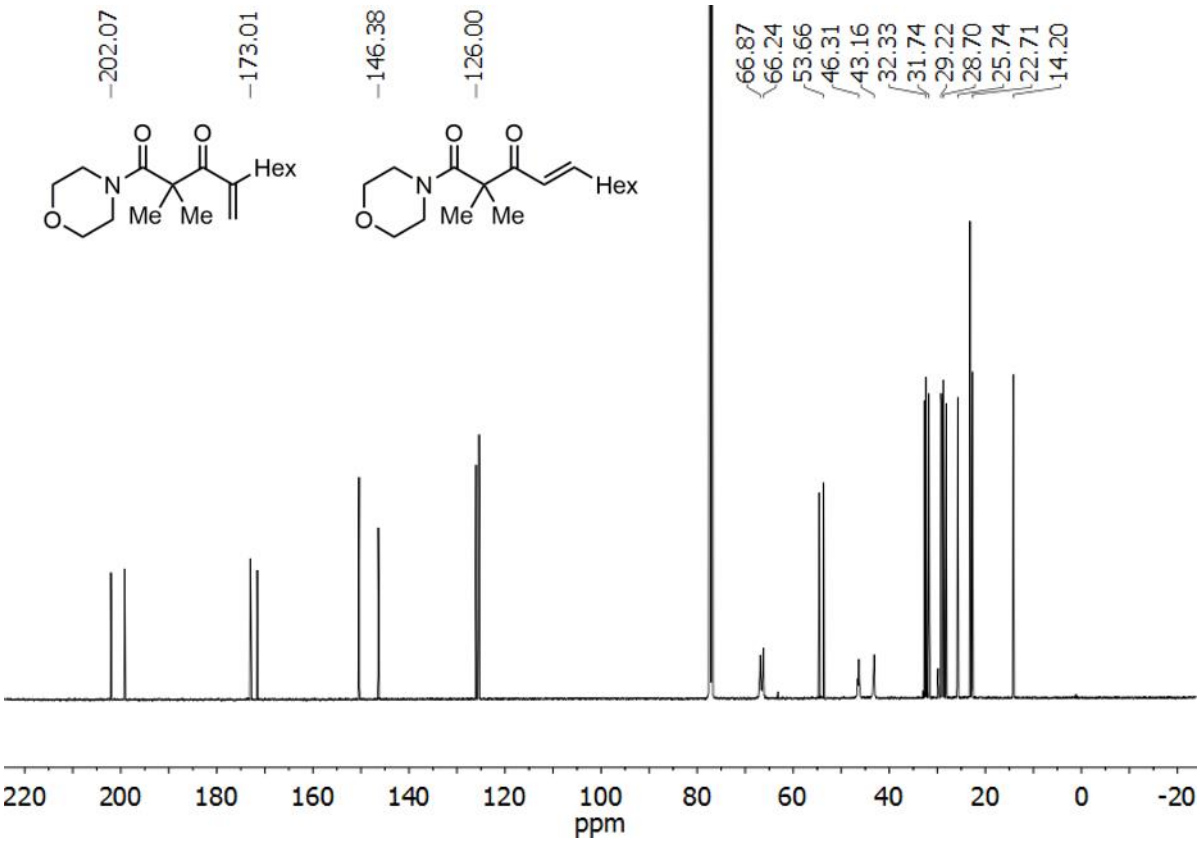

3-hydroxy-2,2-dimethyl-1-(pyrrolidin-1-yl)propan-1-one 3.21: ^{1}H NMR (400 MHz, $CDCl_3$)

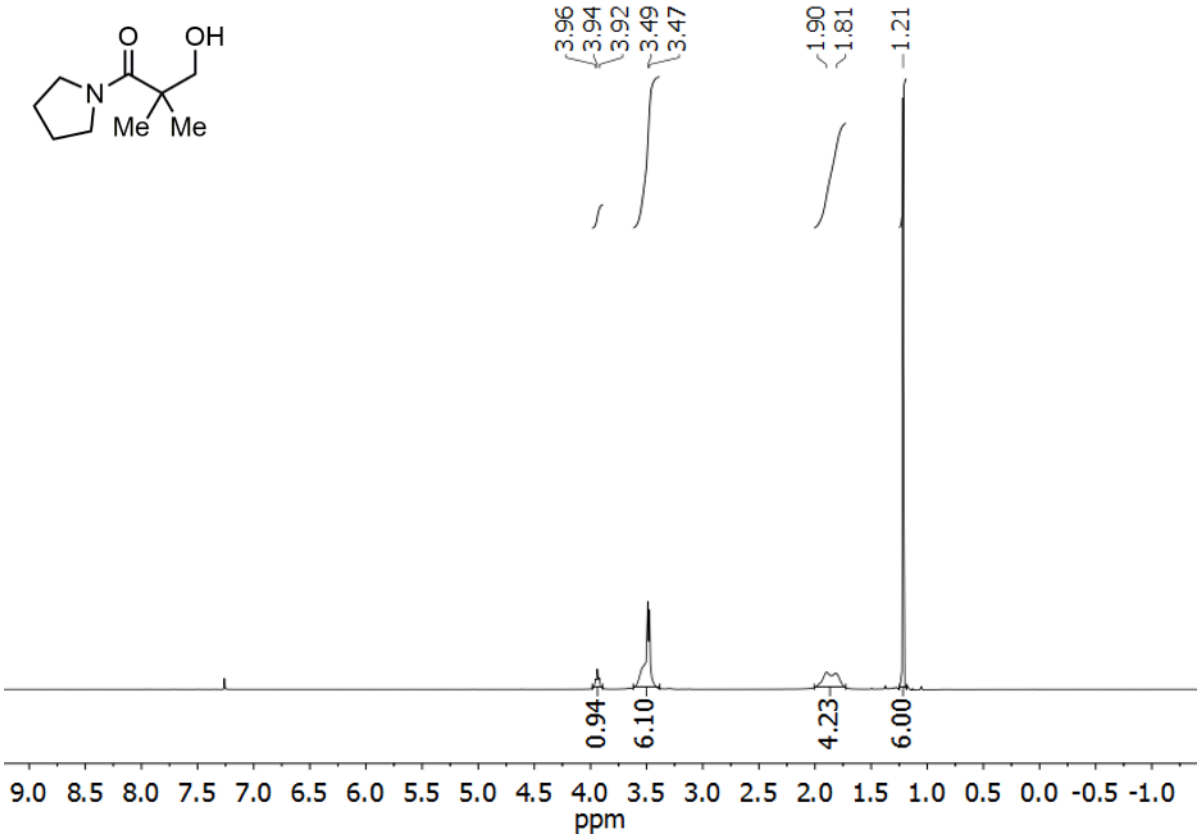

3-hydroxy-2,2-dimethyl-1-(pyrrolidin-1-yl)propan-1-one 3.21: ^{13}C{^{1}H} NMR (400 MHz, $CDCl_3$)

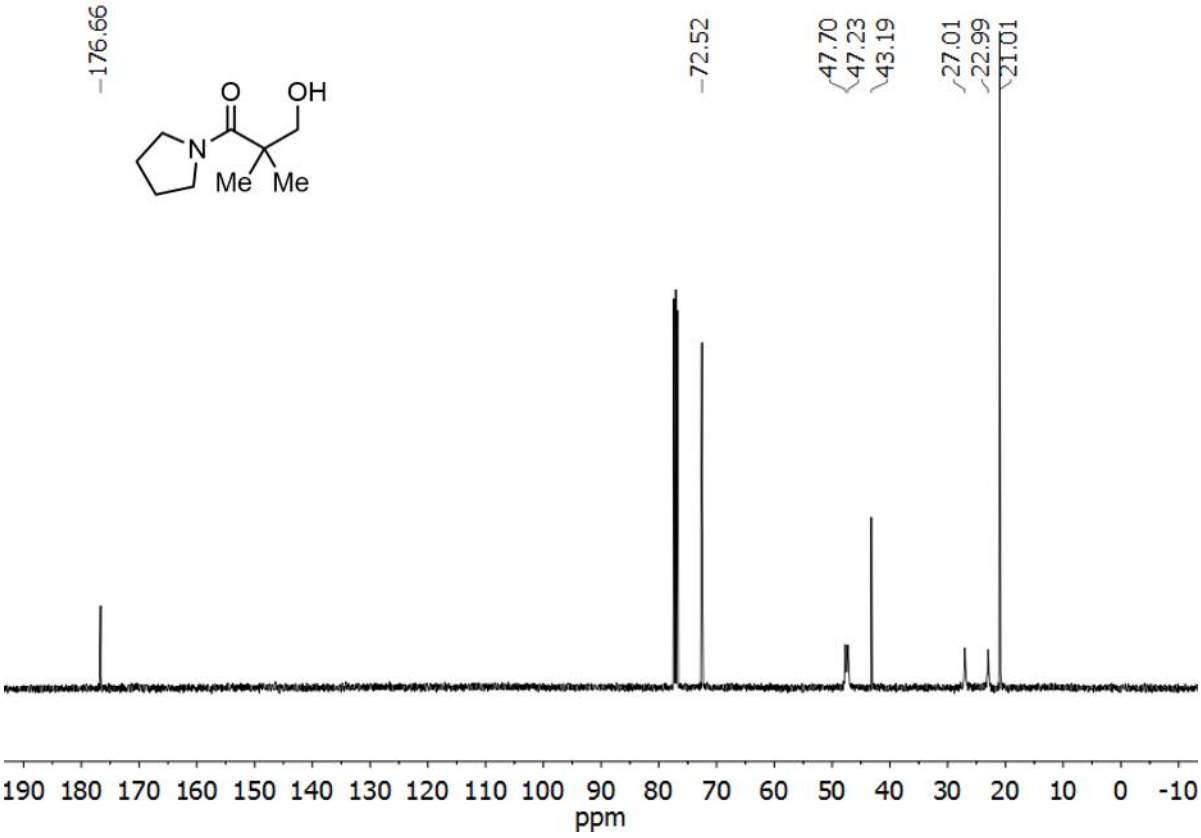

2,2-dimethyl-3-pyrrolidino-3-oxopropanal 3.14b: ^{1}H NMR (400 MHz, $CDCl_3$)

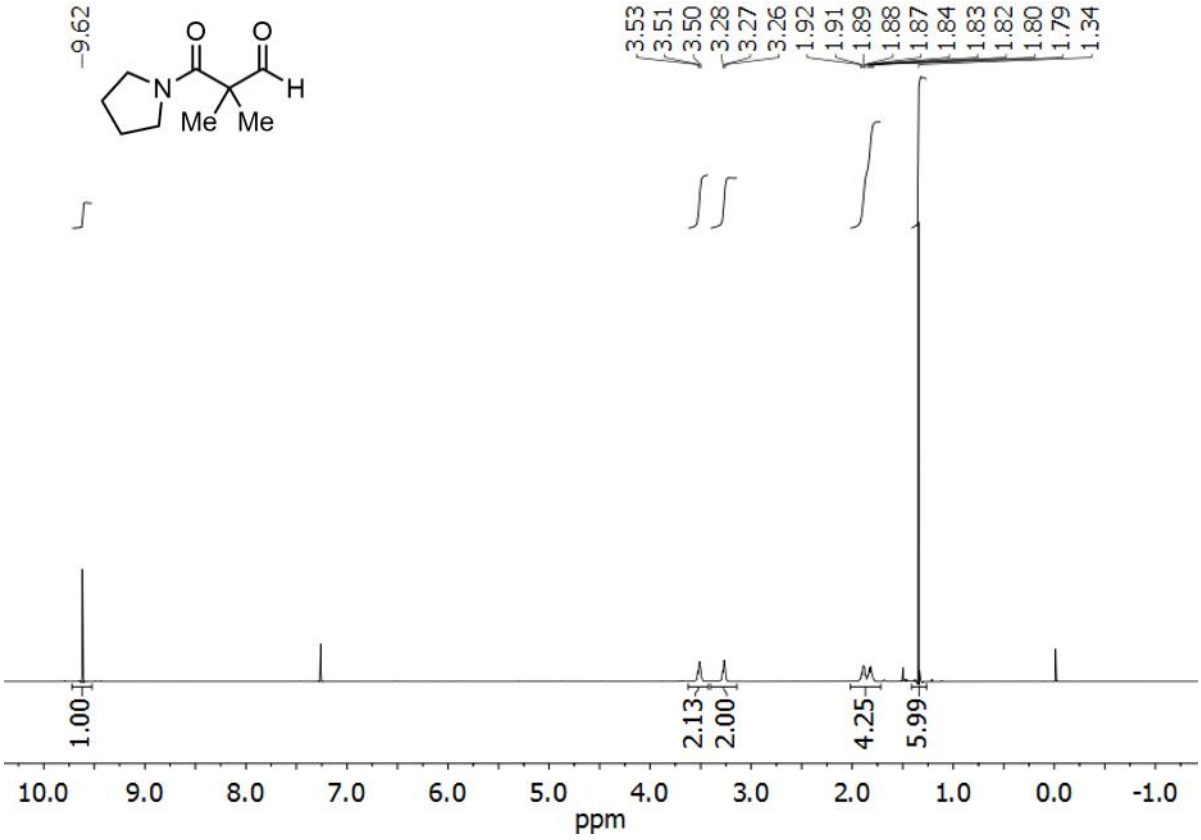

2,2-dimethyl-3-pyrrolidino-3-oxopropanal 3.14b: $^{13}C\{^{1}H\}$ NMR (400 MHz, $CDCl_3$)

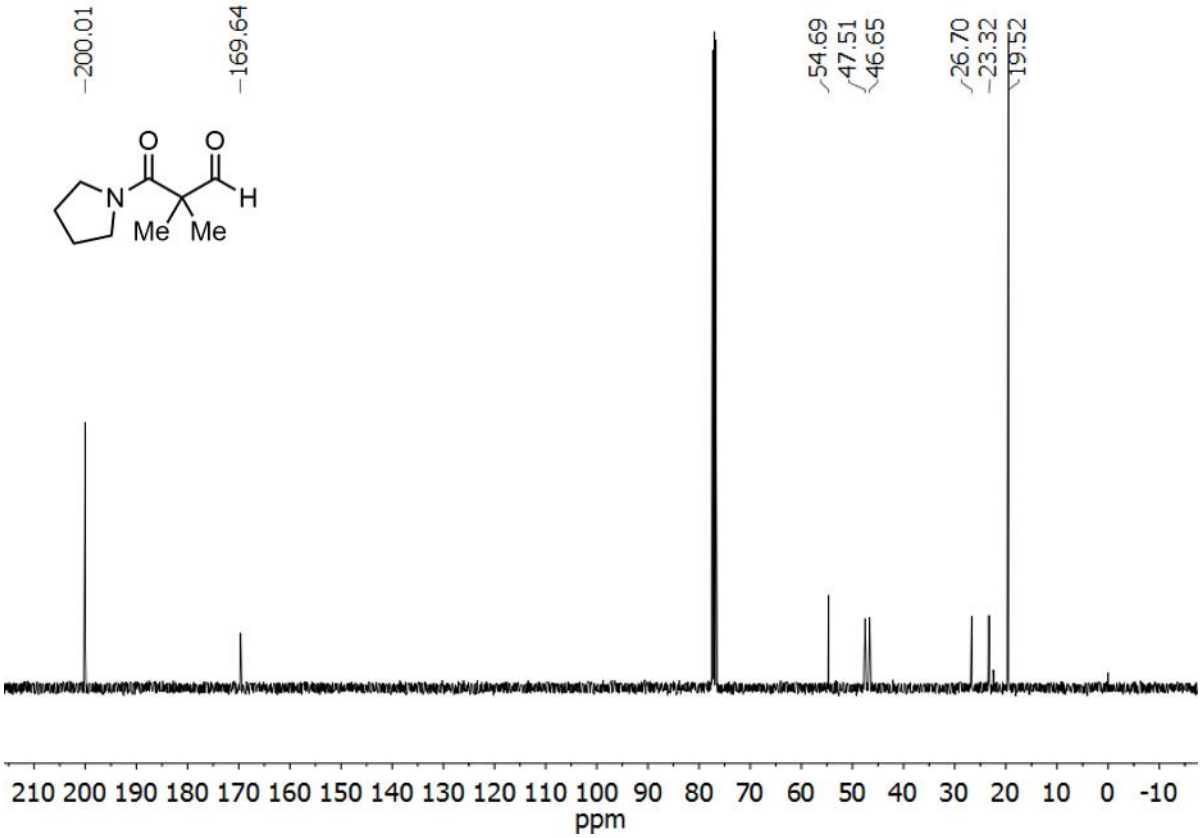

(*E*)-2,2-dimethyl-1-(pyrrolidin-1-yl)undec-4-ene-1,3-dione 3.23a: ^{1}H NMR (400 MHz, $CDCl_3$)

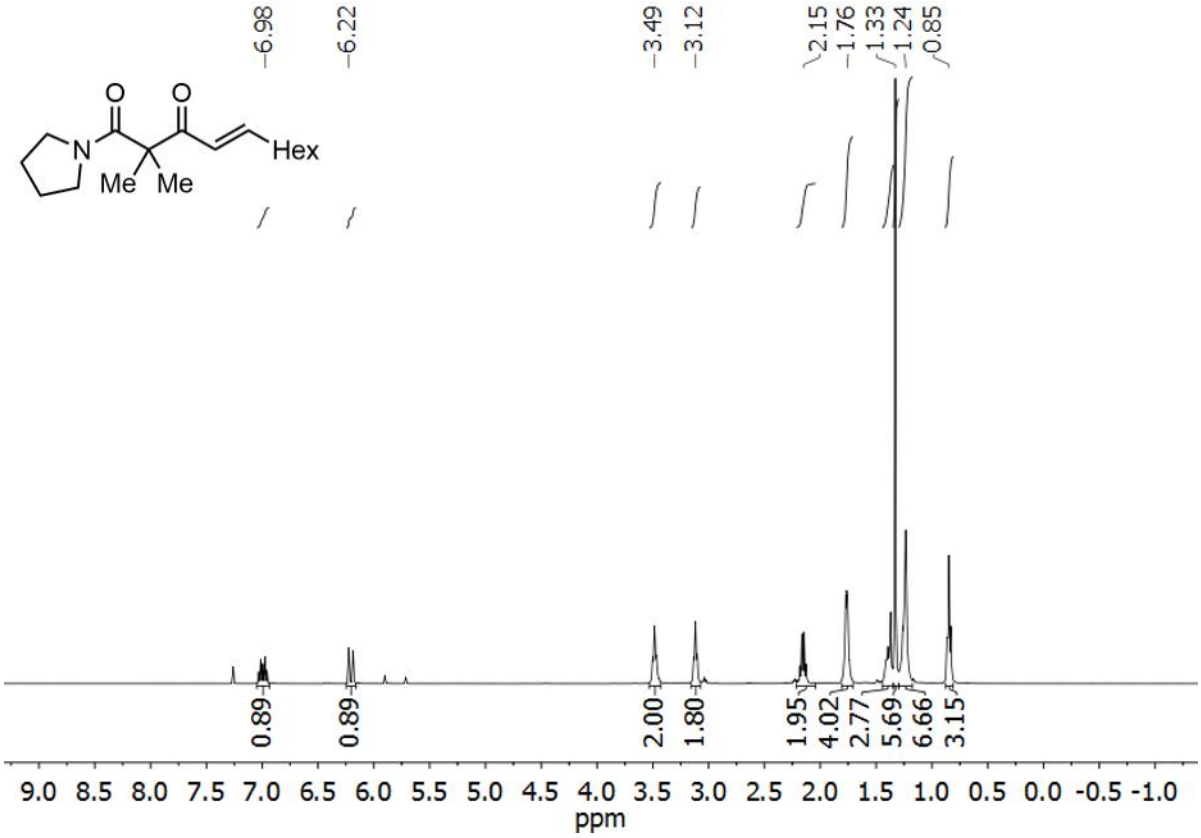

(*E*)-2,2-dimethyl-1-(pyrrolidin-1-yl)undec-4-ene-1,3-dione 3.23a: $^{13}C\{^{1}H\}$ NMR (400 MHz, $CDCl_3$)

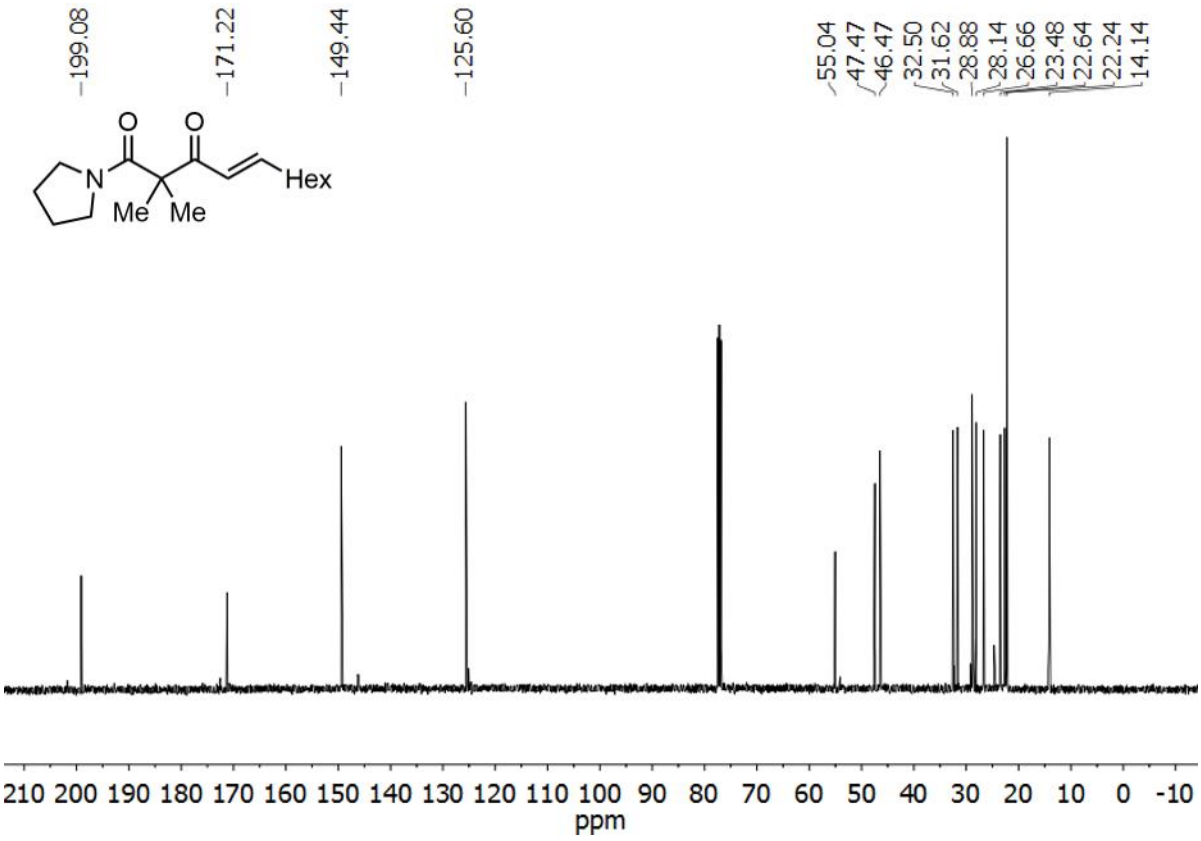

1-(1-(morpholine-4-carbonyl)cyclopentyl)ethan-1-one 4.3: ^{1}H NMR (400 MHz, $CDCl_3$)

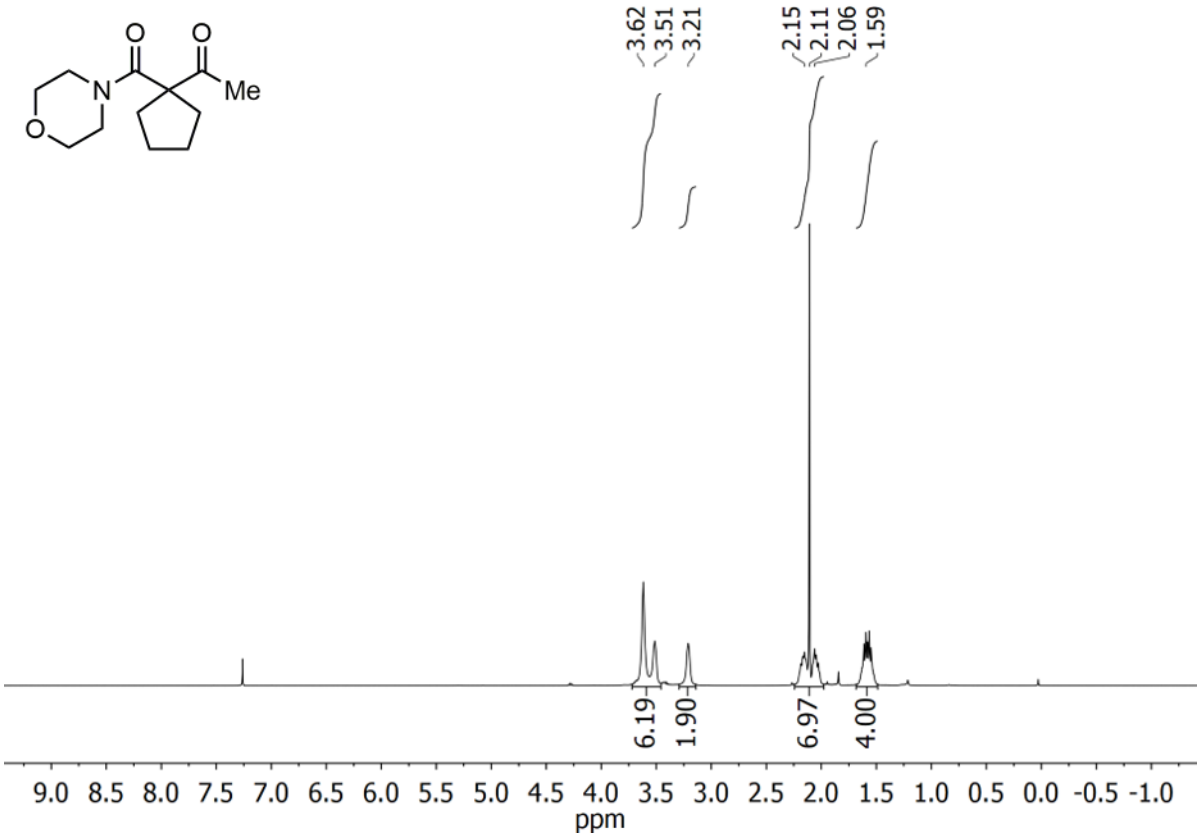

1-(1-(morpholine-4-carbonyl)cyclopentyl)ethan-1-one 4.3: $^{13}C\{^{1}H\}$ NMR (400 MHz, $CDCl_3$)

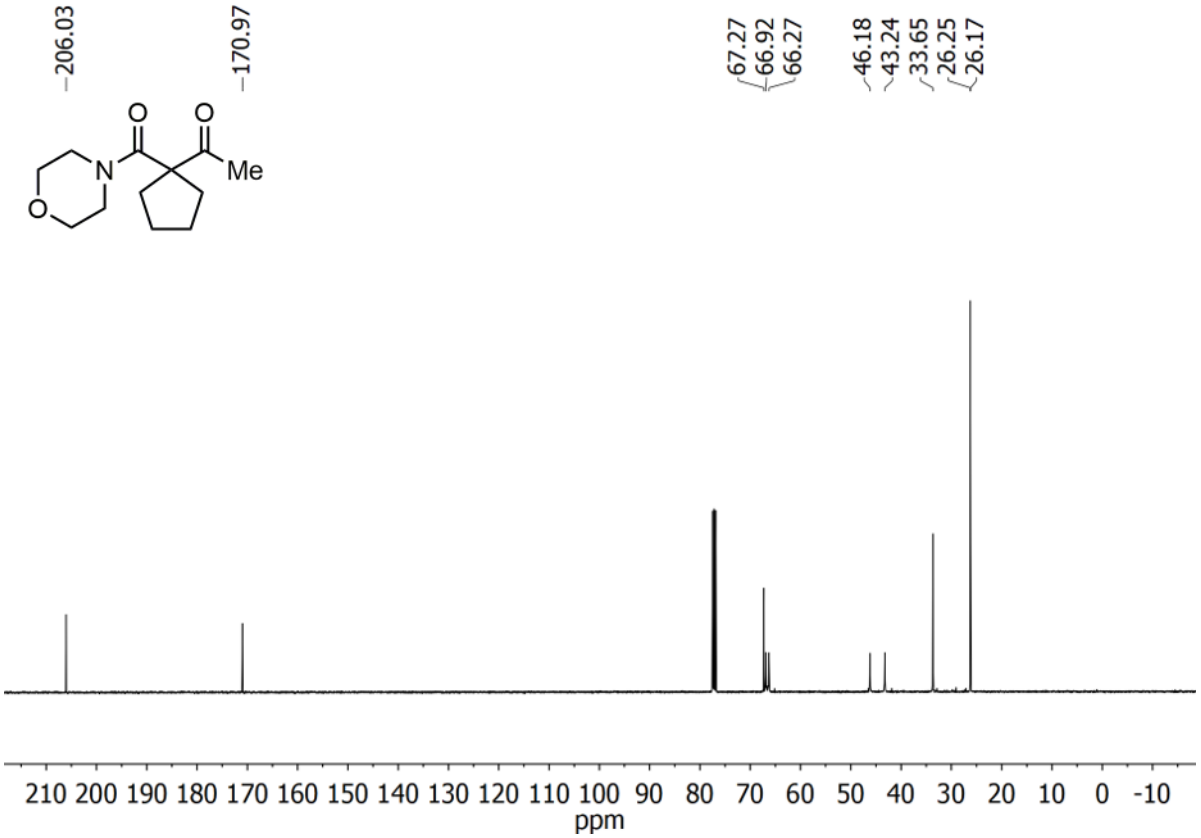

Butyl 4-cyclohexyl-4-oxobutanoate 4.22a: ^{1}H NMR (400 MHz, $CDCl_3$)

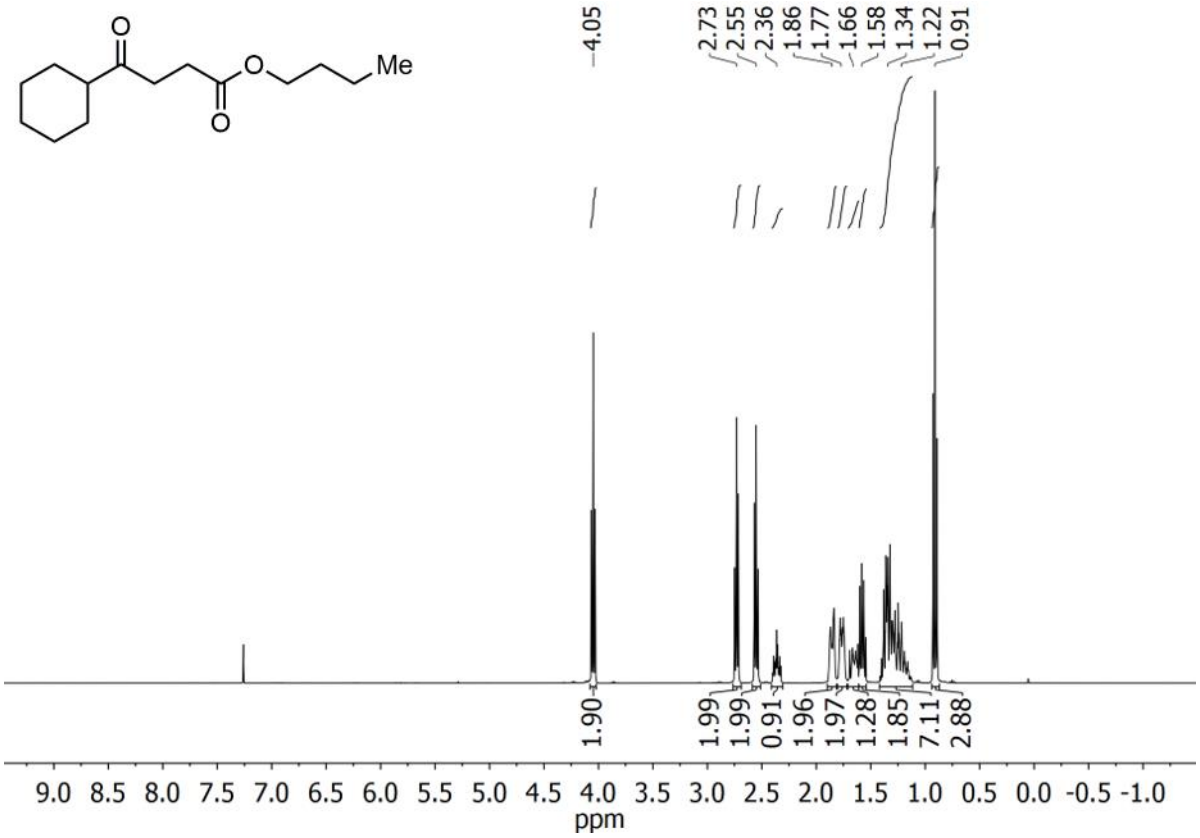

Butyl 4-cyclohexyl-4-oxobutanoate 4.22a: $^{13}C\{^{1}H\}$ NMR (101 MHz, $CDCl_3$)

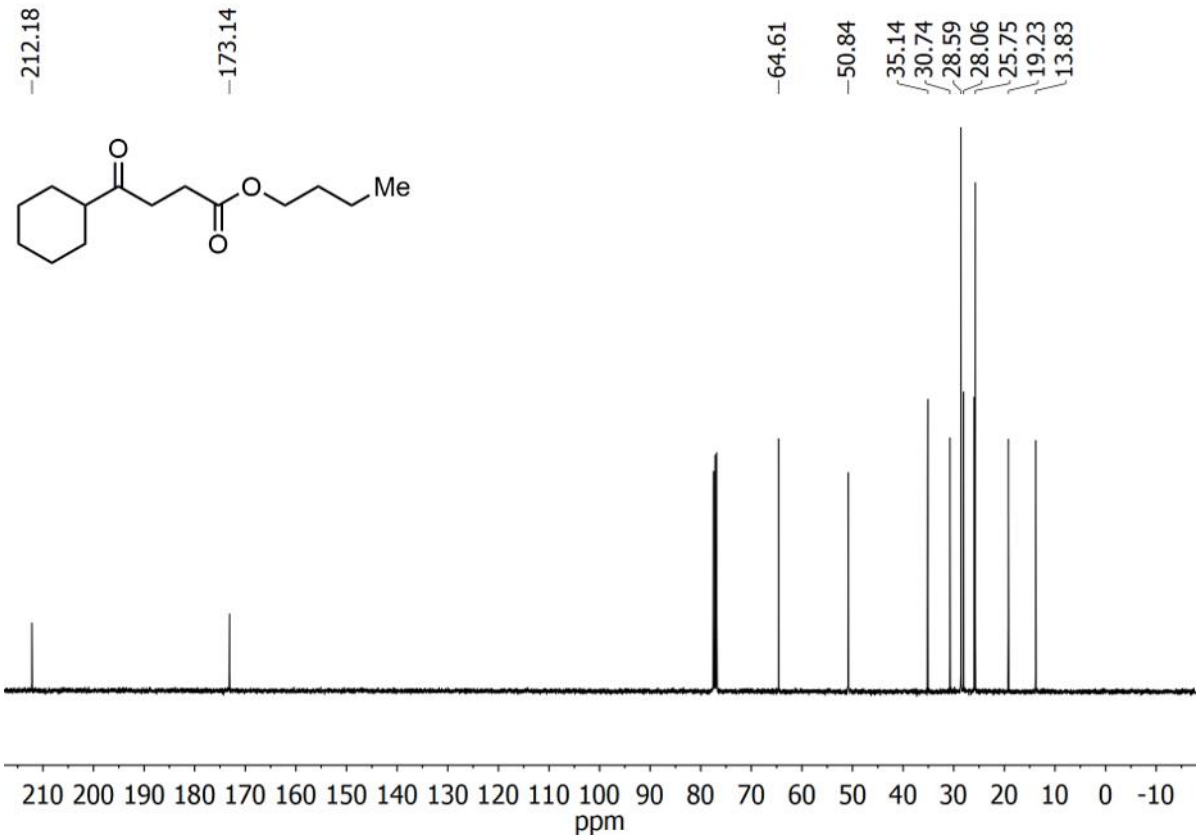

Butyl 4-(1-methylcyclohexyl)-4-oxobutanoate 4.22b: ^{1}H NMR (400 MHz, $CDCl_3$)

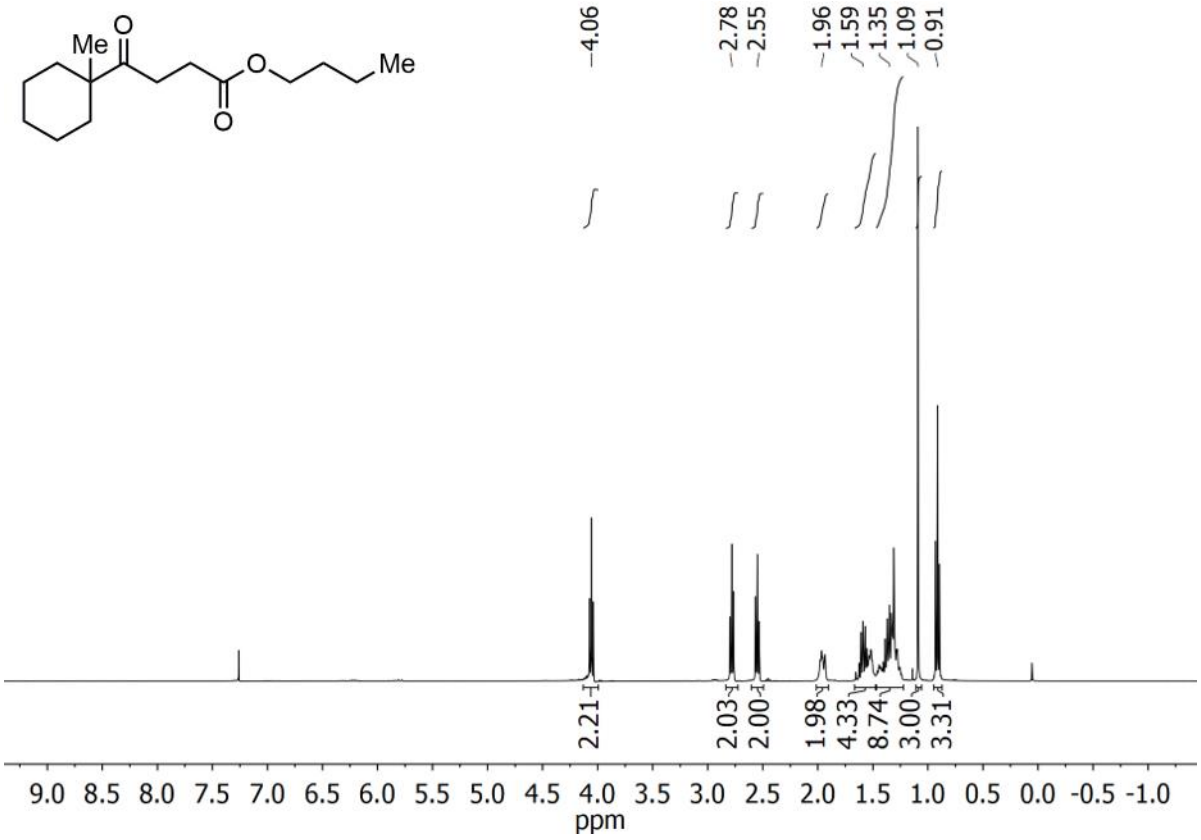

Butyl 4-(1-methylcyclohexyl)-4-oxobutanoate 4.22b: $^{13}C\{^{1}H\}$ NMR (101 MHz, $CDCl_3$)

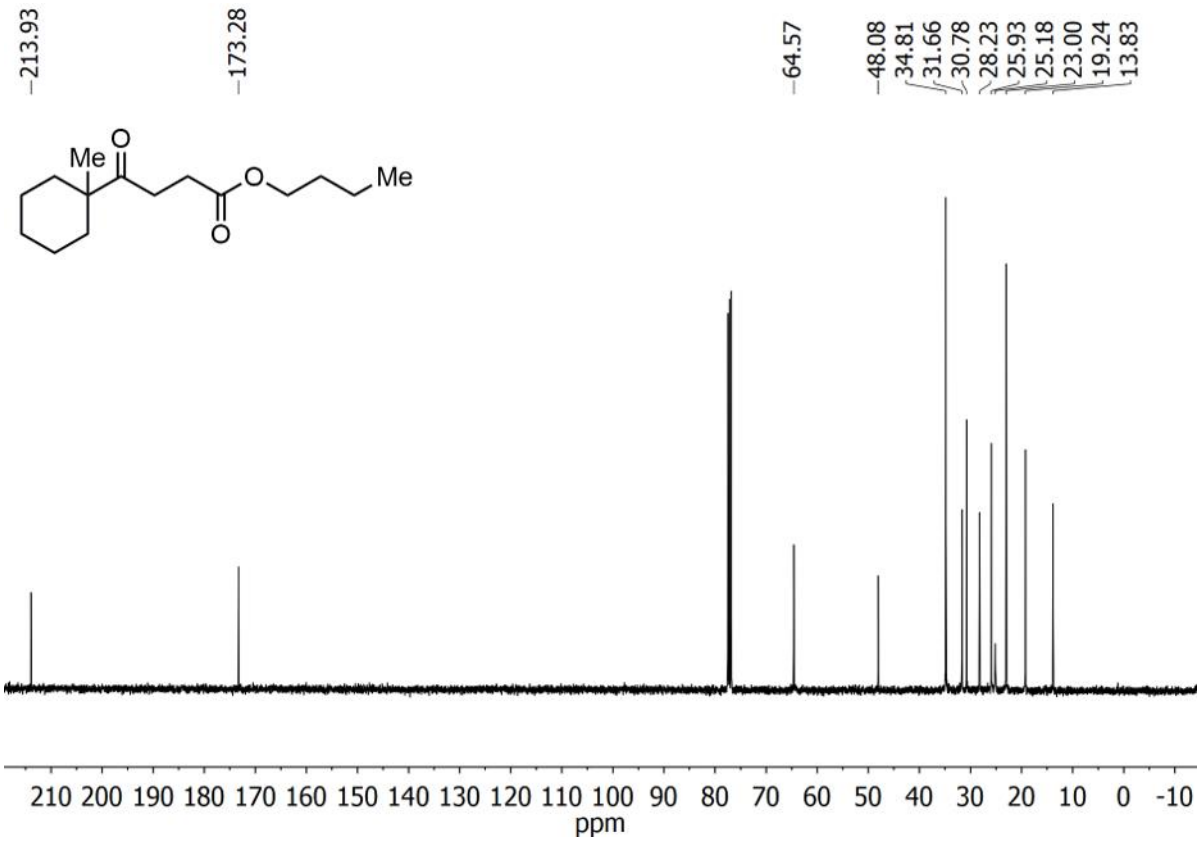

Butyl 4-oxoundecanoate 4.22c: ^{1}H NMR (400 MHz, $CDCl_3$)

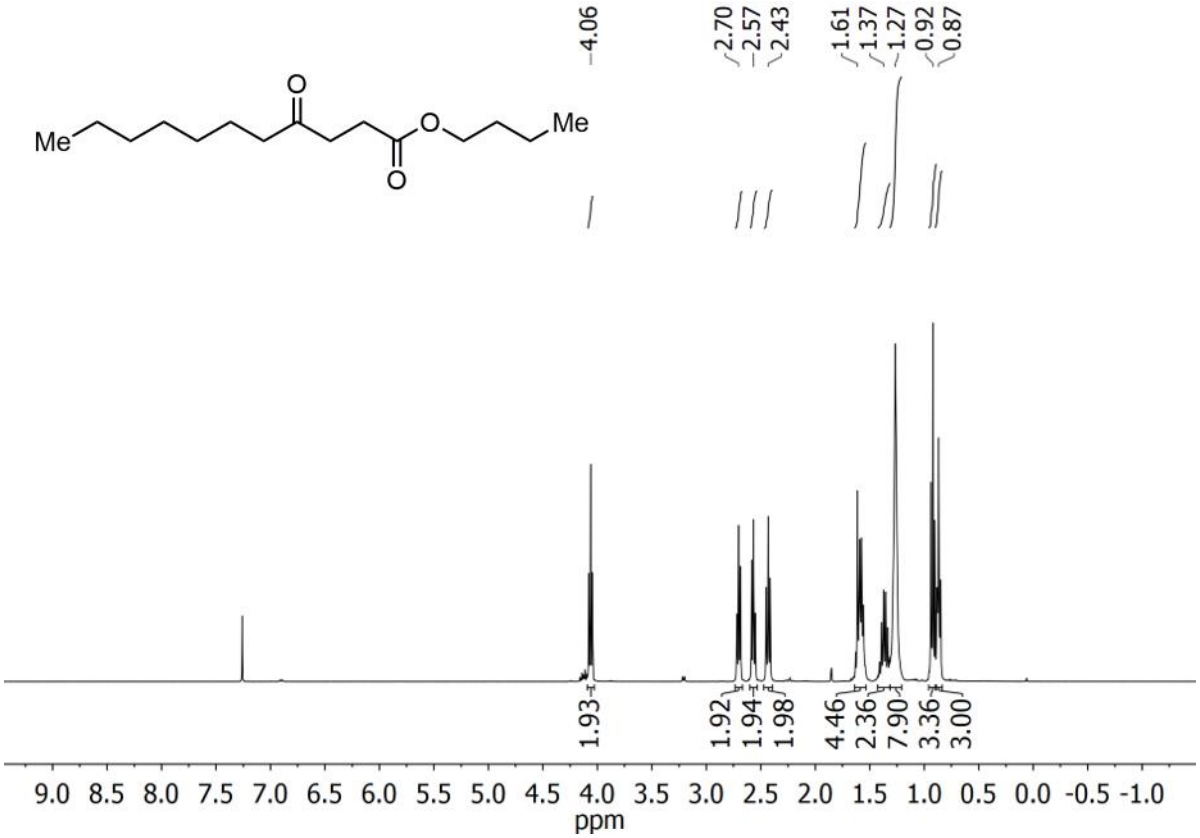

Butyl 4-oxoundecanoate 4.22c: $^{13}C\{^{1}H\}$ NMR (400 MHz, $CDCl_3$)

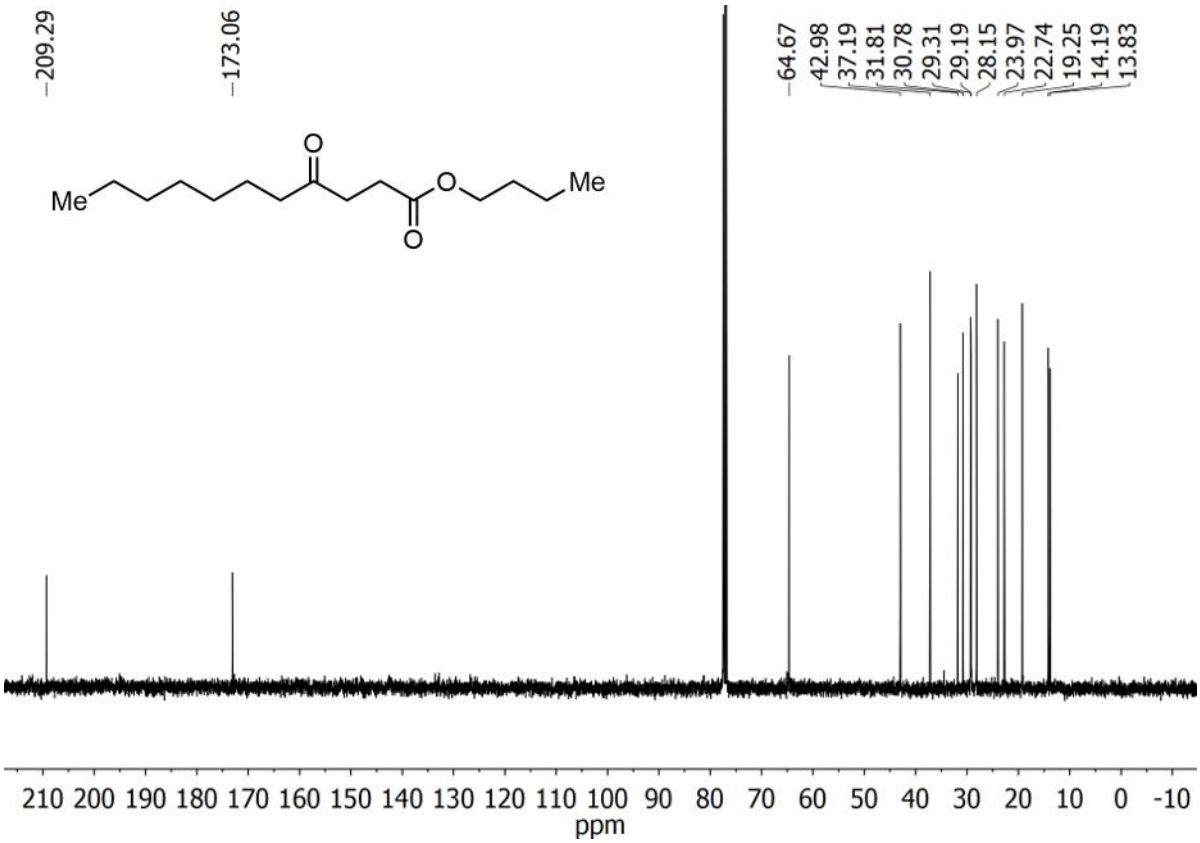

Butyl 4-cyclopentyl-4-oxobutanoate 4.22d: ^{1}H NMR (400 MHz, $CDCl_3$)

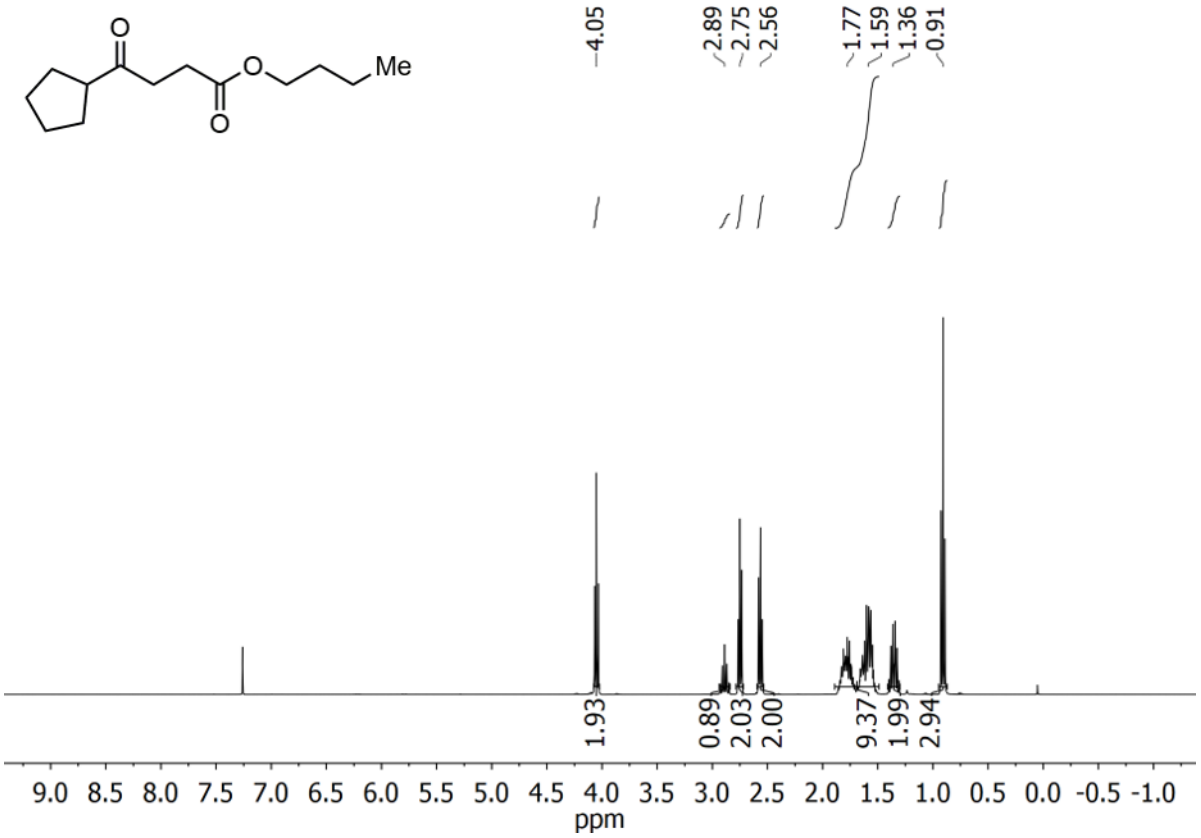

Butyl 4-cyclopentyl-4-oxobutanoate 4.22d: $^{13}C\{^{1}H\}$ NMR (101 MHz, $CDCl_3$)

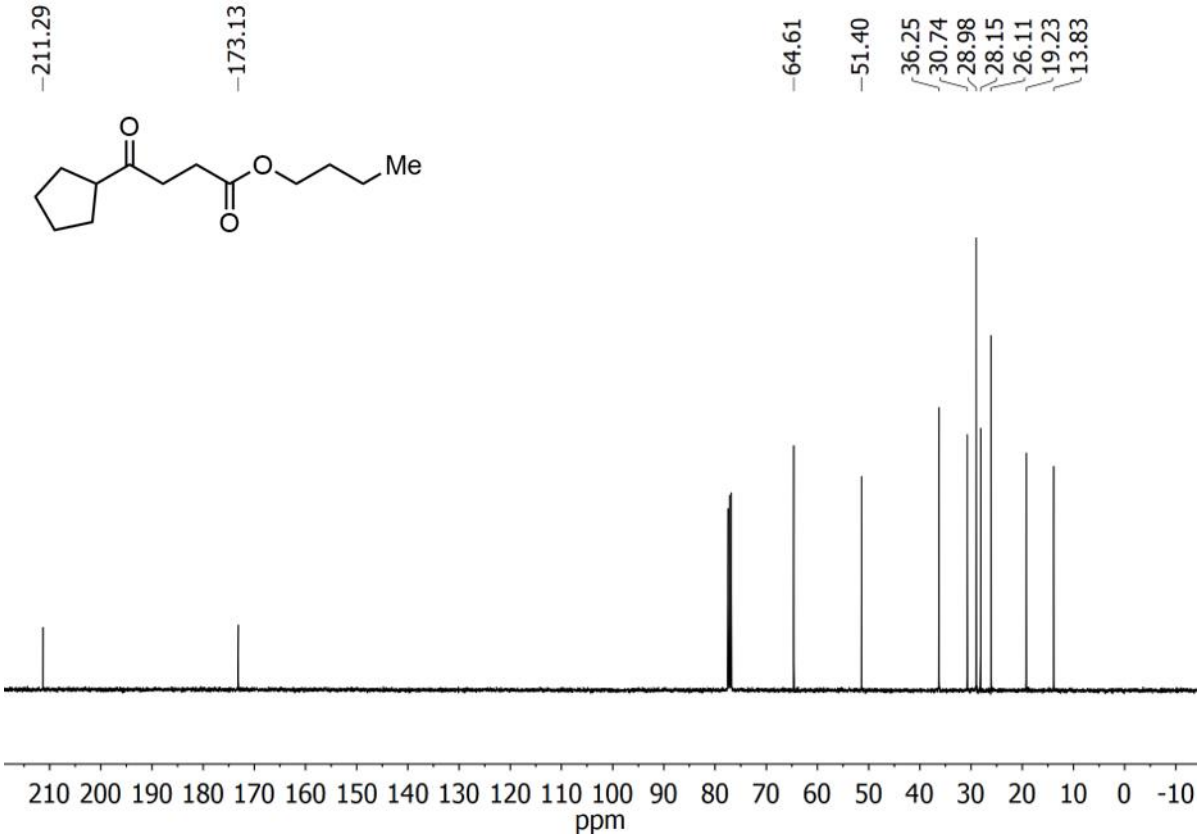

Butyl 5-ethyl-4-oxononanoate 4.22e: ^{1}H NMR (400 MHz, $CDCl_3$)

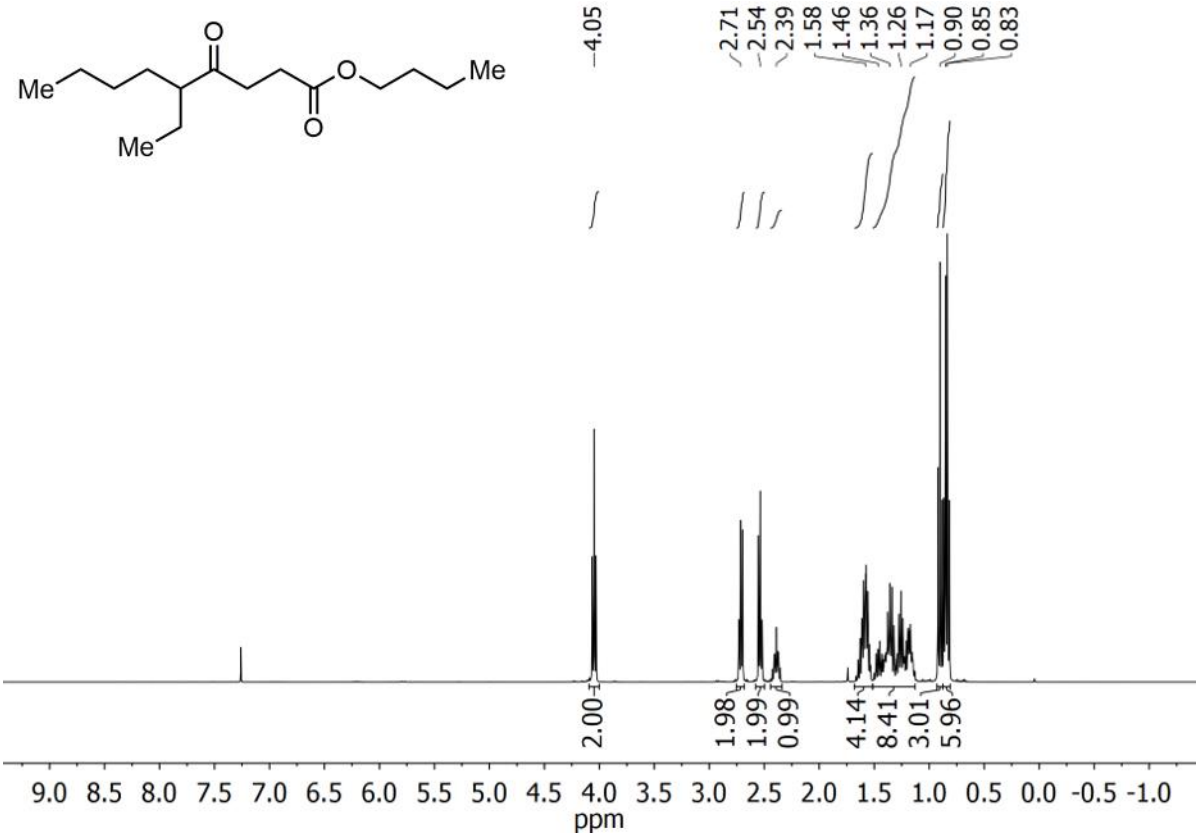

Butyl 5-ethyl-4-oxononanoate 4.22e: $^{13}C\{^{1}H\}$ NMR (400 MHz, $CDCl_3$)

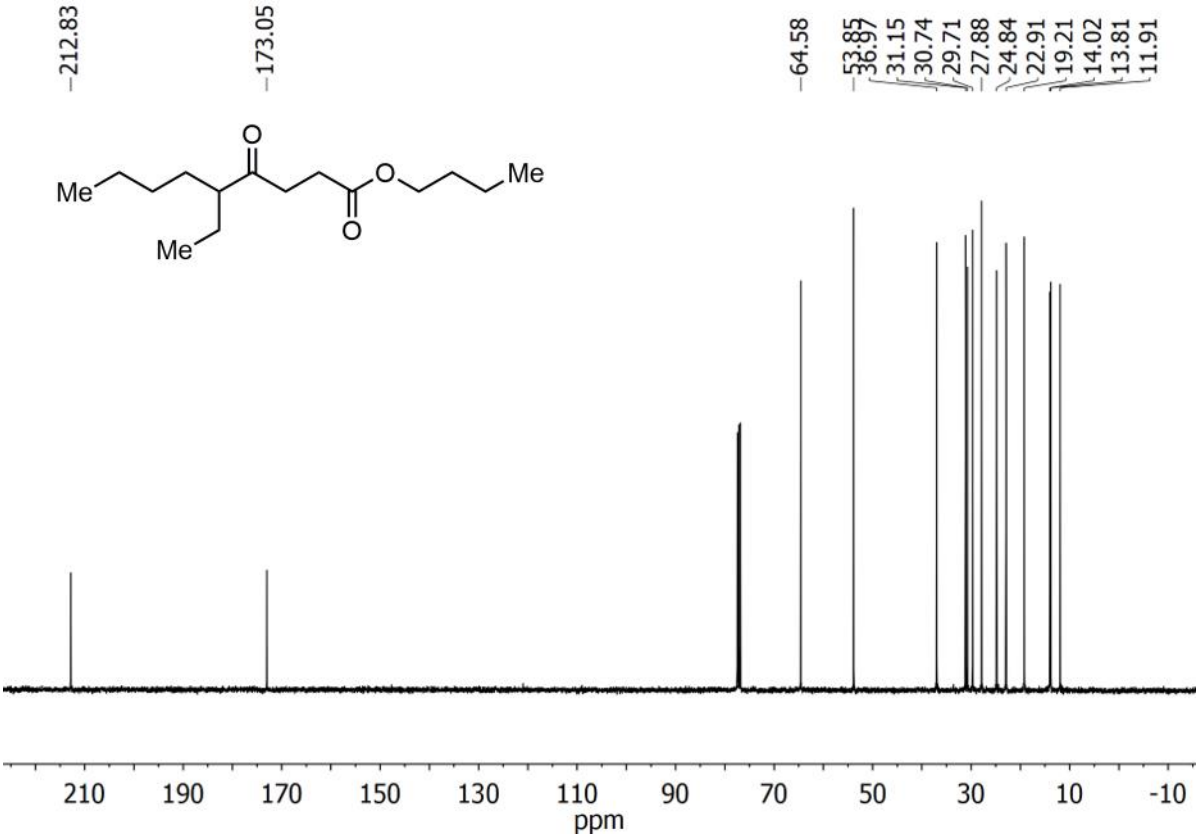

Butyl 4-oxo-4-(tetrahydro-2H-pyran-4-yl)butanoate 4.22f: ^{1}H NMR (400 MHz, $CDCl_3$)

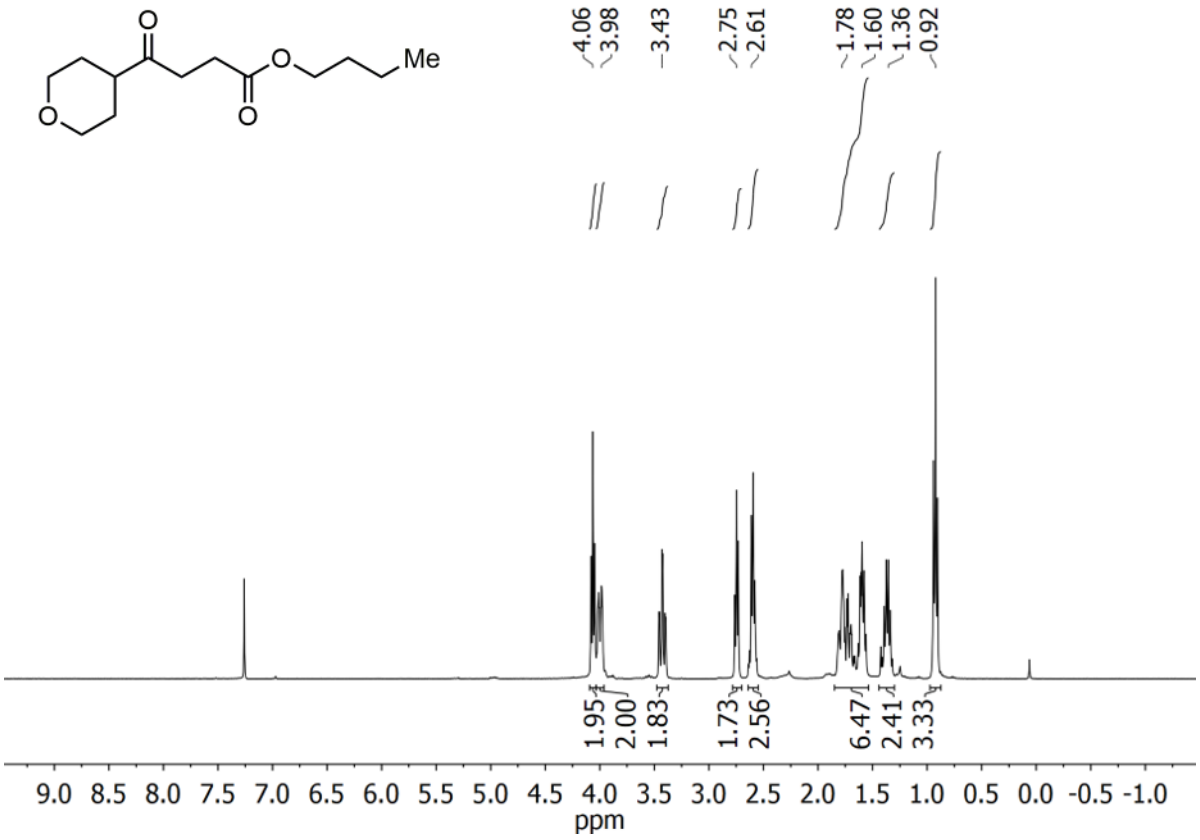

Butyl 4-oxo-4-(tetrahydro-2H-pyran-4-yl)butanoate 4.22f: $^{13}C\{^{1}H\}$ NMR (400 MHz, $CDCl_3$)